U.PORTO

DOUTORAMENTO

BIOTECNOLOGIA MOLECULAR E CELULAR APLICADA ÀS CIÊNCIAS DA SAÚDE

Biophysics of mitotic spindle assembly

Vanessa Nunes

D

2022

U.PORTO

Vanessa Nunes Biophysics of mitotic spindle assembly

Biophysics of mitotic spindle assembly

Vanessa Nunes

D.ICBAS 2022

SEDE ADMINISTRATIVA

INSTITUTO DE CIÊNCIAS BIOMÉDICAS ABEL SALAZAR

FACULDADE DE FARMÁCIA

Vanessa Catarina Ribeiro Nunes

Biophysics of mitotic spindle assembly

Tese de Candidatura ao grau de Doutor em Biotecnologia Molecular e Celular Aplicada às Ciências da Saúde;
Programa Doutoral da Universidade do Porto (Instituto de Ciências Biomédicas Abel Salazar e Faculdade de Farmácia)

Orientador – Doutor Jorge Ferreira
Categoria – Professor Auxiliar/Investigador Principal
Afiliação – i3S – Instituto de Investigação e Inovação em Saúde, FMUP – Faculdade de Medicina da Universidade do Porto.

Coorientador – Doutor Paulo Aguiar
Categoria – Investigador Principal
Afiliação – i3S – Instituto de Investigação e Inovação em Saúde, INEB – Instituto Nacional de Engenharia Biomédica, FMUP – Faculdade de Medicina da Universidade do Porto.

Coorientador – Doutor Matthieu Piel
Categoria – Investigador Principal
Afiliação – Institut Curie/CNRS, Paris, France

Affiliations

The work presented in this thesis was developed in collaboration with the following labs:

- Chromosome Instability & Dynamics Laboratory at Instituto de Investigação e Inovação em Saúde (i3S), Portugal.
- Systems Biology of Cell Polarity and Cell Division at Institut Curie, France.
- Neuroengineering and Computational Neuroscience Laboratory at Instituto de Investigação e Inovação em Saúde (i3S), Portugal.
- Laboratoire Interdisciplinaire de Physique Laboratory at Université Grenoble Alpes, France.
- Epithelial Polarity & Cell Division Laboratory at Instituto de Investigação e Inovação em Saúde (i3S), Portugal.
- Biophysics of Cell Division Laboratory at Faculdade de Medicina da Universidade do Porto (FMUP), Portugal.







Financial Support

The work presented in this thesis was funded by grants from FEDER—Fundo Europeu de Desenvolvimento Regional funds through the COMPETE 2020—Operacional Programme for Competitiveness and Internationalization (POCI), Portugal 2020, and by Portuguese funds through FCT—Fundação para a Ciência e a Tecnologia/Ministério da Ciência, Tecnologia e Ensino Superior in the framework of the projects PTDC/BEX-BCM/1758/2014 (POCI-01–0145-FEDER-016589) and PTDC/BIA-CEL/6704/2020.

Vanessa Nunes was supported by a PhD grant (PD/BD/135545/2018) from Portuguese Foundation for Science and Technology (FCT) in the scope of the BiotechHealth PhD Program (Doctoral Program on Cellular and Molecular Biotechnology Applied to Health Sciences).







Dedicated to my parents.

Acknowledgements

Science is a collective endeavor. Here I express my gratitude to the people that made this work possible.

First and foremost, I would like to thank to **Jorge Ferreira**, my supervisor, for the support, guidance, friendship, critical suggestions, fruitful brainstorming, encouragement, endless patience, and shared knowledge and experience. We have been working together for almost 6 years and, throughout this time, you have supported my personal and professional growth and therefore, shaped myself into a better person and a better scientist. I am very glad to have you as my mentor, supervisor, and friend.

To **Paulo Aguiar**, I want to express my sincere gratitude for all the support, discussions, attention, invaluable inputs, and key resources. Thank you for always being so positive and for following my progress closely. The attitude and enthusiasm with which you approach everything you do is truly inspiring. I am grateful to have you as my co-supervisor.

To **Matthieu Piel,** I want to express my deepest gratitude for keeping the door open for me and giving me the opportunity to work in such a stimulating environment several times. Your lab really feels like my second home. Thank you for sharing your extensive knowledge of microfabrication, for always having the time to discuss and encourage me to give everything a try. This experience has been incredible and has enriched me both personally and professionally.

To **Hélder Maiato**, I want to express my most sincere gratitude for the support, shared knowledge and experience, encouragement, positive attitude, interesting discussions, and valuable scientific advices. Your enthusiasm for cell division was truly inspiring, and I feel privileged to have had the opportunity to develop my PhD project in your lab. I am very glad to have you as my unofficial co-supervisor.

To **all my lab colleagues**, both in Portugal and in France, I want to share my deepest gratitude for all the help and friendship. We struggled, failed, and succeeded together, that is a special kind of bond. A special thanks to **Margarida Dantas** for her involvement in this project and for being my companion throughout this journey and to **Domingos Leite de Castro** for his invaluable help with the MATLAB algorithms.

I want to dedicate my most sincere gratitude to my **parents and sister**, for the unconditional love, support, encouragement, and endless patience. Thank you for being an example of strength and courage and for always believing in me.

Lastly, to **all my friends**, thank you for being there for me all these years and for filling my life with happiness. Your support and friendship have been invaluable.

Thank you!

Thesis Publications

This thesis is in compliance the terms of n.º 2, of Art.º 31º of Decreto-lei n.º 230/2009, as the work here presented is published in peer-reviewed scientific journals, or in preparation for publication, as following detailed.

First-Author Publications:

V. Nunes, D. Castro, M. Dantas, M. Piel, P. Aguiar, H. Maiato, J.G. Ferreira, A mechanical signal regulates Dynein on the nuclear envelope, *In preparation for submission.*

V. Nunes, J.G. Ferreira, From the cytoskeleton to the nucleus: An integrated view on early spindle assembly, Semin. Cell Dev. Biol. 117 (2021) 42–51. https://doi.org/10.1016/j.semcdb.2021.03.006.

V. Nunes, M. Dantas, J.T. Lima, J.G. Ferreira, High-Resolution Analysis of Centrosomes Behavior During Mitosis, in: A.S. Coutts, L. Weston (Eds.), Cell Cycle Oscil. Methods Protoc., Springer US, New York, NY, 2021: pp. 179–194. https://doi.org/10.1007/978-1-0716-1538-6_13.

V. Nunes, M. Dantas, D. Castro, E. Vitiello, I. Wang, N. Carpi, M. Balland, M. Piel, P. Aguiar, H. Maiato, J.G. Ferreira, Centrosome-nuclear axis repositioning drives the assembly of a bipolar spindle scaffold to ensure mitotic fidelity, Mol. Biol. Cell. (2020) mbc.E20-01-0047. https://doi.org/10.1091/mbc.E20-01-0047.

Additional Related Publication:

D. Castro, V. Nunes, J.T. Lima, J.G. Ferreira, P. Aguiar, Trackosome: a computational toolbox to study the spatiotemporal dynamics of centrosomes, nucleus and cellular membrane, J. Cell Sci. (2020). https://doi.org/10.1242/jcs.252254

Abstract

Mitosis is the cellular process by which the duplicated chromosomes are segregated between two identical daughter cells. Accurate chromosome segregation, which is a paramount for maintaining genome integrity, requires the assembly of a microtubule-based structure known as the mitotic spindle. To facilitate spindle assembly and chromosome segregation, the cell is extensively reorganized at the beginning of mitosis. At the nuclear level, the chromosomes condense, and the nuclear envelope (NE) is dismantled. At the cytoplasmic level, cells round up and change their microtubule network organization and dynamics. At this stage, centrosomes, the first microtubule-organizing centers (MTOCs) described, separate and move along the NE to originate the spindle poles. Previous studies have identified molecular and physical requirements for centrosomes separation and early spindle assembly. Yet, none was able to provide an integrated view of these activities nor a comprehensive description of the process.

To provide a spatiotemporal characterization of early mitotic spindle assembly, we used state-of-the-art microscopy and microfabrication techniques together with 3D cellular reconstruction. Firstly, we concluded that during prophase, both centrosomes and the nucleus reorient themselves so that centrosomes are positioned on the shortest nuclear axis at the time of nuclear envelope breakdown (NEB). We have also determined that centrosome motion, which is initially promoted by Kinesin-5 (Eg5 in humans), is then supported by Arp2/3-mediated regulation of microtubule dynamics. On the other hand, Dynein-generated forces on the NE control the reorientation of the nucleus. Interestingly, this nucleus-centrosomes configuration in prophase favors the establishment of an initial spindle scaffold that facilitates proper chromosome capture and segregation.

Secondly, we demonstrated that the nucleus mechanically regulates Dynein recruitment to the NE. We proposed that chromatin condensation-mediated forces are transmitted via the telomeres to SUN proteins at the NE. This mechanical load increases NE tension, which in turn, could produce conformational changes at the nuclear pore complexes (NPCs). We speculated that these changes likely allow the activation of the Dynein adaptors at the NPCs and consequently, loading of Dynein to the NE by mechanisms not yet understood. Since NE-associated Dynein is known to regulate both centrosome separation and NEB, we propose that chromosome condensation, together with CDK1 activity, ensures the coordination of nuclear and cytoplasmic events in the beginning of mitosis. Thus, we propose that mitotic entry is regulated by a combination of biochemical and mechanical pathways.

Resumo

A mitose é o processo celular através do qual os cromossomas duplicados são segregados entre as duas células filhas idênticas. A segregação precisa dos cromossomas, que é fundamental para manter a integridade do genoma, requer a montagem de uma estrutura baseada em microtúbulos conhecida como fuso mitótico. Para facilitar a montagem do fuso e a segregação cromossómica, a célula é extensivamente reorganizada no início da mitose. Ao nível nuclear, os cromossomas condensam e o invólucro nuclear é desmantelado. Ao nível citoplasmático, as células arredondam e mudam a organização e dinâmica da rede de microtúbulos. Nesta fase, os centrossomas, os primeiros centros organizadores de microtúbulos descritos, separam-se e movem-se ao longo do invólucro nuclear para originar os polos do fuso mitótico. Estudos anteriores identificaram os requisitos moleculares e biofísicos para a separação dos centrossomas e montagem inicial do fuso. No entanto, nenhum foi capaz de fornecer uma visão integrada dessas atividades, nem uma descrição abrangente do processo.

Para fornecer uma caracterização espacial- e temporal da montagem inicial do fuso mitótico, utilizamos técnicas de microscopia e microfabricação de última geração, juntamente com reconstrução celular em 3D. Primeiramente, concluímos que durante prófase, tanto os centrossomas como o núcleo se reorientam para que os centrossomas sejam posicionados no eixo nuclear mais curto no momento de ruptura do invólucro nuclear. Determinámos também que o movimento dos centrossomas, que é inicialmente promovido pela cinesina-5 (Eg5 em humanos), é depois suportado pela regulação dos microtúbulos mediada pela Arp2/3. Por outro lado, as forças geradas pela Dineína no invólucro nuclear controlam a reorientação do núcleo. Curiosamente, esta configuração dos centrossomas-núcleo em prófase favorece o estabelecimento de uma estrutura inicial do fuso que facilita a captura e segregação cromossómica adequada.

Em segundo lugar, demonstramos que o núcleo regula mecanicamente o recrutamento de Dineína para o invólucro nuclear. Propusemos que as forças mediadas pela condensação da cromatina são transmitidas através dos telómeros para as proteínas SUN no invólucro nuclear. Esta carga mecânica aumenta a tensão na membrana nuclear, o que por sua vez, deve produzir mudanças conformacionais nos complexos de poro nucleares (CPNs). Especulamos que estas alterações devem permitir a ativação dos adaptadores da Dineína nos CPNs, e, consequentemente, o carregamento de Dineína no invólucro nuclear por mecanismos ainda não compreendidos. Uma vez que a Dineína no invólucro nuclear é conhecida por regular tanto a separação dos centrossomas quanto a ruptura do invólucro nuclear, propomos que a condensação cromossómica, juntamente com a atividade da CDK1, assegura a coordenação dos eventos nucleares e

citoplasmáticos no início da mitose. Assim, propomos que a entrada mitótica é regulada por uma combinação de vias bioquímicas e mecânicas.

List of contents

ACKNOWLEDGEMENTS ..... **VII**

THESIS PUBLICATIONS ..... **IX**

ABSTRACT ..... **XI**

RESUMO ..... **XIII**

LIST OF CONTENTS ..... **XV**

THESIS OUTLINE ..... **XVII**

CHAPTER I **1**

FROM THE CYTOSKELETON TO THE NUCLEUS: AN INTEGRATED VIEW ON EARLY SPINDLE ASSEMBLY **1**

ABBREVIATIONS 2

1. ABSTRACT 3
2. GENERAL INTRODUCTION 3
3. MITOTIC CELL ROUNDING 4
4. MICROTUBULE NETWORK REMODELLING 6
5. PREPARING THE NUCLEUS FOR CHROMOSOME SEGREGATION 6
6. SYNCHRONIZING CYTOPLASMIC AND NUCLEAR EVENTS DURING MITOTIC ENTRY 10
7. EARLY SPINDLE ASSEMBLY 10
8. NUCLEAR MECHANICS MATTER DURING MITOTIC ENTRY 13
9. CONCLUDING REMARKS 15
10. REFERENCES 16

CHAPTER II **31**

CENTROSOME–NUCLEAR AXIS REPOSITIONING DRIVES THE ASSEMBLY OF A BIPOLAR SPINDLE SCAFFOLD TO ENSURE MITOTIC FIDELITY **31**

ABBREVIATIONS 32

1. ABSTRACT 33

2. INTRODUCTION....33
3. RESULTS....34
4. DISCUSSION....50
5. MATERIALS AND METHODS....52
6. REFERENCES....58
7. SUPPLEMENTARY FIGURES....65

CHAPTER III....71

A MECHANICAL SIGNAL REGULATES DYNEIN ON THE NUCLEAR ENVELOPE....71
ABBREVIATIONS....72
1. ABSTRACT....73
2. INTRODUCTION....73
3. RESULTS....75
4. DISCUSSION....91
5. MATERIALS AND METHODS....94
6. REFERENCES....101
7. SUPPLEMENTARY FIGURES....113

CHAPTER VI....119

GENERAL DISCUSSION....119
ABBREVIATIONS....120
1. ACCURATE MITOTIC SPINDLE ASSEMBLY: A PLACE FOR EVERYTHING, EVERYTHING IN ITS PLACE....121
2. THE NUCLEUS AS AN ACTIVE REGULATOR OF MITOTIC ENTRY....126
3. REFERENCES....133

ANNEX A....153

ANNEX B....171

Thesis Outline

The multidisciplinary project underlying this thesis aimed to determine how the physical and molecular factors that control centrosome separation and early spindle assembly in proliferating animal cells are regulated in space and time, in order to ensure mitotic fidelity and prevent aneuploidy onset.

Chapter I includes a general introduction that describes the global cellular reorganization that occurs during mitotic entry, time at which centrosomes separate and the mitotic spindle starts to assemble. This review thoroughly describes the main cytoskeletal and nuclear events that take place during the transition from G2 to mitosis (G2-M) and explores how their coordinated activity contributes to an efficient spindle assembly.

In Chapter II, the first research paper from this PhD project is presented. This manuscript addresses how nucleus and cell shape changes modulate centrosome positioning. In addition, it provides an integrated view on how cytoplasmic players interact to coordinate centrosome separation and early spindle assembly. Lastly, it determines how prophase centrosome positioning impacts mitotic timing and fidelity.

In Chapter III, I present a manuscript that is in preparation for submission. Here, we explore how nuclear mechanics and nucleus-associated components impact centrosome separation and early spindle assembly.

The thesis is concluded with Chapter IV, which includes a general discussion that weaves together the points raised in earlier chapters.

Finally, two additional published papers are annexed to this thesis. The first describes the methodology used in the two research papers presented. The last describes and thoroughly explores the custom MATLAB algorithms that were developed to extract and quantify our live-cell imaging datasets.

CHAPTER I

From the cytoskeleton to the nucleus: An integrated view on early spindle assembly

The content of this chapter is published in the following original review:

V. Nunes, J.G. Ferreira, From the cytoskeleton to the nucleus: An integrated view on early spindle assembly, Semin. Cell Dev. Biol. 117 (2021) 42–51. https://doi.org/10.1016/j.semcdb.2021.03.006.

This is an original review and is presented for the first time in a thesis.

Abbreviations

BicD2	Bicaudal D2
CDK1	Cyclin-Dependent Kinase 1
ER	Endoplasmic Reticulum
ERM	Ezrin/Radixin/Moesin
Faz	Focal Adhesions
INM	Inner Nuclear Membrane
LINC	Linker of Nucleoskeleton and Cytoskeleton
MAPs	Microtubule-Associated Proteins
MyoII	Myosin II
NE	Nuclear Envelope
NEB	Nuclear Envelope Breakdown
Neks	NIMA-related kinases
NPC	Nuclear Pore Complex
ONM	Outer Nuclear Membrane
PCM	Pericentriolar Material
PKC	Protein Kinase C
TCJs	Tricellular Junctions
TOPOII	Topoisomerase II
γ − TuRC	Gamma Tubulin Ring Complex

From the cytoskeleton to the nucleus: An integrated view on early spindle assembly

1. Abstract

Accurate chromosome segregation requires a complete restructuring of cellular organization. Microtubules remodel to assemble a mitotic spindle and the actin cytoskeleton rearranges to form a stiff actomyosin cortex. These cytoplasmic events must be spatially and temporally coordinated with mitotic chromosome condensation and nuclear envelope permeabilization, in order to ensure mitotic timing and fidelity. Here, we discuss the main cytoskeletal and nuclear events that occur during mitotic entry in proliferating animal cells, focusing on their coordinated contribution for early mitotic spindle assembly. We will also explore recent progress in understanding their regulatory biochemical and mechanical pathways.

Keywords: Mitosis, Spindle, Nucleus, Cytoskeleton, Centrosome, Mechanotransduction

2. General introduction

Accurate chromosome segregation requires the efficient assembly of a mitotic spindle. This process is facilitated by a global reorganization of cellular architecture that takes place during the transition from G2 to mitosis (G2-M; [1]). In most eukaryotic cells, this is easily recognizable as a “mitotic cell rounding” event, which occurs due to the transient loss of cellular adhesion [2,3] and cytoskeletal reshaping, contributing to centrosome separation [4] and actomyosin cortex assembly [5]. These cytoplasmic changes occur in tandem with modifications in nuclear organization and structure, such as nuclear pore complex (NPC) disassembly, nuclear lamina depolymerization and nuclear envelope (NE) permeabilization [6], that allow microtubules to capture chromosomes and assemble a mitotic spindle. Driving these changes in cellular architecture is a complex network of signaling cascades, orchestrated by an increase in cyclin-dependent kinase 1 (CDK1) activity [7], which coordinates cytoplasmic and nuclear events [8].

In this review, we focus on the changes in cytoskeletal and nuclear structure that occur during the G2-M transition in proliferating animal cells and discuss how their coordinated activity contributes to an efficient spindle assembly.

3. Mitotic cell rounding

During mitotic entry, almost all metazoan cells lose their flattened and spread morphology to become round. This phenomenon, known as ‘‘mitotic cell rounding”, occurs within a few minutes at the onset of mitosis and is regulated by CDK1 activity [9]. Mitotic rounding plays a key role in generating the necessary intracellular space to accommodate the mitotic spindle [10]. In addition, cell rounding limits the space that astral microtubules have to search for mitotic chromosomes and provides a symmetry that facilitates organelles partitioning [5]. This process involves focal adhesions (FAs) disassembly [3,11], cell margins retraction [11,12], cortical actomyosin assembly [13–17] and osmotic swelling [18,19] (Figure 1).

In interphase, cells are anchored to the extracellular matrix (ECM) by integrin-containing FA complexes. In the beginning of mitosis, FAs are dismantled due to Cyclin B1-CDK1 activity [9,20]. This allows cell margins to retract along beta1-integrin-containing retraction fibres [11,12]. These actin-rich fibers, that lack Myosin II (MyoII) and contain ezrin/radixin/moesin (ERM) proteins, sustain cell attachment to the ECM and support the forces generated by cell margin retraction [5,21]. Cells then remain poorly attached to the outside through retraction fibres [3,11] and reticular adhesions [22]. Overall, this results in a decrease in cell traction forces after FA loss, both in G2 [23,24] and prophase [25].

One significant event triggering cellular deadhesion is the inhibition of Rap1 activity [2]. In fact, in HeLa cells, constitutive activation of Rap1 (Rap1Q63E) blocks FAs disassembly and forces cells to sustain a flatter morphology throughout mitosis, leading to abnormal spindle morphologies [2,26]. Whether this is also required in other systems remains to be determined. Underscoring the importance of FA disassembly there is a hypothetical ‘de-adhesion checkpoint’ that surveys cellular de-adhesion to enable mitotic entry and timely cell cycle progression [20].

Cellular de-adhesion during early mitosis is accompanied by drastic changes in actin cytoskeleton organization. Actin filaments and non-muscle Myo II motors are recruited to the cell cortex to assemble a dense, thin [27] and stiff [14] actomyosin network that is connected to the overlying plasma membrane by ERM proteins [14,17,28]. RhoA, the RhoGEF Ect2 and members of the ERM family regulate this process. Following CDK1-mediated Ect2 translocation [16], RhoA is activated at the plasma membrane [12], culminating in actin filament nucleation [17] and activation of non-muscle Myo II [29] (Figure 1). The establishment of this rigid actomyosin network enables the cell to resist the external myosin-mediated, pushing and pulling forces and the internal spindle-mediated pushing forces on the plasma membrane, supporting the structural integrity of the cell throughout mitosis [12,14].

Entry into mitosis is accompanied by an increase in intracellular pressure [19], cell volume (>10% up to 30%) and cell height [18,30]. This mitotic "swelling" relies on the activity of ion transporters, such as the Na+/H+ exchanger NHE1. This transporter is activated by RhoA at the G2-M transition and allows cells to adjust their hydrostatic pressure in a timely manner [31,32]. As a consequence of mitotic swelling, there is a decrease in intracellular density, which is proposed to facilitate organelle and chromosome movement, as well as influence biochemical reactions due to cytoplasmic dilution [18]. In combination with the reorganization of the cortical actomyosin network, osmotic swelling contributes to the mechanical properties of the cell [33], by producing the internal forces required to overcome the pressures exerted by the external environment, enabling cell rounding [19].

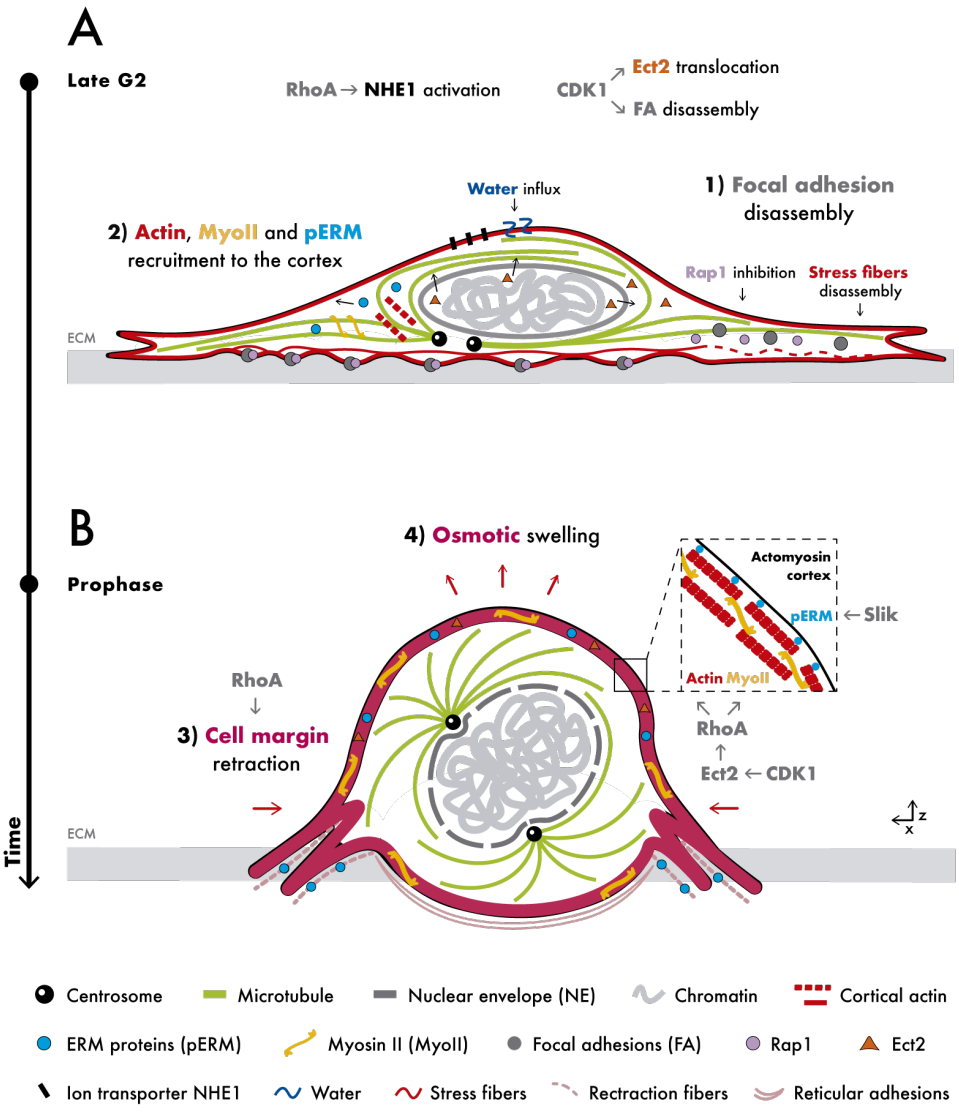


Figure 1: Schematic representation of the events driving cell rounding during late G2 **(A)** and prophase **(B)**. Increased Cyclin B1-CDK1 activity triggers FA disassembly and Ect2 translocation from the nucleus to the cytoplasm. Actin, myosin II and pERM are recruited to the cortex. Increased activity of NHE1 leads to water influx, which causes an increase in cellular volume. In parallel, the stable interphase microtubules are replaced by an array of short and unstable microtubules.

4. Microtubule network remodelling

During the G2-M transition, microtubules change their organization and dynamics to assemble the mitotic spindle. This relies mainly on an increase in centrosome-mediated microtubule nucleation [34] and a decrease in interphase microtubule stability [35] (Figure 1). Upon mitotic entry, the centrosomal microtubule nucleation activity is greatly enhanced due to the recruitment of gamma tubulin ring complex (γ − TuRC) and pericentriolar material (PCM) components, mediated by PLK1 and Aurora kinase A [36]. This allows centrosomes to form a radial array of microtubules and move along the NE [37], originating the spindle poles. Importantly, alterations in centrosome structure and function frequently result in chromosome segregation errors [38] and are often observed in cancer cells [39].

In addition to changes in microtubule organization, microtubules also change their dynamics during the G2-M transition. Accordingly, the extended array of long and stable interphase MTs is completely disassembled and replaced by short and very unstable microtubules [35,37,40]. This event relies on the activity of many microtubule-destabilizing factors such as Op18/stathmin and katanin [37], which increase microtubule catastrophe frequency [41], in combination with the inactivation of the microtubule stabilizer Ensconsin/MAP7 [35]. At the same time, microtubule-associated proteins (MAPs) promote microtubule polymerization, stabilization and bundling, required for spindle assembly [42].

5. Preparing the nucleus for chromosome segregation

As cells prepare to enter mitosis, an extensive reorganization of the nuclear interior and the NE accompanies the previously described cytoplasmic modifications. During mitotic entry, chromatin is reorganized into condensed chromosomes and subsequently exposed to the microtubules, to enable chromosome capture [43] (Figure 2). This requires permeabilization of the nucleus, in a process classically known as NE breakdown (NEB) [6] that gives rise to the characteristic “open mitosis” of higher eukaryotes.

5.1. Chromatin condensation

Entry into mitosis is accompanied by changes in the shape and degree of chromatin compaction. The process of chromosome condensation is reversible until NEB [44], point at which the cell is committed to divide and the rate of chromatin condensation significantly increases. Chromatin reorganization is essential for accurate capture and subsequent segregation of the individual chromosomes driven by the mitotic spindle [43]. This process involves several factors including histones, topoisomerase II (TOPOII), as well as condensin I and II complexes, which represent the major architectural constituents of mitotic chromosomes [43,45] (Figure 2). In mitosis, histone H3 phosphorylation of residue T3 by

Haspin kinase and of residues S10 and S28 by Aurora B kinase, are considered the driving factors for mitotic chromosome formation [46,47]. TOPOII also has a central role in chromatin condensation, since its inhibition partially blocks the process [48,49]. Still, given that impairment of TOPOII decatenation activity does not result in prominent condensation defects, additional factors are required for overall chromosome compaction [50]. In fact, all metazoans have two types of condensin complexes, condensins I and II, that regulate chromosomal organization in mitosis [43,45]. Condensin II is nuclear throughout the cell cycle and accumulates on chromosomes at the beginning of mitosis, supporting their condensation during early prophase. Condensin I, on the other hand, is cytoplasmic and binds to chromosomes only after NEB, a time at which chromosomes have already condensed to a significant degree [51,52]. In HeLa cells, the activity of condensin II is regulated by CDK1 [53] and PLK1 [54], whereas condensin I activity is regulated by Aurora B [55,56] and Aurora A [57]. Condensin depletion delays chromatin condensation [45,58]. Still, the mechanistic contribution of individual condensin complexes to the formation of mitotic chromosomes is not yet completely understood [43,59].

5.2. Restructuring of the Nuclear Envelope

The NE is a dynamic boundary between the nucleus and the cytoplasm. It is made up of two membranes, inner (INM) and outer nuclear membrane (ONM), containing dispersed NPCs, that enable selective movement of macromolecules between the nucleus and the cytoplasm. Underlying the INM is a dense protein meshwork termed nuclear lamina, composed mainly of lamins (A-type and B-type lamins) and lamin-associated proteins [60]. The nuclear lamina is known to sustain nuclear mechanics [61] and contribute to gene expression and chromatin regulation [62].

Underscoring NE plasticity, this structure is able to completely disassemble and reassemble during mitotic entry and exit, respectively [6]. The transition from prophase to prometaphase is defined by NE permeabilization, the key step to the irreversible commitment to mitotic entry [44], which comprises three coordinated events: the disassembly of NPCs, solubilization of the nuclear lamina and fenestration of the NE (Figure 2). Still, the molecular mechanisms driving NE disassembly remain incompletely understood [6,63]. NEB is tightly linked to signaling events controlling mitotic entry. It is triggered by the concerted action of multiple kinases, including CDK1, Aurora A, PLK1 and Protein Kinase C (PKC). These kinases phosphorylate and subsequently release soluble NUPs from NPCs, resulting in the loss of the nuclear permeability barrier and mixing of cytoplasmic and nuclear components. The disassembly of NPCs starts in late prophase [6,63], with the hyperphosphorylation of Nup98 by the combined action of Cyclin B1-CDK1, PLK1, and NIMA-related kinases (Neks) [64]. In fact, CDK1-mediated Nup phosphorylation regulates

overall NPC disassembly [65,66], since CDK1 inhibition impairs NE permeabilization. The subsequent steps in NPC disassembly and dispersal are still poorly understood. Still, the current perspective is that Nup98 phosphorylation and release triggers a synchronous disassembly of the remaining Nups [63,67]. This phosphorylation of Nups might also aid in specifying their later functions during spindle assembly and chromosome segregation [68]. Accordingly, the Nup107-160 complex [69], Nup98 [70] or Tpr [71] were shown to regulate spindle assembly efficiency. However, it is possible that the role of NPCs in this process is indirect, through the regulation of Spindle Assembly Checkpoint robustness [72]. Finally, defects in the kinetics of NE permeabilization impair accurate spindle assembly and chromosome segregation [73,74]. Therefore, the NE appears as a key player in the G2-M transition, either by directly regulating mitotic progression or by allowing timely access of microtubules to chromosomes.

Following NPC release, the nuclear lamina depolymerizes. Whereas A-type lamins are solubilized into the nucleoplasm, B-type lamins are removed to the endoplasmic reticulum (ER), following the change in NE permeability [75]. As result of lamin depolymerization, proteins of the NE detach from the nuclear lamina and chromatin, moving into the ER and allowing chromatin to be disengaged from the NE [6,63]. Both lamina disassembly and removal of proteins are under the regulation of CDK1 and PKC [1,76]. Permeabilization of the NE, with a consequent loss of the nucleo-cytoplasmic boundary, is completed during late prophase. At this point, NE membranes are reabsorbed by the ER, exposing chromatin to the spindle machinery. This process relies on dynein-mediated microtubule pulling forces, that lead to NE invaginations around the centrosomes and fenestration on the distal side of the nucleus [77,78], eventually leading to NE disruption and subsequent membrane removal from the chromatin [63]. Whether NE fenestration is a direct consequence of NPC removal or driven by microtubule-mediated mechanical stretching of the nuclear lamina is still unclear. Regardless, alternative pathways for NE permeabilization must exist, since the process still occurs in the absence of microtubules [77,78]. Indeed, it is conceivable that F-actin may act together with microtubules in promoting NEB, as was shown in meiosis [79], or that NE–chromosome interactions could also regulate NE disassembly by directing kinase activity, and providing spatial cues for NE disassembly [80].

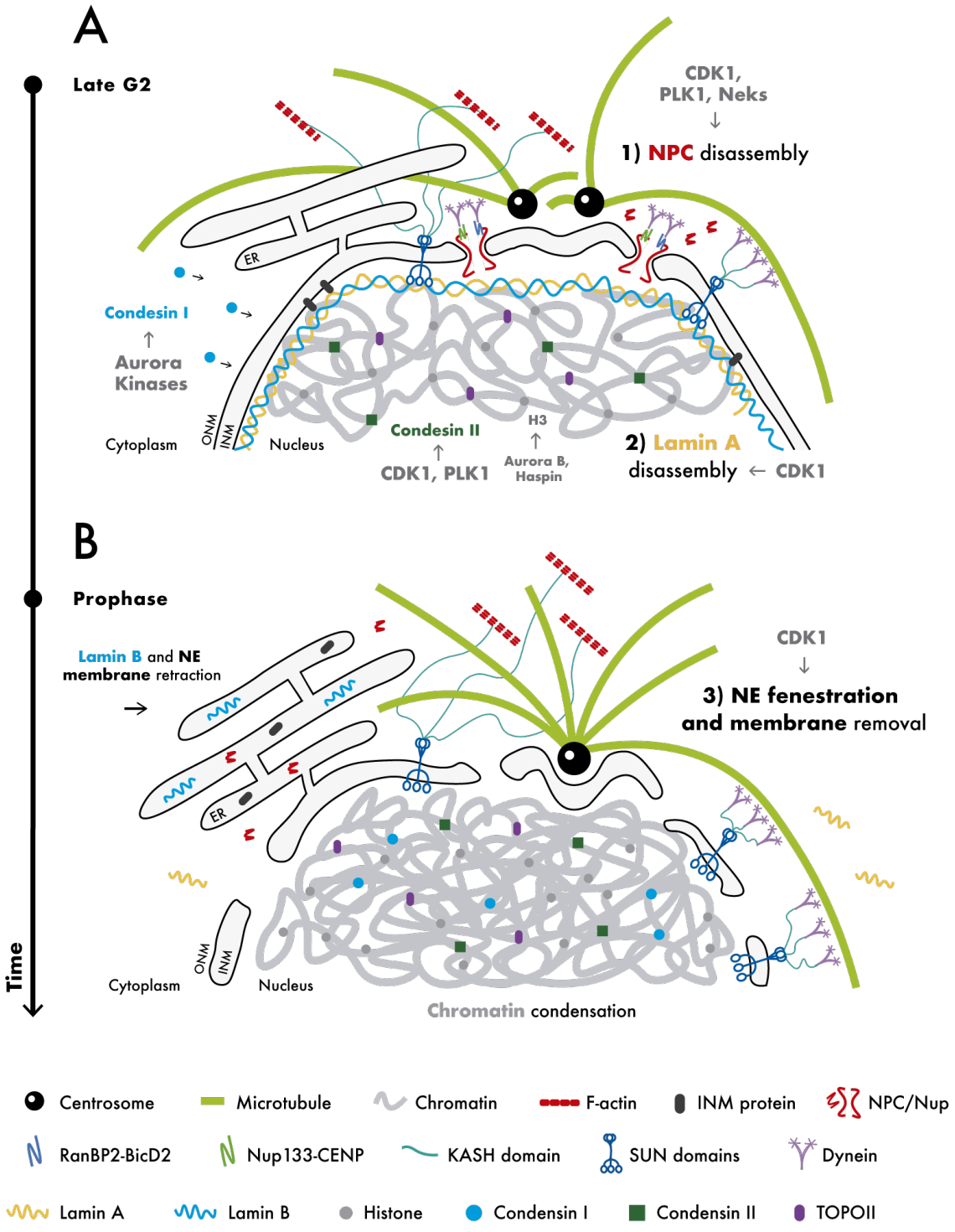


Figure 2: Schematic representation of the events driving NEB during late G2 **(A)** and prophase **(B)**. NEB is initially triggered by NPC disassembly. Concomitantly, nuclear lamina depolymerization is initiated with the solubilization of A-type lamins. Later, B-type lamins and INM proteins are removed to the ER, releasing chromatin from its interactions with the NE. Lastly, NE fenestration driven by dynein-mediated microtubule pulling leads to complete NE disintegration. Chromatin condensation accompanies NEB. Histones, TOPOII and condensin I and II complexes are recruited to chromatin and assist its reorganization into condensed chromosomes. It remains unclear how all these components functionally cooperate to drive chromatin condensation.

6. Synchronizing cytoplasmic and nuclear events during mitotic entry

The nuclear and cytoplasmic events that take place during mitotic entry need to be coordinated to ensure timely mitotic spindle assembly and ensure mitotic fidelity. All these morphological alterations are coupled to the cell cycle through the activity and localization of the Cyclin B1-CDK1 complex [7,8], that promotes the G2-M transition [81,82] and directly contributes to several structural changes required for mitotic entry, including centrosome separation [83], microtubule remodeling and disassembly of the nuclear lamina [63,65]. Cyclin B1-CDK1 activation is regulated by the Cdc25 phosphatase [84] and indirectly controlled by PLK1 and Aurora A kinases [85,86]. This likely starts at the centrosome, where Cyclin B1-CDK1, PLK1 and Cdc25C concentrate during late interphase [87,88]. Cyclin B1-CDK1 activation immediately triggers its rapid translocation into the nucleus, allowing synchronization of cytoplasmic and nuclear events at mitotic onset [8]. A similar role could also be played by PLK1, since its activity starts in the nucleus and subsequently increases in the cytoplasm before mitotic entry [89,90], thereby regulating mitotic onset [91] and assisting in centrosome maturation and spindle assembly [92,93]. Interestingly, in human cultured cells, imposing tension on the nucleus is sufficient to trigger nuclear accumulation of transcription factors such as YAP [94], AP1 and TEAD [95]. Whether Cyclin B1-CDK1 localization and activity are also dependent on mechanical forces remains an exciting line of research for the future.

7. Early Spindle Assembly

The mitotic spindle is a highly dynamic bipolar structure made up of microtubules and their associated motor and non-motor proteins [37]. Spindle assembly depends on two parallel mechanisms that ensure the robustness and coordination of the process. Accordingly, during the initial stages of mitosis, astral microtubules nucleated by the centrosome can eventually bind to kinetochores [96–98]. In alternative, kinetochores can attach to non-centrosomal microtubules that are nucleated in their vicinity [99–101]. These randomly oriented microtubules are then aligned with the spindle, likely through CENP-E activity [99].

During late G2, the duplicated centrosomes move along the NE to establish the two spindle poles. While centrosome separation was originally proposed to occur independently of NEB [102,103], recent works show that the two events are coordinated to ensure centrosome positioning on opposite sides of the nucleus [25,104]. Nonetheless, both insufficient centrosome separation or centrosomes mispositioning at NEB, can cause deviant spindle morphologies and increased chromosome missegregation events [102,105,106].

Orientation of the metaphase spindle depends on a combination of internal and external cues [107–112], through mechanisms that are not yet completely understood. Human cultured cells appear to rely on the distribution of retraction fibres, which reflect the interphase adhesion geometry [108,112], to activate cortical force generators that act on the microtubule network to orient the spindle [113,114]. However, there are alternative mechanisms. Accordingly, a cell-intrinsic signal generated by Ran-GTP determines spindle orientation by displacing cortical force generators from the vicinity of chromatin [111,115]. Importantly, this mechanism does not seem to require external cues [115]. Moreover, in epithelial tissues, tricellular junctions (TCJs) localize microtubule force generators to orient the spindle [107]. Importantly, before NEB, the mitotic cortex is still being assembled [17,116] and many of these cortical force generators are not yet in place [111,114]. Consequently, prophase and metaphase centrosome positioning are fundamentally different. In prophase, centrosomes do not align according to external cues. Instead, internal cues provided by the cytoskeleton and nucleus preferentially position the centrosomes on the shortest nuclear axis at NEB [25]. This particular centrosome configuration, together with the ring-like chromosome distribution, favors the exposure of kinetochores to microtubules and facilitates chromosome capture [25,104].

7.1. Mechanisms driving centrosome separation

Initial centrosome separation is driven by the combined action of molecular motors [4,117,118] together with actomyosin [119,120] and microtubules [121,122]. Nevertheless, there is growing evidence that nucleus-associated components such as the Linker of Nucleoskeleton and Cytoskeleton (LINC) complex [123,124] and nuclear lamina [125,126] are also involved in this process (Figure 3). However, how the forces generated by all these components are functionally coordinated to ensure efficient spindle assembly remains unclear.

The main driver of centrosome separation is the microtubule motor protein kinesin-5 (Eg5 in humans), which is recruited to the centrosomes in early prophase, following phosphorylation by CDK1, PLK1 [83,127] and Aurora A [128]. This centrosomal enrichment of Eg5 initiates the centrosome separation process [4,129], by crosslinking and sliding apart antiparallel microtubules [122,130]. Inhibition or depletion of Eg5, before centrosome separation, induces monopolar spindles in almost all tested organisms [129]. However, Eg5 inhibition after the spindle has assembled has little effect on bipolarity, suggesting its activity is essential only for initial centrosome separation [123].

In addition to Eg5, dynein is also required for centrosome separation. Dynein localizes to various subcellular compartments including microtubule plus-ends, the cell cortex and the NE [131]. Dynein assists in centrosome separation and positioning by generating pulling

forces on microtubules either towards the cortex [114] or along the NE [132]. These pulling forces will drive centrosome motion only when asymmetric interactions between centrosomes and the cell cortex/NE are established [122]. While cortical dynein is required to position the spindle in metaphase, NE-associated dynein seems to be the main driver of initial centrosome separation [123,133]. Dynein is specifically recruited to the NE in late G2, through multiple pathways that are under the regulation of CDK1 [134]. Firstly, RanBP2/ Nup358 recruits the adaptor protein Bicaudal D2 (BICD2), which promotes dynein recruitment [133]. Later on, CENP-F is recruited to the NE, where it interacts with Nup133 and recruits NudE/NudEL. These then tether dynein/dynactin to the Nup133 scaffold [132]. Both pathways act in tandem to promote dynein recruitment to NPCs. In parallel, the LINC complex also mediates dynein/dynactin recruitment to the NE [135,136]. This NE dynein pool is then able to tether centrosomes to the nucleus [132,133] and direct nuclear and centrosome movement [25,137].

Lastly, kinesin-14 motors (HSET, in human cells) also regulate centrosome separation and early spindle assembly by directly regulating microtubule nucleation and organization at the spindle poles [138]. Importantly, these minus-end directed motors such as kinesin-14 can counteract kinesin-5 activity by generating inward pulling forces on interpolar microtubule bundles [139], thereby regulating spindle length [140,141]. How these motor activities are spatiotemporally coordinated to ensure centrosome positioning on the shortest nuclear axis [25] remains to be determined.

7.2. Actomyosin and microtubule crosstalk promotes centrosome separation

The actin cytoskeleton also plays a key role in centrosome separation [25,119,142], spindle assembly [143,144] and chromosome positioning [145], through mechanisms not yet completely understood. Studies performed in *Drosophila* embryos and human cells suggest that, prior to NEB, centrosome separation relies on Arp2/3- and Formin-mediated actin turnover at the cortex, independently of myosin [119]. Contrarily, after NEB, MyoII-based cortical flows seem to be responsible for driving late centrosome separation [142]. While Arp2/3 activity seems dispensable from NEB to anaphase onset [5], Arp2/3-mediated F-actin networks were previously described during mitosis, surrounding the centrosome [25,146], the nucleus [124,145] or simply spanning the cell cortex [147] (Figure 3). These networks around the centrosome could act as a physical barrier, blocking microtubule growth and triggering their disassembly [146,148]. Remarkably, centrosomes can directly regulate Arp2/3 F-actin assembly through PCM1 and cell adhesion [149,150], suggesting that the centrosomal F-actin nucleation could be coordinated with mitotic entry. Accordingly, in early mitosis, centrosomal recruitment of PCM1 mediated by PLK1, coupled with low cell adhesion, allow the centrosomes to nucleate actin filaments and limit microtubule growth.

This might contribute to the microtubule reorganization observed during the G2-M transition [40] and assist in prophase centrosome positioning [25,124]. In certain cells types, an actin network surrounding the nucleus has also been involved in centrosome [124] or chromosome positioning [145]. These transient G2/prophase perinuclear actin structures were shown to interact with centrosomal microtubules to regulate centrosome positioning and separation before NEB. In combination with Myo-II-mediated contraction, this seems to facilitate initial chromosome–microtubule interaction [145]. Later, during prometaphase, cortical actin assists in centrosome separation and spindle positioning either by serving as an anchoring site for astral microtubules, providing mechanical resistance to microtubule-generated forces or through the recruitment of dynein to the cell cortex [15,119,151].

8. Nuclear mechanics matter during mitotic entry

During mitotic entry, both the NE and chromatin are extensively reorganized. How these nuclear changes directly impact early spindle assembly, remains poorly understood. Nevertheless, there is growing evidence to support an active role for the nucleus and nucleus-associated components in spindle assembly and chromosome segregation [124,136,152].

The nuclear lamina and chromatin are the main regulators of both nuclear shape and its mechanical response [153]. As cells transition from G2 to mitosis, chromatin condenses and the nuclear lamina disassembles, suggesting modifications in the mechanical properties of the nucleus. Indeed, despite the lack of measurements of nuclear mechanics at this stage, alterations in the pattern of NE fluctuations are indicative of these changes [154]. These NE fluctuations are actively driven by both chromatin and cytoskeleton [155], but their purpose is not yet clear. It is conceivable that such fluctuations might assist nuclear transport or diffusion flows, since it has been demonstrated that applying an oscillating field to a membrane increases the flux through nanopores [155,156]. If so, NE fluctuations during the G2-M transition could be important for assisting in the nucleo-cytoplasmic shuttling of key molecules such as Cyclin B1-CDK1 complexes, CENP-F or Ect2, ensuring the coordination between nuclear and cytoplasmic events.

In addition to the other nuclear components, the LINC complex is also involved in key processes during the G2-M transition. This complex plays a crucial role in force transmission across the NE [157,158] and is comprised of the SUN domain-containing proteins (SUN1-5), located on the INM that interact with lamins and chromatin, and KASH domain-containing proteins (nesprins-1–4, KASH5) located on the ONM that associate with various elements of the cytoskeleton [159]. Since the LINC complex physically links the nucleus and the cytoplasm, it is well positioned to mediate the interaction between the

centrosomes and nucleus [124,136,152]. Accordingly, actin-LINC complex disruption affects centrosome positioning and increases chromosome missegregation [124]. This is likely due to the LINC-mediated recruitment of dynein to the NE [74,123]. Moreover, co-depletion of SUN1 and SUN2 impairs NEB, leading to mitotic spindle defects [74]. Taken together, these observations suggest that nucleus-cytoskeleton coupling could play an important role in determining spindle assembly efficiency (Figure 3).

In the future, it would be interesting to perform a detailed characterization of the mechanical properties of the nucleus during the G2-M transition and its contribution for early spindle assembly.

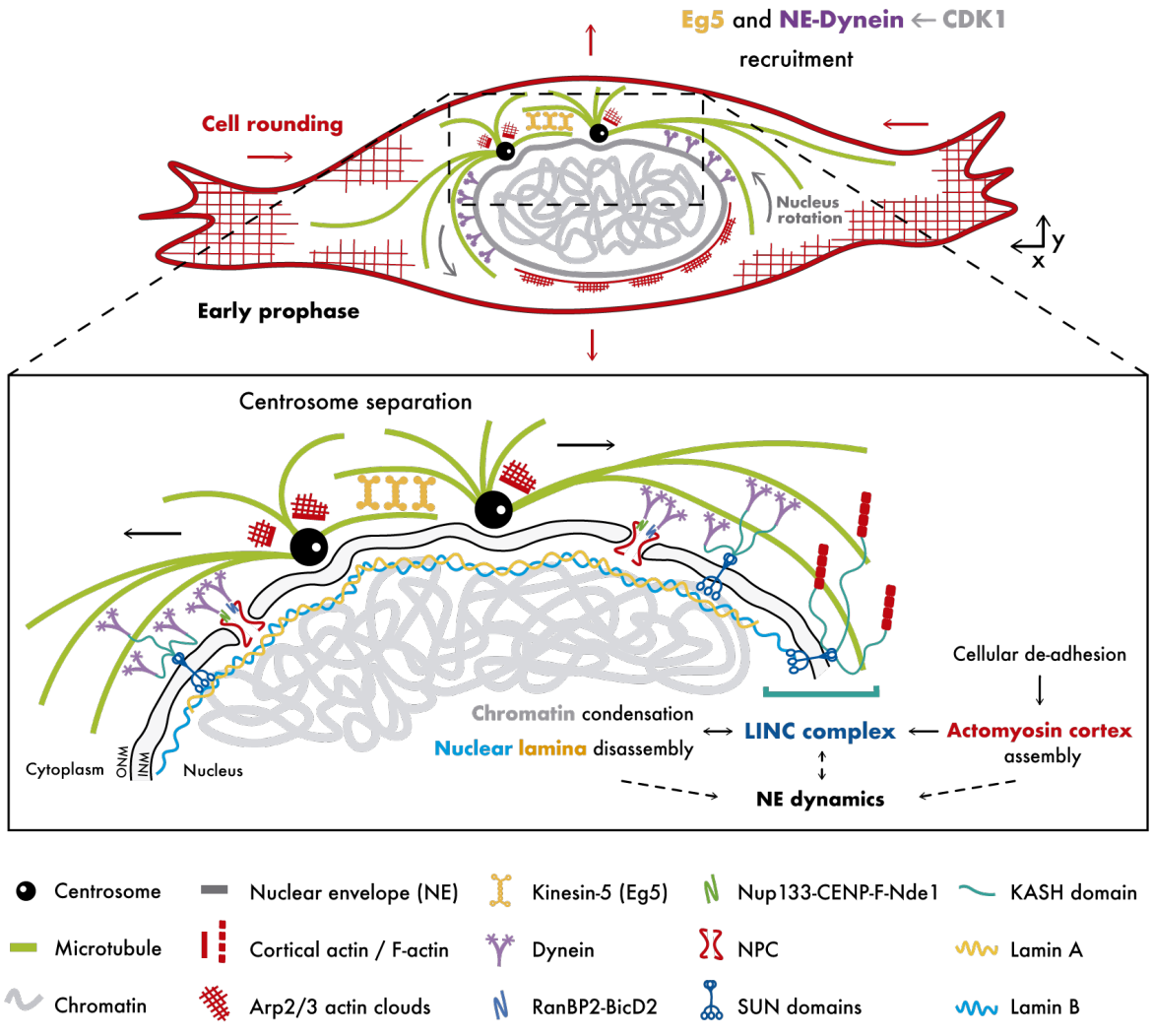


Figure 3: Mechanisms driving prophase centrosome separation. Centrosomes are separated by the combined action of Eg5 and NE-dynein, together with the actin and microtubule cytoskeletons. Dynein loading on the NE is primarily mediated by Nup binding. An additional mechanism driving NE dynein loading involves binding to the LINC complex, which mediates force transmission between the nucleus and the cytoskeleton.

9. Concluding remarks

Entry into mitosis involves an overall cellular reorganization that culminates in the assembly of the mitotic spindle. To assemble the spindle, centrosomes are separated during prophase by the combined action of the molecular motors, together with the actin and microtubule cytoskeletons. This mechanism is further aided by cell rounding, which generates sufficient space to accommodate the spindle. Remarkably, all these events are under the regulation of CDK1, which ensures cytoplasmic/nuclear coordination, timely NEB and efficient spindle assembly.

Notwithstanding the large amount of knowledge on the mechanisms of early spindle assembly, the role of nuclear mechanics and nuclear-associated components in this process is still poorly understood. An integrated view, that takes into account the contributions of the biochemical and mechanical pathways involved in the G2-M transition, could provide new insight on the regulation of spindle formation and its consequences for chromosome segregation. With the emergence of new tools that allow us to probe the mechanical properties of cells, combined with advanced imaging techniques and improved theoretical modelling, we expect to obtain a comprehensive description and understanding of this highly choreographed mechanism.

10. References

[1] L. Champion, M.I. Linder, U. Kutay, Cellular Reorganization during Mitotic Entry, Trends Cell Biol. 27 (2017) 26–41. https://doi.org/10.1016/j.tcb.2016.07.004.

[2] V.T. Dao, A.G. Dupuy, O. Gavet, E. Caron, J. de Gunzburg, Dynamic changes in Rap1 activity are required for cell retraction and spreading during mitosis, J. Cell Sci. 122 (2009) 2996–3004. https://doi.org/10.1242/jcs.041301.

[3] C.L. Dix, H.K. Matthews, M. Uroz, S. McLaren, L. Wolf, N. Heatley, Z. Win, P. Almada, R. Henriques, M. Boutros, X. Trepat, B. Baum, The Role of Mitotic Cell-Substrate Adhesion Re-modeling in Animal Cell Division, Dev. Cell. 45 (2018) 132-145.e3. https://doi.org/10.1016/j.devcel.2018.03.009.

[4] C.M. Whitehead, R.J. Winkfein, J.B. Rattner, The relationship of HsEg5 and the actin cytoskeleton to centrosome separation, Cell Motil. Cytoskeleton. 35 (1996) 298–308. https://doi.org/10.1002/(SICI)1097-0169(1996)35:4<298::AID-CM3>3.0.CO;2-3.

[5] N. Ramkumar, B. Baum, Coupling changes in cell shape to chromosome segregation, Nat. Rev. Mol. Cell Biol. 17 (2016) 511–521. https://doi.org/10.1038/nrm.2016.75.

[6] R. Ungricht, U. Kutay, Mechanisms and functions of nuclear envelope remodelling, Nat. Rev. Mol. Cell Biol. 18 (2017) 229–245. https://doi.org/10.1038/nrm.2016.153.

[7] O. Gavet, J. Pines, Progressive activation of CyclinB1-Cdk1 coordinates entry to mitosis, Dev. Cell. 18 (2010) 533–543. https://doi.org/10.1016/j.devcel.2010.02.013.

[8] O. Gavet, J. Pines, Activation of cyclin B1-Cdk1 synchronizes events in the nucleus and the cytoplasm at mitosis, J. Cell Biol. 189 (2010) 247–259. https://doi.org/10.1083/jcb.200909144.

[9] M.C. Jones, J.A. Askari, J.D. Humphries, M.J. Humphries, Cell adhesion is regulated by CDK1 during the cell cycle, J. Cell Biol. 217 (2018) 3203–3218. https://doi.org/10.1083/jcb.201802088.

[10] C. Cadart, E. Zlotek-Zlotkiewicz, M. Le Berre, M. Piel, H.K. Matthews, Exploring the function of cell shape and size during mitosis, Dev. Cell. 29 (2014) 159–169. https://doi.org/10.1016/j.devcel.2014.04.009.

[11] L.P. Cramer, T.J. Mitchison, Investigation of the mechanism of retraction of the cell margin and rearward flow of nodules during mitotic cell rounding, Mol. Biol. Cell. 8 (1997) 109–119. https://doi.org/10.1091/mbc.8.1.109.

[12] A.S. Maddox, K. Burridge, RhoA is required for cortical retraction and rigidity during mitotic cell rounding, J. Cell Biol. 160 (2003) 255–265. https://doi.org/10.1083/jcb.200207130.

[13] P. Chugh, E.K. Paluch, The actin cortex at a glance, J. Cell Sci. 131 (2018). https://doi.org/10.1242/jcs.186254.

[14] P. Kunda, A.E. Pelling, T. Liu, B. Baum, Moesin Controls Cortical Rigidity, Cell Rounding, and Spindle Morphogenesis during Mitosis, Curr. Biol. 18 (2008) 91–101. https://doi.org/10.1016/j.cub.2007.12.051.

[15] P. Kunda, B. Baum, The actin cytoskeleton in spindle assembly and positioning, Trends Cell Biol. 19 (2009) 174–179. https://doi.org/10.1016/j.tcb.2009.01.006.

[16] H.K. Matthews, U. Delabre, J.L. Rohn, J. Guck, P. Kunda, B. Baum, Changes in Ect2 Localization Couple Actomyosin-Dependent Cell Shape Changes to Mitotic Progression, Dev. Cell. 23 (2012) 371–383. https://doi.org/10.1016/j.devcel.2012.06.003.

[17] A. Rosa, E. Vlassaks, F. Pichaud, B. Baum, Ect2/Pbl Acts via Rho and Polarity Proteins to Direct the Assembly of an Isotropic Actomyosin Cortex upon Mitotic Entry, Dev. Cell. 32 (2015) 604–616. https://doi.org/10.1016/j.devcel.2015.01.012.

[18] E. Zlotek-Zlotkiewicz, S. Monnier, G. Cappello, M. Le Berre, M. Piel, Optical volume and mass measurements show that mammalian cells swell during mitosis, J. Cell Biol. 211 (2015) 765–774. https://doi.org/10.1083/jcb.201505056.

[19] M.P. Stewart, J. Helenius, Y. Toyoda, S.P. Ramanathan, D.J. Muller, A.A. Hyman, Hydrostatic pressure and the actomyosin cortex drive mitotic cell rounding, Nature. 469 (2011) 226–230. https://doi.org/10.1038/nature09642.

[20] S. Marchesi, F. Montani, G. Deflorian, R. D'Antuono, A. Cuomo, S. Bologna, C. Mazzoccoli, T. Bonaldi, P.P. Di Fiore, F. Nicassio, DEPDC1B coordinates de-adhesion events and cell-cycle progression at mitosis, Dev. Cell. 31 (2014) 420–433. https://doi.org/10.1016/j.devcel.2014.09.009.

[21] O.M. Lancaster, B. Baum, Shaping up to divide: coordinating actin and microtubule cytoskeletal remodelling during mitosis, Semin. Cell Dev. Biol. 34 (2014) 109–115. https://doi.org/10.1016/j.semcdb.2014.02.015.

[22] J.G. Lock, M.C. Jones, J.A. Askari, X. Gong, A. Oddone, H. Olofsson, S. Göransson, M. Lakadamyali, M.J. Humphries, S. Strömblad, Reticular adhesions are a distinct class of cell-matrix adhesions that mediate attachment during mitosis, Nat. Cell Biol. 20 (2018) 1290–1302. https://doi.org/10.1038/s41556-018-0220-2.

[23] M. Uroz, S. Wistorf, X. Serra-Picamal, V. Conte, M. Sales-Pardo, P. Roca-Cusachs, R. Guimerà, X. Trepat, Regulation of cell cycle progression by cell-cell and cell-matrix forces, Nat. Cell Biol. 20 (2018) 646–654. https://doi.org/10.1038/s41556-018-0107-2.

[24] B. Vianay, F. Senger, S. Alamos, M. Anjur-Dietrich, E. Bearce, B. Cheeseman, L. Lee, M. Théry, Variation in traction forces during cell cycle progression, Biol. Cell. 110 (2018) 91–96. https://doi.org/10.1111/boc.201800006.

[25] V. Nunes, M. Dantas, D. Castro, E. Vitiello, I. Wang, N. Carpi, M. Balland, M. Piel, P. Aguiar, H. Maiato, J.G. Ferreira, Centrosome-nuclear axis repositioning drives the assembly of a bipolar spindle scaffold to ensure mitotic fidelity, Mol. Biol. Cell. (2020) mbc.E20-01-0047. https://doi.org/10.1091/mbc.E20-01-0047.

[26] O.M. Lancaster, M. Le Berre, A. Dimitracopoulos, D. Bonazzi, E. Zlotek-Zlotkiewicz, R. Picone, T. Duke, M. Piel, B. Baum, Mitotic rounding alters cell geometry to ensure efficient bipolar spindle formation, Dev. Cell. 25 (2013) 270–283. https://doi.org/10.1016/j.devcel.2013.03.014.

[27] A.G. Clark, K. Dierkes, E.K. Paluch, Monitoring actin cortex thickness in live cells, Biophys. J. 105 (2013) 570–580. https://doi.org/10.1016/j.bpj.2013.05.057.

[28] S. Carreno, I. Kouranti, E.S. Glusman, M.T. Fuller, A. Echard, F. Payre, Moesin and its activating kinase Slik are required for cortical stability and microtubule organization in mitotic cells, J. Cell Biol. 180 (2008) 739–746. https://doi.org/10.1083/jcb.200709161.

[29] N. Watanabe, T. Kato, A. Fujita, T. Ishizaki, S. Narumiya, Cooperation between mDia1 and ROCK in Rho-induced actin reorganization, Nat. Cell Biol. 1 (1999) 136–143. https://doi.org/10.1038/11056.

[30] C. Cadart, S. Monnier, J. Grilli, P.J. Sáez, N. Srivastava, R. Attia, E. Terriac, B. Baum, M. Cosentino-Lagomarsino, M. Piel, Size control in mammalian cells involves modulation of both growth rate and cell cycle duration, Nat. Commun. 9 (2018) 3275. https://doi.org/10.1038/s41467-018-05393-0.

[31] L.K. Putney, D.L. Barber, Na-H Exchange-dependent Increase in Intracellular pH Times G2/M Entry and Transition*, J. Biol. Chem. 278 (2003) 44645–44649. https://doi.org/10.1074/jbc.M308099200.

[32] T. Tominaga, D.L. Barber, Na–H Exchange Acts Downstream of RhoA to Regulate Integrin-induced Cell Adhesion and Spreading, Mol. Biol. Cell. 9 (1998) 2287–2303. https://doi.org/10.1091/mbc.9.8.2287.

[33] A.V. Taubenberger, B. Baum, H.K. Matthews, The Mechanics of Mitotic Cell Rounding, Front. Cell Dev. Biol. 8 (2020). https://doi.org/10.3389/fcell.2020.00687.

[34] P. Meraldi, E.A. Nigg, The centrosome cycle, FEBS Lett. 521 (2002) 9–13. https://doi.org/10.1016/s0014-5793(02)02865-x.

[35] N. Mchedlishvili, H.K. Matthews, A. Corrigan, B. Baum, Two-step interphase microtubule disassembly aids spindle morphogenesis, BMC Biol. 16 (2018) 14. https://doi.org/10.1186/s12915-017-0478-z.

[36] P.T. Conduit, A. Wainman, J.W. Raff, Centrosome function and assembly in animal cells, Nat. Rev. Mol. Cell Biol. 16 (2015) 611–624. https://doi.org/10.1038/nrm4062.

[37] D.A. Compton, Spindle Assembly in Animal Cells, Annu. Rev. Biochem. 69 (2000) 95–114. https://doi.org/10.1146/annurev.biochem.69.1.95.

[38] B.D. Vitre, D.W. Cleveland, Centrosomes, chromosome instability (CIN) and aneuploidy, Curr. Opin. Cell Biol. 24 (2012) 809–815. https://doi.org/10.1016/j.ceb.2012.10.006.

[39] S.A. Godinho, R. Picone, M. Burute, R. Dagher, Y. Su, C.T. Leung, K. Polyak, J.S. Brugge, M. Thery, D. Pellman, Oncogene-like induction of cellular invasion from centrosome amplification, Nature. 510 (2014) 167–171. https://doi.org/10.1038/nature13277.

[40] Y. Zhai, P.J. Kronebusch, P.M. Simon, G.G. Borisy, Microtubule dynamics at the G2/M transition: abrupt breakdown of cytoplasmic microtubules at nuclear envelope breakdown and implications for spindle morphogenesis., J. Cell Biol. 135 (1996) 201–214. https://doi.org/10.1083/jcb.135.1.201.

[41] S.S.L. Andersen, Spindle assembly and the art of regulating microtubule dynamics by MAPs and Stathmin/Op18, Trends Cell Biol. 10 (2000) 261–267. https://doi.org/10.1016/S0962-8924(00)01786-4.

[42] J.G. Ferreira, A.L. Pereira, H. Maiato, Microtubule plus-end tracking proteins and their roles in cell division, Int. Rev. Cell Mol. Biol. 309 (2014) 59–140. https://doi.org/10.1016/B978-0-12-800255-1.00002-8.

[43] W. Antonin, H. Neumann, Chromosome condensation and decondensation during mitosis, Curr. Opin. Cell Biol. 40 (2016) 15–22. https://doi.org/10.1016/j.ceb.2016.01.013.

[44] C.L. Rieder, Mitosis in vertebrates: the G2/M and M/A transitions and their associated checkpoints, Chromosome Res. Int. J. Mol. Supramol. Evol. Asp. Chromosome Biol. 19 (2011) 291–306. https://doi.org/10.1007/s10577-010-9178-z.

[45] K. Kinoshita, T. Hirano, Dynamic organization of mitotic chromosomes, Curr. Opin. Cell Biol. 46 (2017) 46–53. https://doi.org/10.1016/j.ceb.2017.01.006.

[46] K.M. Johansen, J. Johansen, Regulation of chromatin structure by histone H3S10 phosphorylation, Chromosome Res. Int. J. Mol. Supramol. Evol. Asp. Chromosome Biol. 14 (2006) 393–404. https://doi.org/10.1007/s10577-006-1063-4.

[47] M. Kschonsak, C.H. Haering, Shaping mitotic chromosomes: From classical concepts to molecular mechanisms, Bioessays. 37 (2015) 755–766. https://doi.org/10.1002/bies.201500020.

[48] G.J. Gorbsky, Cell cycle progression and chromosome segregation in mammalian cells cultured in the presence of the topoisomerase II inhibitors ICRF-187 [(+)-1,2-bis(3,5-dioxopiperazinyl-1-yl)propane; ADR-529] and ICRF-159 (Razoxane), Cancer Res. 54 (1994) 1042–1048.

[49] K. Samejima, I. Samejima, P. Vagnarelli, H. Ogawa, G. Vargiu, D.A. Kelly, F. de Lima Alves, A. Kerr, L.C. Green, D.F. Hudson, S. Ohta, C.A. Cooke, C.J. Farr, J. Rappsilber, W.C. Earnshaw, Mitotic chromosomes are compacted laterally by KIF4 and condensin and axially by topoisomerase IIα, J. Cell Biol. 199 (2012) 755–770. https://doi.org/10.1083/jcb.201202155.

[50] P.R. Andreassen, F.B. Lacroix, R.L. Margolis, Chromosomes with two intact axial cores are induced by G2 checkpoint override: evidence that DNA decatenation is not required to template the chromosome structure, J. Cell Biol. 136 (1997) 29–43. https://doi.org/10.1083/jcb.136.1.29.

[51] T. Ono, Y. Fang, D.L. Spector, T. Hirano, Spatial and temporal regulation of Condensins I and II in mitotic chromosome assembly in human cells, Mol. Biol. Cell. 15 (2004) 3296–3308. https://doi.org/10.1091/mbc.e04-03-0242.

[52] L.C. Green, P. Kalitsis, T.M. Chang, M. Cipetic, J.H. Kim, O. Marshall, L. Turnbull, C.B. Whitchurch, P. Vagnarelli, K. Samejima, W.C. Earnshaw, K.H.A. Choo, D.F. Hudson, Contrasting roles of condensin I and condensin II in mitotic chromosome formation, J. Cell Sci. 125 (2012) 1591–1604. https://doi.org/10.1242/jcs.097790.

[53] S. Abe, K. Nagasaka, Y. Hirayama, H. Kozuka-Hata, M. Oyama, Y. Aoyagi, C. Obuse, T. Hirota, The initial phase of chromosome condensation requires Cdk1-mediated phosphorylation of the CAP-D3 subunit of condensin II, Genes Dev. 25 (2011) 863–874. https://doi.org/10.1101/gad.2016411.

[54] Y. Kagami, M. Ono, K. Yoshida, Plk1 phosphorylation of CAP-H2 triggers chromosome condensation by condensin II at the early phase of mitosis, Sci. Rep. 7 (2017) 5583. https://doi.org/10.1038/s41598-017-05986-7.

[55] J.J. Lipp, T. Hirota, I. Poser, J.-M. Peters, Aurora B controls the association of condensin I but not condensin II with mitotic chromosomes, J. Cell Sci. 120 (2007) 1245–1255. https://doi.org/10.1242/jcs.03425.

[56] K.S. Collette, E.L. Petty, N. Golenberg, J.N. Bembenek, G. Csankovszki, Different roles for Aurora B in condensin targeting during mitosis and meiosis, J. Cell Sci. 124 (2011) 3684–3694. https://doi.org/10.1242/jcs.088336.

[57] E. Poser, R. Caous, U. Gruneberg, F.A. Barr, Aurora A promotes chromosome congression by activating the condensin-dependent pool of KIF4A, J. Cell Biol. 219 (2019). https://doi.org/10.1083/jcb.201905194.

[58] D.F. Hudson, P. Vagnarelli, R. Gassmann, W.C. Earnshaw, Condensin is required for nonhistone protein assembly and structural integrity of vertebrate mitotic chromosomes, Dev. Cell. 5 (2003) 323–336. https://doi.org/10.1016/s1534-5807(03)00199-0.

[59] A.S. Belmont, Mitotic chromosome structure and condensation, Curr. Opin. Cell Biol. 18 (2006) 632–638. https://doi.org/10.1016/j.ceb.2006.09.007.

[60] P. De Magistris, W. Antonin, The Dynamic Nature of the Nuclear Envelope, Curr. Biol. CB. 28 (2018) R487–R497. https://doi.org/10.1016/j.cub.2018.01.073.

[61] R.P. Martins, J.D. Finan, F. Guilak, D.A. Lee, Mechanical regulation of nuclear structure and function, Annu. Rev. Biomed. Eng. 14 (2012) 431–455. https://doi.org/10.1146/annurev-bioeng-071910-124638.

[62] J. Kind, B. van Steensel, Genome-nuclear lamina interactions and gene regulation, Curr. Opin. Cell Biol. 22 (2010) 320–325. https://doi.org/10.1016/j.ceb.2010.04.002.

[63] S. Güttinger, E. Laurell, U. Kutay, Orchestrating nuclear envelope disassembly and reassembly during mitosis, Nat. Rev. Mol. Cell Biol. 10 (2009) 178–191. https://doi.org/10.1038/nrm2641.

[64] E. Laurell, K. Beck, K. Krupina, G. Theerthagiri, B. Bodenmiller, P. Horvath, R. Aebersold, W. Antonin, U. Kutay, Phosphorylation of Nup98 by Multiple Kinases Is Crucial for NPC Disassembly during Mitotic Entry, Cell. 144 (2011) 539–550. https://doi.org/10.1016/j.cell.2011.01.012.

[65] M.I. Linder, M. Köhler, P. Boersema, M. Weberruss, C. Wandke, J. Marino, C. Ashiono, P. Picotti, W. Antonin, U. Kutay, Mitotic Disassembly of Nuclear Pore Complexes Involves CDK1- and PLK1-Mediated Phosphorylation of Key Interconnecting Nucleoporins, Dev. Cell. 43 (2017) 141-156.e7. https://doi.org/10.1016/j.devcel.2017.08.020.

[66] C. Macaulay, E. Meier, D.J. Forbes, Differential mitotic phosphorylation of proteins of the nuclear pore complex, J. Biol. Chem. 270 (1995) 254–262. https://doi.org/10.1074/jbc.270.1.254.

[67] E. Dultz, E. Zanin, C. Wurzenberger, M. Braun, G. Rabut, L. Sironi, J. Ellenberg, Systematic kinetic analysis of mitotic dis- and reassembly of the nuclear pore in living cells, J. Cell Biol. 180 (2008) 857–865. https://doi.org/10.1083/jcb.200707026.

[68] A. Ibarra, M.W. Hetzer, Nuclear pore proteins and the control of genome functions, Genes Dev. 29 (2015) 337–349. https://doi.org/10.1101/gad.256495.114.

[69] A.V. Orjalo, A. Arnaoutov, Z. Shen, Y. Boyarchuk, S.G. Zeitlin, B. Fontoura, S. Briggs, M. Dasso, D.J. Forbes, The Nup107-160 nucleoporin complex is required for correct bipolar spindle assembly, Mol. Biol. Cell. 17 (2006) 3806–3818. https://doi.org/10.1091/mbc.e05-11-1061.

[70] M.K. Cross, M.A. Powers, Nup98 regulates bipolar spindle assembly through association with microtubules and opposition of MCAK, Mol. Biol. Cell. 22 (2011) 661–672. https://doi.org/10.1091/mbc.E10-06-0478.

[71] N. Schweizer, C. Ferrás, D.M. Kern, E. Logarinho, I.M. Cheeseman, H. Maiato, Spindle assembly checkpoint robustness requires Tpr-mediated regulation of Mad1/Mad2 proteostasis, J. Cell Biol. 203 (2013) 883–893. https://doi.org/10.1083/jcb.201309076.

[72] V. Rodriguez-Bravo, J. Maciejowski, J. Corona, H.K. Buch, P. Collin, M.T. Kanemaki, J.V. Shah, P.V. Jallepalli, Nuclear pores protect genome integrity by assembling a premitotic and Mad1-dependent anaphase inhibitor, Cell. 156 (2014) 1017–1031. https://doi.org/10.1016/j.cell.2014.01.010.

[73] A. Fernández-Álvarez, C. Bez, E.T. O'Toole, M. Morphew, J.P. Cooper, Mitotic Nuclear Envelope Breakdown and Spindle Nucleation Are Controlled by Interphase Contacts between Centromeres and the Nuclear Envelope, Dev. Cell. 39 (2016) 544–559. https://doi.org/10.1016/j.devcel.2016.10.021.

[74] Y. Turgay, L. Champion, C. Balazs, M. Held, A. Toso, D.W. Gerlich, P. Meraldi, U. Kutay, SUN proteins facilitate the removal of membranes from chromatin during nuclear envelope breakdown, J. Cell Biol. 204 (2014) 1099–1109. https://doi.org/10.1083/jcb.201310116.

[75] S.D. Georgatos, A. Pyrpasopoulou, P.A. Theodoropoulos, Nuclear envelope breakdown in mammalian cells involves stepwise lamina disassembly and microtubule-drive deformation of the nuclear membrane, J. Cell Sci. 110 (Pt 17) (1997) 2129–2140.

[76] L.-C. Tseng, R.-H. Chen, Temporal control of nuclear envelope assembly by phosphorylation of lamin B receptor, Mol. Biol. Cell. 22 (2011) 3306–3317. https://doi.org/10.1091/mbc.E11-03-0199.

[77] D. Salina, K. Bodoor, D.M. Eckley, T.A. Schroer, J.B. Rattner, B. Burke, Cytoplasmic Dynein as a Facilitator of Nuclear Envelope Breakdown, Cell. 108 (2002) 97–107. https://doi.org/10.1016/S0092-8674(01)00628-6.

[78] J. Beaudouin, D. Gerlich, N. Daigle, R. Eils, J. Ellenberg, Nuclear Envelope Breakdown Proceeds by Microtubule-Induced Tearing of the Lamina, Cell. 108 (2002) 83–96. https://doi.org/10.1016/S0092-8674(01)00627-4.

[79] M. Mori, K. Somogyi, H. Kondo, N. Monnier, H.J. Falk, P. Machado, M. Bathe, F. Nédélec, P. Lénárt, An Arp2/3 Nucleated F-Actin Shell Fragments Nuclear Membranes at Nuclear Envelope Breakdown in Starfish Oocytes, Curr. Biol. 24 (2014) 1421–1428. https://doi.org/10.1016/j.cub.2014.05.019.

[80] A. Fernández-Álvarez, J.P. Cooper, Chromosomes Orchestrate Their Own Liberation: Nuclear Envelope Disassembly, Trends Cell Biol. 27 (2017) 255–265. https://doi.org/10.1016/j.tcb.2016.11.005.

[81] L.J. Holt, B.B. Tuch, J. Villén, A.D. Johnson, S.P. Gygi, D.O. Morgan, Global analysis of Cdk1 substrate phosphorylation sites provides insights into evolution, Science. 325 (2009) 1682–1686. https://doi.org/10.1126/science.1172867.

[82] J.A. Ubersax, E.L. Woodbury, P.N. Quang, M. Paraz, J.D. Blethrow, K. Shah, K.M. Shokat, D.O. Morgan, Targets of the cyclin-dependent kinase Cdk1, Nature. 425 (2003) 859–864. https://doi.org/10.1038/nature02062.

[83] E. Smith, N. Hégarat, C. Vesely, I. Roseboom, C. Larch, H. Streicher, K. Straatman, H. Flynn, M. Skehel, T. Hirota, R. Kuriyama, H. Hochegger, Differential control of Eg5-dependent centrosome separation by Plk1 and Cdk1, EMBO J. 30 (2011) 2233–2245. https://doi.org/10.1038/emboj.2011.120.

[84] A.W. Murray, Recycling the cell cycle: cyclins revisited, Cell. 116 (2004) 221–234. https://doi.org/10.1016/s0092-8674(03)01080-8.

[85] T. Hirota, N. Kunitoku, T. Sasayama, T. Marumoto, D. Zhang, M. Nitta, K. Hatakeyama, H. Saya, Aurora-A and an interacting activator, the LIM protein Ajuba, are required for mitotic commitment in human cells, Cell. 114 (2003) 585–598. https://doi.org/10.1016/s0092-8674(03)00642-1.

[86] P. Lénárt, M. Petronczki, M. Steegmaier, B. Di Fiore, J.J. Lipp, M. Hoffmann, W.J. Rettig, N. Kraut, J.-M. Peters, The small-molecule inhibitor BI 2536 reveals novel insights into mitotic roles of polo-like kinase 1, Curr. Biol. CB. 17 (2007) 304–315. https://doi.org/10.1016/j.cub.2006.12.046.

[87] J. Bonnet, P. Coopman, M.C. Morris, Characterization of centrosomal localization and dynamics of Cdc25C phosphatase in mitosis, Cell Cycle Georget. Tex. 7 (2008) 1991–1998. https://doi.org/10.4161/cc.7.13.6095.

[88] M. Jackman, C. Lindon, E.A. Nigg, J. Pines, Active cyclin B1-Cdk1 first appears on centrosomes in prophase, Nat. Cell Biol. 5 (2003) 143–148. https://doi.org/10.1038/ncb918.

[89] O. Afanzar, G.K. Buss, T. Stearns, J.E. Ferrell Jr, The nucleus serves as the pacemaker for the cell cycle, ELife. 9 (2020) e59989. https://doi.org/10.7554/eLife.59989.

[90] W. Bruinsma, M. Aprelia, J. Kool, L. Macurek, A. Lindqvist, R.H. Medema, Spatial Separation of Plk1 Phosphorylation and Activity, Front. Oncol. 5 (2015) 132. https://doi.org/10.3389/fonc.2015.00132.

[91] W. Bruinsma, J.A. Raaijmakers, R.H. Medema, Switching Polo-like kinase-1 on and off in time and space, Trends Biochem. Sci. 37 (2012) 534–542. https://doi.org/10.1016/j.tibs.2012.09.005.

[92] V. Archambault, D.M. Glover, Polo-like kinases: conservation and divergence in their functions and regulation, Nat. Rev. Mol. Cell Biol. 10 (2009) 265–275. https://doi.org/10.1038/nrm2653.

[93] S. Zitouni, C. Nabais, S.C. Jana, A. Guerrero, M. Bettencourt-Dias, Polo-like kinases: structural variations lead to multiple functions, Nat. Rev. Mol. Cell Biol. 15 (2014) 433–452. https://doi.org/10.1038/nrm3819.

[94] A. Elosegui-Artola, I. Andreu, A.E.M. Beedle, A. Lezamiz, M. Uroz, A.J. Kosmalska, R. Oria, J.Z. Kechagia, P. Rico-Lastres, A.-L.L. Roux, C.M. Shanahan, X. Trepat, D. Navajas, S. Garcia-Manyes, P. Roca-Cusachs, Force Triggers YAP Nuclear Entry by Regulating Transport across Nuclear Pores, Cell. 171 (2017) 1397-1410.e14. https://doi.org/10.1016/j.cell.2017.10.008.

[95] J. Aureille, V. Buffière-Ribot, B.E. Harvey, C. Boyault, L. Pernet, T. Andersen, G. Bacola, M. Balland, S. Fraboulet, L. Van Landeghem, C. Guilluy, Nuclear envelope deformation controls cell cycle progression in response to mechanical force, EMBO Rep. 20 (2019) e48084. https://doi.org/10.15252/embr.201948084.

[96] S.L. Prosser, L. Pelletier, Mitotic spindle assembly in animal cells: a fine balancing act, Nat. Rev. Mol. Cell Biol. 18 (2017) 187–201. https://doi.org/10.1038/nrm.2016.162.

[97] A. Khodjakov, C.L. Rieder, Centrosomes Enhance the Fidelity of Cytokinesis in Vertebrates and Are Required for Cell Cycle Progression, J. Cell Biol. 153 (2001) 237–242. https://doi.org/10.1083/jcb.153.1.237.

[98] S. Moutinho-Pereira, N. Stuurman, O. Afonso, M. Hornsveld, P. Aguiar, G. Goshima, R.D. Vale, H. Maiato, Genes involved in centrosome-independent mitotic spindle assembly in Drosophila S2 cells, Proc. Natl. Acad. Sci. 110 (2013) 19808. https://doi.org/10.1073/pnas.1320013110.

[99] V. Sikirzhytski, F. Renda, I. Tikhonenko, V. Magidson, B.F. McEwen, A. Khodjakov, Microtubules assemble near most kinetochores during early prometaphase in human cells, J. Cell Biol. 217 (2018) 2647–2659. https://doi.org/10.1083/jcb.201710094.

[100] A. Khodjakov, L. Copenagle, M.B. Gordon, D.A. Compton, T.M. Kapoor, Minus-end capture of preformed kinetochore fibers contributes to spindle morphogenesis, J. Cell Biol. 160 (2003) 671–683. https://doi.org/10.1083/jcb.200208143.

[101] H. Maiato, C.L. Rieder, A. Khodjakov, Kinetochore-driven formation of kinetochore fibers contributes to spindle assembly during animal mitosis, J. Cell Biol. 167 (2004) 831–840. https://doi.org/10.1083/jcb.200407090.

[102] K. Kaseda, A.D. McAinsh, R.A. Cross, Dual pathway spindle assembly increases both the speed and the fidelity of mitosis, Biol. Open. 1 (2012) 12–18. https://doi.org/10.1242/bio.2011012.

[103] J.B. Rattner, M.W. Berns, Centriole behavior in early mitosis of rat kangaroo cells (PTK2)., Chromosoma. 54 (1976) 387–395. https://doi.org/10.1007/bf00292817.

[104] V. Magidson, C.B. O'Connell, J. Lončarek, R. Paul, A. Mogilner, A. Khodjakov, The Spatial Arrangement of Chromosomes during Prometaphase Facilitates Spindle Assembly, Cell. 146 (2011) 555–567. https://doi.org/10.1016/j.cell.2011.07.012.

[105] H.-J. Nam, R. Naylor, J.M. van Deursen, Centrosome dynamics as a source of chromosomal instability, Trends Cell Biol. 25 (2015) 65–73. https://doi.org/10.1016/j.tcb.2014.10.002.

[106] W.T. Silkworth, I.K. Nardi, R. Paul, A. Mogilner, D. Cimini, Timing of centrosome separation is important for accurate chromosome segregation, Mol. Biol. Cell. 23 (2011) 401–411. https://doi.org/10.1091/mbc.e11-02-0095.

[107] F. Bosveld, O. Markova, B. Guirao, C. Martin, Z. Wang, A. Pierre, M. Balakireva, I. Gaugue, A. Ainslie, N. Christophorou, D.K. Lubensky, N. Minc, Y. Bellaïche, Epithelial tricellular junctions act as interphase cell shape sensors to orient mitosis, Nature. 530 (2016) 495–498. https://doi.org/10.1038/nature16970.

[108] J. Fink, N. Carpi, T. Betz, A. Bétard, M. Chebah, A. Azioune, M. Bornens, C. Sykes, L. Fetler, D. Cuvelier, M. Piel, External forces control mitotic spindle positioning, Nat. Cell Biol. 13 (2011) 771–778. https://doi.org/10.1038/ncb2269.

[109] S.W. Grill, J. Howard, E. Schäffer, E.H.K. Stelzer, A.A. Hyman, The Distribution of Active Force Generators Controls Mitotic Spindle Position, Science. 301 (2003) 518–521. https://doi.org/10.1126/science.1086560.

[110] O. Hertwig, Das Problem der Befruchtung und der Isotropie des Eies: eine Theorie der Vererbung, Fischer, 1884.

[111] T. Kiyomitsu, I.M. Cheeseman, Chromosome- and spindle-pole-derived signals generate an intrinsic code for spindle position and orientation, Nat. Cell Biol. 14 (2012) 311–317. https://doi.org/10.1038/ncb2440.

[112] M. Théry, V. Racine, A. Pépin, M. Piel, Y. Chen, J.-B. Sibarita, M. Bornens, The extracellular matrix guides the orientation of the cell division axis, Nat. Cell Biol. 7 (2005) 947–953. https://doi.org/10.1038/ncb1307.

[113] S.W. Grill, A.A. Hyman, Spindle Positioning by Cortical Pulling Forces, Dev. Cell. 8 (2005) 461–465. https://doi.org/10.1016/j.devcel.2005.03.014.

[114] S. Kotak, C. Busso, P. Gönczy, Cortical dynein is critical for proper spindle positioning in human cells, J. Cell Biol. 199 (2012) 97–110. https://doi.org/10.1083/jcb.201203166.

[115] A. Dimitracopoulos, P. Srivastava, A. Chaigne, Z. Win, R. Shlomovitz, O.M. Lancaster, M. Le Berre, M. Piel, K. Franze, G. Salbreux, B. Baum, Mechanochemical Crosstalk Produces Cell-Intrinsic Patterning of the Cortex to Orient the Mitotic

Spindle, Curr. Biol. CB. 30 (2020) 3687-3696.e4. https://doi.org/10.1016/j.cub.2020.06.098.

[116] S.P. Ramanathan, J. Helenius, M.P. Stewart, C.J. Cattin, A.A. Hyman, D.J. Muller, Cdk1-dependent mitotic enrichment of cortical myosin II promotes cell rounding against confinement, Nat. Cell Biol. 17 (2015) 148–159. https://doi.org/10.1038/ncb3098.

[117] A. De Simone, F. Nédélec, P. Gönczy, Dynein Transmits Polarized Actomyosin Cortical Flows to Promote Centrosome Separation, Cell Rep. 14 (2016) 2250–2262. https://doi.org/10.1016/j.celrep.2016.01.077.

[118] J.A. Raaijmakers, R.G.H.P. van Heesbeen, J.L. Meaders, E.F. Geers, B. Fernandez-Garcia, R.H. Medema, M.E. Tanenbaum, Nuclear envelope-associated dynein drives prophase centrosome separation and enables Eg5-independent bipolar spindle formation, EMBO J. 31 (2012) 4179–4190. https://doi.org/10.1038/emboj.2012.272.

[119] J. Cao, J. Crest, B. Fasulo, W. Sullivan, Cortical Actin Dynamics Facilitate Early-Stage Centrosome Separation, Curr. Biol. 20 (2010) 770–776. https://doi.org/10.1016/j.cub.2010.02.060.

[120] R. Uzbekov, I. Kireyev, C. Prigent, Centrosome separation: respective role of microtubules and actin filaments, Biol. Cell. 94 (2002) 275–288. https://doi.org/10.1016/S0248-4900(02)01202-9.

[121] E.N. Cytrynbaum, J.M. Scholey, A. Mogilner, A Force Balance Model of Early Spindle Pole Separation in Drosophila Embryos, Biophys. J. 84 (2003) 757–769. https://doi.org/10.1016/S0006-3495(03)74895-4.

[122] M.E. Tanenbaum, R.H. Medema, Mechanisms of centrosome separation and bipolar spindle assembly, Dev. Cell. 19 (2010) 797–806. https://doi.org/10.1016/j.devcel.2010.11.011.

[123] V. Nunes, M. Dantas, E. Vitiello, I. Wang, N. Carpi, M. Balland, M. Piel, P. Aguiar, H. Maiato, J.G. Ferreira, Spatial Asymmetries of the Prophase Nucleus Regulate Dynein Recruitment to Ensure Mitotic Fidelity, BioRxiv. (2019) 526939. https://doi.org/10.1101/526939.

[124] T. Stiff, F.R. Echegaray-Iturra, H.J. Pink, A. Herbert, C.C. Reyes-Aldasoro, H. Hochegger, Prophase-Specific Perinuclear Actin Coordinates Centrosome Separation and Positioning to Ensure Accurate Chromosome Segregation, Cell Rep. 31 (2020) 107681. https://doi.org/10.1016/j.celrep.2020.107681.

[125] T. Dechat, T. Shimi, S.A. Adam, A.E. Rusinol, D.A. Andres, H.P. Spielmann, M.S. Sinensky, R.D. Goldman, Alterations in mitosis and cell cycle progression caused by a mutant lamin A known to accelerate human aging, Proc. Natl. Acad. Sci. 104 (2007) 4955–4960. https://doi.org/10.1073/pnas.0700854104.

[126] R. Qi, N. Xu, G. Wang, H. Ren, S. Li, J. Lei, Q. Lin, L. Wang, X. Gu, H. Zhang, Q. Jiang, C. Zhang, The lamin-A/C-LAP2α-BAF1 protein complex regulates mitotic spindle assembly and positioning, J. Cell Sci. 128 (2015) 2830–2841. https://doi.org/10.1242/jcs.164566.

[127] M.T. Bertran, S. Sdelci, L. Regué, J. Avruch, C. Caelles, J. Roig, Nek9 is a Plk1-activated kinase that controls early centrosome separation through Nek6/7 and Eg5, EMBO J. 30 (2011) 2634–2647. https://doi.org/10.1038/emboj.2011.179.

[128] R. Giet, R. Uzbekov, F. Cubizolles, K. Le Guellec, C. Prigent, The Xenopus laevis aurora-related protein kinase pEg2 associates with and phosphorylates the kinesin-related protein XlEg5, J. Biol. Chem. 274 (1999) 15005–15013. https://doi.org/10.1074/jbc.274.21.15005.

[129] N.P. Ferenz, A. Gable, P. Wadsworth, Mitotic functions of kinesin-5, Semin. Cell Dev. Biol. 21 (2010) 255–259. https://doi.org/10.1016/j.semcdb.2010.01.019.

[130] L.C. Kapitein, E.J.G. Peterman, B.H. Kwok, J.H. Kim, T.M. Kapoor, C.F. Schmidt, The bipolar mitotic kinesin Eg5 moves on both microtubules that it crosslinks, Nature. 435 (2005) 114–118. https://doi.org/10.1038/nature03503.

[131] J.R. Kardon, R.D. Vale, Regulators of the cytoplasmic dynein motor, Nat. Rev. Mol. Cell Biol. 10 (2009) 854–865. https://doi.org/10.1038/nrm2804.

[132] S. Bolhy, I. Bouhlel, E. Dultz, T. Nayak, M. Zuccolo, X. Gatti, R. Vallee, J. Ellenberg, V. Doye, A Nup133-dependent NPC-anchored network tethers centrosomes to the nuclear envelope in prophase, J. Cell Biol. 192 (2011) 855–871. https://doi.org/10.1083/jcb.201007118.

[133] D. Splinter, M.E. Tanenbaum, A. Lindqvist, D. Jaarsma, A. Flotho, K.L. Yu, I. Grigoriev, D. Engelsma, E.D. Haasdijk, N. Keijzer, J. Demmers, M. Fornerod, F. Melchior, C.C. Hoogenraad, R.H. Medema, A. Akhmanova, Bicaudal D2, dynein, and kinesin-1 associate with nuclear pore complexes and regulate centrosome and nuclear positioning during mitotic entry, PLoS Biol. 8 (2010) e1000350. https://doi.org/10.1371/journal.pbio.1000350.

[134] A.D. Baffet, D.J. Hu, R.B. Vallee, Cdk1 Activates Pre-mitotic Nuclear Envelope Dynein Recruitment and Apical Nuclear Migration in Neural Stem Cells, Dev. Cell. 33 (2015) 703–716. https://doi.org/10.1016/j.devcel.2015.04.022.

[135] H.N. Fridolfsson, N. Ly, M. Meyerzon, D.A. Starr, UNC-83 coordinates kinesin-1 and dynein activities at the nuclear envelope during nuclear migration, Dev. Biol. 338 (2010) 237–250. https://doi.org/10.1016/j.ydbio.2009.12.004.

[136] X. Zhang, K. Lei, X. Yuan, X. Wu, Y. Zhuang, T. Xu, R. Xu, M. Han, SUN1/2 and Syne/Nesprin-1/2 complexes connect centrosome to the nucleus during

neurogenesis and neuronal migration in mice, Neuron. 64 (2009) 173–187. https://doi.org/10.1016/j.neuron.2009.08.018.

[137] J. Wu, K.C. Lee, R.B. Dickinson, T.P. Lele, How dynein and microtubules rotate the nucleus, J. Cell. Physiol. 226 (2011) 2666–2674. https://doi.org/10.1002/jcp.22616.

[138] Z.-Y. She, W.-X. Yang, Molecular mechanisms of kinesin-14 motors in spindle assembly and chromosome segregation, J. Cell Sci. 130 (2017) 2097–2110. https://doi.org/10.1242/jcs.200261.

[139] N. Pavin, I.M. Tolić, Self-Organization and Forces in the Mitotic Spindle, Annu. Rev. Biophys. 45 (2016) 279–298. https://doi.org/10.1146/annurev-biophys-062215-010934.

[140] S. Cai, L.N. Weaver, S.C. Ems-McClung, C.E. Walczak, Kinesin-14 Family Proteins HSET/XCTK2 Control Spindle Length by Cross-Linking and Sliding Microtubules, Mol. Biol. Cell. 20 (2008) 1348–1359. https://doi.org/10.1091/mbc.e08-09-0971.

[141] G. Goshima, J.M. Scholey, Control of Mitotic Spindle Length, Annu. Rev. Cell Dev. Biol. 26 (2010) 21–57. https://doi.org/10.1146/annurev-cellbio-100109-104006.

[142] J. Rosenblatt, L.P. Cramer, B. Baum, K.M. McGee, Myosin II-dependent cortical movement is required for centrosome separation and positioning during mitotic spindle assembly, Cell. 117 (2004) 361–372. https://doi.org/10.1016/s0092-8674(04)00341-1.

[143] P.-C. Chan, R.Y.C. Hsu, C.-W. Liu, C.-C. Lai, H.-C. Chen, Adducin-1 is essential for mitotic spindle assembly through its interaction with myosin-X, J. Cell Biol. 204 (2013) 19–28. https://doi.org/10.1083/jcb.201306083.

[144] M. Plessner, J. Knerr, R. Grosse, Centrosomal Actin Assembly Is Required for Proper Mitotic Spindle Formation and Chromosome Congression, IScience. 15 (2019) 274–281. https://doi.org/10.1016/j.isci.2019.04.022.

[145] A.J. Booth, Z. Yue, J.K. Eykelenboom, T. Stiff, G.G. Luxton, H. Hochegger, T.U. Tanaka, Contractile acto-myosin network on nuclear envelope remnants positions human chromosomes for mitosis, ELife. 8 (2019) e46902. https://doi.org/10.7554/eLife.46902.

[146] D. Inoue, D. Obino, J. Pineau, F. Farina, J. Gaillard, C. Guerin, L. Blanchoin, A.-M. Lennon-Duménil, M. Théry, Actin filaments regulate microtubule growth at the centrosome, EMBO J. 38 (2019) e99630. https://doi.org/10.15252/embj.201899630.

[147] M. Mitsushima, K. Aoki, M. Ebisuya, S. Matsumura, T. Yamamoto, M. Matsuda, F. Toyoshima, E. Nishida, Revolving movement of a dynamic cluster of actin filaments during mitosis, J. Cell Biol. 191 (2010) 453–462. https://doi.org/10.1083/jcb.201007136.

[148] A. Colin, P. Singaravelu, M. Théry, L. Blanchoin, Z. Gueroui, Actin-Network Architecture Regulates Microtubule Dynamics, Curr. Biol. 28 (2018) 2647-2656.e4. https://doi.org/10.1016/j.cub.2018.06.028.

[149] F. Farina, J. Gaillard, C. Guérin, Y. Couté, J. Sillibourne, L. Blanchoin, M. Théry, The centrosome is an actin-organizing centre, Nat. Cell Biol. 18 (2016) 65–75. https://doi.org/10.1038/ncb3285.

[150] D. Obino, F. Farina, O. Malbec, P.J. Sáez, M. Maurin, J. Gaillard, F. Dingli, D. Loew, A. Gautreau, M.-I. Yuseff, L. Blanchoin, M. Théry, A.-M. Lennon-Duménil, Actin nucleation at the centrosome controls lymphocyte polarity, Nat. Commun. 7 (2016) 10969. https://doi.org/10.1038/ncomms10969.

[151] H. Tuncay, B.F. Brinkmann, T. Steinbacher, A. Schürmann, V. Gerke, S. Iden, K. Ebnet, JAM-A regulates cortical dynein localization through Cdc42 to control planar spindle orientation during mitosis, Nat. Commun. 6 (2015) 8128. https://doi.org/10.1038/ncomms9128.

[152] I. Minn, M.M. Rolls, W. Hanna-Rose, C.J. Malone, SUN-1 and ZYG-12, Mediators of Centrosome–Nucleus Attachment, Are a Functional SUN/KASH Pair in Caenorhabditis elegans, Mol. Biol. Cell. 20 (2009) 4586–4595. https://doi.org/10.1091/mbc.e08-10-1034.

[153] A.D. Stephens, E.J. Banigan, S.A. Adam, R.D. Goldman, J.F. Marko, Chromatin and lamin A determine two different mechanical response regimes of the cell nucleus, Mol. Biol. Cell. 28 (2017) 1984–1996. https://doi.org/10.1091/mbc.e16-09-0653.

[154] D. Castro, V. Nunes, J.T. Lima, J.G. Ferreira, P. Aguiar, Trackosome: a computational toolbox to study the spatiotemporal dynamics of centrosomes, nucleus and cellular membrane, J. Cell Sci. (2020). https://doi.org/10.1242/jcs.252254.

[155] F.-Y. Chu, S.C. Haley, A. Zidovska, On the origin of shape fluctuations of the cell nucleus, Proc. Natl. Acad. Sci. 114 (2017) 10338–10343. https://doi.org/10.1073/pnas.1702226114.

[156] T. Menais, S. Mossa, A. Buhot, Polymer translocation through nano-pores in vibrating thin membranes, Sci. Rep. 6 (2016) 38558. https://doi.org/10.1038/srep38558.

[157] C.S. Janota, F.J. Calero-Cuenca, E.R. Gomes, The role of the cell nucleus in mechanotransduction, Curr. Opin. Cell Biol. 63 (2020) 204–211. https://doi.org/10.1016/j.ceb.2020.03.001.

[158] M. Maurer, J. Lammerding, The Driving Force: Nuclear Mechanotransduction in Cellular Function, Fate, and Disease, Annu. Rev. Biomed. Eng. 21 (2019) 443–468. https://doi.org/10.1146/annurev-bioeng-060418-052139.

[159] D.N. Simon, K.L. Wilson, The nucleoskeleton as a genome-associated dynamic “network of networks,” Nat. Rev. Mol. Cell Biol. 12 (2011) 695–708. https://doi.org/10.1038/nrm3207.

CHAPTER II

Centrosome–nuclear axis repositioning drives the assembly of a bipolar spindle scaffold to ensure mitotic fidelity

The content of this chapter is published in the following original research paper:

V. Nunes, M. Dantas, D. Castro, E. Vitiello, I. Wang, N. Carpi, M. Balland, M. Piel, P. Aguiar, H. Maiato, J.G. Ferreira, Centrosome-nuclear axis repositioning drives the assembly of a bipolar spindle scaffold to ensure mitotic fidelity, Mol. Biol. Cell. (2020) mbc.E20-01-0047. https://doi.org/10.1091/mbc.E20-01-0047.

This is an original research paper and is presented for the first time in a thesis.

Abbreviations

DHC	Dynein Heavy Chain
DMEM	Dulbecco's Modified Eagle Medium
FBN	Fibronectin
FBS	Fetal Bovine Serum
NE	Nuclear Envelope
NEB	Nuclear Envelope Breakdown
PBS	Phosphate-Buffered Saline
PCA	Principal Components Analysis
PLL	Poly-L-Lysine
RT	Room Temperature
SAC	Spindle Assembly Checkpoint
siRNAs	Small Interfering RNAs
SMIFH2	Small-Molecule Inhibitor of Formins
TBS	Triphosphate-Buffered Saline
TFM	Traction Force Microscopy

Centrosome–nuclear axis repositioning drives the assembly of a bipolar spindle scaffold to ensure mitotic fidelity

1. Abstract

During the initial stages of cell division, the cytoskeleton is extensively reorganized so that a bipolar mitotic spindle can be correctly assembled. This process occurs through the action of molecular motors, cytoskeletal networks, and the nucleus. How the combined activity of these different components is spatiotemporally regulated to ensure efficient spindle assembly remains unclear. To investigate how cell shape, cytoskeletal organization, and molecular motors cross-talk to regulate initial spindle assembly, we use a combination of micropatterning with high-resolution imaging and 3D cellular reconstruction. We show that during prophase, centrosomes and nucleus reorient so that centrosomes are positioned on the shortest nuclear axis at nuclear envelope (NE) breakdown. We also find that this orientation depends on a combination of centrosome movement controlled by Arp2/3-mediated regulation of microtubule dynamics and Dynein-generated forces on the NE that regulate nuclear reorientation. Finally, we observe this centrosome configuration favors the establishment of an initial bipolar spindle scaffold, facilitating chromosome capture and accurate segregation, without compromising division plane orientation.

2. Introduction

Chromosome segregation requires the assembly of a bipolar mitotic spindle. While multiple pathways contribute to spindle assembly [1], in human somatic cells centrosomes play a dominant role. During prophase, centrosome separation occurs independently of nuclear envelope breakdown (NEB) in a kinesin–5-dependent manner [2]. Accordingly, depletion or inhibition of kinesin-5 prevents centrosome separation, generating monopolar spindles and mitotic arrest [3]. Other players have been involved in this process, including Myosin II [4], actin [5], microtubule pushing forces [6,7], and Dynein, both at the nucleus [8–12] and at the cell cortex [6,11]. How the forces generated by these components are functionally coordinated to ensure efficient spindle assembly remains unclear.

Entry into mitosis involves loss of interphase adhesion complexes [13–15], changes in interphase microtubule organization [16,17], and dynamics [18] and retraction of cell margins [19,20]. This enables mitotic cells to round up and assemble a stiff actin cortex [20–22]. Although the changes observed in the microtubule and actin cytoskeletons during early mitosis occur simultaneously, they are thought to be independently regulated [16,23]. However, several lines of evidence suggest a functional connection between the two cytoskeletal systems at this stage. Actin helps in initial centrosome separation [5] and

spindle assembly [24,25], and its accumulation on the nuclear envelope (NE) facilitates chromosome congression [26]. Moreover, actin localizes to centrosomes in an Arp2/3-dependent manner [27,28] to assist in microtubule network re-modeling [28,29].

Once the mitotic spindle is assembled, cortical force generators determine metaphase spindle orientation [30–33]. These are activated by external cues [34] and generate pulling forces on astral microtubules [35–37] to align the spindle with the long cell axis [38], ultimately defining the division plane. However, whether centrosome separation and early spindle assembly follow the same cortical cues remains unknown. Defining how external and internal signals are integrated during mitosis to ensure efficient spindle assembly and robust division plane orientation is essential, since prophase centrosome positioning is required for accurate chromosome segregation [39,40].

Here, we performed a high-resolution analysis of centrosome, cytoskeleton, and nuclear behavior during mitotic entry in human cells, followed by 3D cellular reconstruction and centrosome tracking. We show that during mitotic entry, the centrosomes axis does not align according to external cues. Instead, the centrosomes and nucleus reorient so that centrosomes are positioned on the shortest nuclear axis at NEB. This depends on a combination of Dynein-dependent nuclear movement and Arp2/3-medi-ated centrosome positioning. As a result, the formation of an initial bipolar spindle scaffold is facilitated, ensuring maximum exposure of kinetochores to microtubules and improving chromosome segregation fidelity.

3. Results

3.1. Centrosomes position on the shortest nuclear axis at NEB

To characterize mitotic spindle assembly at high spatiotemporal resolution, we performed 4D imaging in HeLa cells. We observed that when cells were seeded on a substrate that does not activate integrin signaling (poly-l-lysine; PLL), centrosomes separated independently of NEB (Supplemental Figure S1A), as reported previously [2,39]. However, when seeded on integrin-activating fibronectin (FBN), ~82% of the cells separated their centrosomes to opposite sides of the nucleus before NEB. Moreover, cells that had an increased spreading area at NEB showed longer intercentrosome distances (Supplemental Figure S1B), suggesting that centrosome separation prior to NEB is a function of the adhesion area. To normalize cell area and shape in 2D, we seeded cells on defined FBN micropatterns and monitored centrosome dynamics, cell membrane, and nuclear shape (Figure 1A), which were subsequently reconstructed using specifically developed computational algorithms (Supplemental Figure S2). Centro-some dynamics relative to the micropattern was defined by two angles, theta and phi, reflecting movements

in xy (azimuth) and xz (inclination), respectively (Figure 1B). These varied between 0° (aligned with the long axis of the pattern) and 90° (perpendicular to the pattern). We anticipated that separated centrosomes should align with the long axis of the micropattern due to the distribution of retraction fibers imposed by extracellular matrix organization [30,34]. However, during mitotic entry, centrosomes deviated from the underlying micropattern, as observed by the high variability of theta and phi (Figure 1B). This was accompanied by a movement of the nucleus relative to the long axis of the pattern, as well as a decrease in cell area (Figure 1C). Due to the shape asymmetry of the line micropattern, we could calculate cell membrane eccentricity, which varied between 1 (completely elongated cell) and 0 (spherical cell). As cells progressed toward NEB, membrane eccentricity decreased (Figure 1D), which was due to a retraction of the long cell axis (Figure 1E, 0°) and a simultaneous increase in cell width, perpendicularly to the pattern (Figure 1, E and F, 90°; ***p<0.001). Interestingly, during the rounding process, the centrosomes and nucleus reoriented so that centrosomes were positioned on the shortest nuclear axis at NEB (~80% of cells; Figure 1, G–I; Supplemental Movie S1).

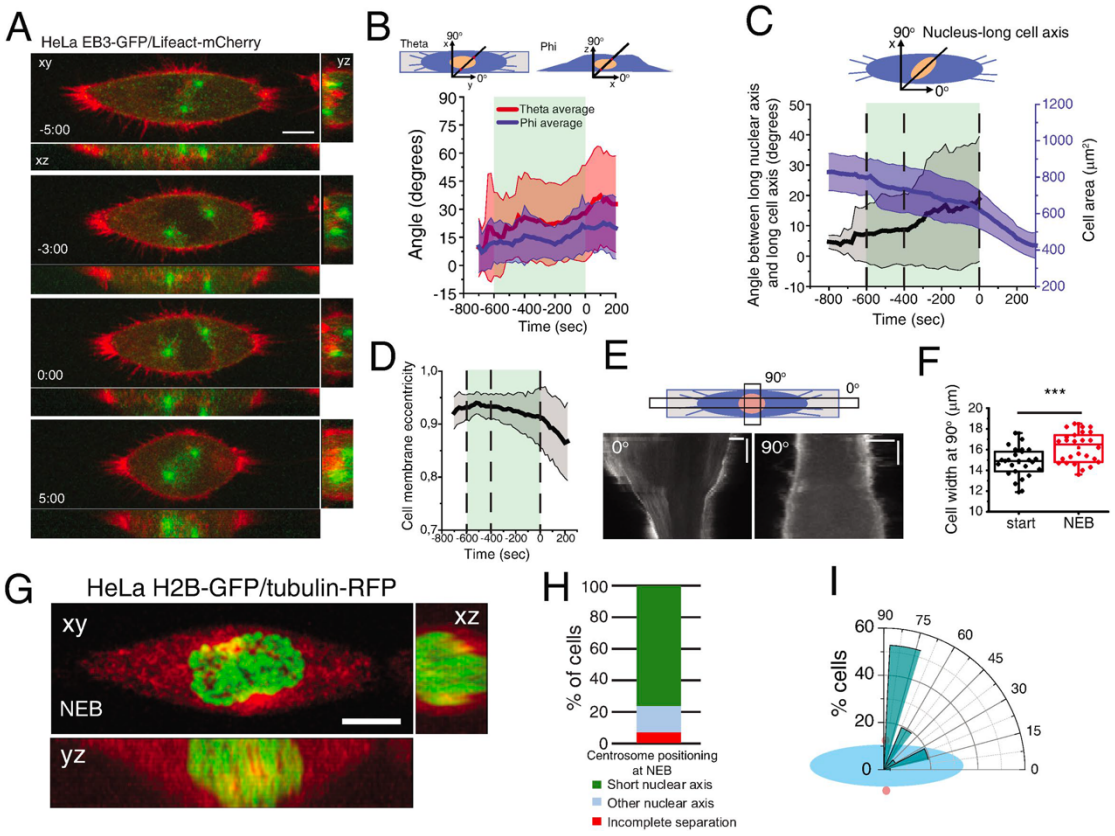


Figure 1: Characterization of early spindle assembly. **(A)** Frames from a movie of a cell seeded on a line micropattern showing movement of the centrosomes toward the shortest nuclear axis. Time is in minutes:seconds. Time zero corresponds to NEB. **(B)** Characterization of centrosome orientation vector in xy (theta; red) and z (phi; blue) for cells seeded on line micropatterns (*n* = 30). Line corresponds to average and

shaded area to SD. **(C)** Quantification of cell area (μm^2; blue) and angle between nucleus-long cell axis (black) for cells on line micropatterns (n = 37). Lines correspond to average and shaded areas represent SD. **(D)** Cell membrane eccentricity during mitotic entry for cells on line micropatterns. Line represents average value and shaded area represents SD. **(E)** Kymograph from cell expressing Lifeact-mCherry seeded on a line micropattern, during mitotic cell rounding. Zero degrees corresponds to the long cell axis and 90° to the perpendicular orientation. **(F)** Cell width (μm) perpendicular to the pattern (n = 16; ***p < 0.001). **(G)** Representative frame from a movie of a cell expressing H2B-GFP/tubulin-RFP showing centrosome and nucleus orientation at NEB. **(H)** Quantification of centrosome separation behavior at NEB for cells seeded on line micropatterns. **(I)** Polar plot quantifying centrosome positioning (red circles) relative to the longest nuclear axis (blue ellipse) at NEB for cells seeded on line micropatterns. All experiments were replicated at least three times.

3.2. Centrosome positioning requires nuclear and centrosome movement

Our observations suggest that prophase centrosome positioning on the shortest nuclear axis is a result of the combined motion of centrosomes and nuclear reorganization. To directly test this, we analyzed the relative contribution of each component for the positioning of centrosomes on the shortest nuclear axis. We reasoned that if positioning on the shortest nuclear axis depended exclusively on centrosome movement (centrosome dominant), the centrosomes-long nuclear axis angle would tend to 90° and the nucleus would remain aligned with the micropattern. On the other hand, if this mechanism required only nuclear reorientation, then the nucleus long axis–long cell axis angle would tend to 90°, and the centrosomes movement would be residual. If both components were involved, then we would observe a combined contribution of both nucleus and centrosomes (Figure 2, A–E). Accordingly, when cell rounding was limited, the nucleus aligned with the long cell axis and centrosomes deviated from the pattern (“centrosome dominant;” Figure 2, A and B). When cell rounding is more pronounced, the long nuclear axis tends to deviate from the long cell axis (“nucleus dominant;” Figure 2, A and C). In intermediate cases, both centrosomes and nucleus deviated from the long cell axis (Figure 2, A and D).

Since the nucleus undergoes extensive changes during prophase, we decided to clarify if the nucleus-dominant behavior is due to nuclear rotation or a change in nuclear shape. As cells progressed toward NEB, nuclear irregularity increased (Figure 2F) and eccentricity decreased (Figure 2G), suggesting that nuclear shape is indeed changing. Next, to evaluate if nuclei also rotated during this stage, we performed photobleaching of H2B-GFP (Figure 2H). Under these conditions, 32% of the nuclei rotated, whereas 68% remained aligned with the long cell axis (Figure 2, H and I). Moreover, a significant percentage of aligned nuclei showed significant deformation (Figure 2I), leading to the generation of a new short axis. We conclude that nuclear orientation during prophase is determined by a combination of nuclear rotation and deformation.

Taken together, our results reveal that multiple components contribute for centrosome positioning on the shortest nuclear axis. Accordingly, at earlier time points (600 s before NEB) when cells had not rounded up significantly, nuclear movement was limited and correct positioning depended mainly on centrosome motion and nuclear deformation (Figure 2, J and M). However, as rounding progressed, the nucleus was now able to reorient (Figure 2, K, L, and N), contributing to correct centrosome positioning (Figure 2O, *p<0.05). Overall, these observations suggest that cell rounding enables nuclear reorientation to facilitate the positioning of centrosomes on the shortest nuclear axis at NEB (Figure 2P).

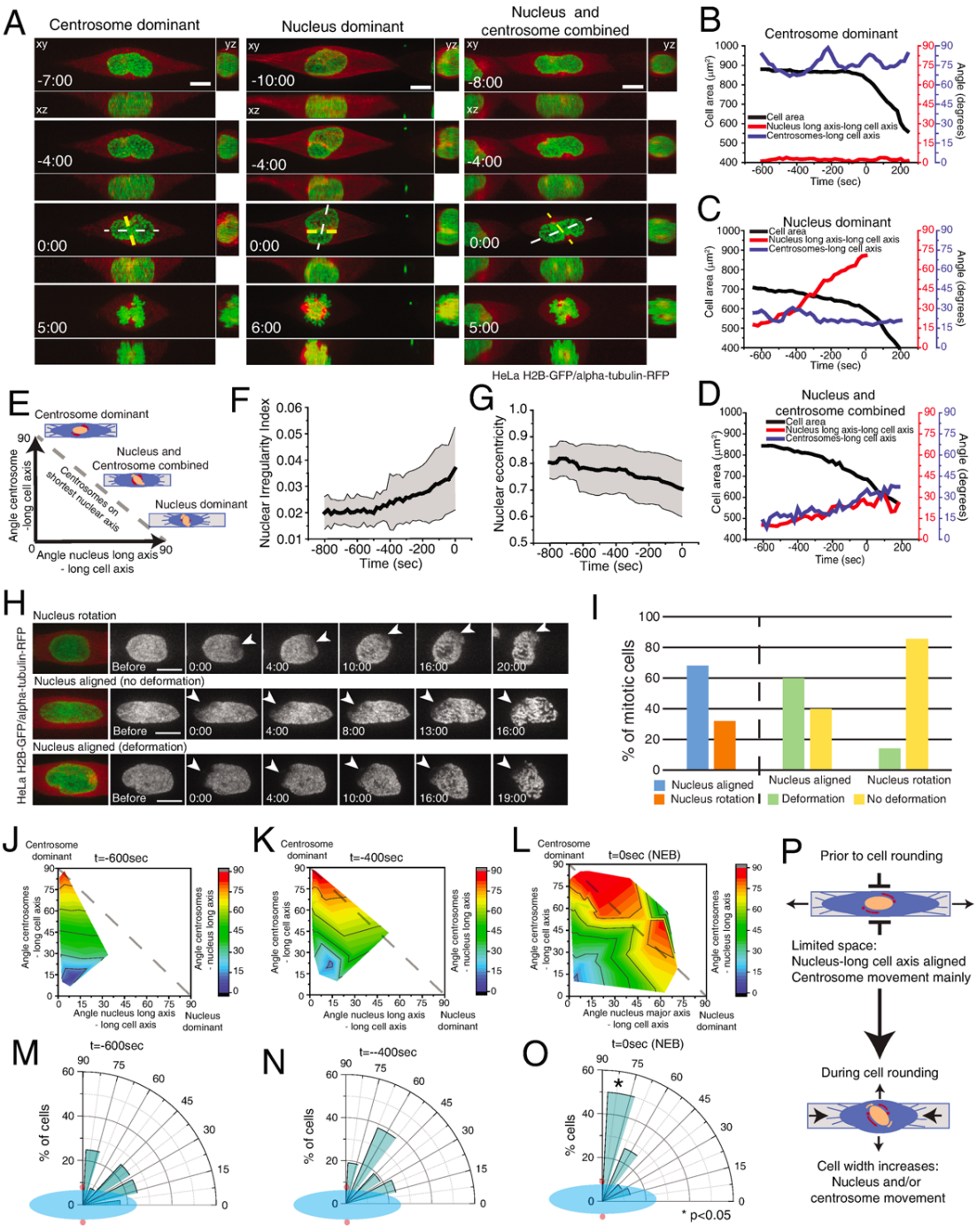


Figure 2: Centrosome positioning requires centrosome and nucleus movement. **(A)** Selected frames from movies of HeLa cells expressing H2B-GFP/alpha-tubulin-RFP seeded on line micropatterns showing different pathways for centrosomes–nucleus axis orientation (*n = 38*). White line shows the long nuclear axis and yellow lines show centrosomes axis. Time lapse is 20 s. Time is in minutes:seconds. Time zero corresponds to NEB. Scale bars, 10 µm. Representative plots showing the correlation between centrosome-long cell axis (blue), long nuclear axis-long cell axis (red), and cell area (black) for centrosome-dominant **(B)**, nucleus-dominant **(C)**, and nucleus–centrosome-combined **(D)** pathways. **(E)** Positioning of centrosomes on the shortest nuclear axis can be achieved by a combination of centrosome movement and nuclear rotation. Quantification of nuclear irregularity index **(F)** and nuclear eccentricity **(G)** for cells entering mitosis. **(H)** Time-lapse imaging of photobleached H2B-GFP during mitotic entry (*n = 22*). Time lapse is 20 s. Scale bars, 10 µm. Time is in minutes:seconds. **(I)** Quantification of the percentage of nuclei that rotate or deform during mitotic entry. Quantification of the contribution of centrosome displacement (angle between centrosomes-long cell axis) and nucleus displacement (angle nucleus long axis-long cell axis) for centrosome positioning on the shortest nuclear axis (angle centrosomes-long nuclear axis) at –600 s **(J)**, –400 s **(K)**, and NEB **(L)**. Distribution of centrosome positioning (red circles) relative to the longest nuclear axis (blue ellipse) at –600 s **(M)**, –400 s **(N)**, and NEB **(O)**. **(P)** Before cell rounding, centrosome–nucleus axis orientation depends mainly on centrosome movement due to the limitation in space. During mitotic rounding, cell width increases, allowing nuclear rotation.

3.3. Centrosome positioning on the shortest nuclear axis depends on cell adhesion area but not cell shape

Our initial observations were obtained with cells seeded on line micropatterns that have a highly polarized shape. To determine whether centrosome positioning on the shortest nuclear axis was a result of shape polarization or a more general feature, we compared cells on circles and rectangles during mitotic entry (Figure 3A). Strikingly, changing from a polarized shape such as a rectangle to an unpolarized large circle did not block the capacity of centrosomes to position on the shortest nuclear axis (78% of cells on rectangles and 75% of cells on large circles; Figure 3, A–D). However, correct positioning depended on the initial spreading area, as seeding cells in small circles led to erratic centrosome movement and only 25% of cells placed centrosomes on the short nuclear axis (Figure 3, A, B, and E, *p=0.02). In addition, although nuclear shape changed when cells were seeded on small circles (Figure 3F; ***p<0.001), with nuclei becoming more rounded, cell shape did not interfere with nucleus orientation relative to the micropattern (Figure 3, G–I), As a result, cells on small circles lost the coordination of movement between centrosomes and nucleus, when compared with the other micropatterns. Taken together, these data indicated that centrosomes position on the shortest nuclear axis at NEB in a cell area-dependent manner but independently of cell shape.

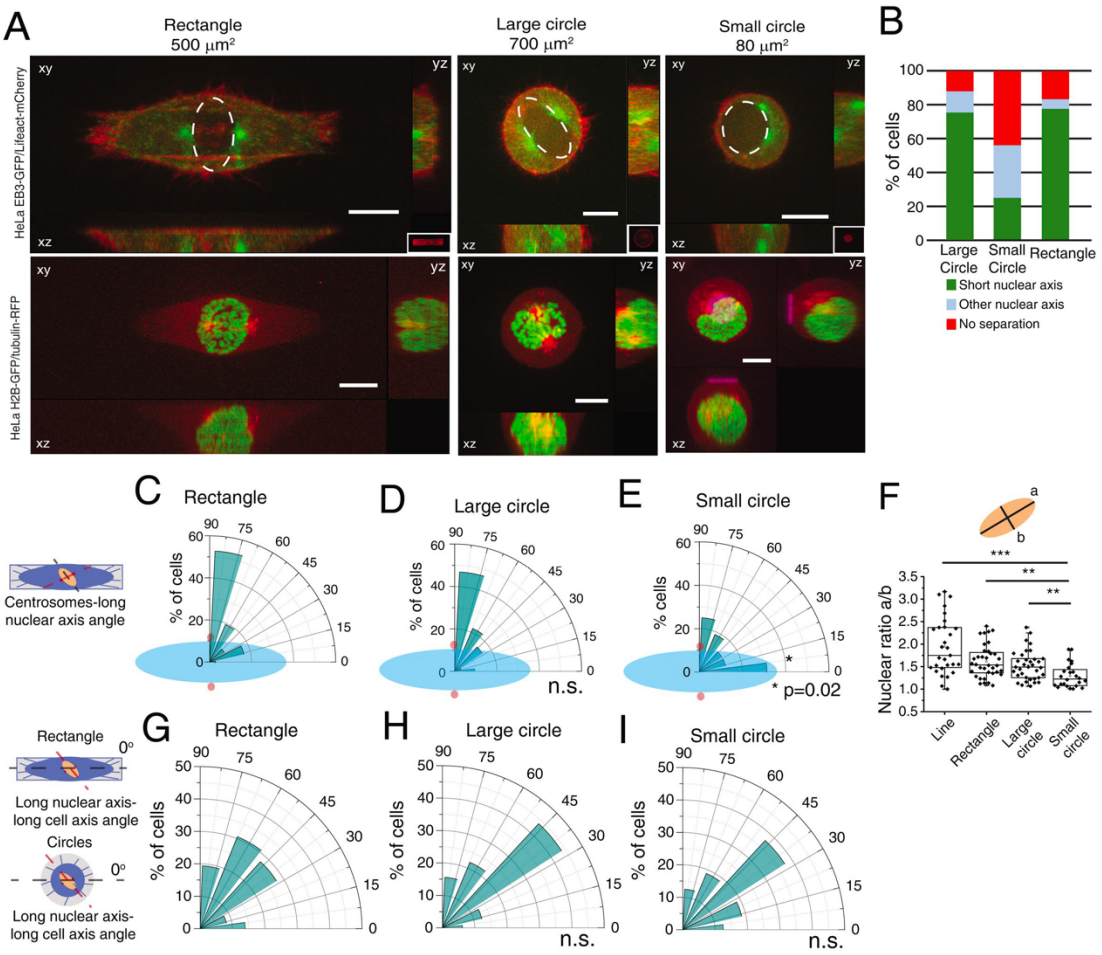


Figure 3: Centrosome positioning on the shortest nuclear axis depends on cell adhesion area. **(A)** Representative images from cells at NEB expressing EB3-GFP/Lifeact-mCherry (top panels) or H2B-GFP/alpha-tubulin-RFP (bottom panels) seeded on rectangles (500 μm^2; *n = 36*), large circles (700 μm^2; *n = 32*), or small circles (80 μm^2; *n = 16*) showing lateral projections (xz and yz). Scale bars, 10 μm. Ellipses highlight nuclear shape at NEB. **(B)** Quantification of centrosome separation behavior at NEB for cells seeded on the different micropatterns. Polar plot quantifying centrosome positioning (red circles) relative to the longest nuclear axis (blue ellipse) at NEB for cells seeded on rectangles **(C)**, large circles **(D)**, or small circles **(E)**. **(F)** Quantification of nuclear shape asymmetry, as defined by the ratio long nuclear axis/short nuclear axis, for cells seeded on different micropatterns (****p < 0.001; **p < 0.01*). Polar plot quantifying alignment of the long nuclear axis with the long cell axis at NEB for cells on rectangles **(G)**, large circles **(H)**, and small circles **(I)**. For cells seeded on circles, 0 was defined horizontally.

3.4. Cell rounding allows the centrosomes–nucleus axis to reorient in prophase

Metaphase spindle orientation is determined by the distribution of actin-based retraction fibers and this depends on extracellular matrix organization [30,34]. Therefore, it would be reasonable to assume that centrosomes should orient according to the same cues during prophase. However, our results showed that prior to NEB (and simultaneously with cell rounding), the centrosomes reoriented away from the underlying retraction fiber

distribution imposed by the micropattern, but according to the shortest nuclear axis. This suggests that the rounding process changes the manner in which cells interact with the extracellular matrix. To confirm this, we performed Traction Force Microscopy (TFM) analysis on cells seeded on rectangles (Supplemental Figure S3A). Under these conditions, cells showed a well-defined traction axis that correlated with the initial centrosome separation axis (theta; Supplemental Figure S3, A–C). On mitotic rounding, both cell area and the contractile energy exerted on the substrate decreased (Supplemental Figure S3D), leading us to conclude that mitotic rounding decreases the force exerted by the cell on the substrate. These observations, together with our previous results, suggest that interfering with cellular adhesion during mitotic rounding could affect the centrosome–nucleus axis orientation. Mitotic rounding is comprised of two parallel pathways that involve adhesion disassembly and cortical retraction [20]. To test which of these processes is required for centrosome positioning during prophase, we decided to express a mutant form of Rap1 (Rap1Q63E; Rap1*) that interferes with focal adhesion disassembly, effectively blocking mitotic rounding [13]. As expected, Rap1* expression affected cell rounding (Figure 4, A, B, D, and E) and delayed focal adhesion disassembly (Supplemental Figure S4 and A, B, **p<0.002). To confirm these results, we decided to deplete the RhoGEF Ect2 by RNAi, as this protein was previously shown to interfere with mitotic cell rounding [41]. Accordingly, Ect2-depleted cells showed delayed cell rounding (Supplemental Figure S4C, ***p< 0.001). Importantly, affecting adhesion disassembly was sufficient to impair centrosome (Figure 4B, E; ***p<0.001) and nuclear reorientation (Figure 4, C and F, *p<0.05; Supplemental Figure S4D, *p<0.03), when compared with controls. This eventually resulted in a failure to position centrosomes on the shortest nuclear axis at NEB (Figure 4, J, K, M, and N, **p<0.01; Supplemental Figure S4E, **p<0.002). Inversely, interfering with cortical retraction by inhibiting ROCK with Y27632 did not impair centrosome movement or nuclear reorientation (Figure 4, G–I, ***p<0.001), which allowed correct positioning of centrosomes (Figure 4, L and O). We concluded that adhesion disassembly in prophase is required for positioning of centrosomes on the shortest nuclear axis by allowing both nuclear reorientation and efficient centrosome movement.

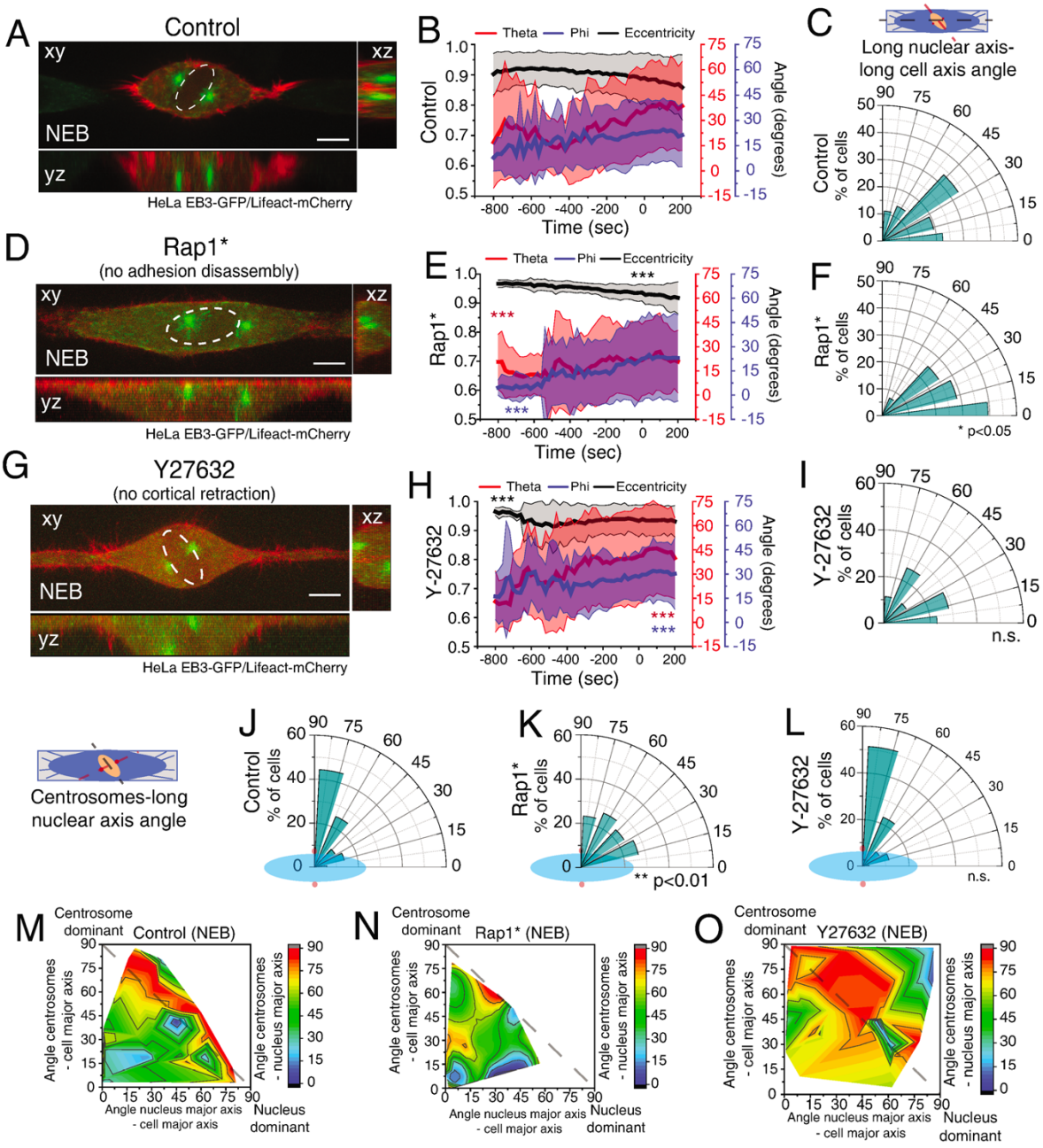


Figure 4: Adhesion complex disassembly is required to establish the centrosomes–nucleus axis at NEB. Representative time frame from a movie of HeLa cells expressing EB3-GFP/Lifeact-mCherry treated with DMSO (**A**; *n = 38*), Rap1* (**D**; *n = 28*), or Y-27632 (**G**; *n = 35*) at NEB. Correlation of cell membrane eccentricity (black), theta (red), and phi (blue) for controls **(B)**, Rap1* **(E)** and Y-27632 **(H)**. Lines correspond to average values and shaded areas correspond to SD. Inhibiting adhesion disassembly limits centrosome movement (***$p < 0.001$). Polar plot quantifying alignment of the long nuclear axis with the long cell axis at NEB for DMSO **(C)**, Rap1* (**F**; *$p < 0.05$), and Y-27632 **(I)**. Polar plot quantifying centrosome positioning (red circles) relative to the longest nuclear axis (blue ellipse) at NEB for controls **(J)**, Rap1* (**K**; **$p < 0.01$) or Y-27632 **(L)**. Quantification of the contribution of centrosome displacement (angle between centrosomes-long cell axis) and nucleus displacement (angle nucleus long axis-long cell axis) for centrosome positioning on the shortest nuclear axis (angle centrosomes-long nuclear axis) for controls **(M)**, Rap1* **(N)**, or Y-27632 **(O)** at NEB. All experiments were replicated at least three times.

3.5. Dynein on the NE is required for nuclear rotation during prophase

Next, we wanted to systematically dissect which factors influence the positioning of centrosomes on the shortest nuclear axis by either regulating nuclear rotation or centrosome movement. It is known that kinesin-5 is essential for centrosome separation [2,3]. To assess whether it is also required to position centrosomes on the shortest nuclear axis, we treated cells with an Eg5 inhibitor (STLC) when centrosomes were already on opposite sides of the nucleus (Late stage) or when centrosomes were still not fully separated (Early stage). Early Eg5 inhibition significantly decreased pole-to-pole distance, preventing centrosome positioning on the shortest nuclear axis (Supplemental Figure S5, A–C). When Eg5 was inhibited in the Late stage, centrosomes moved toward the shortest nuclear axis, simultaneously with mitotic cell rounding (Supplemental Figure S5D, dashed line). We concluded that kinesin-5 is required for initial centrosome separation but not directionality.

In addition to kinesin-5, additional factors contribute to early centrosome separation such as Dynein [9,42], actin [2,5,43,44], and microtubules [2,7], making these likely candidates to mediate centrosomes–nucleus orientation. We started by depleting total Dynein Heavy Chain (DHC), which induced defects in centrosome positioning, probably due to a delayed cell rounding (Supplemental Figure S6, A–C, ***$p<0.001$). However, in mitosis Dynein can be found in different subcellular localizations. During prophase, Dynein is loaded on the NE through two pathways involving RanBP2-BicD2 and Nup133-CENP-F-NudE/NudEL [8,10,45,46]. Later on, it localizes to the cell cortex through the LGN-Gαi-NuMA complex, which can be prevented by inhibiting Gαi activity with per-tussis toxin (PTx) [33,47]. To determine if prophase centrosome positioning required any of these specific pools of Dynein, we interfered with NE Dynein by depleting either NudE/NudEL or BicD2 by RNAi (Supplemental Figure S6, D and E). Depletion of NudE+NudEL, but not BicD2, led to a small but significant detachment of centrosomes from the NE (Figure 5A and Supplemental Figure S6F, ***$p<0.001$; Supplemental Movie S2). However, both treatments impaired reorientation of the nucleus relative to the long cell axis (Figure 5, B–D, ***$p<0.001$). This effect was independent of cell rounding, as depleting NudE+NudEL or BicD2 had opposing effects on cell rounding (Figure 5E, ***$p<0.001$) but showed a similar defect in nuclear reorientation. Consequently, centrosomes no longer positioned on the shortest nuclear axis (Figure 5, F–H, ***$p<0.001$). Notably, this effect was independent of centrosomes distance to the nucleus (Supplemental Figure S6, F and G), indicating that nuclear reorientation requires Dynein-mediated forces. Next, to determine whether cortical Dynein was also required for nuclear rotation, we treated cells with PTx during mitotic entry (Figure 5I). Under these conditions, Dynein was selectively removed from the cortex but not the NE (Supplemental Figure S6, H and I). When Dynein was prevented from accumulating

in the cortex, cells rounded up prematurely (Figure 5J, ***p<0.001), leading to increased nuclear rotation (Figure 5K, **p=0.002) and centrosome movement (Figure 5L; theta, **p<0.01; phi, *p= 0.04). Overall, this did not affect centrosome positioning on the shortest nuclear axis at NEB (Figure 5, M and N), which is in agreement with the presence of Dynein on the NE following PTx treatment. Moreover, Dynein accumulation on the NE was independent on cell rounding, as treating cells with PTx or expressing Rap1* had opposite effects on rounding, but did not interfere with NE Dynein (Supplemental Figure S6, H–K).

Next, we wanted to determine whether the actin cytoskeleton was required for nuclear reorientation during prophase, since it is involved in nuclear rotation during interphase [48]. For that reason, we interfered with the activity of actin nucleators Arp2/3 or formins by depleting the Arp2/3 subunit, ArpC4, with RNAi or with the small-molecule inhibitor of formins, SMIFH2. Interfering with either actin nucleator did not affect cell rounding (Figure 5O) or nuclear orientation (Figure 5, P and Q). Similar results regarding nuclear orientation were obtained when we used a small-molecule inhibitor of Arp2/3 (CK666; our unpublished observations). Overall, we concluded that NE Dynein, coupled with loss of cortical Dynein, ensured the correct centrosome–nucleus axis at NEB by facilitating nuclear reorientation.

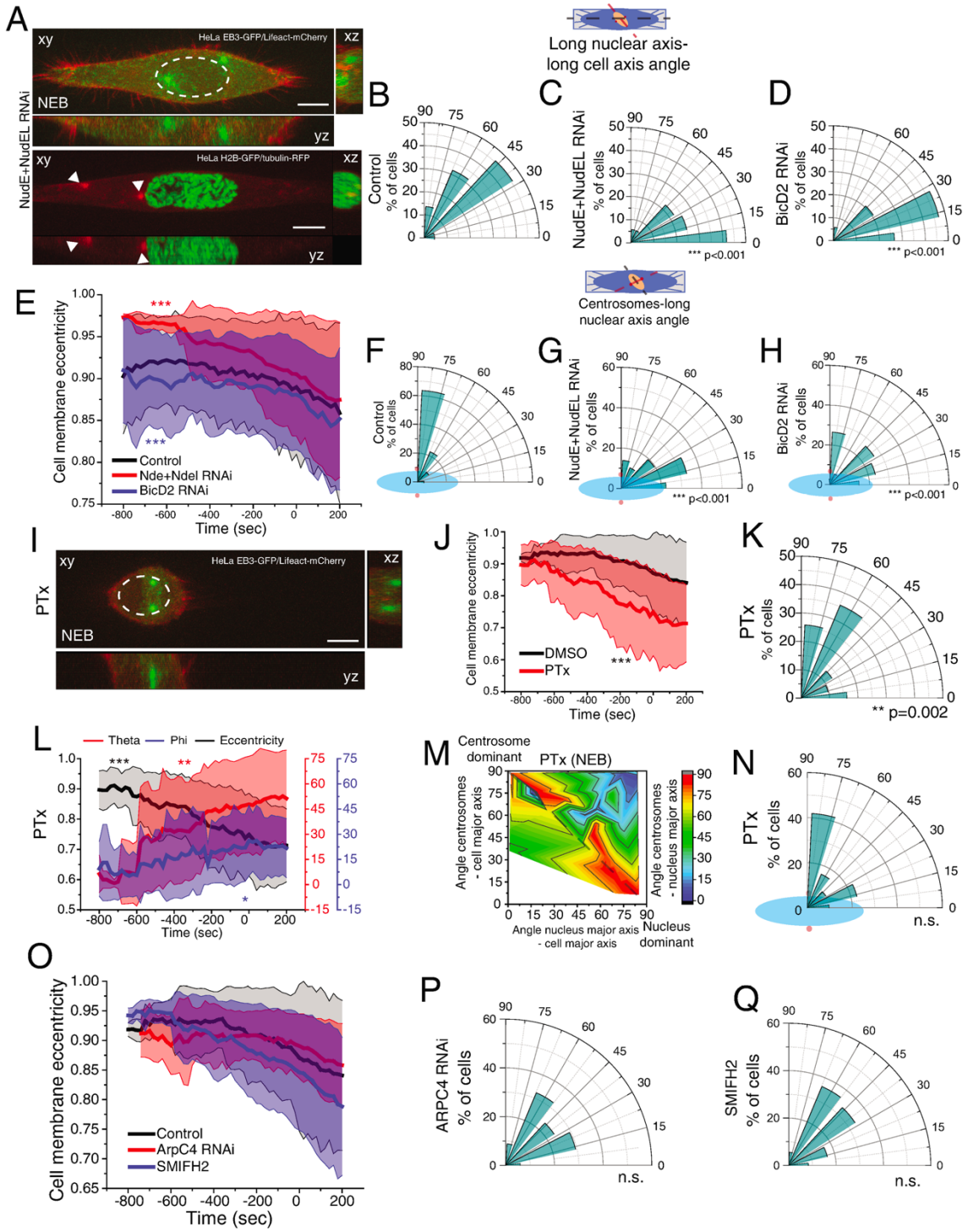


Figure 5: Dynein on the NE is required for nuclear rotation. **(A)** Images of HeLa cells expressing EB3-GFP/Lifeact-mCherry (top panel; *n = 36*) or H2B-GFP/tubulin-RFP (bottom panel; *n = 25*) treated with NudE+NudEL RNAi. White arrowheads indicate centrosome position. Time lapse is 20 s. Scale bar, 10 µm. Polar plot quantifying alignment of the long nuclear axis with the long cell axis at NEB for controls **(B)**, NudE+NudEL RNAi (**C**; ***$p < 0.001$), or BicD2 RNAi (**D**; ***$p < 0.001$; $n = 34$). **(E)** Cell membrane eccentricity for controls, NudE+NudEL RNAi, and BicD2 RNAi. Lines correspond to average values and shaded areas correspond to SD (***$p < 0.001$). Polar plot quantifying centrosome positioning (red circles) relative to the longest nuclear axis (blue ellipse) at NEB for controls **(F)**, cells treated with RNAi for NudE+NudEL **(G)**, or BicD2 **(H)**. **(I)** Time frame from cells expressing EB3-GFP/Lifeact-mCherry treated with PTx ($n = 31$). Scale bar, 10 µm. **(J)**

Cell membrane eccentricity for controls and PTx-treated cells. Lines correspond to average values and shaded areas correspond to SD (****p < 0.001*). **(K)** Polar plot quantifying alignment of the long nuclear axis with the long cell axis at NEB for cells treated with PTx. **(L)** Correlation of cell membrane eccentricity (black), theta (red), and phi (blue) for PTx cells. **(M)** Quantification of the contribution of centrosome displacement (angle between centrosomes-long cell axis) and nucleus displacement (angle nucleus long axis-long cell axis) for centrosome positioning on the shortest nuclear axis (angle centrosomes-long nuclear axis) at NEB for cells treated with PTx. **(N)** Polar plot quantifying centrosome positioning (red circles) relative to the longest nuclear (blue ellipse) at NEB for cells treated with PTx. **(O)** Cell membrane eccentricity for controls (*n = 38*), ArpC4 RNAi (*n = 34*), and SMIFH2 (*n = 36*). Lines correspond to average values and shaded areas correspond to SD (***p < 0.001). Polar plot quantifying alignment of the long nuclear axis with the long cell axis at NEB for ArpC4 RNAi **(P)** and SMIFH2 **(Q)**. All experiments were replicated at least three times.

3.6. Arp2/3 activity is required for centrosome orientation during prophase

The experiments above support a model where Dynein-mediated forces act on the NE to induce nuclear reorientation. However, they do not take into account the contribution of centrosome movement for positioning on the shortest nuclear axis. This is particularly relevant since we showed that Arp2/3 activity did not affect nuclear orientation (Figure 5, O–Q) but was required for centrosome positioning on the shortest nuclear axis (Figure 6, A–C, ***p<0.001, Supplemental Movie S3). It is possible the Arp2/3-mediated branched actin network directly affects centrosome movement and positioning, in line with previously published in vitro work [49]. Accordingly, we observed that depleting ArpC4 by RNAi leads to increased centrosome movement (Figure 6D, ***p<0.001). Inversely, interfering with formins activity (Figure 6E) or with any of the Dynein pools (Supplemental Figure S7, A–C) did not affect centrosome movement, suggesting this process required the presence of a branched actin network, but was independent of NE Dynein or centrosome distance to the NE. Interestingly, expression of Rap1* did not affect overall centrosome movement, indicating that adhesion disassembly is primarily required for nuclear reorientation (Supplemental Figure S7D and Figure 4F).

It was recently shown, using reconstituted in vitro approaches, that the Arp2/3-mediated branched actin network controls centrosome movement by regulating microtubule dynamics [49]. To assess whether centrosome positioning depended on Arp2/3 regulation of microtubule dynamics, we started by performing high-resolution imaging of cells expressing EB3-GFP/Lifeact-mCherry during prophase (Figure 6F). We consistently observed the presence of actin near the centrosome that correlated with a decrease in microtubule nucleation (Figure 6, F, white arrowheads, and G). Next, to interfere with the Arp2/3-mediated actin network, we treated cells with the Arp2/3 inhibitor, CK666, and analyzed astral microtubule dynamics using the plusTipTracker software [50]. Treatment with CK666 during prophase increased the number of microtubule growths, as well as

microtubule speed and length, when compared with controls (Figure 6, H–L, ***p<0.001), in line with the microtubule-destabilizing effect of branched actin networks [29,29,49]. Microtubule destabilization during early mitosis is crucial to allow proper spindle assembly [16,18]. To determine whether Arp2/3 activity was required for microtubule cytoskeleton reorganization and early spindle assembly, we filmed HeLa cells expressing H2B-GFP/tubulin-RFP during mitotic entry and quantified the levels of tubulin-RFP fluorescence intensity in controls and ArpC4 RNAi cells. In controls, we observed a decrease in tubulin fluorescence intensity over time (Figure 6, M and N, ***p<0.001), reflecting the disassembly of the interphase microtubule cytoskeleton [16]. By comparison, tubulin fluorescence intensity in ArpC4-depleted cells did not vary significantly (Figure 6, M and N), supporting a role for Arp2/3 activity in prophase microtubule destabilization. To further confirm that microtubule destabilization was important for centrosome movement and positioning during prophase, we treated cells with low doses of the microtubule stabilizer, Taxol. As expected, stabilizing microtubules with Taxol treatment led to increased centrosome movement (Supplemental Figure S7E, ***p<0.001) and incorrect centrosome positioning at NEB (Supplemental Figure S7F, **p=0.008), independently of cell rounding (Supplemental Figure S7H) or nuclear reorientation (Supplemental Figure S7G). Thus, we concluded that Arp2/3 regulates microtubule dynamics to facilitate cytoskeleton reorganization, centrosome movement, and correct positioning during prophase.

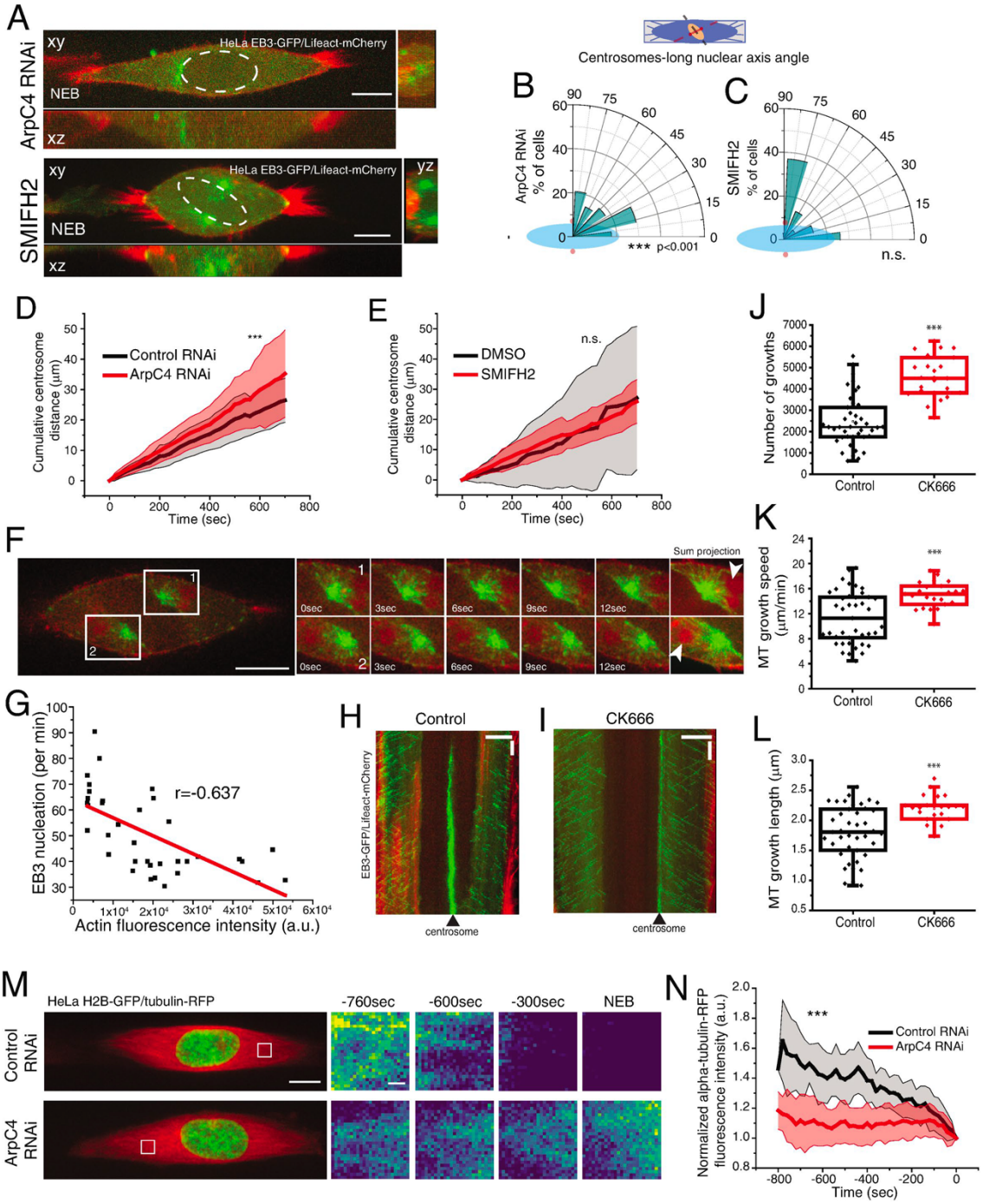


Figure 6: Arp2/3 activity regulates centrosome movement. **(A)** Representative images of HeLa cells expressing EB3-GFP/Lifeact-mCherry after treatment with ArpC4 RNAi or SMIFH2 at NEB. Scale bar, 10 µm. **(B)** Polar plots quantifying centrosome positioning (red circles) relative to the longest nuclear axis (blue ellipse) at NEB for cells treated with ArpC4 RNAi **(B)** or SMIFH2 **(C)**. Cumulative centrosome distance measured for cells treated with ArpC4 RNAi **(D)** or SMIFH2 **(E)**. **(F)** HeLa cell expressing EB3-GFP/Lifeact-mCherry filmed with a 500-ms time lapse to show how the presence of actin limits microtubule growth. Scale bar, 10 µm. Time is in seconds. **(G)** Correlation between actin fluorescence intensity (a.u.) and EB3 nucleation (per minute). Kymograph of cells expressing EB3-GFP/Lifeact-mCherry for control **(H)** or CK666-treated **(I)** cells. Horizontal scale bar, 10 µm; vertical scale bar, 30 s. Microtubule dynamics parameters for control (*79,899 tracks; 41 cells*) and CK666-treated cells (*79,957 tracks; 23 cells; ***p < 0.001*) indicating number of growths **(J)**, growth speed

(**K**; μm/min), and growth length (**L**; μm). **(M)** Representative images of HeLa cells expressing H2B-GFP/tubulin-RFP filmed during mitotic entry. Scale bar, 10 μm. White box corresponds to area used for insets on the right. Insets represent tubulin fluorescence intensity visualized with a Viridis LUT. Scale bar, 1 μm. **(N)** Quantification of normalized tubulin-RFP fluorescence intensity for controls and ArpC4 RNAi-treated cells (****p < 0.001*).

3.7. Centrosome positioning on the shortest nuclear axis facilitates spindle assembly

Centrosome positioning at NEB is known to affect mitotic fidelity [39,40]. Here, we tested specifically whether positioning on the shortest nuclear axis affected spindle assembly efficiency. We imaged cells on FBN or PLL and correlated centrosome positioning, mitotic timing, and missegregation events (Figure 7A; Supplemental Movies S4 and S5). Seeding cells on PLL affected centrosome separation ("incomplete separation;" 23% for PLL and 8% for FBN) and positioning on the shortest nuclear axis (51% for PLL and 72% for FBN), when compared with FBN (Figure 7B). Consequently, PLL-seeded cells had increased missegregation events (19.2%) when compared with FBN (5.7%) (Figure 7C). These were mainly lagging chromosomes in cells with incomplete centrosome separation (Figure 7D), as was described previously [40]. We concluded that the extent of centrosome separation increases chromosome segregation fidelity. Next, we determined whether centrosome positioning affects mitotic timing. Cells on PLL had a significant delay in anaphase onset when compared with cells on FBN (Figure 7E, *p<0.05). This delay was due to cells that separate, but do not position centrosomes on the shortest nuclear axis (Figure 7F, "other axis;" 72 ± 29 min, ***p<0.001), as opposed to cells with centrosomes on the "shortest axis" (40 ± 18 min). To confirm if the increased mitotic timing observed was due to a delay in Spindle Assembly Checkpoint (SAC) satisfaction, we filmed HeLa cells expressing Mad2-GFP/SiR-tubulin. By monitoring Mad2 removal from kinetochores, we can determine how efficiently microtubules attach to kinetochores [51], leading to SAC satisfaction. We seeded cells in PLL and followed them as they progressed through mitosis (Figure 7G). We then correlated Mad2 removal from kinetochores with the centrosome–nucleus axis at NEB (Figure 7, H and I). Interestingly, we observed that cells which place their centrosomes on the shortest nuclear axis remove Mad2 faster from the kinetochores (Figure 7, G–I, r = –0.756). We concluded that centrosome positioning on the shortest nuclear axis ensures timely progression through mitosis by ensuring faster SAC satisfaction.

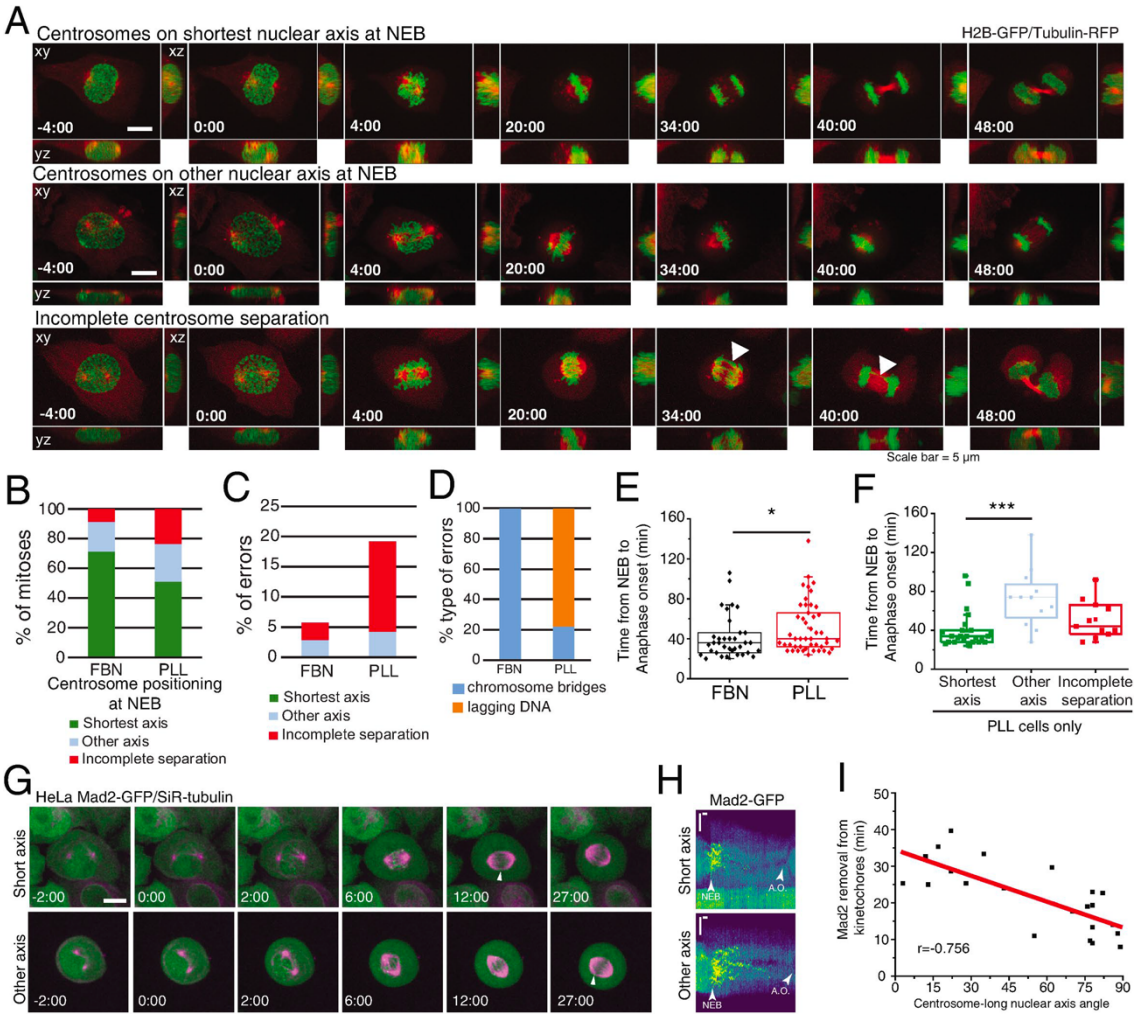


Figure 7: Centrosome positioning on the shortest nuclear axis facilitates spindle assembly. **(A)** HeLa cells expressing H2B-GFP/alpha-tubulin-RFP during mitosis. The top panel represents a cell with centrosomes on the shortest nuclear axis at NEB, the middle panel represents a cell with centrosomes on a random nuclear axis, and the bottom panel represents a cell with incomplete centrosomes separation. Time lapse is 2 min. Scale bar, 5 µm. **(B)** Proportion of cells that place centrosomes on shortest axis (green), other axis (blue), or have incomplete separation (red) at NEB, depending on the coating (FBN or PLL). Quantification of the proportion **(C)** and type of missegregation events **(D)** for cells seeded on FBN (*n = 35*) or PLL (*n = 47*). **(E)** Quantification of the time between NEB and anaphase onset for cells seeded on FBN or PLL (****p < 0.001*). **(F)** Timings from NEB to anaphase onset, for cells seeded on PLL, according to their centrosome separation status (****p < 0.001*; n.s., not significant). **(G)** HeLa cells expressing Mad2-GFP/SiR-tubulin during mitosis. The top panel represents a cell with centrosomes on shortest nuclear axis at NEB and the bottom panel represents a cell with centrosomes on a random nuclear axis. White arrowheads indicate Mad2-positive kinetochores. Time lapse is 20 s. Time is in minutes:seconds. Scale bar, 10 µm. **(H)** Representative kymographs of Mad2-GFP (Viridis LUT) for cells with centrosomes on the shortest nuclear axis (top panel) and cells with centrosomes on a random axis (bottom panel). Horizontal scale bar, 100 s. Vertical scale bar, 5 µm. A.O., anaphase onset. **(I)** Correlation between the time for Mad2 removal from kinetochores and centrosome-long nuclear axis and NEB, with a Pearson s correlation coefficient = –0.756.

4. Discussion

At the transition from G2 to mitosis, interphase adhesion complexes disassemble [13,14,52], cell margins retract [19,20], and microtubule organization and dynamics change [16,18]. This leads to a global reorganization of cellular geometry that is required to form a stiff mitotic cortex [21] and help bipolar spindle assembly [53]. During this stage, Dynein is loaded on the NE through multiple pathways mediated by RanBP2 [45] and Nup133 [8]. This allows centrosome tethering to the NE which assists in centrosome separation [9], NEB [54,55], and early spindle assembly [8]. How these processes are spatiotemporally coordinated to ensure efficient spindle assembly remained unclear.

Here, we propose a model in which efficient spindle assembly requires a combination of centrosome movement and nuclear reorientation to position centrosomes on the shortest nuclear axis at NEB. Our observations suggest that microtubule remodeling during early mitosis is essential for centrosome movement, partly through the action of Arp2/3-mediated microtubule regulation, but also likely through the inactivation of interphase microtubule stabilizers [16]. Although the Arp2/3 complex does not seem to be relevant for mitotic progression [53] or mitotic cortex structure [56], its activity was recently proposed to assist in microtubule remodeling at mitotic exit [29]. In particular, recruitment of Arp2/3 to the centrosome during this stage leads to increased actin filament nucleation, accompanied by decrease in centrosomal microtubule density. Our results (Figure 6) suggest that Arp2/3 may function in a similar manner during mitotic entry to decrease microtubule density and assist in cytoskeletal reorganization. This is in line with previous works that propose a role for Arp2/3 in fine-tuning changes in microtubule dynamics [29,49] and could contribute to the microtubule reorganization observed during the G2/M transition [18]. Globally, this would trigger centrosome repositioning during prophase.

In combination with centrosome movement, we propose that Dynein-mediated forces on the NE also contribute to correct centrosome positioning by regulating nuclear reorientation, as was already described in other systems [57–59]. During prophase, centrosomes separate to opposite sides of the nucleus [7]. This event creates an asymmetry in the centrosomal microtubule arrays due to the presence of an intact nucleus between them, biasing microtubule nucleation along the surface of the NE. At the same time, Dynein is loaded on the NE [8,45]. This allows Dynein to capture centrosomal microtubules, likely stabilizing them [60] and generating pulling forces that are sufficient to assist in NEB [54,55]. Due to the asymmetry in the centrosomal microtubule arrays and the dynamic nature of microtubules, these pulling forces exert a rotational torque on the prophase nucleus [58,59]. This torque is then translated into nuclear reorientation, once cell rounding occurs. This hypothesis is supported by our data showing that adhesion disassembly or PTx-triggered cell rounding is sufficient to allow nuclear rotation (Figures 4

and 5), whereas blocking deadhesion constrains nuclear reorientation (Figure 4, Supplemental Figure S4, and [61]).

Importantly, the positioning of centrosomes on the shortest nuclear axis during prophase is clearly distinct from the mechanism driving metaphase spindle orientation. During metaphase, external cues [30,34,62] activate cortical force generators [31–33] and transmit pulling forces to astral microtubules [6,34,36,37] to ensure robust centrosome positioning. However, before NEB, the mitotic cortex is not fully assembled [63,64] and cortical force generators are not yet in place [32,33]. Consequently, at this stage, centrosomes do not align according to external cues but follow internal cues provided by the cytoskeleton and nucleus.

Chromosome capture during early mitosis was proposed to occur through a “search-and-capture” mechanism [65]. Subsequent work demonstrated that timely spindle assembly could not rely solely on the search-and-capture mechanism [66], but depended on the contribution of kinetochore-driven microtubule nucleation [67], kinetochore compaction [68], and chromosome motion [69] and distribution [70].

However, these facilitating mechanisms often require that centrosomes deviate from the external cues [70,71] to ensure efficient chromosome capture. These reports are in line with our observations that the centrosome–nuclear axis orients away from the underlying micropattern during early spindle assembly. We propose that centrosome positioning on the shortest nuclear axis favors the assembly of a bipolar spindle scaffold to ensure maximum exposure of kinetochores to microtubules [53]. In combination with the spatial distribution of chromosomes in a ring configuration [70], this would accelerate spindle assembly, minimizing the probability of generating erroneous attachments. In agreement with this hypothesis, we observed that centrosome mispositioning significantly delayed mitosis and Mad2 removal from kinetochores (Figure 7), whereas failure to separate centrosomes altogether generated chromosome missegregation events, as previously described [40]. In summary, we propose a model where centrosomes–nucleus axis orientation during prophase facilitates the formation of an initial bipolar spindle scaffold to ensure mitotic fidelity.

5. Materials and Methods

5.1. Cell lines and transfections

Cell lines were cultured in Dulbecco's Modified Eagle Medium (DMEM; Life Technologies) supplemented with 10% fetal bovine serum (FBS; Life Technologies) and grown in a 37°C humidified incubator with 5% CO2. HeLa cell line expressing histone H2B-GFP/mRFP-α-tubulin was generated in our lab using lentiviral vectors. For this purpose, HEK293T cells at 50–70% con-fluence were cotransfected with lentiviral packaging vectors (16.6 μg of Pax2 and 5.6 μg of pMD2) and 22.3 μg of LV-H2B-GFP (a gift from Elaine Fuchs, Addgene plasmid 25999) or pRRL-mRFP-α-tubulin plasmids, using 30 μg of Lipofectamine2000 (Life Technologies). After transfection, the virus-containing supernatant was collected, centrifuged, filtered, and stored at –80°C. HeLa parental cells were then transduced with each lentivirus in the presence of polybrene (1:1000) in standard culture media for 24 h. The lentiviruses were used individually, giving time for cells to recover between transductions. After the second transduction, H2B-GFP/mRFP-α-tubulin double-positive cells were isolated by fluorescence-activated cell sorting (FACS; FACS Aria II). For transient over-expression of pRK5-Rap1[Q63E] plasmids (a gift from Jean de Gunzburg), cells were transfected with the corresponding plasmid using Lipofectamine2000 (Life Technologies). Briefly, cells at 50–70% con-fluence were incubated for 6 h with 5 μl of Lipofectamine 2000 and 0.6 μg/ml DNA. DNA–lipid complexes were previously diluted in Opti-Minimal Essential Medium (Opti-MEM; Alfagene) and incubated for 30 min before adding to the cells. Prior to and during transfection, cell medium was changed to a reduced serum medium (DMEM supplemented with 5% FBS). Cells were analyzed 48 h after transfection. HeLa Mad2-GFP cells were previously described [72].

5.2. Micropatterning

Micropatterns to control individual cell shape and adhesion pattern were produced as previously described [73]. Briefly, glass coverslips (22 × 22 mm No. 1.5, VWR) were activated with plasma (Zepto Plasma System, Diener Electronic) for 1 min and incubated with 0.1 mg/ml PLL(20)-g[3,5]-PEG(2) (SuSoS) in 10 mM HEPES at pH 7.4, for 1 h, at room temperature (RT). After rinsing and air-drying, the coverslips were placed on a synthetic quartz photomask (Delta Mask), previously activated with deep-UV light (PSD-UV, Novascan Technologies) for 5 min; 3 μl of MiliQ water were used to seal each coverslip to the mask. The coverslips were then irradiated through the photomask with the UV lamp for 5 min. Afterward, coverslips were incubated with 25 μg/ml FBN (Sigma-Aldrich) and 5 μg/ml Alexa 546– or 647–conjugated fibrinogen (Thermo Fisher Scientific) in 100 mM NaHCO3 at pH 8.6, for 1 h, at RT. Cells were seeded at a density of 50,000 cells/coverslip and allowed

to spread for ~10–15 h before imaging. Nonattached cells were removed by changing the medium ~2–5 h after seeding.

5.3. Drug treatments

PTx was used at 40 nM (Merck). To inhibit the activity of the Arp2/3 complex, we used 100 µM of CK666 (Tocris Bioscience). ROCK inhibitor Y-27632 was used at a concentration of 20 µM (Sigma-Al-drich). The small molecule inhibitor of formin-mediated actin assembly, SMIFH2, was used at 30 µM. To interfere with the microtubule cytoskeleton, we used Taxol (20 nM) (Sigma-Aldrich). To inhibit Eg5, STLC was added at 5 µM. All the drugs used were added to the culture medium 30 min–1 h before live-cell imaging or fixation. Control cells were treated with DMSO (Sigma-Aldrich) only.

5.4. RNAi experiments

Cells were transfected with small interfering RNAs (siRNAs) using Lipofectamine RNAi Max (Life Technologies). Specifically, 5 µl of Lipofectamine and 20 nM of each siRNA were diluted and incubated in Opti-MEM (Alfagene) for 30 min. The siRNA–lipid complexes were then added to 50–70% confluence cells cultured, during transfection (6 h), in reduced serum medium (DMEM supplemented with 5% FBS). Commercial ON-TARGETplus SMARTpool siRNAs (Dharmacon) were used for BICD2, ARPC4, and Ect2 depletions. For DHC depletion, the following oligos were ordered: 5′-GAACU-AGACUUGGUUAAUU-3′ and 5′-AAUUAACCAAGUCUAGUUC-3′. For combined NudE+NudEL, depletion the following oligos were ordered: 5’-GCUUGAAUCAGGCCAUCGA-3’ and 5’-UCGAUGGCCUGAUUCAAGC-3’ for NudE and 5’-GGAUGAAGCAAGAGAU-UUA-3’ and 5’-UAAAUCUCUUGCUUCAUCC-3’ for NudEL. Commercial ON-TARGETplus SMARTpool nontargeting siRNAs and mock transfections were used as controls. For all siRNAs used, cells were analyzed 72 h after transfection, except for Ect2 RNAi where cells were analyzed 24–48 h post-transfection. Protein depletion efficiency was monitored by immunoblotting and phenotypic analysis.

5.5. Time-lapse microscopy

For time-lapse microscopy, 12–24 h before the experiments 1.5×10^5 cells were seeded on coverslips coated with FBN (25 µg/ml; F1141, Sigma) or PLL (25 µg/ml; F1141, Sigma). When micropatterns were used, 5×10^4 cells were seeded on coverslips coated with FBN (25 µg/ml; F1141, Sigma). Prior to each experiment, cell culture medium was changed from DMEM with 10% FBS to Leibovitz’s-L15 medium (Life Technologies) supplemented with 10% FBS and Anti-biotic-Antimycotic 100X (AAS; Life Technologies). When SiR-dyes were used, they were added to the culture medium 30 min–1 h before

acquisition (20 nM Sir-tubulin or 10 nM Sir-DNA; Spirochrome). Live-cell imaging was performed using temperature-controlled Nikon TE2000 microscopes equipped with a modified Yokogawa CSU-X1 spinning-disk head (Yokogawa Electric), an electron multiplying iXon+ DU-897 EM-CCD camera (Andor), and a filter wheel. Three laser lines were used for excitation at 488, 561, and 647 nm. For nuclear pore fluctuation analysis, an oil-immersion 100× 1.4 NA Plan-Apo DIC (Nikon) was used. All the remaining experiments were done with an oil-immersion 60× 1.4 NA Plan-Apo DIC (Nikon). Image acquisition was controlled by NIS Elements AR software. For centrosome tracking, 17–21 z-stacks with a 0.5-µm separation were collected every 20 s. For mitotic timing quantifications, 13 z-stacks with a 0.7-µm separation were collected every 2 min. For microtubule dynamics measurements, a single z-stack was collected every 500 ms.

5.6. Quantitative analysis of centrosomes, cell membrane, and nucleus membrane

Detailed quantitative analysis of centrosomes location and membranes topology (cell and nucleus) was performed using custom-made MATLAB scripts (MathWorks, USA; R2018a). The image analysis took advantage of the different labeling for centrosomes, cell membrane, and nuclear membrane. The scripts were separated into three modules with specific workflows: 1) centrosomes tracking and 2) nuclear and cellular membrane reconstruction. Tracking of centrosomes position/trajectories was performed in 3D space using image stacks with a pixel size of 0.190 µm and z-step of 0.7 µm. Images were preprocessed using a Laplacian of Gaussian filter with a user-defined kernel size, associated with the centrosome radius in pixels. Image segmentation was performed using Otsu's method, and morphological operators were used to improve the mask and obtain the centrosomes 3D coordinates. Error correction methods, such as automatic thresholding adjustment or in the limit frame elimination, were implemented to take care of frames where the standard method was unable to uniquely identify two centrosomes. For the visualization of the centrosomes trajectories (space and time), the centrosomes coordinates were interpolated using cubic splines. Different metrics, such as the distance between centrosomes (pole-to-pole), were calculated to analyze and characterize the trajectories. Cellular and nuclear membranes were reconstructed in 3D space taking advantage of specific labeling. For each membrane, a mask was produced using Otsu's method and improved with a sequence of morphological operators (namely image close, dilation and erosion, small objects removal). The orientation axis for the membranes were calculated using principal components analysis (PCA) of a large sample of membrane surface points. This method using PCA was found to be more robust than ellipsoid fitting to the membrane surface (followed by extraction of the axis vectors). From the centrosomes locations and

nuclear membrane reconstruction, it was possible to calculate the angle between the centrosomes axis and the nucleus major axis.

5.7. Preparation of micropatterned hydrogels with nanobeads

First, 32-mm coverslips were plasma cleaned for 30 s and then incubated with a drop of PLL-PEG 0.1 mg/ml in HEPES 10 mM, pH 7.4, for 30 min at RT as described previously [74]. Coverslips are then put upright to let the excess PLL-PEG run off and placed on a rectangle shape quartz photomask (Top-pan) on a 3-µl drop of MilliQ water. The coverslips on the photo-mask are then exposed to deep UV for 5 min. Then, coverslips are detached from the photomask and incubated with 20 µg/ml FBN (Sigma) and 20 µg/ml Alexa 546–conjugated fibrinogen (Invitrogen) in phosphate-buffered saline (PBS) for 30 min at RT. To prepare the gels, a 42-µl drop of a 40-KPa mix of polyacrylamide and bisacrylamide (Sigma) containing 0.1 µl carboxylate-modified polystyrene fluorescent beads (Invitrogen) is placed onto the FBN-coated coverslips and then covered with a second coverslip and pretreated with Bind-silane solution (100% ethanol solution containing 18.5 µl Bind Silane; GE Healthcare Life Science) and 161 µl 10% acetic acid (Sigma) for 5 min. Gels are polymerized for 30 min and finally the gel is retrieved with the silanized coverslip. FBN proteins are trapped within the acrylamide mesh. Gels are stored in PBS at 4°C.

5.8. TFM imaging and analyses

For TFM live-cell imaging, rectangle micropatterned coverslips are mounted in dedicated chambers and supplemented with L-15/10% FBS medium. A Leica SP8 confocal microscope was used to acquire the images using a 40× objective (oil immersion, numerical aperture 1.3) with a temperature control chamber set at 37°C. Cells were imaged every 3 min; 488- and 533-nm lasers were used in sequential scanning mode. All the laser parameters and imaging setups are controlled through the LAS X system. Cellular traction forces were calculated using a method previously described [75]. Briefly, at each time point, the image of the fluorescent beads embedded in the substrate was compared with a reference image corresponding to a relaxed substrate and taken after washing away the cells. After correcting for experimental drift, the displacement field was obtained by a two-step process consisting of cross-correlation on 9.6-µm subimages followed by particle tracking to improve the spatial resolution. The final displacement field was interpolated to a regular grid with 1.2-µm spacing. Traction stress reconstruction was performed with the assumption that the substrate is a linear elastic half-space using Fourier transform traction cytometry and zeroth order regularization. The stress map was defined on the same 1.2-µm-period grid. From this stress map and the cell mask, we checked that the out of equilibrium force is less than 10% of the sum of forces magnitude, as a quality criterion for

all cells and time points. The contractile energy, which is the mechanical energy transferred from the cell to the substrate, was computed from the traction map by integrating the scalar product of the displacement and stress vectors over the cell surface. To determine the principal direction of contraction of each cell, we calculated and diagonalized the first moment tensor of the stress. The eigenvector corresponding to the larger eigenvalue gives the direction of the main force dipole. The degree of force polarization is obtained by comparing both eigenvalues. All the calculations are performed in MATLAB (MathWorks, USA; R2018a).

5.9. Immunofluorescence

Cells were fixed with 4% PFA in cytoskeleton buffer (274 mM NaCl, 2.2 mM Na2HPO4, 10 mM KCL, 0.8 mM KH2PO4, 4 mM EDTA, 4 mM MgCl2, 10 mM Pipes, 10 nM glucose, pH 6.1) and subsequently permeabilized with 0.5% Triton X-100 (Sigma-Aldrich) in 1× PBS for 5 min. After washing in 0.1% Triton X-100, cells were blocked with 10% FBS in 0.1% Triton X-100 in PBS for 30 min. All the primary antibodies were diluted in blocking solution and incubated for 1 h at room temperature. After this incubation, the cells were washed with 0.1% Triton X-100 in 1× PBS and incubated with the respectively secondary antibody for 1 h at room temperature. The secondary antibodies were diluted in blocking solution. DNA was stained with DAPI, which was added to the secondary antibodies solution (1 µg/ml, Sigma-Aldrich). After incubation with the secondary antibodies and DAPI the cover-slips were washed with 0.1% Triton X-100 in 1× PBS and sealed on glass slides mounted with 20 mM Tris, pH 8, 0.5 N-propyl gallate, and 90% glycerol. The following primary antibodies were used: rat anti-alpha Tubulin (1:500 Bio-Rad) and pFAK(Y397) (1:100, Invitrogen). Alexa Fluor 488, 568, and 647 (1:2000, Invitrogen) were used as secondary antibodies. Where indicated, SiR-actin was used at a concentration of 20 nM (Spirochrome). Images were acquired using an AxioImager Z1 (63×, Plan oil differential interference con-tract objective lens, 1.4 NA; all from Carl Zeiss) which is coupled with a CCD camera (ORCA-R2; Hamamatsu Photonics) using the Zen software (Carl Zeiss).

5.10. Western blotting

HeLa cell extracts were collected after trypsinization and centrifuged at 1200 rpm for 5 min, washed, and resuspended in 30–50 µl of lysis buffer (NP-40, 20 nM HEPES/KOH, pH 7.9; 1 mM EDTA, pH 8; 1 mM EGTA; 150 mM NaCl; 0.5% NP40; 10% glycerol, 1:50 protease inhibitor; 1:100 Phenylmethylsulfonyl fluoride). The samples were then flash frozen in liquid nitrogen and kept on ice for 30 min. After centrifugation at 14,000 rpm for 8 min at 4°C, the supernatant was collected and protein concentration determined by the Bradford protein assay (Bio-Rad). The proteins were run on 7–15% SDS–PAGE gels (50

µg/lane) and transferred using the iBlot Gel Transfer Device (Thermo Scientific) to a nitrocellulose Hybond-C membrane. With the exception of DHC RNAi samples, all others were transferred using a wet blot apparatus for 3 h at 70 V, with constant amperage. Afterward, the membranes were blocked with 5% milk in Triphosphate-Buffered Saline (TBS) with 0.1% Tween-20 (TBS-T) for 1 h at room temperature. The primary antibodies used were: mouse anti-Nde1 (1:500, Abnova), rabbit anti-ARPC4 (1:500, Bethyl Laboratories), rabbit anti-BICD2 (1:250, Atlas Antibodies), mouse anti-Dynein intermediate chain 74.1 (1:1000, Merck), and rat anti-alpha tubulin (1:1000, Bio-Rad). All primary antibodies were incubated overnight at 4°C with shaking. After three washes in TBS-T, the membranes were incubated with the secondary antibody for 1 h at room temperature. The secondary antibodies used were anti-mouse-HRP and anti-rabbit-HRP at 1:5000. After several washes with TBS-T, the detection was performed with Clarity Western ECL Substrate (Bio-Rad).

5.11. Statistical analysis and data presentation

Each experiment was repeated independently at least three times and sample sizes are defined in each figure legend. We used three to six independent experiments or biologically independent samples for statistical analysis. For knockdown experiments, the knock-down efficiency of each experiment was measured by quantifying immunoblots. When data are represented as box-whisker plots, the box size represents 75% of the population and the line inside the box represents the median of the sample. The size of the bars (whiskers) represents the maximum (in the upper quartile) and the mini-mum (in the lower quartile) values. Statistical analysis for multiple group comparison was performed using a parametric one-way analysis of variance (ANOVA) when the samples had a normal distribu-tion. When the sample did not have a normal distribution, multiple group comparison was done using a nonparametric ANOVA (Kruskal–Wallis). All pairwise multiple comparisons were subsequently analyzed using either post-hoc Student–Newman–Keuls (parametric) or Dunn's (nonparametric) tests. When comparing only two experimental groups, a parametric t test was used when the sample had a normal distribution, or a nonparametric Mann–Whitney test was used for samples without normal distribution. Distribution normalities were assessed using the Kolmogorov–Smirnov test. No power calculations were used. All statistical analyses were per-formed using SigmaStat 3.5 (Systat Software).

6. References

[1] S.L. Prosser, L. Pelletier, Mitotic spindle assembly in animal cells: a fine balancing act, Nat Rev Mol Cell Biol. 18 (2017) 187–201. https://doi.org/10.1038/nrm.2016.162.

[2] C.M. Whitehead, R.J. Winkfein, J.B. Rattner, The relationship of HsEg5 and the actin cytoskeleton to centrosome separation, Cell Motil. Cytoskeleton. 35 (1996) 298–308. https://doi.org/10.1002/(SICI)1097-0169(1996)35:4<298::AID-CM3>3.0.CO;2-3.

[3] T.M. Kapoor, T.U. Mayer, M.L. Coughlin, T.J. Mitchison, Probing Spindle Assembly Mechanisms with Monastrol, a Small Molecule Inhibitor of the Mitotic Kinesin, Eg5, J Cell Biol. 150 (2000) 975–988.

[4] J. Rosenblatt, L.P. Cramer, B. Baum, K.M. McGee, Myosin II-dependent cortical movement is required for centrosome separation and positioning during mitotic spindle assembly, Cell. 117 (2004) 361–372. https://doi.org/10.1016/s0092-8674(04)00341-1.

[5] J. Cao, J. Crest, B. Fasulo, W. Sullivan, Cortical Actin Dynamics Facilitate Early-Stage Centrosome Separation, Current Biology. 20 (2010) 770–776. https://doi.org/10.1016/j.cub.2010.02.060.

[6] E.N. Cytrynbaum, J.M. Scholey, A. Mogilner, A Force Balance Model of Early Spindle Pole Separation in Drosophila Embryos, Biophysical Journal. 84 (2003) 757–769. https://doi.org/10.1016/S0006-3495(03)74895-4.

[7] M.E. Tanenbaum, R.H. Medema, Mechanisms of centrosome separation and bipolar spindle assembly, Dev Cell. 19 (2010) 797–806. https://doi.org/10.1016/j.devcel.2010.11.011.

[8] S. Bolhy, I. Bouhlel, E. Dultz, T. Nayak, M. Zuccolo, X. Gatti, R. Vallee, J. Ellenberg, V. Doye, A Nup133-dependent NPC-anchored network tethers centrosomes to the nuclear envelope in prophase, J Cell Biol. 192 (2011) 855–871. https://doi.org/10.1083/jcb.201007118.

[9] J.A. Raaijmakers, R.G.H.P. van Heesbeen, J.L. Meaders, E.F. Geers, B. Fernandez-Garcia, R.H. Medema, M.E. Tanenbaum, Nuclear envelope-associated dynein drives prophase centrosome separation and enables Eg5-independent bipolar spindle formation, The EMBO Journal. 31 (2012) 4179–4190. https://doi.org/10.1038/emboj.2012.272.

[10] A.D. Baffet, D.J. Hu, R.B. Vallee, Cdk1 Activates Pre-mitotic Nuclear Envelope Dynein Recruitment and Apical Nuclear Migration in Neural Stem Cells, Dev Cell. 33 (2015) 703–716. https://doi.org/10.1016/j.devcel.2015.04.022.

[11] A. De Simone, F. Nédélec, P. Gönczy, Dynein Transmits Polarized Actomyosin Cortical Flows to Promote Centrosome Separation, Cell Rep. 14 (2016) 2250–2262. https://doi.org/10.1016/j.celrep.2016.01.077.

[12] V. Boudreau, R. Chen, A. Edwards, M. Sulaimain, P.S. Maddox, PP2A-B55/SUR-6 collaborates with the nuclear lamina for centrosome separation during mitotic entry, Mol Biol Cell. 30 (2019) 876–886. https://doi.org/10.1091/mbc.E18-10-0631.

[13] V.T. Dao, A.G. Dupuy, O. Gavet, E. Caron, J. de Gunzburg, Dynamic changes in Rap1 activity are required for cell retraction and spreading during mitosis, J. Cell. Sci. 122 (2009) 2996–3004. https://doi.org/10.1242/jcs.041301.

[14] C.L. Dix, H.K. Matthews, M. Uroz, S. McLaren, L. Wolf, N. Heatley, Z. Win, P. Almada, R. Henriques, M. Boutros, X. Trepat, B. Baum, The Role of Mitotic Cell-Substrate Adhesion Re-modeling in Animal Cell Division, Developmental Cell. 45 (2018) 132-145.e3. https://doi.org/10.1016/j.devcel.2018.03.009.

[15] J.G. Lock, M.C. Jones, J.A. Askari, X. Gong, A. Oddone, H. Olofsson, S. Göransson, M. Lakadamyali, M.J. Humphries, S. Strömblad, Reticular adhesions are a distinct class of cell-matrix adhesions that mediate attachment during mitosis, Nature Cell Biology. 20 (2018) 1290–1302. https://doi.org/10.1038/s41556-018-0220-2.

[16] N. Mchedlishvili, H.K. Matthews, A. Corrigan, B. Baum, Two-step interphase microtubule disassembly aids spindle morphogenesis, BMC Biology. 16 (2018) 14. https://doi.org/10.1186/s12915-017-0478-z.

[17] N.M. Rusan, U.S. Tulu, C. Fagerstrom, P. Wadsworth, Reorganization of the microtubule array in prophase/prometaphase requires cytoplasmic dynein-dependent microtubule transport, J Cell Biol. 158 (2002) 997–1003. https://doi.org/10.1083/jcb.200204109.

[18] Y. Zhai, P.J. Kronebusch, P.M. Simon, G.G. Borisy, Microtubule dynamics at the G2/M transition: abrupt breakdown of cytoplasmic microtubules at nuclear envelope breakdown and implications for spindle morphogenesis., J Cell Biol. 135 (1996) 201–214. https://doi.org/10.1083/jcb.135.1.201.

[19] L.P. Cramer, T.J. Mitchison, Investigation of the mechanism of retraction of the cell margin and rearward flow of nodules during mitotic cell rounding, Mol. Biol. Cell. 8 (1997) 109–119. https://doi.org/10.1091/mbc.8.1.109.

[20] A.S. Maddox, K. Burridge, RhoA is required for cortical retraction and rigidity during mitotic cell rounding, Journal of Cell Biology. 160 (2003) 255–265. https://doi.org/10.1083/jcb.200207130.

[21] P. Kunda, A.E. Pelling, T. Liu, B. Baum, Moesin Controls Cortical Rigidity, Cell Rounding, and Spindle Morphogenesis during Mitosis, Current Biology. 18 (2008) 91–101. https://doi.org/10.1016/j.cub.2007.12.051.

[22] S. Carreno, I. Kouranti, E.S. Glusman, M.T. Fuller, A. Echard, F. Payre, Moesin and its activating kinase Slik are required for cortical stability and microtubule organization

in mitotic cells, Journal of Cell Biology. 180 (2008) 739–746. https://doi.org/10.1083/jcb.200709161.

[23] B.D. Matthews, C.K. Thodeti, J.D. Tytell, A. Mammoto, D.R. Overby, D.E. Ingber, Ultra-rapid activation of TRPV4 ion channels by mechanical forces applied to cell surface beta1 integrins, Integr Biol (Camb). 2 (2010) 435–442. https://doi.org/10.1039/c0ib00034e.

[24] P.-C. Chan, R.Y.C. Hsu, C.-W. Liu, C.-C. Lai, H.-C. Chen, Adducin-1 is essential for mitotic spindle assembly through its interaction with myosin-X, J Cell Biol. 204 (2014) 19–28. https://doi.org/10.1083/jcb.201306083.

[25] M. Plessner, J. Knerr, R. Grosse, Centrosomal Actin Assembly Is Required for Proper Mitotic Spindle Formation and Chromosome Congression, IScience. 15 (2019) 274–281. https://doi.org/10.1016/j.isci.2019.04.022.

[26] A.J. Booth, Z. Yue, J.K. Eykelenboom, T. Stiff, G.G. Luxton, H. Hochegger, T.U. Tanaka, Contractile acto-myosin network on nuclear envelope remnants positions human chromosomes for mitosis, ELife. 8 (2019) e46902. https://doi.org/10.7554/eLife.46902.

[27] F. Farina, J. Gaillard, C. Guérin, Y. Couté, J. Sillibourne, L. Blanchoin, M. Théry, The centrosome is an actin-organizing centre, Nature Cell Biology. 18 (2016) 65–75. https://doi.org/10.1038/ncb3285.

[28] F. Farina, N. Ramkumar, L. Brown, D. Samandar Eweis, J. Anstatt, T. Waring, J. Bithell, G. Scita, M. Thery, L. Blanchoin, T. Zech, B. Baum, Local actin nucleation tunes centrosomal microtubule nucleation during passage through mitosis, EMBO J. 38 (2019) e99843. https://doi.org/10.15252/embj.201899843.

[29] D. Inoue, D. Obino, J. Pineau, F. Farina, J. Gaillard, C. Guerin, L. Blanchoin, A.-M. Lennon-Duménil, M. Théry, Actin filaments regulate microtubule growth at the centrosome, The EMBO Journal. 38 (2019) e99630. https://doi.org/10.15252/embj.201899630.

[30] M. Théry, V. Racine, A. Pépin, M. Piel, Y. Chen, J.-B. Sibarita, M. Bornens, The extracellular matrix guides the orientation of the cell division axis, Nature Cell Biology. 7 (2005) 947–953. https://doi.org/10.1038/ncb1307.

[31] M. Théry, A. Jiménez-Dalmaroni, V. Racine, M. Bornens, F. Jülicher, Experimental and theoretical study of mitotic spindle orientation, Nature. 447 (2007) 493–496. https://doi.org/10.1038/nature05786.

[32] T. Kiyomitsu, I.M. Cheeseman, Chromosome- and spindle-pole-derived signals generate an intrinsic code for spindle position and orientation, Nat. Cell Biol. 14 (2012) 311–317. https://doi.org/10.1038/ncb2440.

[33] S. Kotak, C. Busso, P. Gönczy, Cortical dynein is critical for proper spindle positioning in human cells, J Cell Biol. 199 (2012) 97–110. https://doi.org/10.1083/jcb.201203166.

[34] J. Fink, N. Carpi, T. Betz, A. Bétard, M. Chebah, A. Azioune, M. Bornens, C. Sykes, L. Fetler, D. Cuvelier, M. Piel, External forces control mitotic spindle positioning, Nature Cell Biology. 13 (2011) 771–778. https://doi.org/10.1038/ncb2269.

[35] S.W. Grill, A.A. Hyman, Spindle Positioning by Cortical Pulling Forces, Developmental Cell. 8 (2005) 461–465. https://doi.org/10.1016/j.devcel.2005.03.014.

[36] S.W. Grill, J. Howard, E. Schäffer, E.H.K. Stelzer, A.A. Hyman, The Distribution of Active Force Generators Controls Mitotic Spindle Position, Science. 301 (2003) 518–521. https://doi.org/10.1126/science.1086560.

[37] F. Bosveld, O. Markova, B. Guirao, C. Martin, Z. Wang, A. Pierre, M. Balakireva, I. Gaugue, A. Ainslie, N. Christophorou, D.K. Lubensky, N. Minc, Y. Bellaïche, Epithelial tricellular junctions act as interphase cell shape sensors to orient mitosis, Nature. 530 (2016) 495–498. https://doi.org/10.1038/nature16970.

[38] O. Hertwig, Das Problem der Befruchtung und der Isotropie des Eies: eine Theorie der Vererbung, Fischer, 1884.

[39] K. Kaseda, A.D. McAinsh, R.A. Cross, Dual pathway spindle assembly increases both the speed and the fidelity of mitosis, Biology Open. 1 (2012) 12–18. https://doi.org/10.1242/bio.2011012.

[40] W.T. Silkworth, I.K. Nardi, R. Paul, A. Mogilner, D. Cimini, Timing of centrosome separation is important for accurate chromosome segregation, Mol Biol Cell. 23 (2012) 401–411. https://doi.org/10.1091/mbc.E11-02-0095.

[41] H.K. Matthews, U. Delabre, J.L. Rohn, J. Guck, P. Kunda, B. Baum, Changes in Ect2 Localization Couple Actomyosin-Dependent Cell Shape Changes to Mitotic Progression, Developmental Cell. 23 (2012) 371–383. https://doi.org/10.1016/j.devcel.2012.06.003.

[42] R.G.H.P. van Heesbeen, J.A. Raaijmakers, M.E. Tanenbaum, R.H. Medema, Nuclear envelope-associated dynein cooperates with Eg5 to drive prophase centrosome separation, Commun Integr Biol. 6 (2013). https://doi.org/10.4161/cib.23841.

[43] W. Wang, L. Chen, Y. Ding, J. Jin, K. Liao, Centrosome separation driven by actin-microfilaments during mitosis is mediated by centrosome-associated tyrosine-phosphorylated cortactin, J Cell Sci. 121 (2008) 1334–1343. https://doi.org/10.1242/jcs.018176.

[44] F. Winkler, M. Gummalla, L. Künneke, Z. Lv, A. Zippelius, T. Aspelmeier, J. Grosshans, Fluctuation Analysis of Centrosomes Reveals a Cortical Function of Kinesin-1, Biophys J. 109 (2015) 856–868. https://doi.org/10.1016/j.bpj.2015.07.044.

[45] D. Splinter, M.E. Tanenbaum, A. Lindqvist, D. Jaarsma, A. Flotho, K.L. Yu, I. Grigoriev, D. Engelsma, E.D. Haasdijk, N. Keijzer, J. Demmers, M. Fornerod, F. Melchior, C.C. Hoogenraad, R.H. Medema, A. Akhmanova, Bicaudal D2, dynein, and kinesin-1 associate with nuclear pore complexes and regulate centrosome and nuclear positioning during mitotic entry, PLoS Biol. 8 (2010) e1000350. https://doi.org/10.1371/journal.pbio.1000350.

[46] D.J.-K. Hu, A.D. Baffet, T. Nayak, A. Akhmanova, V. Doye, R.B. Vallee, Dynein Recruitment to Nuclear Pores Activates Apical Nuclear Migration and Mitotic Entry in Brain Progenitor Cells, Cell. 154 (2013) 1300–1313. https://doi.org/10.1016/j.cell.2013.08.024.

[47] G.E. Woodard, N.-N. Huang, H. Cho, T. Miki, G.G. Tall, J.H. Kehrl, Ric-8A and Gi alpha recruit LGN, NuMA, and dynein to the cell cortex to help orient the mitotic spindle, Mol Cell Biol. 30 (2010) 3519–3530. https://doi.org/10.1128/MCB.00394-10.

[48] A. Kumar, A. Maitra, M. Sumit, S. Ramaswamy, G.V. Shivashankar, Actomyosin contractility rotates the cell nucleus, Sci Rep. 4 (2014) 3781. https://doi.org/10.1038/srep03781.

[49] A. Colin, P. Singaravelu, M. Théry, L. Blanchoin, Z. Gueroui, Actin-Network Architecture Regulates Microtubule Dynamics, Current Biology. 28 (2018) 2647-2656.e4. https://doi.org/10.1016/j.cub.2018.06.028.

[50] K.T. Applegate, S. Besson, A. Matov, M.H. Bagonis, K. Jaqaman, G. Danuser, plusTipTracker: Quantitative image analysis software for the measurement of microtubule dynamics, J Struct Biol. 176 (2011) 168–184. https://doi.org/10.1016/j.jsb.2011.07.009.

[51] J.C. Waters, R.H. Chen, A.W. Murray, E.D. Salmon, Localization of Mad2 to kinetochores depends on microtubule attachment, not tension, J Cell Biol. 141 (1998) 1181–1191. https://doi.org/10.1083/jcb.141.5.1181.

[52] S. Marchesi, F. Montani, G. Deflorian, R. D'Antuono, A. Cuomo, S. Bologna, C. Mazzoccoli, T. Bonaldi, P.P. Di Fiore, F. Nicassio, DEPDC1B coordinates de-adhesion events and cell-cycle progression at mitosis, Dev. Cell. 31 (2014) 420–433. https://doi.org/10.1016/j.devcel.2014.09.009.

[53] O.M. Lancaster, M. Le Berre, A. Dimitracopoulos, D. Bonazzi, E. Zlotek-Zlotkiewicz, R. Picone, T. Duke, M. Piel, B. Baum, Mitotic rounding alters cell geometry to ensure efficient bipolar spindle formation, Dev Cell. 25 (2013) 270–283. https://doi.org/10.1016/j.devcel.2013.03.014.

[54] J. Beaudouin, D. Gerlich, N. Daigle, R. Eils, J. Ellenberg, Nuclear Envelope Breakdown Proceeds by Microtubule-Induced Tearing of the Lamina, Cell. 108 (2002) 83–96. https://doi.org/10.1016/S0092-8674(01)00627-4.

[55] D. Salina, K. Bodoor, D.M. Eckley, T.A. Schroer, J.B. Rattner, B. Burke, Cytoplasmic Dynein as a Facilitator of Nuclear Envelope Breakdown, Cell. 108 (2002) 97–107. https://doi.org/10.1016/S0092-8674(01)00628-6.

[56] P. Chugh, A.G. Clark, M.B. Smith, D.A.D. Cassani, K. Dierkes, A. Ragab, P.P. Roux, G. Charras, G. Salbreux, E.K. Paluch, Actin cortex architecture regulates cell surface tension, Nat Cell Biol. 19 (2017) 689–697. https://doi.org/10.1038/ncb3525.

[57] C.M. Pomerat, Rotating nuclei in tissue cultures of adult human nasal mucosa, Experimental Cell Research. 5 (1953) 191–196. https://doi.org/10.1016/0014-4827(53)90104-9.

[58] J.R. Levy, E.L.F. Holzbaur, Dynein drives nuclear rotation during forward progression of motile fibroblasts, Journal of Cell Science. 121 (2008) 3187–3195. https://doi.org/10.1242/jcs.033878.

[59] J. Wu, K.C. Lee, R.B. Dickinson, T.P. Lele, How dynein and microtubules rotate the nucleus, Journal of Cellular Physiology. 226 (2011) 2666–2674. https://doi.org/10.1002/jcp.22616.

[60] A.G. Hendricks, J.E. Lazarus, E. Perlson, M.K. Gardner, D.J. Odde, Y.E. Goldman, E.L.F. Holzbaur, Dynein Tethers and Stabilizes Dynamic Microtubule Plus-Ends, Curr Biol. 22 (2012) 632–637. https://doi.org/10.1016/j.cub.2012.02.023.

[61] M. Versaevel, T. Grevesse, S. Gabriele, Spatial coordination between cell and nuclear shape within micropatterned endothelial cells, Nature Communications. 3 (2012) 671. https://doi.org/10.1038/ncomms1668.

[62] F. Toyoshima, E. Nishida, Integrin-mediated adhesion orients the spindle parallel to the substratum in an EB1- and myosin X-dependent manner, EMBO J. 26 (2007) 1487–1498. https://doi.org/10.1038/sj.emboj.7601599.

[63] S.P. Ramanathan, J. Helenius, M.P. Stewart, C.J. Cattin, A.A. Hyman, D.J. Muller, Cdk1-dependent mitotic enrichment of cortical myosin II promotes cell rounding against confinement, Nature Cell Biology. 17 (2015) 148–159. https://doi.org/10.1038/ncb3098.

[64] A. Rosa, E. Vlassaks, F. Pichaud, B. Baum, Ect2/Pbl Acts via Rho and Polarity Proteins to Direct the Assembly of an Isotropic Actomyosin Cortex upon Mitotic Entry, Developmental Cell. 32 (2015) 604–616. https://doi.org/10.1016/j.devcel.2015.01.012.

[65] M.W. Kirschner, T. Mitchison, Microtubule dynamics, Nature. 324 (1986) 621–621. https://doi.org/10.1038/324621a0.

[66] R. Wollman, E.N. Cytrynbaum, J.T. Jones, T. Meyer, J.M. Scholey, A. Mogilner, Efficient chromosome capture requires a bias in the “search-and-capture” process during mitotic-spindle assembly, Curr Biol. 15 (2005) 828–832. https://doi.org/10.1016/j.cub.2005.03.019.

[67] H. Maiato, C.L. Rieder, A. Khodjakov, Kinetochore-driven formation of kinetochore fibers contributes to spindle assembly during animal mitosis, Journal of Cell Biology. 167 (2004) 831–840. https://doi.org/10.1083/jcb.200407090.

[68] V. Magidson, R. Paul, N. Yang, J.G. Ault, C.B. O’Connell, I. Tikhonenko, B.F. McEwen, A. Mogilner, A. Khodjakov, Adaptive changes in the kinetochore architecture facilitate proper spindle assembly, Nat Cell Biol. 17 (2015) 1134–1144. https://doi.org/10.1038/ncb3223.

[69] R. Paul, R. Wollman, W.T. Silkworth, I.K. Nardi, D. Cimini, A. Mogilner, Computer simulations predict that chromosome movements and rotations accelerate mitotic spindle assembly without compromising accuracy, PNAS. 106 (2009) 15708–15713. https://doi.org/10.1073/pnas.0908261106.

[70] V. Magidson, C.B. O’Connell, J. Lončarek, R. Paul, A. Mogilner, A. Khodjakov, The Spatial Arrangement of Chromosomes during Prometaphase Facilitates Spindle Assembly, Cell. 146 (2011) 555–567. https://doi.org/10.1016/j.cell.2011.07.012.

[71] A. Toso, J.R. Winter, A.J. Garrod, A.C. Amaro, P. Meraldi, A.D. McAinsh, Kinetochore-generated pushing forces separate centrosomes during bipolar spindle assembly, J Cell Biol. 184 (2009) 365–372. https://doi.org/10.1083/jcb.200809055.

[72] N. Schweizer, C. Ferrás, D.M. Kern, E. Logarinho, I.M. Cheeseman, H. Maiato, Spindle assembly checkpoint robustness requires Tpr-mediated regulation of Mad1/Mad2 proteostasis, Journal of Cell Biology. 203 (2013) 883–893. https://doi.org/10.1083/jcb.201309076.

[73] A. Azioune, M. Storch, M. Bornens, M. Théry, M. Piel, Simple and rapid process for single cell micro-patterning, Lab Chip. 9 (2009) 1640–1642. https://doi.org/10.1039/b821581m.

[74] T. Vignaud, H. Ennomani, M. Théry, Polyacrylamide hydrogel micropatterning, Methods Cell Biol. 120 (2014) 93–116. https://doi.org/10.1016/B978-0-12-417136-7.00006-9.

[75] K. Mandal, I. Wang, E. Vitiello, L.A.C. Orellana, M. Balland, Cell dipole behaviour revealed by ECM sub-cellular geometry, Nat Commun. 5 (2014) 5749. https://doi.org/10.1038/ncomms6749.

7. Supplementary Figures

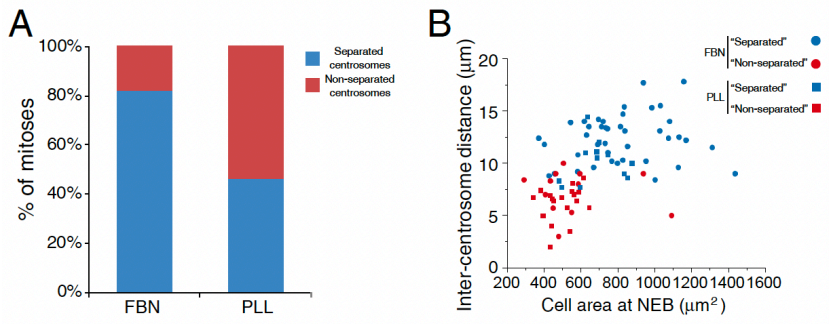


Figure S1: Effect of substrate coating on centrosome separation efficiency, related to Figure 1. **(A)** HeLa cells expressing H2B-GFP/mRFP-alpha-tubulin were seeded either on FBN (*n=59*) or PLL (*n=41*) and imaged to determine whether they separated ("Separated") or not ("Nonseparated") their centrosomes during mitotic entry. **(B)** Correlation between inter-centrosome distance (µm) and cell area at NEB (µm^2) for cells seeded in FBN or PLL, taking into account their centrosome separation pathway. Cells with decreased area have lower inter-centrosome distances.

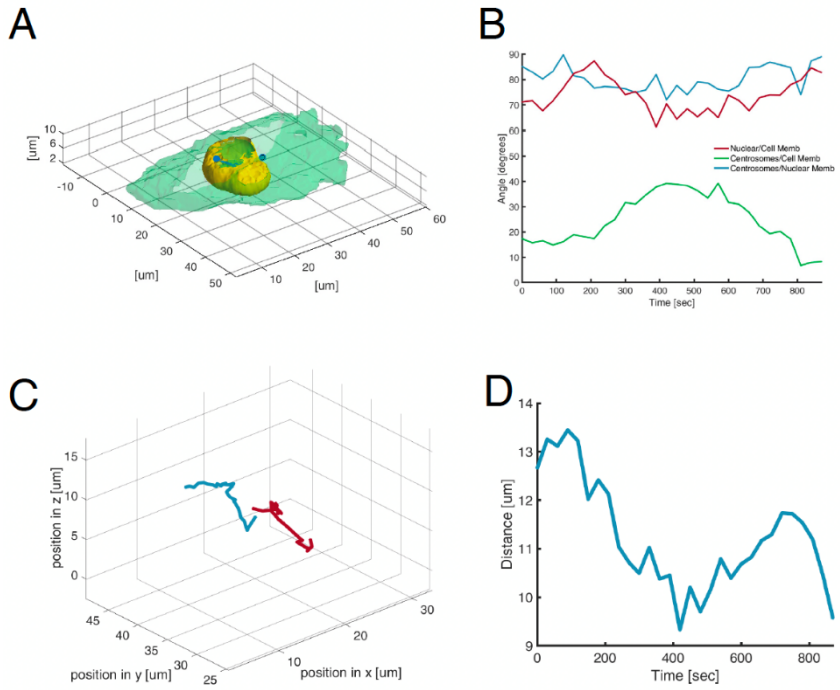


Figure S2: Computational analysis of centrosomes, cell shape and nuclear shape, related to Figure 1. **(A)** Representative reconstruction of HeLa cell seeded on a line micropattern, showing centrosomes (blue), nucleus (yellow) and cell membrane (green). Centrosomes are connected by a vector that runs through the nucleus centroid. **(B)** Plot quantifying angles between centrosomes/nucleus long axis (green), centrosomes/cell membrane (blue) and cell membrane/nucleus (red) over time. **(C)** Representative 4D reconstruction of centrosomes trajectories. **(D)** Representative plot showing pole-to-pole distance over time.

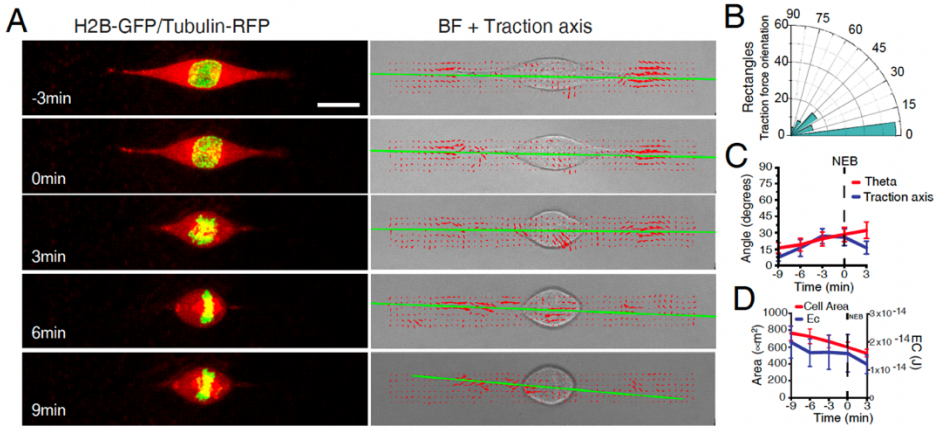


Figure S3: Cell rounding changes the forces exerted by cells on the substrate, related to Figure 4. **(A)** Frames from a movie of a HeLa cell expressing H2B-GFP/alpha-tubulin-RFP (left panel) seeded on a PAA hydrogel with a rectangle micropattern. Right panel corresponds to brightfield (BF) image overlaid with the corresponding traction force map (red arrows). Green line corresponds to the main direction of the force dipole. Time is in min. NEB = 0min. **(B)** Traction force orientation for cells on rectangles (*n=14*). **(C)** Correlation between centrosome orientation axis (theta; red) and traction axis (blue). Lines corresponds to average values. Error bars correspond to SEM. **(D)** Correlation between contractile energy (EC; blue) and cell area (red) for cells seeded on rectangles. Lines corresponds to average values. Error bars correspond to SEM.

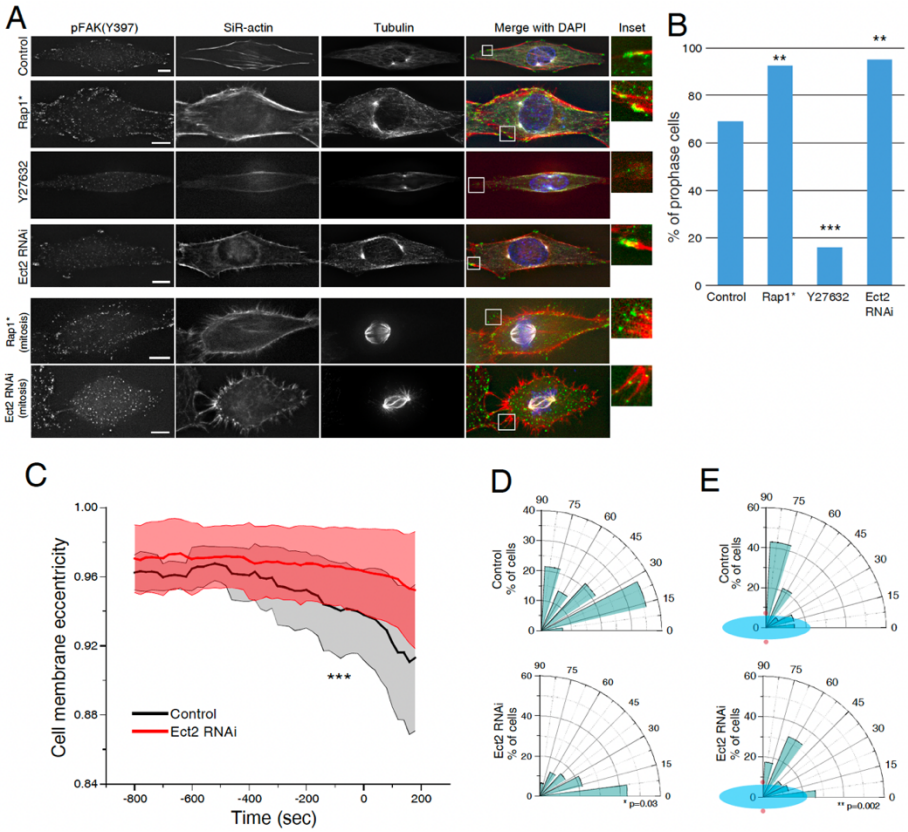


Figure S4: Adhesion disassembly is required for centrosome positioning on the shortest nuclear axis, related to Figure 4. **(A)** Immunofluorescence images of pFAK(Y397), SiR-actin, alpha-tubulin and DAPI for controls (*n=29*), Rap1* (*n=53; **p=0.002*), Y27632 (*n=50; ***p<0.001*) and Ect2 RNAi (*n=40; **p<0.003*). Scale

bars, 10µm. Insets show pFAK(Y397) in green and SiRactin in red. **(B)** Quantification of the percentage of prophase cells with focal adhesions. **(C)** Cell membrane eccentricity for controls (*n=16*) and Ect2 RNAi (*n=66; *** p<0.001*). **(D)** Polar plot quantifying alignment of the long nuclear axis with the long cell axis at NEB for Controls and Ect2 RNAi (** p=0.03*). **(E)** Polar plot quantifying centrosome positioning (red circles) relative to the longest nuclear axis (blue ellipse) at NEB for controls and Ect2 RNAi cells (*** p=0.002*).

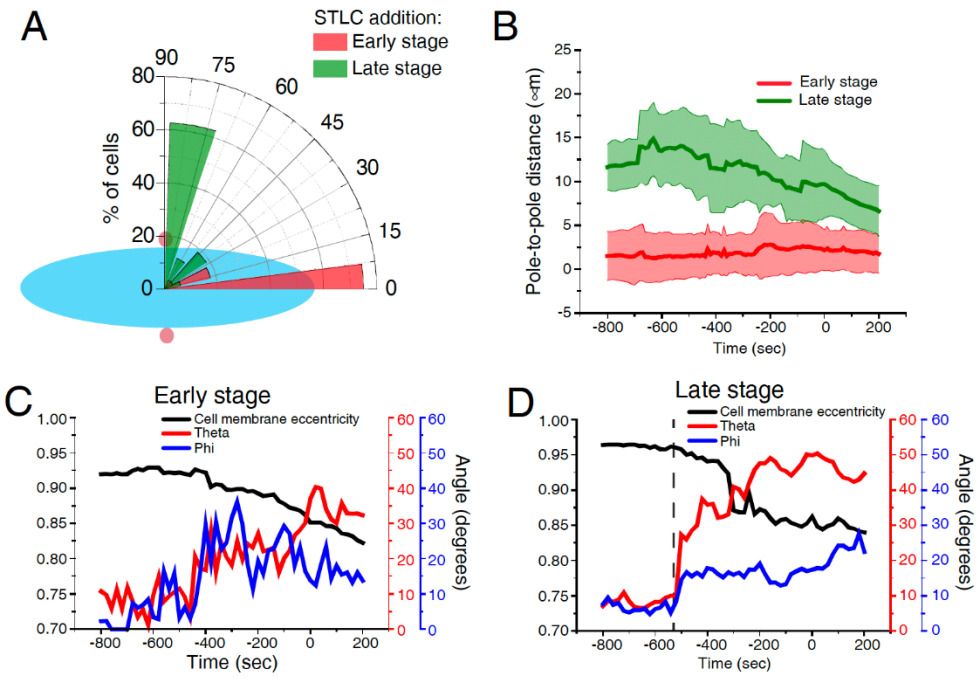


Figure S5: Eg5 is required for early centrosome separation but not centrosome positioning, related to Figure 5. **(A)** Polar plot quantifying centrosome positioning (red circles) relative to the longest nuclear axis (blue ellipse) at NEB for cells treated with STLC when centrosomes were already on opposite sides of the nucleus (Late stage; green; *n=12*) or when centrosomes were still not completely separated (Early stage; red; *n=30*). **(B)** Inter-centrosome distance for cells treated with STLC in either the Early stage (red) or the Late stage (green) of centrosome separation. Note how intercentrosome distance only decreases in Late stage cells when cell rounding begins (~550sec before NEB). Lines correspond to averages and shaded areas correspond to SD. Correlation between the average theta values (red; corresponding to centrosomes xy orientation), average phi values (blue; corresponding to centrosomes z orientation) and cell membrane eccentricity (black) for cells in early **(C)** or late **(D)** stage of centrosome separation. The long axis of the micropattern was oriented horizontally and defined as a reference point, corresponding to a value of zero for theta and phi.

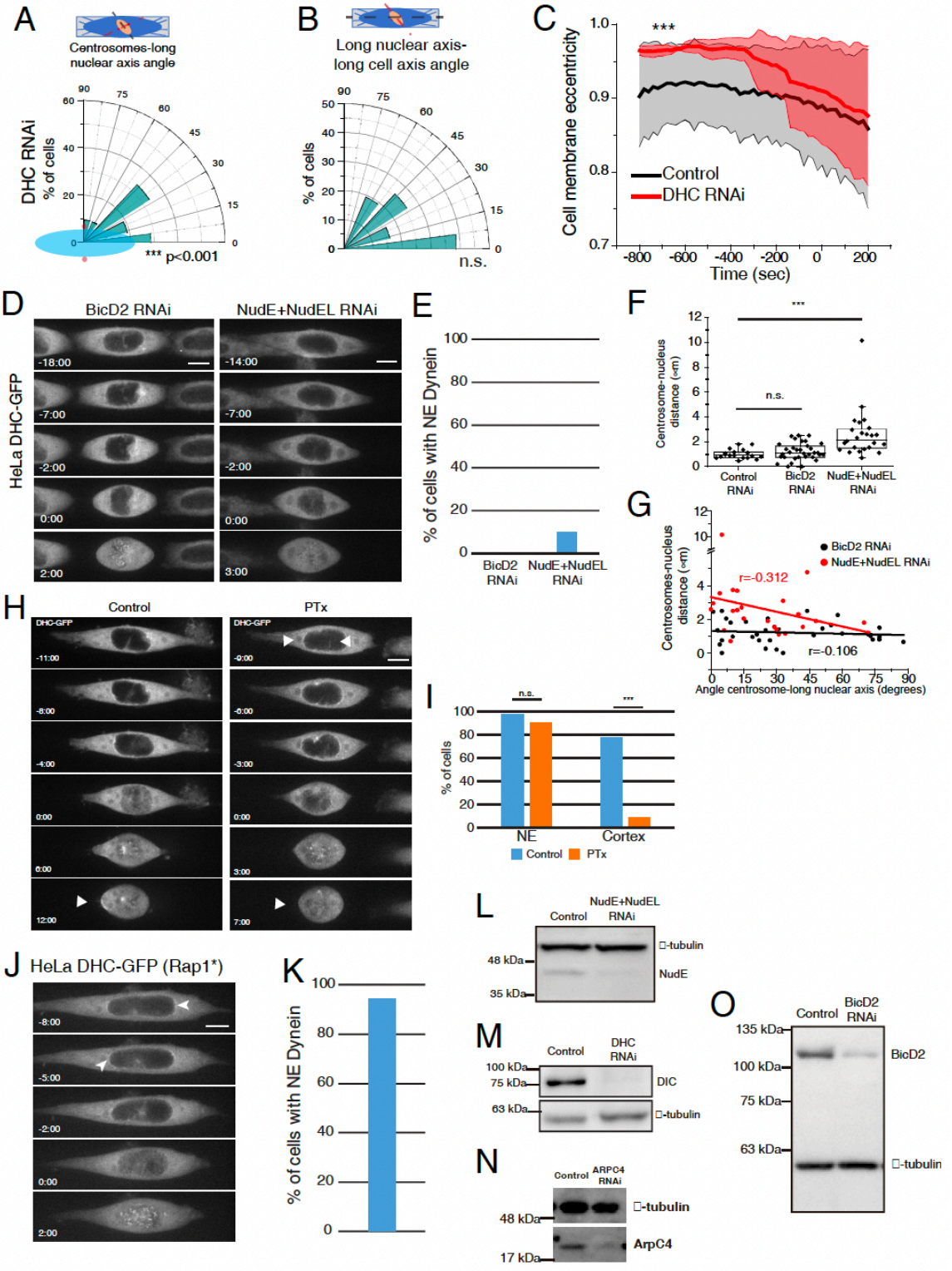


Figure S6: Nuclear envelope Dynein is required for centrosome positioning, related to Figure 5. Polar plots for DHC RNAi-treated cells (*n=21*) quantifying centrosome positioning (red circles) relative to the longest nuclear (**A**; *** *p<0.001*) or alignment of the long nuclear axis with the long cell axis **(B)** at NEB. **(C)** Cell membrane eccentricity for controls and DHC RNAi-treated cells. Line correspond to averages and shaded areas correspond to SD (****p<0.001*). **(D)** Representative images of cells expressing DHC-GFP treated with BicD2 (*n=11*) or NudE+NudEL RNAi (*n=10*). **(E)** Quantification of the percentage of cells with NE Dynein. **(F)**

Quantification of centrosome-nucleus distance (µm) for controls (*n=18*), BicD2 RNAi (*n=33*) and NudE+NudEL RNAi (*n=24; *p<0.05*). **(G)** Correlation between the centrosomes-long nuclear axis angle and the centrosome nucleus distance. Note the lack of correlation between the two variables (r=-0.312 for NudE+NudEL RNAi and r=-0.106 for BicD2 RNAi). **(H)** Representative images of HeLa DHCGFP control cells (left panel; *n=27*) or treated with PTx (right panel; *n=11*) during mitotic entry. Note how PTx specifically abolishes DHC accumulation on the cell cortex (white arrowhead; *** *p<0.001*). **(I)** Quantification of the percentage of cells showing DHC accumulation on the NE and cell cortex. **(J)** Representative images of a cell expressing DHC-GFP and Rap1*. **(K)** Quantification of the percentage of cells expressing Rap1* with NE Dynein. Scale bars, 10µm. Time-lapse is 20sec. Time is in min:sec. Representative immunoblots to confirm depletion efficiency by RNAi of NudE+NudEL **(L)**, DHC **(M)**, ArpC4 **(N)** BicD2 **(O)**.

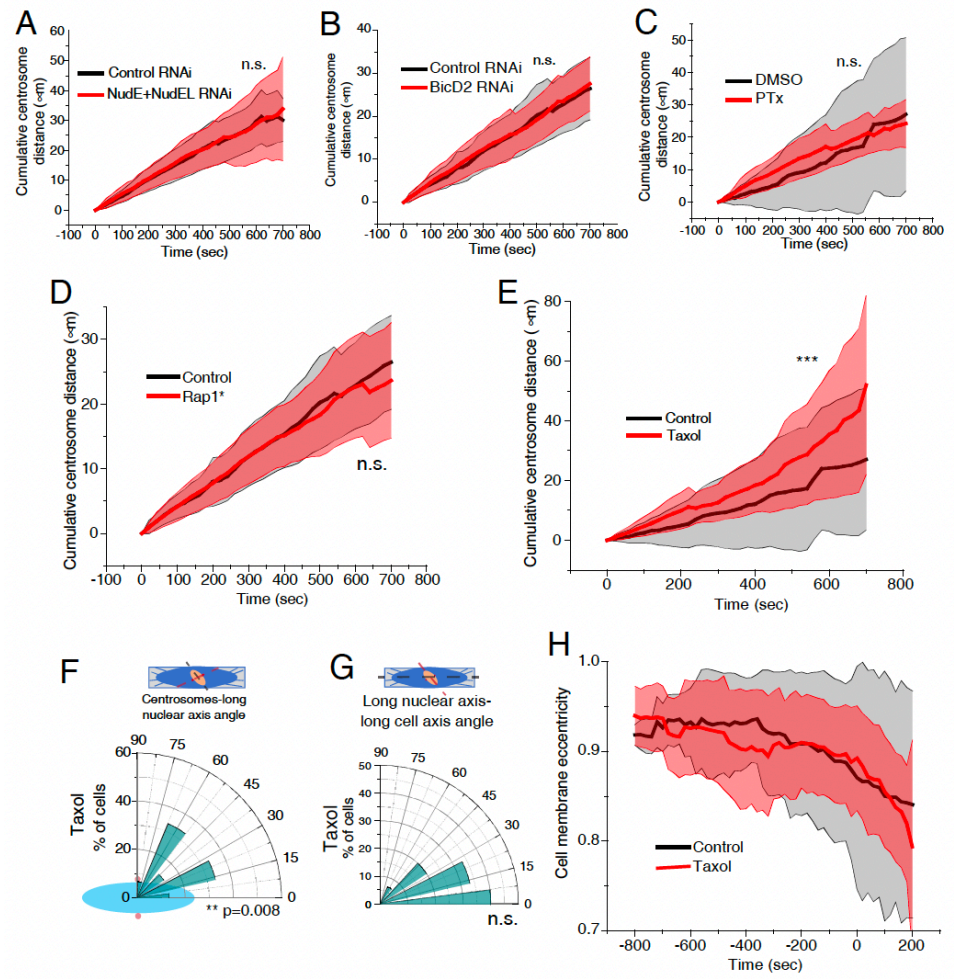


Figure S7: Microtubule stabilization affects centrosome positioning, related to Figure 6. Quantification of centrosome distance over time for controls and BicD2 **(A)**, NudE+NudEL RNAi **(B)**, PTx **(C)**, Rap1* **(D)** and Taxol-treated cells (**E**; ****p<0.001*). Polar plots for Taxol-treated cells quantifying centrosome positioning (red circles) relative to the longest nuclear (**F**; ** *p=0.008*) or alignment of the long nuclear axis with the long cell axis **(G)** at NEB. **(H)** Cell membrane eccentricity for controls and Taxol-treated cells. Line correspond to averages and shaded areas correspond to SD.

CHAPTER III

A mechanical signal regulates Dynein on the nuclear envelope

The content of this chapter is currently in preparation for submission.

V. Nunes, D. Castro, M. Dantas, M. Piel, P. Aguiar, H. Maiato, J.G. Ferreira, A mechanical signal regulates Dynein on the nuclear envelope, *In preparation for submission.*

Abbreviations

BicD2	Bicaudal D2
CDK1	Cyclin-Dependent Kinase 1
DMEM	Dulbecco's Modified Eagle Medium
ECM	Extracellular Matrix
ER	Endoplasmic Reticulum
FBN	Fibronectin
FBS	Fetal Bovine Serum
FT	Fourier transform
HDAC	Histone Deacetylase
INM	Inner Nuclear Membrane
LINC	Linker of Nucleoskeleton and Cytoskeleton
NE	Nuclear Envelope
NEP	Nuclear Envelope Permeabilization
NL	Nuclear Lamina
Noco	Nocodozole
NPC	Nuclear Pore Complex
PBS	Phosphate-Buffered Saline
PCA	Principal Components Analysis
PDMS	Polydimethylsiloxane
PFA	Paraformaldehyde
PPL	Poly-L-lysine
RT	Room Temperature
SAFs	Spindle Assembly Factors
siRNAs	Small Interfering RNAs
TBS	Triphosphate-Buffered Saline
TBS-T	Triphosphate-Buffered Saline with 0.1% Tween-20
TOPOII	Topoisomerase II
VPA	Valproic Acid

A mechanical signal regulates Dynein loading on the nuclear envelope

1. Abstract

Increasing evidence shows that the nucleus is an active player during mitotic entry. Accordingly, chromosomes and other nucleus-associated components, which directly contribute for mitotic spindle assembly, also regulate nuclear mechanics. Importantly, in preparation for mitosis, cells undergo an extensive cytoplasmic and nuclear reorganization. These nuclear modifications are expected to elicit changes in the mechanical properties of the nucleus.

To address how these changes directly impact early spindle assembly, we followed mitotic entry in cells with compromised nuclear organization and structure, measured nuclear envelope (NE) fluctuations and extracted high-resolution quantitative data for both centrosome and nucleus-related metrics. Our results allow us to propose a model where mitotic chromosome condensation increases intranuclear stiffness. This increased stiffness is transmitted by telomeres to SUN proteins at NE. In turn, this SUN protein-mediated strain on the nucleus is transmitted to the Bicaudal D2 (BicD2) and NudE/NudEL pathways, triggering Dynein loading to the NE. This recruitment of Dynein then ensures centrosome-NE tethering and correct centrosome positioning on the shortest nuclear axis, at nuclear envelope permeabilization (NEP). We propose that during the transition from G2 to mitosis, a mechanical signaling pathway triggered by chromosome condensation aids to set the time for mitotic entry and coordinate cytoplasmic and nuclear events.

2. Introduction

The transition from G2 to mitosis (G2-M) encompasses an extensive cytoplasmic and nuclear reorganization [1]. Cytoplasmic changes involve a rearrangement in the microtubule cytoskeleton, reflected in a decrease in interphase microtubule stability [2] and an enhancement of centrosome-mediated microtubule nucleation [3]. Globally, these modifications allow centrosomes to nucleate a radial array of microtubules and separate along the NE to originate the spindle poles [4]. Simultaneously, cells also round up, a phenomenon known as “mitotic cell rounding” [5]. This involves a temporary disassembly of their adhesion complexes [6,7], retraction of cell margins [8,9], assembly of an actomyosin cortex [10–14], and osmotic swelling [15,16]. One of the most distinctive features of this cytoskeletal organization is the separation of the duplicated centrosomes. In fact, initial separation is known to be aided by mitotic cell rounding [5,27,28] and the actomyosin cytoskeleton [29,30], and is driven by the combined action of molecular motors

[31–33], and microtubules [34,35]. During metaphase, separated centrosomes are positioned according to external cues that recruit force generators the cell cortex, and generate forces on astral microtubules [36–39]. However, we have recently shown that in earlier stages of mitosis, centrosomes do not follow external cues but follow internal signals to position on the shortest nuclear axis [28]. This centrosome configuration at NEP suggests that, in addition to the cues provided by the cytoskeleton and the extracellular microenvironment, intrinsic nuclear cues might be guiding centrosome separation and positioning in the beginning of mitosis.

Modifications in nuclear organization and structure also occur during mitotic entry, along with the described cytoplasmic events. In fact, as cells progress into mitosis, chromatin compaction changes significantly [17,18], a process dependent on several factors including histones post-translational modifications, topoisomerase II (TOPOII) activity, as well as association of condensin I and II complexes with mitotic chromosomes [17,18]. Importantly, the process of chromosome condensation is reversible until NEP. Therefore, NEP is considered the crucial step for the irreversible commitment to mitosis [19]. Another essential nuclear modification is NE disassembly. Although not completely understood, this process comprises three coordinated events: the disassembly of nuclear pore complexes (NPC; [20,21]), the depolymerization of the nuclear lamina (NL), with corresponding solubilization of A-type lamins into the nucleoplasm and removal of B-type lamins to the endoplasmic reticulum (ER; [1,22]), and finally, microtubule- and dynein-mediated fenestration of the NE [23,24]. Driving all these modifications is a complex network of signaling cascades under the regulation of cyclin-dependent kinase 1 (CDK1; [25]), which ensures the coordination between cytoplasmic and nuclear processes [26].

Increasing evidence points toward nucleus-associated components, such as the NL [40–42] and the Linker of Nucleoskeleton and Cytoskeleton (LINC) complex [43], as having an important role on early spindle assembly. In fact, it has been shown that Lamin B is a constitutive component of a spindle-associated matrix that tethers numerous spindle assembly factors (SAFs) promoting microtubule assembly and organization [42]. In addition, Lamin A/C, together with BAF and LAP2α, were shown to bind to actomyosin filaments and Dynein on the cell cortex in order to properly position the mitotic spindle [41]. Moreover, depleting lamins triggered defects in spindle assembly [40]. On the other hand, the LINC complex, was proposed to mediate nucleus-centrosome tethering and help in NEP [43]. Moreover, co-depletion of SUN1 and SUN2, components of the LINC complex that are located on the inner nuclear membrane (INM) and interact with lamins and chromatin, impairs NEP, ultimately leading to mitotic spindle defects [44]. Taken together, these observations suggest that changing the organization of the NE impact early spindle assembly.

Currently, it is becoming increasingly clear that many cellular processes are, to some extent, mechanically regulated. In fact, nuclear mechanics appear to directly assist in cell cycle progression [45–48], in particular during G2-M transition [49]. Interestingly, the NL and chromatin, which are extensively remodeled during mitotic entry, jointly regulate nuclear mechanics [50]. Previous studies demonstrate that chromatin condensation or Lamin A/C overexpression increase nuclear stiffness [51–54]. On the other hand, chromatin decompaction, histone hypermethylation or Lamin A/C depletion were shown to decrease nuclear rigidity and induce nuclear blebbing [55–59]. Importantly, lamins themselves, by tethering chromatin to the NE, are required for the organization of chromatin [60–64]. Alongside with lamins and INM proteins, telomeres appear to play an important role in the organization of the chromatin at the NE. In fact, in mammalian cells, telomere tethering at the NE has been proposed to aid in chromatin organization both in the beginning of meiosis [65] as in the end of mitosis [66]. How nuclear mechanics impacts centrosome separation and early spindle assembly during the G2-M transition has not been addressed yet.

In this study, we addressed how the modifications in nuclear organization and structure that occur during the G2-M transition impact centrosome separation and early spindle assembly. We found that mitotic chromosome condensation provides a mechanical cue required for Dynein loading on the NE. This mechanical signal involves chromosome coupling to the NE via the telomeres, which is transmitted to SUN1 and SUN2 at the NE, triggering NE-Dynein loading.

3. Results

3.1. Characterization of nucleus behavior during mitotic entry

We started by performing a detailed characterization of the cell and nuclear changes that occur in preparation for mitosis. We followed mitotic entry in HeLa cells expressing H2B-GFP/Tubulin-RFP seeded on 10 μm line-micropatterns using high-resolution live-cell imaging (Fig 1A). These micropatterns induce a highly reproducible cell shape polarization, with well-defined long cell and nuclear axes, allowing us to track dynamic changes in cell and nuclear shape relative to the micropattern. We then performed 3D cellular reconstructions (Fig. 1A') and extracted nuclear shape and orientation metrics (Fig. 1B and C), using a previously developed tool, Trackosome [67]. We observed that, as cells progressed into mitosis, centrosomes oriented towards the short nuclear axis, as we previously described (Fig. 1B; green line; [28]). Given that the long nuclear axis remained aligned with the long cell axis up until the moment of NEP (Fig. 1B; blue line), this meant that separating centrosomes deviated from the long cell axis (Fig. 1B; purple line) and away from cortical force generators. This centrosome-nucleus reorientation occurred without

global changes in cell or nuclear shape, as measured by their eccentricity throughout time (Fig. 1C). These results, in combination with our previous observations [28], indicate that centrosome orientation at NEP might be determined by a nuclear signal and not by external signals. To determine the nature of this nuclear signal, we performed a detailed spatiotemporal analysis of the prophase nucleus. We image cells expressing the nucleoporin POM121-3xGFP in interphase (Fig. 1D) and early mitosis (Fig. 1E) with high temporal resolution (100 msec), and measured active and thermally driven NE fluctuations using Trackosome [67]. In interphase cells, the individual fluctuation maps displayed scarce minor NE undulations (Fig. 1D and D`). In agreement, the corresponding Fourier transform (FT) of the fluctuations curves (uf) showed the highest FT peaks, corresponding to low wavelengths, as illustrated in Figure S1A (highest FT peak (λ1) with a wavelength of 0,0775 μm). This results from the larger membrane displacements seen around the arc landmarks, such as the membrane undulation seen around the 17 μm arc landmark in Figure 1D'. Therefore, in interphase cells, the NE membrane barely deviates from its initial position and only shows subtle nuclear membrane movements (Fig. 1D). On the contrary, prophase cells presented individual fluctuation maps showing frequent major membrane displacements (Fig. 1E), such as those observed around the 25 μm or 53 μm arc landmarks (Fig. 1E'). Accordingly, the corresponding FT curves showed highest peaks corresponding to higher wavelengths, as illustrated in Figure S1B (highest FT peaks (λ1-λ3) with wavelengths of 0,1026 μm, 0,0583 μm, and 0,0289 μm, respectively). In addition, prophase cells also showed an increase in the fluctuation amplitude for the low frequency components (values beyond the peak; S1B and 1F), which reflect the occurrence of membrane wrinkles and nucleus-wide deformations (Fig. 1E). Hence, and in agreement with previous studies [67,68], as cells transition into mitosis there is an increase in the fluctuation amplitude for the whole range of wavelengths, with a significant difference between the median FT curves across cells for each experimental group (Fig. 1F; ****$p<0.0001$).

Overall, we conclude that mitotic entry is accompanied by an increase in thermally and actively driven NE undulations, which possibly reflect an altered mechanical state of the nucleus [69].

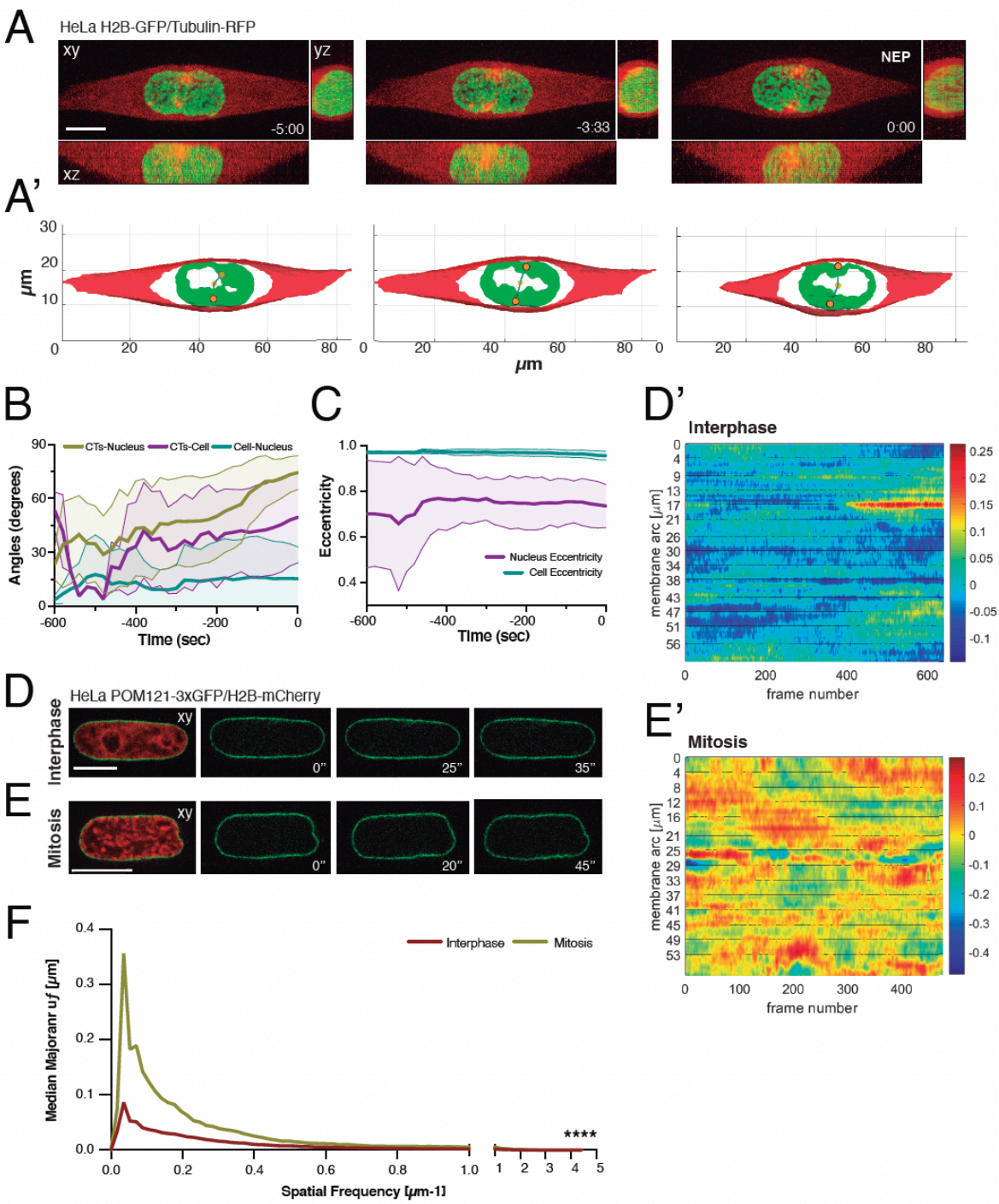


Figure 1: Characterization of nucleus behavior during mitotic entry. **(A**) Representative images from movie of a HeLa cell expressing H2B-GFP/Tubulin-RFP seeded on a 10 μm line micropattern, during mitotic entry. Time is in min:sec. Time zero corresponds to NEP. Scale bar, 10 μm **(A')** 3D reconstruction of the representative time-frame presented in A, showing centrosomes (yellow), nucleus (green) and cell membrane (red), depicting nucleus shape changes during mitotic entry. Centrosomes are connected by a vector that runs through the nucleus centroid. **(B)** Plot quantifying angles between centrosomes/nucleus long axis (green), centrosomes/cell membrane long axis (purple) and cell membrane long axis/nucleus long axis (blue) over time. Lines correspond to average values (n=24) and shaded areas correspond to SD. Time zero corresponds to NEP. **(C)** Cell membrane eccentricity (blue) and nuclear membrane eccentricity (purple) over time. Lines correspond to average values (n=24) and shaded areas correspond to SD. Time zero corresponds to NEP.

Representative images from movies of interphase **(D)** and prophase **(E)** HeLa cells expressing POM121-3xGFP/H2B-mCherry seeded on a 10 μm line micropatterns. The NE, labeled with POM121-3xGFP (green), is shown at three different time points to illustrate the degree of membrane undulation in each group. Time is in sec. Time zero corresponds to the first recorded frame. Scale bar, 10 μm. **(D'-E')** Corresponding maps of the fluctuations amplitude, u_f, obtained for all the frames from the videos in D and E, respectively. The *y*-axis corresponds to the arc around the median membrane. **(F)** Interphase (n=36) and early mitosis (n=34; ****p<0.0001) medians of the majorant frequency-dependent fluctuations, u_f, obtained by finding the maximum amplitude of the spatial Fourier transform (FT) for each frequency across frames. These FT curve show the maximum fluctuation amplitude of each wavelength; thus, its peaks reveal the median amplitude and wavelength of the most significant curvatures of the NE for each experimental group.

3.2. Interfering with nuclear mechanics affects centrosome positioning

Next, we set out to determine how the mechanical properties of the nucleus might affect centrosome positioning. It is well established that nuclear mechanics rely on the amount and distribution of nuclear lamins, chromatin condensation state and nuclear-cytoskeletal coupling [50,51,70,71]. Whether these have any effect on spindle assembly, remains unknown. We started by interfering with the nuclear-cytoskeletal coupling by expressing a dominant-negative KASH construct (Fig. 2B and D), which displaces endogenous nesprins from the NE, disrupting the LINC complex and effectively blocking force propagation to the nucleus [72,73]. Under this condition, cells exhibited frequent major NE membrane undulations (Fig. 2B-B'), when compared to control cells (Fig 2A-A'), with a significant difference between the median FT curves across cells, for each experimental group (Fig. 2C; ****p<0.0001). In addition, the long nuclear axis was more frequently perpendicular to the long cell axis (Fig. 2E; ****p<0.0001). This is likely due to a faster cell rounding (Fig. S2A), which allows unrestricted nuclear movement [74]. Overall, the observed changes confirm that interfering with nucleo-cytoskeletal coupling affects nuclear behaviour. However, centrosomes still positioned on the short nuclear axis at NEP (Fig. 2F).

Next, we affected nuclear mechanics by directly interfering with the NL using RNAi-mediated Lamin A depletion (Fig. S2B-C) and followed mitotic entry. Evaluation of NE fluctuations revealed that Lamin A depleted cells (Fig. S2C) exhibited an increase in the fluctuation amplitude (Fig. 2H-H' and I; ****p<0.0001), when compared to controls (Fig. 2G-G' and I). Importantly, the fluctuation amplitude increased for the entire range of wavelengths, namely for the low frequency components that are indicative of nucleus-wide deformations (Fig. 2I; ****p<0.0001). These changes are in agreement with the decreased nuclear stiffness that is observed upon Lamin A depletion [56,57]. This change in nuclear behaviour was accompanied by an increase on nucleus irregularity metrics just prior to NEP (Fig 2K), that correlated with centrosome-nucleus angle reorientation (Fig. 2J; dotted blue

line; ****p<0.0001). These results are indicative that centrosomes in Lamin A depleted cells do not migrate along the NE but deform the nucleus to generate a local short axis. Consequently, centrosome positioning at NEP was not altered when compared to controls (Fig. 2L-M). Overall, we concluded that Lamin A, similarly to the LINC-complex, is required to constrain NE undulations during prophase but does not change centrosome-nucleus axis orientation, due to an artificial deformation of the nucleus.

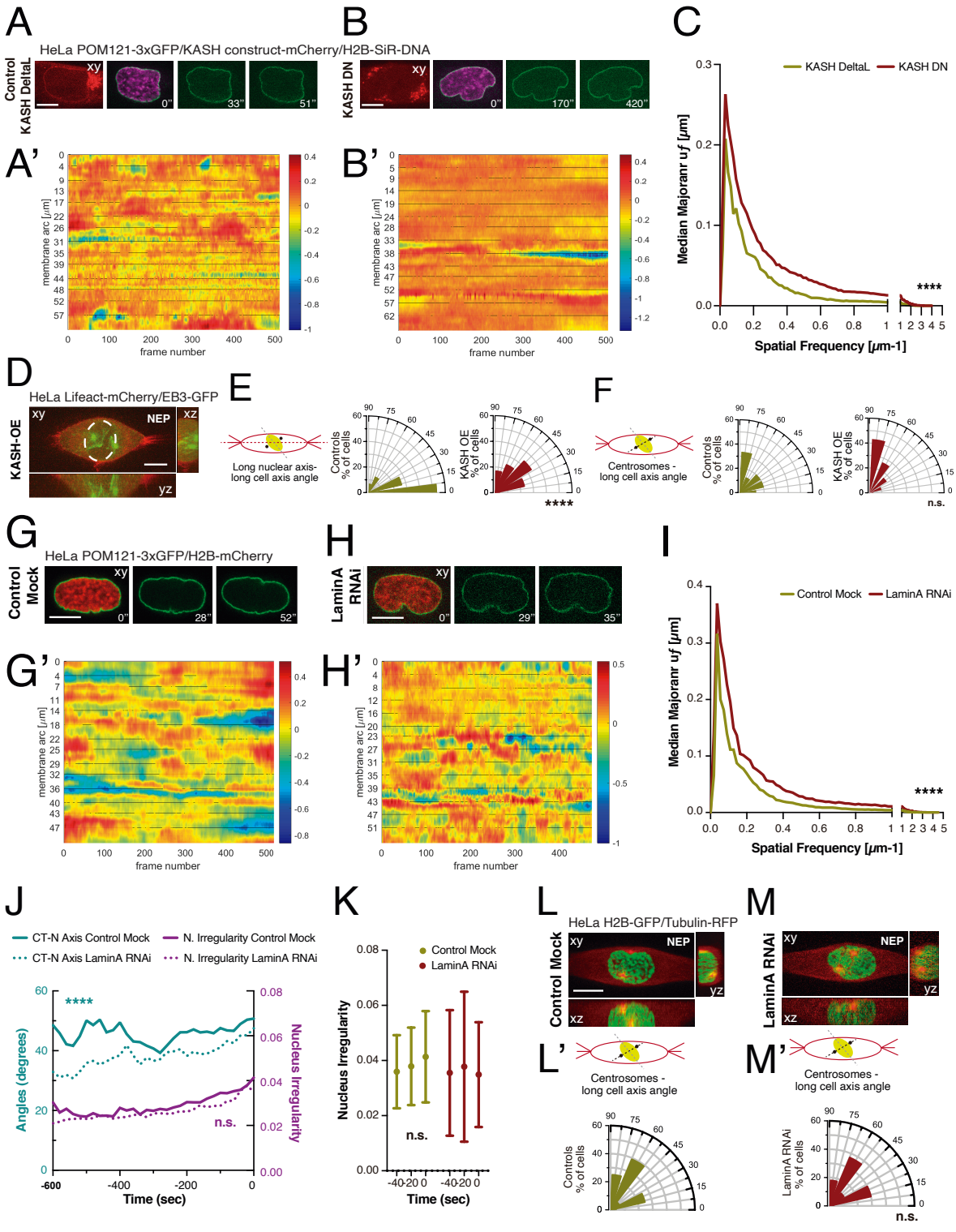


Figure 2: Nucleus-cytoskeleton connection and Lamin A restrain NE fluctuations. **(A-B)** Representative images from movies of cells expressing either mCherry-KASH-DeltaL (controls; **A**) or mRFP1-KASH-DN (KASH DN; **B**) constructs together with POM121-3xGFP/SiR-DNA, seeded on 10 μm line micropatterns. The NE labeled with POM121-3xGFP (green) is shown at two different time points to illustrate the degree of membrane undulation in each group. Time is in sec. Time zero corresponds to the first recorded frame. Scale bar, 10 μm. **(A'-B')** Corresponding maps of the fluctuations amplitude, u_f, obtained for all the frames from the videos in A and B, respectively. The *y*-axis corresponds to the arc around the median membrane. **(C)** Medians of the majorant frequency-dependent fluctuations, u_f, for cells expressing either mCherry-KASH-deltaL (controls; green; n=21) or mRFP1-KASH-DN (KASH DN; red; n=35; ****p<0.0001) constructs. Cells expressing KASH DN construct exhibited a significant increase in the membrane undulations in mitosis. **(D)** Representative time-frame from cell expressing EB3-GFP/Lifeact-mCherry, transfected with a pEGFP-KASH construct (KASH OE) at NEP. Scale bar, 10 μm. **(E)** Polar plots quantifying alignment of the long nuclear axis with the long cell axis at NEP for controls (n=15) and cells expressing pEGFP-KASH (KASH OE; n=30; ****p<0.0001). **(F)** Polar plots quantifying centrosome positioning relative to the longest nuclear at NEP for controls (n=15) and cells expressing pEGFP-KASH (KASH OE; n=30; n.s. - not significant). Representative images from movies of mock-transfected **(G)** and LaminA RNAi-treated **(H)** cells expressing POM121-3xGFP/H2B-mCherry, seeded on 10 μm line micropatterns. The NE labeled with POM121-3xGFP (green) is shown at two different time points to illustrate the degree of membrane undulation in each group. Time is in sec. Time zero corresponds to the first recorded frame. Scale bar, 10 μm. **(G'-H')** Corresponding maps of the fluctuations amplitude, u_f, obtained for all the frames from the videos in G and H, respectively. The *y*-axis corresponds to the arc around the median membrane. **(I)** Medians of the majorant frequency-dependent fluctuations, u_f, for mock-transfected (green; n=23) and Lamin A RNAi-treated (red; n=20; ****p<0.0001) cells. Lamin A depletion caused a significant increase in the membrane undulations in mitosis. **(J)** Polar plot quantifying centrosome positioning relative to the longest nuclear axis, at NEP, for cells treated with Lamin A RNAi (n=33; n.s. - not significant). **(J)** Plot showing both centrosomes/nucleus long axis (green) and nuclear membrane irregularity (purple) overtime for mock-transfected (straight lines; n=28) and Lamin A RNAi-treated (dotted lines; n=33) cells. Lines correspond to average values. Time zero corresponds to NEP. **(K)** Plot featuring the last three time points of nuclear membrane irregularity of J. **(L**) Representative time-frame of a mock-transfected HeLa cell expressing H2B-GFP/Tubulin-RFP seeded on a 10 μm line micropattern at NEP. **(L'**) Polar plot quantifying centrosome positioning relative to the longest nuclear axis for mock-transfected control cells (n=28) at NEP. **(M**) Representative image of HeLa cell expressing H2B-GFP/Tubulin-RFP seeded on a 10 μm line micropattern treated with Lamin A RNAi at NEP. **(M')** Polar plot quantifying centrosome positioning relative to the longest nuclear axis, at NEP, for cells treated with Lamin A RNAi (n=33; n.s. - not significant).

During mitotic entry, chromatin undergoes extensive reorganization to form mitotic chromosomes. This reorganization leads to a drastic change in chromosome stiffness [50,51]. To determine if chromatin condensation and organization affected nuclear behaviour during the G2-M transition, we treated cells with TOPOII inhibitor (ICRF-193; Fig. 3B), known to alter the biophysical properties and compaction of mitotic chromosomes [75], or with a histone deacetylase (HDAC) inhibitor (Valproic Acid (VPA); Fig. 3C) that induces histone hyperacetylation without affecting chromosome stiffness [55]. Cells treated with ICRF-193 exhibited a more roundish nucleus in the beginning of mitosis (Fig. 3D; red line;

****p<0.0001), when compared to controls (Fig. 3D; green line), as well as faster cell rounding (Fig. S2D; red line; ****p<0.0001). ICRF-193 treatment also increased the fluctuation amplitude for the whole range of wavelengths (Fig. 3K, K' and M; red line; ****p<0.0001). This was likely not due to an effect on the NL, since we did not observe significant changes in Lamin B1 and Lamin A levels after treatment with ICRF-193 (Fig. S3). Importantly, ICRF-193 treatment prevented centrosome positioning on the shortest nuclear axis (Fig. 3B, G and I; straight red line; **p<0.01) when compared to controls (Fig. 3A, F and I; straight green line). On the other hand, treatment with VPA induced faster cell rounding (Fig. S2D; blue line; ****p<0.0001) and reduced nucleus irregularity until NEP (Fig. 3E; blue line; ****p<0.0001). However, unlike ICRF-193-treated cells, these showed NE fluctuations similar to what was observed in controls (Fig. 3J, J', L, L' and M). Taken together, these changes suggest that modifying chromosome stiffness can modify nuclear behavior during mitotic entry. Remarkably, unlike ICRF-193, VPA treatment, did not change nucleus orientation (Fig. 3I; blue dashed line; ****p<0.0001), centrosome movement (Fig. 3I; dotted blue line), or centrosome-nucleus axis positioning at NEP (Fig. 3C, H and I; straight blue line), when compared to controls (Fig. 3A, F and I; green lines).

Overall, these data indicate that accurate positioning of centrosomes on the shortest nuclear axis at NEP is dependent on correct mitotic chromosome compaction but does not require the NL or nucleo-cytoskeletal coupling.

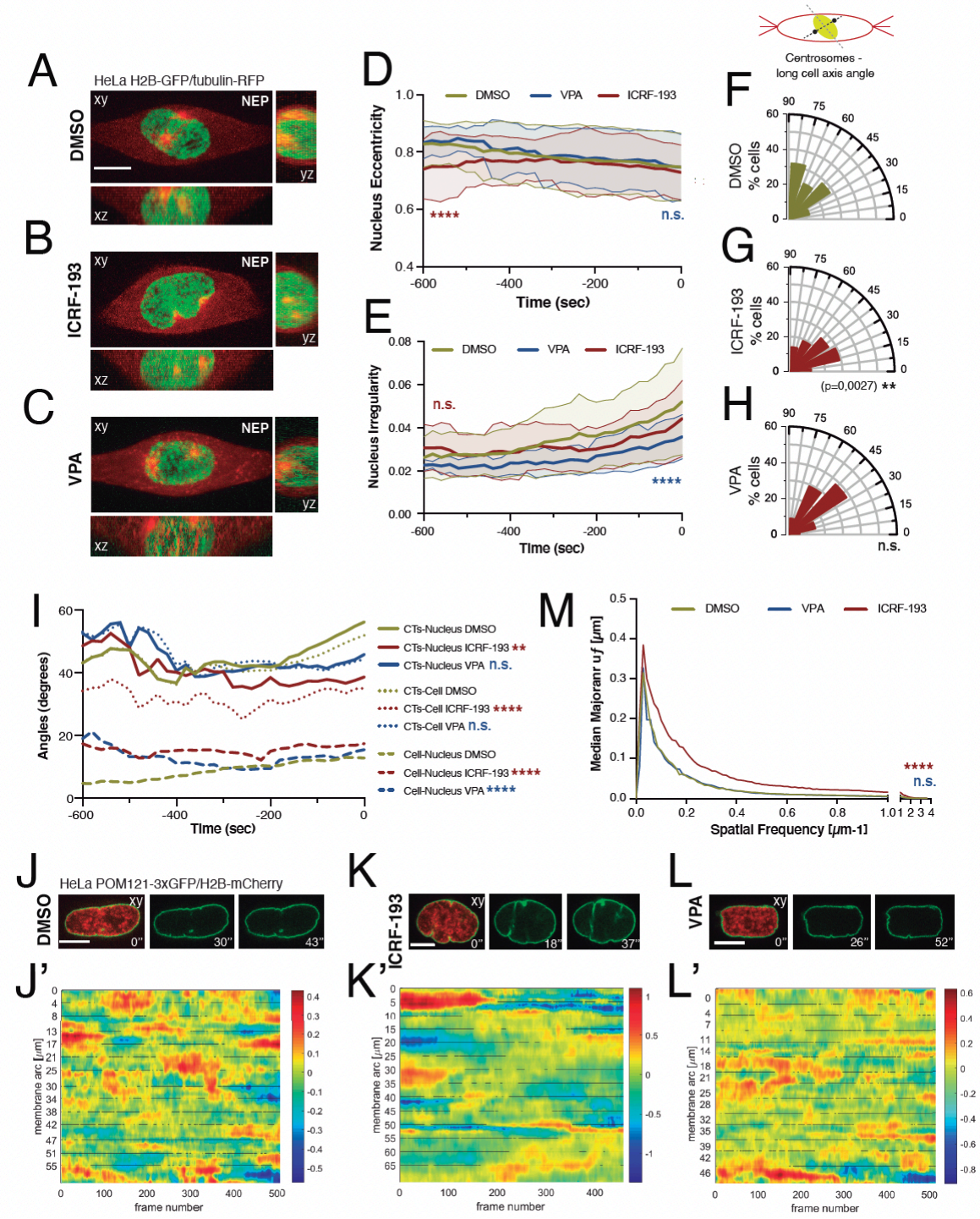


Figure 3: Chromatin condensation is required for centrosome positioning on the shortest nuclear axis. Representative images of HeLa cells expressing H2B-GFP/Tubulin-RFP seeded on a 10 µm line micropatterns at NEP, treated with DMSO **(A),** ICRF-193 **(B)** and VPA **(C). (D)** Nuclear membrane eccentricity over time for cells treated with DMSO (green; n=50), ICRF-193 (red; n=42; ****p<0.0001) and VPA (blue; n=34; n.s. - not significant). Lines correspond to average values and shaded areas correspond to SD. Time zero corresponds to NEP. **(E)** Nuclear membrane irregularity over time for cells treated with DMSO (green; n=50), ICRF-193 (red; n=42; n.s. - not significant) and VPA (blue; n=34; ****p<0.0001). Lines correspond to average values and shaded areas correspond to SD. Time zero corresponds to NEP. Polar plots quantifying centrosome positioning relative to the longest nuclear axis, at NEP, for cells treated with DMSO (**F;** n=50), ICRF-193 (**G**; n=42; **p<0.01) and

VPA (**H**; n=34; n.s. - not significant). **(I)** Plot quantifying angles between centrosomes/nucleus long axis (straight lines; ICRF-193 **p<0.01; VPA n.s. - not significant), centrosomes/cell membrane long axis (dotted lines; ICRF-193 ****p<0.0001; VPA n.s. - not significant) and cell membrane long axis/nucleus long axis (dashed lines; ICRF and VPA ****p<0.0001) over time for cells treated with DMSO (green; n=50), ICRF-193 (red; n=42) and VPA (blue; n=34). Lines correspond to average values and shaded areas correspond to SD. Time zero corresponds to NEP. Representative images from movies of DMSO **(J)**, ICRF-193 **(K)** and VPA-treated **(L)** cells expressing POM121-3xGFP/H2B-mCherry, seeded on 10 μm line micropatterns. The NE labeled with POM121-3xGFP (green) is shown at two different time points to illustrate the degree of membrane undulation in each group. Time is in sec. Time zero corresponds to the first recorded frame. Scale bar, 10 μm. **(J'-L')** Corresponding maps of the fluctuations amplitude, u_f, obtained for all the frames from the videos in J, K and L, respectively. The *y*-axis corresponds to the arc around the median membrane. **(M)** Medians of the majorant frequency-dependent fluctuations, u_f, for DMSO (green; n=30), ICRF-193 (red; n=29; ****p<0.0001) and VPA-treated (blue; n=27; n.s. - not significant) cells. ICRF-193 treatment caused a significant increase in the membrane undulations in mitosis.

3.3. Chromosome condensation regulates NE-Dynein loading

Given that NE-associated Dynein is required for centrosome positioning on the shortest nuclear axis [28,76], we wondered whether the defects we observed in centrosome positioning upon mitotic chromosome disruption could be due to an impairment of Dynein function. We started by analyzing DHC-GFP distribution on the NE during prophase using both live-cell imaging (Fig. 4A and D) and immunofluorescence analysis (Fig. 4G, H, J, K and L; controls). We then measured Dynein levels on NE (Fig. 4I M; controls; green boxes). As can be observed in Figures 4A and D, in control cells, Dynein accumulates at the NE and centrosomes prior to NEP. To test whether chromatin compaction contributes for NE-Dynein loading, we analyzed Dynein distribution on the NE after treatment with ICRF-193. Interestingly, inhibition of TOPOII (Fig. 4B, E and G) induced a loss of Dynein specifically on the NE (Fig. 4I; ****p<0.0001), without interfering with Dynein recruitment to the kinetochore or cell cortex (Fig. S4). While VPA treatment also induced a mild decrease in NE-Dynein (Fig. 4C, F, G, and I, *p<0.05), the effects on NE-Dynein were significantly severer following ICRF-193 treatment (****p<0.0001). To further confirm if chromosome condensation was indeed required for NE-Dynein recruitment, we interfered with this process using alternative methods. Specifically, we inactivated both condensins I and II using RNAi-mediated depletion of SMC2 (Fig. S5A-B), a SMC subunit shared between the two condensins [77]. Importantly, SMC2-depleted cells also showed a loss of Dynein on the NE (Fig. 4H and 4I; purple box; ****p<0.0001).

Loading of Dynein on the NE is biochemically regulated by CDK1 and occurs through the RanBP2-BicD2 [78,79] and Nup133-CENP-F-NudE/NudEL [76,80] pathways. To determine whether ICRF-193 treatment affected NE-Dynein recruitment through its known adaptors, we assessed whether BicD2 and NudE/NudEL localization on the NE was

affected after ICRF-193 treatment. We observed that both adaptors localized normally to the NE following treatment with ICRF-193, even though Dynein was not detected (Fig. S3B-C). These results confirm that chromosome condensation affects both NE-Dynein loading and centrosome positioning.

Next, we wanted to determine how chromosome condensation, which occurs inside the nucleus, could regulate NE-Dynein loading on the cytoplasmic side. We reasoned there must be a physical coupling between these structures, relaying the forces generated by chromosome stiffening to the NE. One possibility is that chromosome coupling to the NE via the telomeres could provide such link. To test this, we performed RNAi-mediated depletion of TRF1, a telomeric DNA-binding protein proposed to act as key regulator of telomere length [81]. Interestingly, TRF1 depletion (Fig.S5C-D) compromised Dynein recruitment to the NE (Fig. 4H and I; orange box; *p<0.05). Interestingly, neither interfering with the NL with Lamin A RNAi (known to also mediated chromatin tethering to the NE [82,83]), nor with the LINC-complex through expression of DN-KASH,), had any effect on NE-Dynein recruitment (Fig. 4J, L, and M), when compared with controls. Inversely, Lamin A depletion even increased NE-Dynein levels (Fig. 4J and L; orange box; * p<0.05), similarly to what we observed following incubation with Nocodazole (Noco; Fig. 4K and L; blue box; ****p<0.0001), previously known to enrich NE-Dynein levels [79,80]. Interestingly, Lamin A RNAi and Noco treatment had opposite effects on NE fluctuation dynamics. Whereas Lamin A RNAi increased NE undulations (Fig. 2G-I), Noco abolished them (Fig. S6). This suggests that NE undulations rely on the MT network but occur independently of NE-Dynein levels. Lastly, interfering with cellular contractility by inhibiting ROCK with Y27632 also did not affect NE-Dynein recruitment (Fig. 4K and L). Overall, we concluded that chromosome compaction during mitotic entry regulates NE-Dynein recruitment, independently of its known adaptors, via a telomere-mediated tethering of chromosomes to the NE.

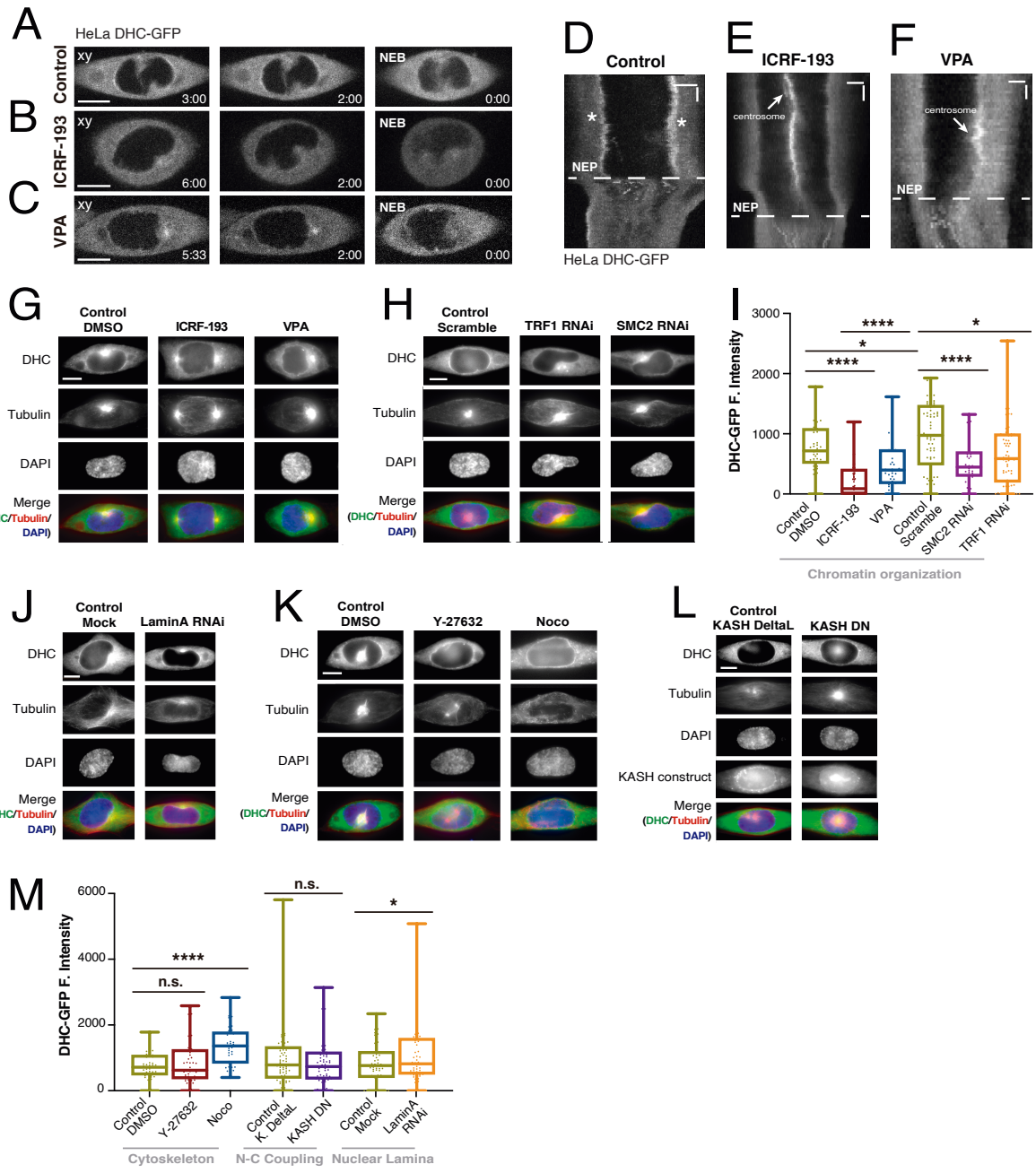


Figure 4: Chromosome condensation is required for NE-Dynein recruitment. Representative images from movies of DMSO **(A),** ICRF-193 **(B)** and VPA-treated **(C)** cells expressing DHC-GFP seeded on 10 µm line micropatterns, during mitotic entry. Time is in min:sec. Time zero corresponds to NEP. Scale bar, 10 µm. Kymographs of DMSO **(D)**, ICRF-193 **(E)** and VPA-treated **(F)** cells expressing DHC-GFP (not related with A-C). White arrowheads indicate NE-Dynein. Horizontal scale bar, 10 µm. Vertical scale bar 100sec. **(G)** Immunofluorescence images of DHC-GFP, alpha-tubulin and DAPI for controls (DMSO), ICRF-193 and VPA-treated cells expressing DHC-GFP seeded on 10 µm line micropatterns. DHC-GFP images correspond to sum projections. DAPI and alpha-tubulin correspond to maximal intensity projections. Scale bar, 10 µm. **(H)** Immunofluorescence images of DHC-GFP, alpha-tubulin and DAPI for controls (scramble), TRF1 RNAi, SMC2 RNAi-treated cells expressing DHC-GFP seeded on 10 µm line micropatterns. DHC-GFP images correspond to sum projections. DAPI and alpha-tubulin correspond to maximal intensity projections. Scale bar, 10 µm. **(I)** Quantification of NE-associated DHC-GFP fluorescence intensity in prophase for controls (green boxes: DMSO

ON; n=43 and scrambled RNAi (200nM); n=74), ICRF-193 (red box; n=71; ****p<0.0001), VPA (blue box; n=39; * p<0.05), SMC2 RNAi (purple box; n=33; ****p<0.0001) and TRF1 RNAi (orange box; n=68; * p<0.05)-treated cells. For quantification purposes, sum-projected images covering the middle nucleus region were used**. (J)** Immunofluorescence images of DHC-GFP, alpha-tubulin and DAPI for controls (scrambled RNAi) and LaminA RNAi-treated cells expressing DHC-GFP seeded on 10 µm line micropatterns. DHC-GFP images correspond to sum projections. DAPI and alpha-tubulin correspond to maximal intensity projections. Scale bar, 10 µm. **(K)** Immunofluorescence images of DHC-GFP, alpha-tubulin and DAPI for controls (DMSO), Y-27632 and, Nocodozole-treated cells expressing DHC-GFP seeded on 10 µm line micropatterns. DHC-GFP images correspond to sum projections. DAPI and alpha-tubulin correspond to maximal intensity projections. Scale bar, 10 µm. **(L)** Immunofluorescence images of DHC-GFP, alpha-tubulin, DAPI, and KASH constructs (Control - mCherry-KASH-deltaL; Dominant Negative - mRFP1-KASH-DN) for controls cells (KASH DeltaL). DHC-GFP images correspond to sum projections. DAPI, alpha-tubulin and KASH constructs correspond to maximal intensity projections. Scale bar, 10 µm. **(I)** Quantification of NE-associated DHC-GFP fluorescence intensity in prophase for controls (green: DMSO; n=43, scramble (20nM); n=51, KASH DeltaL; n=67), Y-27632 (red box; n=44; n.s. - not significant), Nocodozole (blue box; n=36; ****p<0.0001), LaminA RNAi (orange box; n=53; * p<0.05) and KASH DN-treated (purple box; n=63; n.s. - not significant) cells. For quantification purposes, sum-projected images covering the middle nucleus region were used. **(M)** Quantification of NE-associated DHC-GFP fluorescence intensity in prophase for controls (KASH DeltaL; green; n=67) and KASH DN-treated (red; n=63; n.s. - not significant) cells. For quantification purposes, sum-projected images covering the middle nucleus region were used.

3.4. NE-Dynein loading is mechanosensitive

Given our observations that interfering with chromatin condensation affect NE-Dynein loading and that compressive forces induce chromatin condensation [84], we wondered whether mechanical confinement of the nucleus could rescue NE-Dynein loading in cells with compromised chromosome condensation (Fig. 5A). To test this hypothesis, we interfered with chromatin using different treatments and applied a reversible confinement on cells, followed by live-cell imaging and immunofluorescence analysis DHC-GFP (Fig. 5C-D and E). Under confinement, both control and treated-cells exhibited low levels of Dynein on the NE (Fig. 5B-D), possibly due to a decrease in NE-Dynein density [85]. Confinement release was sufficient to immediately restore Dynein localization both in controls (Fig. 5B-C) as in ICRF-193, VPA and SMC2 RNAi-treated cells (Fig. 5B, D-F). Interestingly, confinement also restored Dynein localization in TRF1-depleted cells (Fig.5E-F). Overall, this suggests that confinement-induced mitotic chromosome condensation triggers a mechanical signal important for Dynein loading and overrides the deficiency in telomeric chromatin-NE coupling.

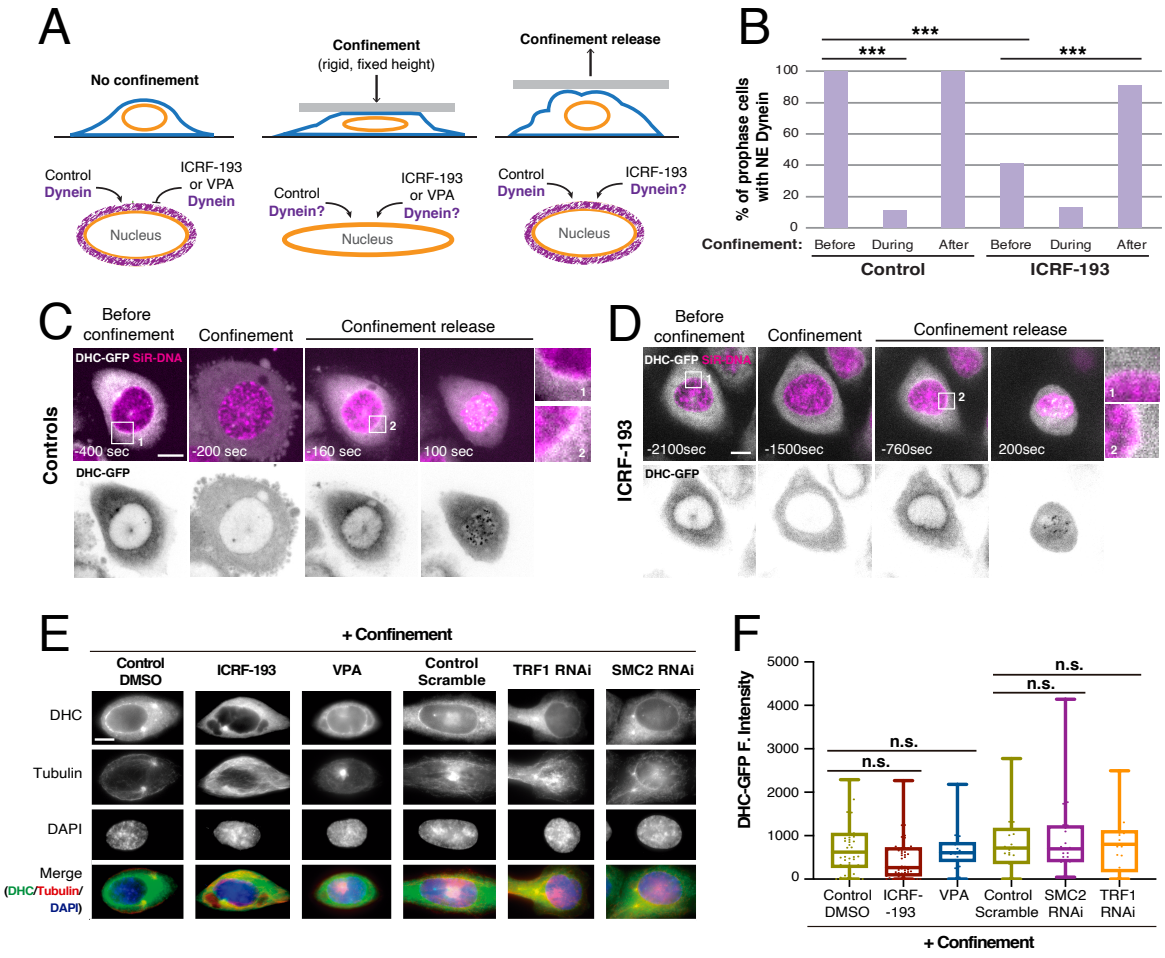


Figure 5: Dynein is loaded on the NE following mechanical stimulation. **(A)** Experimental setup to test the effect of confinement on Dynein loading on the prophase nucleus. **(B)** Quantification of the percentage of prophase cells with Dynein on the NE before, during and after confinement (controls, n=14; ICRF-193, n=22; ***p<0.001). **(C)** Frames from movie of control HeLa cell expressing DHC-GFP and SiR-DNA (n=27), seeded on a 10 µm line micropattern, before, during and after confinement. Time lapse is 20sec. Time zero corresponds to NEP. Scale bar, 10 µm. **(D)** Frames from movie of HeLa cell treated with ICRF-193 (n=23), expressing DHC-GFP and stained with SiR-DNA, seeded on a 10 µm line micropattern, before, during and after confinement. Time lapse is 20sec. Time zero corresponds to NEP. Scale bar, 10 µm. **(E)** Immunofluorescence images of DHC-GFP, alpha-tubulin and DAPI for controls (DMSO ON and scrambled RNAi), ICRF-193, VPA, TRF1 RNAi and SMC2 RNAi-treated cells expressing DHC-GFP, seeded on 10 µm line micropatterns, after confinement release DHC-GFP images correspond to sum projections. DAPI, alpha-tubulin and KASH constructs correspond to maximal intensity projections. Scale bar, 10 µm (**F)** Quantification of DHC-GFP intensity in prophase for controls (green; DMSO ON; n=48 and scrambled RNAi; n=28), ICRF-193 (red; n=56; n.s. - not significant), VPA (blue; n=22; n.s. - not significant), TRF1 RNAi (orange; n=23; n.s. - not significant) and SMC2 RNAi-treated (n=24; purple; n.s. - not significant) cells after confinement and release. For quantification purposes, sum-projected images covering the middle nucleus region were used.

Next, we wanted to determine if the mechanical regulation of NE-Dynein recruitment required the classical Dynein adaptors. To test this hypothesis, we treated cells with ICRF-193 in combination with RNAi depletion of BicD2 or NudE/NudEL (Fig. S6A-B) and subjected these cells to mechanical confinement, followed by quantification of NE-Dynein levels. Strikingly, mechanical confinement in the presence of ICRF-193 following either NudE/NudEL or BicD2 depletions, was able to rescue Dynein loading on the NE (Fig. 6A-C). These observations indicate that both pathways are redundant, and that Dynein loading requires a mechanical signal.

Finally, we set out to determine how the mechanical stimulus could be transmitted across the NE. Transduction of mechanical forces to the nucleus requires an intact SUN-KASH connection [71]. Our previous observations showed that physical coupling of telomeres to the NE is important for Dynein loading (Fig. 4H-I) and that KASH disruption did not affect Dynein (Fig. 4L-M). We reasoned this physical coupling could be mediated by SUN proteins. Importantly, SUN1/2 were previously shown to be required for NE Dynein loading during neuronal development [86] and mitotic entry [44]. To test whether SUN proteins could mediate the mechanoresponsive recruitment of Dynein to the NE during prophase, we depleted SUN1 or SUN2 by RNAi and assessed NE-Dynein levels. Both SUN1 and SUN2 depletions induced NE-Dynein loss (Fig. 6D-F). Interestingly, SUN2 depletion (Fig. 6F; blue box; ****$p<0.0001$) led to a more pronounced reduction of NE-Dynein levels than SUN1 depletion (Fig. 6F; red box; **$p<0.01$). Importantly, mechanical stimulation was not able to restore NE-Dynein recruitment following SUN1 or SUN2-depletions (Fig. 6D-F). This indicates that SUN proteins are directly responsible for the mechanical regulation of Dynein loading on the NE. This was further confirmed with co-depletion of SUN1/2 using shRNA (Fig. S7C-D). Overall, our data suggests that SUN1 and SUN2 transmit mechanical forces imposed by mitotic chromosomes across the NE to allow loading of Dynein on the NE, via the BicD2 and NudE/NudEL pathways.

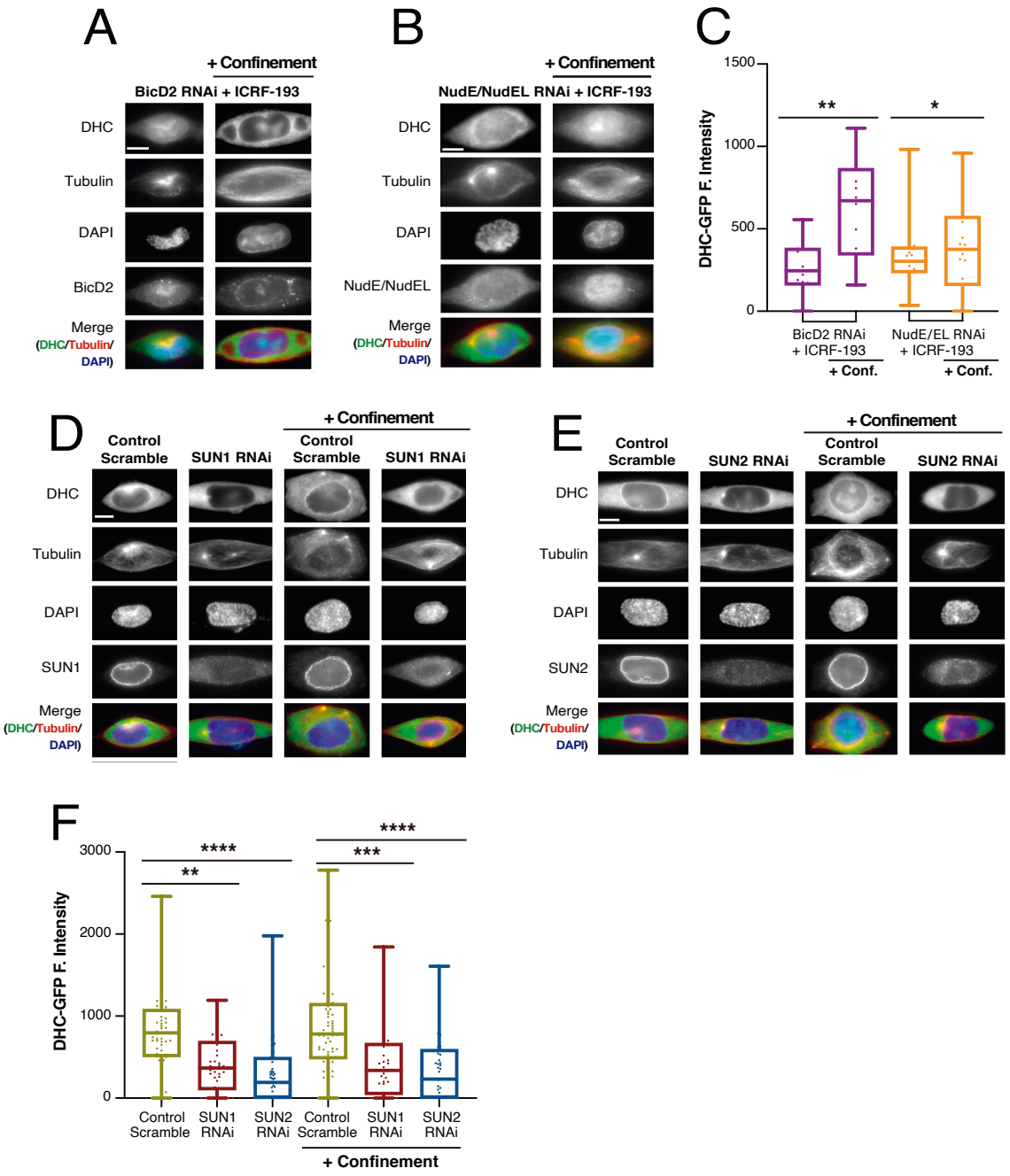


Figure 6: SUN1/2 are required for the mechanosensitive loading of Dynein. **(A)** Immunofluorescence images of DHC-GFP, alpha-tubulin, DAPI and BicD2 for cells expressing DHC-GFP, seeded on 10 μm line micropatterns, treated with ICRF-193 and BicD2 RNAi, before and after confinement release. DHC-GFP images correspond to sum projections. DAPI, alpha-tubulin and BicD2 correspond to maximal intensity projections. Scale bar, 10 μm. **(B)** Immunofluorescence images of DHC-GFP, alpha-tubulin, DAPI, and NudE for cells expressing DHC-GFP, seeded on 10 μm line micropatterns, treated with ICRF-193 and NudE+NudEL RNAi before and after confinement release. DHC-GFP images correspond to sum projections. DAPI, alpha-tubulin and NudE correspond to maximal intensity projections. Scale bar, 10 μm**. (C)** Quantification of DHC-GFP intensity for prophase cells treated with ICRF-193+BicD2 RNAi without confinement (purple; n=16; n.s. - not significant), ICRF-193+BicD2 RNAi after confinement release (n=10; n.s. - not significant), ICRF-193+NudE RNAi without confinement (orange; n=15; *p<0.05) and ICRF-193+NudE RNAi after confinement release (orange; n=14; *p<0.05). For quantification purposes, sum-projected images covering the middle nucleus region

were used. **(D)** Immunofluorescence images of DHC-GFP, alpha-tubulin, DAPI and SUN, for control (scrambled RNAi) cells before and after confinement and release and cells treated with SUN1 RNAi before and after confinement and release. Cells are expressing DHC-GFP and are seeded on 10 µm line micropatterns. DHC-GFP images correspond to sum projections. DAPI, alpha-tubulin and SUN1 correspond to maximal intensity projections. Scale bar, 10 µm. **(E)** Immunofluorescence images of DHC-GFP, alpha-tubulin, DAPI and SUN2, for control (scrambled RNAi) cells and after confinement and release and cells treated with SUN2 RNAi, before and after confinement and release. Cells are expressing DHC-GFP and are seeded on 10 µm line micropatterns. DHC-GFP images correspond to sum projections. DAPI, alpha-tubulin and SUN2 correspond to maximal intensity projections. Scale bar, 10 µm. **(F)** Quantification of DHC-GFP intensity in prophase for controls before (green; n=53) and after confinement and release (green; n=65), cells treated with SUN1 RNAi before (red; n=40; **p<0.01) and after confinement and release (red; n=26; ***p<0.001) and cell treated with SUN2 RNAi before (blue; n=61; ****p<0.0001) and after confinement and release (blue; n=43; ****p<0.0001). For quantification purposes, sum-projected images covering the middle nucleus region were used.

In summary, we propose a model where mitotic chromosome condensation increases intranuclear stiffness, which is transmitted by telomeres to SUN1 and SUN2 proteins at the NE. As a consequence, the mechanical strain imposed on SUN proteins triggers NE-Dynein loading via BicD2 or NudE/NudEL pathways. This ensures centrosome-NE tethering and correct positioning on the short nuclear axis at NEP (Fig. 7).

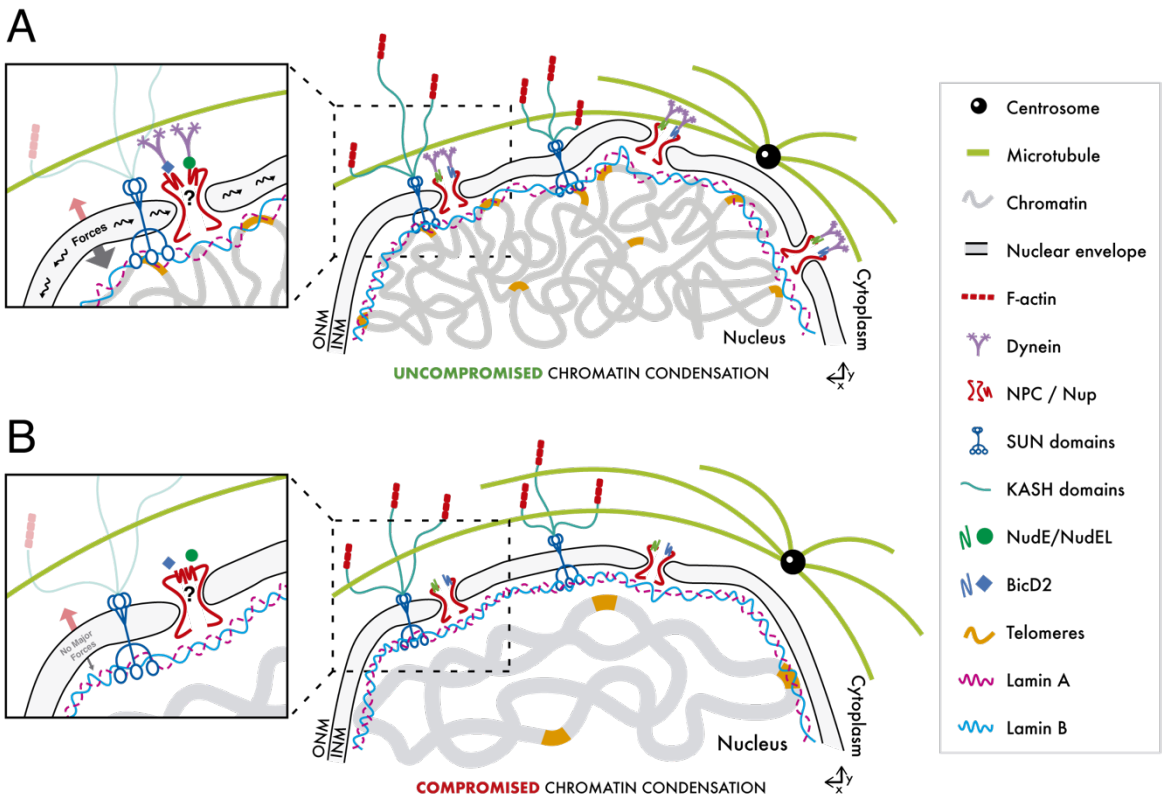


Figure 7: Proposed model for prophase NE-Dynein recruitment. **(A)** The model we propose postulate that at early prophase, chromosome condensation-mediated forces (grey arrow) are transmitted to the

telomeres, which tether chromatin to the NE alongside with lamins and INM proteins. Telomeres then propagate this mechanical signal to the SUN proteins also at the NE. This mechanical load applied on SUN proteins triggers Dynein recruitment to the NE through BicD2 or NudE/NudEL pathways, which ensures centrosome-NE coupling. We speculate that both Dynein adaptors are activated due to NE tension-driven conformational changes at the NPCs. **(B)** When chromatin condensation is impaired, the NE is only subjected to cytoskeleton-mediated forces (red arrow), which appear to be irrelevant for this process. Dynein recruitment is abolished under such conditions despite the recruitment of Dynein adaptors to the NE. This condition often leads to centrosome detachment from the NE.

4. Discussion

Growing evidence demonstrate that chromosomes [87–93] and other nuclear-associated elements, such as the NL [40–42] and the LINC complex [43,94,95], directly contribute to mitotic spindle assembly. Interestingly, alongside with this active role in spindle formation, all these components also regulate nuclear mechanics [50,51,70,71]. Importantly, mitotic entry is characterized by organizational and functional changes of NE proteins and chromatin [1], which imply a change on the mechanical properties of the nucleus. In this study we addressed how these changes contribute to early spindle assembly. Here, we propose that chromatin condensation produces intranuclear mechanical forces that are transmitted by the telomeres to the SUN proteins at the NE. In turn, SUN proteins relay this mechanical signal to the NE via the BicD2 or NudE/NudEL pathways, triggering Dynein recruitment, through a mechanism not yet understood. This Dynein pool then ensures centrosome-NE coupling and proper positioning on the short nuclear axis at NEP (Fig. 7).

Our NE fluctuation measurements, which can be used to estimate the mechanical properties of the nucleus, have shown that these nuclear properties change in preparation for mitosis (Fig. 1D-F). At this stage, our study and others report an increase in the amplitude of the NE undulations that correlates with chromatin condensation [67–69]. Interfering with nucleo-cytoskeletal coupling and Lamin A depletion, impact nuclear mechanics, leading to increased amplitude of NE fluctuations (Fig. 2A-C and G-I; [68]). However, given that both treatments did not affect NE-Dynein levels (Fig. 4J, L and M), we concluded that only chromosome condensation provides the mechanical signal for NE-Dynein recruitment. Nevertheless, these cells do not behave normally during mitotic entry. Accordingly, we show that upon Lamin A depletion and LINC complex disruption, the nucleus is easily deformable by the separating centrosomes, leading to the formation of an ectopic, abnormal short nuclear axis (Fig. 2). This leads to an erroneous centrosome-nucleus configuration that would contribute for the mitotic problems previously described [40–44].

To date, research that focused on mechanotransduction pathways have considered that the mechanical stimuli are generated exclusively from cytoskeletal activities or from the cellular environment [96–99]. Here, we propose that the mechanical force generated by chromatin condensation constitutes, in itself, a source of mechanical stimuli for the cell. Supporting this idea, our previous study has shown that there is a reduction on the forces exerted by the cell on the extracellular matrix (ECM) accompanying mitotic cell rounding [28]. This strongly suggests an absence of substantial external mechanical stimulation at this stage. Additionally, previous studies have shown that the nucleus, which is thought to initially act as a mechanosensor, can subsequently act as a mechanotransducer and therefore modulate cytoskeleton or nuclear elements in response to strain (e.g. nuclear tension-mediated activation of YAP/TAZ pathway; [100,101]. In fact, the mechanical properties of the nucleus, the stiffest organelle in the cell, have the potential to influence the mechanics of the entire cell [102]. Importantly, while chromatin decompaction or histone hypermethylation decrease nuclear rigidity and often lead to the formation of nuclear blebs [51,55,57,58], chromatin condensation increases nuclear stiffness [51,53,54]. Lastly, although in somatic cells mitosis seems to be initiated simultaneously in all subcellular localizations [26], in larger cells the nucleus has been shown to concentrate Cdc25C and Cyclin B-CDK1 to ensure proper timing for both cytoplasmic and nuclear events [103,104].

The nucleus is physically connected to the cytoplasm through the LINC complex [71,105–107]. In our study we have shown that chromosome condensation-mediated forces are transmitted to the SUN proteins at the NE by the telomeric regions of chromosomes (Fig. 4-6). Accordingly, in somatic cells both SUN1 and SUN2 were considered to act as chromatin tethers at the NE [108,109]. Contrarywise, in mitotic cells, SUN1 does not colocalize with telomeres and, therefore, seems to interact solely with the NL and KASH proteins [109]. Upon mitotic exit in human cells, telomeres are anchored to the NE and interact with SUN1 in order to aid in chromatin organization during the process of NE reassembly [66]. Nevertheless, telomere distribution is still controversial. So far, different cell types at different stages exhibited distinct localization patterns [110–112]. This suggests that telomere positioning is a dynamic process, whose details are still not entirely understood. Therefore, a detailed spatiotemporal characterization of telomere behaviour during mitosis is still lacking.

In other experimental systems, Dynein-mediated forces are transmitted to the telomeres by SUN1-KASH5 bridges to modulate meiotic chromosome dynamics [109,113–119]. The formation of a meiotic chromosome bouquet, similarly to mitotic chromosome ring configuration [120], appears to aid mitotic spindle assembly efficiency, by facilitating homolog chromosome pairing [65,117]. Contrarily to this mechanism, our results indicate that KASH proteins are not driving Dynein recruitment to the NE during mitotic prophase

(Fig. 4L-M). Thus, alternative cellular components are required to mediate this process. Our results show that both Dynein adaptors, BicD2 and NudE/NudEL, localize to the NE after chromatin condensation impairment (Fig. S3). This suggests that loss of NE-Dynein is not due to a loss or mislocalization of these Dynein adaptors, but likely due to their lack of activity. Interestingly, both pathways driving NE-Dynein recruitment rely on the association of Dynein adaptors (BicD2 and NudE/NudEL) with the nucleoporins (RanBP2/Nup358 and Nup133, respectively) in the NPCs [76,79,121]. Thus, we speculate that chromatin condensation could generate pulling forces at the NE that induce conformational changes at the NPCs, activating these adaptors to promote NE-Dynein association. Supporting this idea, it was previously demonstrated that both SUN1 and SUN2 can directly interact with the NPCs [122]. In addition, NPC conformation and nucleocytoplasmic transport activity was reported to be modulated by NE membrane tension [101,123–125]. Also, a recent study demonstrated that in the beginning of mitosis, chromatin remodeling is initiated at the nuclear pores [126]. Importantly, this idea could explain how cell confinement, either by inducing transient chromatin condensation [84], or imposing mechanical strain on SUN proteins [127], is able to restore NE Dynein localization (Fig. 5). In this context, NE-Dynein recruitment might be a simple physical process regulated by chromatin-mediated tension in the NE. Still, we cannot exclude potential modulatory contributions of other accessory proteins and mechanisms.

Remarkably, NE-Dynein-mediated forces were shown to assist prophase centrosome separation [28], early spindle assembly [76], and NEP [24]. Consequently, chromosome condensation-mediated forces likely regulate and coordinate all these processes by determining timely Dynein loading. If that is the case, acutely impairing chromosome condensation might directly impact CyclinB1 nuclear translocation. Indeed, it was recently reported that mechanical confinement induced rapid Cyclin B1 translocation [49]. Nevertheless, challenging this hypothesis, abolishing cellular contractility, which was found to be required to facilitate Cyclin B1 nuclear translocation [49], did not impact NE-Dynein recruitment (Fig. 4K and M).

In conclusion, we propose that a new mechanical signaling pathway, which relies on chromosome condensation and regulates NE-Dynein recruitment, contributing to set the time for mitotic entry.

5. Materials and Methods

5.1. Cell lines

Cell lines were cultured in Dulbecco's Modified Eagle Medium (DMEM; Life Technologies) supplemented with 10% fetal bovine serum (FBS; Life Technologies) and grown in a 37˚C humidified incubator with 5% CO2. HeLa Lifeact-mCherry/EB3-GFP and HeLa DHC-GFP lines were a kind gift from Matthieu Piel and Iain Cheeseman, respectively. HeLa POM121-3xGFP and HeLa POM121-3xGFP/H2B-mCherry cell lines were kindly made available by Katharine Ullman.

5.1.1. Cell transduction with lentiviruses

HeLa cell line expressing histone H2B-GFP/mRFP-α-tubulin was generated in our lab using lentiviral vectors. For virus production, HEK293T cells at 50%-70% confluence were co-transfected with the lentiviral packaging vectors (16.6 µg of Pax2 and 5.6 µg of pMD2) together with 22.3 µg of LV-H2B-GFP (a gift from Elaine Fuchs, Addgene 545 plasmid 25999) or pRRL-mRFP-α-tubulin plasmids, and 30 µg of Lipofectamine2000 (Life Technologies). 48 - 72 h after transfection, the virus-containing supernatant was collected, centrifuged, filtered, and stored at –80°C. For cell transduction, HeLa parental cells were incubated with the previously produced lentivirus in the presence of polybrene (1:1000) in standard culture media, for 24 h. The lentiviruses were used separately, giving time for cells to recover between transductions. H2B-GFP/mRFP-α-tubulin double-positive cells were then isolated by fluorescence-activated cell sorting (FACS; FACS Aria II).

5.1.2. Transient transfection and plasmids

For transient overexpression of pEGFP-KASH (kindly provided by Christophe Guilluy), mRFP1-KASH-DN or mRFP1-KASH-deltaL (kindly provided by Edgar Gomes), cells were transiently transfected with the corresponding plasmid using Lipofectamine2000 (Life Technologies), according to the manufacturer's instructions. Briefly, 5 µl of Lipofectamine 2000 and 0.6 µg/ml of DNA of interest were diluted and incubated in Opti-Minimal Essential Medium (Opti-MEM; Alfagene) for 30 min. Cells at 50%–70% confluence were then incubated with the DNA-lipid complexes for 6 h. Prior to and during transfection, cells were cultured in reduced serum medium (DMEM supplemented with 5% FBS). Transfected cells were analyzed 72 h after transfection.

5.2. RNAi experiments

Cells were transfected with small interfering RNAs (siRNAs) using Lipofectamine RNAi Max (Life Technologies), according to the manufacturer's instructions. Briefly, 5 µl of

Lipofectamine and each siRNA were diluted and incubated in Opti-MEM (Alfagene) for 30 min. Different concentrations of siRNA were used: 20 nM for Lamin A RNAi, 40 nM for SUN1 and SUN2 RNAi and 200 nM for SMC2 and TRF1 RNAi. Cells at 50%–70% confluence were then incubated with the siRNA-lipid complexes for 6 h. Prior to and during transfection, cells were cultured in reduced serum medium (DMEM supplemented with 5% FBS). For all siRNAs used, cells were analyzed 48 - 72 h after transfection. Protein depletion efficiency was monitored by immunoblotting or immunohistochemistry. The following commercial ONTARGETplus siRNAs (Dharmacon) were used: Lamin A/C (#LQ-004978-00-0010), BicD2 (#L-014060-00-0020), SUN1 (#L-025277-00-0020), SUN2 (#L-009959-01-0020) and TERF1 (#L-010542-02-0020). For combined NudE/NudEL depletion the following oligos were ordered from Sigma-Aldrich 5`-GCUUGAAUCAGGCCAUCGA-3` and 5`-UCGAUGGCCUGAUUCAAGC-3` for NudE and 5`-GGAUGAAGCAAGAGAUUUA3`and 5`-UAAAUCUCUUGCUUCAUCC-3`for NudEL. For SMC2 depletion the following oligo was ordered from Sigma-Aldrich 5′-UGCUAUCACUGGCUUAAAUTT-3′ [128]. Both commercial ONTARGETplus non-targeting Pool siRNAs (Dharmacon #D-001810-10-20) and mock transfections were used as controls.

5.3. Drug treatments

Inhibition of Topoisomerase II was done using 10 μM of ICRF-193 (Merck-Millipore). Inhibition of histone deacetylases (HDACs) was done using 1.5 μM of VPA (Sigma-Aldrich). To interfere with the microtubule cytoskeleton, we used 20 nM of nocodazole (Sigma-Aldrich). Y-27632 (Sigma-Aldrich) was used at a concentration of 20 μM to inhibit ROCK. ICRF-193 and VPA were added to the culture medium 8 – 16 h before live-cell imaging or fixation. Nocodozole was added 30 min – 1 h before the experiments. Control cells were treated with DMSO (Sigma-Aldrich) only.

5.4. Micro-patterning

To control individual cell shape and adhesion pattern, micro-patterns were produced as previously described [129,130]. Succinctly, glass coverslips, previously activated with plasma (Zepto Plasma System, Diener Electronic) for 1 min, were incubated with 0.1 mg/ml of PLL(20)-g[3,5]-PEG(2) (SuSoS) in 10 mM HEPES at pH 7.4, for 30 min, at room temperature (RT). After rinsing and air-drying, the coverslips were sealed onto a synthetic quartz photomask (Delta Mask), previously activated with deep-UV light (PSD-UV, Novascan Technologies) for 5 min, using 3 μl of MiliQ water. The coverslips were then irradiated through the photomask with the UV lamp for 5 min and incubated with 25 μg/ml of fibronectin (FBN; Sigma-Aldrich) in 100 mM NaHCO3 at pH 8.6, for 1 h, at RT. To monitor patterning efficiency and quality, 5 μg/ml of Alexa546 or 647-conjugated fibrinogen (Thermo

Fisher Scientific) was added to the FBN solution. 50.000-75 000 cells were seeded per patterned-coverslip and allowed to for ~10–15 h before imaging. To wash out non-attached cells the cell medium was changed ~2–5 h after seeding.

5.5. Cell confinement

For cell confinement experiments, confinement slides made of a glass coverslips covered by a microstructured layer of PDMS designed with a regular array of micropillars (diameter 449 µm, 1 mm spacing, 8 µm height) were used to confine cells in two dimensions (geometric confinement). Confinement slide fabrication has been previously described elsewhere [131]. Briefly, a drop of polydimethylsiloxane (PDMS, RTV615, GE) mixture (8/1 w/w PDMS A/crosslinker B) was poured on top of a microfabricated mold. 10-mm glass coverslips, previously activated with plasma for 2 min (Zepto system, Diener Electronics), were placed on top of the PDMS drop and gently pushed with tweezers to obtain a very thin layer of PDMS under the coverslips. The mold containing the coverslips was then baked on the hot plate at 95ºC for 15 min. After removing the excess of PDMS, the coverslips were released from the mold with the help of isopropanol and a razor blade, rinsed with isopropanol and air dried. Confinement coverslips were used without any treatment but were incubated with the appropriate culture media and drugs (when used) for at least 1 h before each experiment.

The confinement slides were applied onto cells using two different setups, the dynamic and the static cell confinement setups, described previously [130,131]. To perform dynamic cell confinement experiments, the so-called cell confiner device was assembled as described previously [131]. Briefly, using a custom-made mold a suction cup made of a PDMS mixture (10/1 w/w PDMS A/crosslinker B) was baked on the hot plat at 80ºC for 1h and left to dry overnight. After unmolding the device, a puncher (0.75 mm) was used to create a hole to plug the device into the vacuum generator apparatus (Elveflow). The confinement slide was placed onto the piston of the device. Lastly, the device was sealed on top of the cell culture substrate and cell confinement was modulated by increasing or decreasing the pressure on the vacuum line.

Static cell confinement experiments were done using a commercially available modified 6-well lid (4DCell). In this case, PDMS pillars were stuck on the lid and hold the confinement slides. When 6-well plate was closed with the lid, the pillars pushed the confinement slides onto the culture substrate and confined the cells.

5.6. Time-lapse microscopy

For time-lapse microscopy, a day prior to imaging cells were seeded on FBN-patterned-coverslips. Before each experiment, the cell culture medium was replaced with

Leibovitz's-L15 medium (Life Technologies) supplemented with 10% FBS and Antibiotic-Antimycotic 100X (AAS; Life Technologies). When SiR-dyes (20 nM Sir-tubulin or 10 nM Sir-DNA; Spirochrome) and/or drugs (acute pharmacological inhibition) were used, they were added to the culture medium before acquisition. Live-cell imaging was performed using temperature-controlled Nikon TE2000 microscopes equipped with a modified Yokogawa CSU-X1 spinning-disc head (Yokogawa Electric), an electron multiplying iXon+ DU-897 EM-CCD camera (Andor) and a filter-wheel. The following laser lines were used for excitation: 488, 561 and 647nm. The experiments were done with an oil-immersion 60x 1.4 NA Plan-Apo DIC (Nikon), except for the nuclear pore fluctuation analysis, in which an oil-immersion 100x 1.4 NA Plan-Apo DIC (Nikon) was used. Image acquisition was controlled by NIS Elements AR software. For centrosome tracking, 17-21 z-stacks with a 0.5 µm or 0.7 µm separation were collected every 20 sec. For NE fluctuation analysis, a single z-stack was collected every 100 msec.

5.7. Immunofluorescence

For DHC, SUN1, SUN2, Lamin A/C, Lamin B1, BicD2 and NudE/NudEL immunostainings cells were seeded on FBN-patterned-coverslips and fixed with 4% Paraformaldehyde (PFA) in Cytoskeleton Buffer (274 mM NaCl, 2.2mM Na2HPO4, 10mM KCL, 0.8 mM KH2PO4, 4 mM EDTA, 4 mM MgCl2, 10 mM Pipes, 10 nM Glucose, pH 6.1) for 8 min. Subsequently, cells were permeabilized with 0.5% Triton X-100 (Sigma- Aldrich) in 1x phosphate-buffered saline (PBS) for 5 min, and washed with 0.1% Triton X-100, 2x for 5 min. The cells were then blocked with 10% FBS in 0.1% Triton X-100 in PBS for 30 min. After blocking, the cells were incubated with the primary antibodies diluted in blocking solution, for 1 h at RT. Next, the cells were washed with 10% Triton X-100 in 1x PBS, 2x for 5 min and subsequently incubated with the respectively secondary antibody, diluted in blocking solution, and DAPI (1ug/ml, Sigma-Aldrich) for 45 min at RT. Lastly, cells were washed with 0.1% Triton X-100 in 1x PBS, 2x for 5 min, and sealed on glass slides mounted with 20 mM Tris pH8, 0.5 N-propyl gallate and 90% glycerol.

For SMC2 and TRF1 immunostainings cells were seeded on Poly-L-lysine-(PPL)-coated coverslips (50 µg/ml; Sigma, P8920). For SMC2 immunostaining, cells were washed with 1x PBS for 1 min, pre-extracted with 0.5% Triton-X100 for 30 sec and fixed with 4% PFA in Cytoskeleton Buffer (274 mM NaCl, 2.2mM Na2HPO4, 10mM KCL, 0.8 mM KH2PO4, 4 mM EDTA, 4 mM MgCl2, 10 mM Pipes, 10 nM Glucose, pH 6.1) for 8 min. Next, cells were permeabilized with 0.5% Triton-X100 for 3 min, washed with 0.1% Triton-X100 for 2x for 3 min and blocked with 10% FBS in 0.1% Triton X-100 in PBS for 30 min. After blocking, the cells were incubated with the primary antibodies followed by the secondary antibodies and sealed on glass coverslips as described for the initial immunostainings. For

TRF1 immunostaining, cells were washed with 1x PBS for 1 min, pre-extracted with 0.5% Triton-X100 for 30 sec and fixed with 4% PFA for 8 min. Next, cells were permeabilized with TBS-T with 0.25% Triton-X100 for 3 min, washed with 0.1% Triton-X100 for 2x for 3 min and blocked with 5% BSA with TBS-T for 30 min. After blocking, the cells were incubated with the primary antibodies followed by the secondary antibodies and sealed on glass coverslips as described for the initial immunostainings.

The following primary antibodies were used: mouse anti-Lamin A/C (1:500, Abcam), rabbit anti-Lamin B1 (1:500, Abcam), rat anti-alpha Tubulin (1:500, Bio-Rad), rabbit anti-NudE/NudEL antibody (1:500, gift from Richard Vallee), rabbit anti-BicD2 (1:500, Atlas Antibodies) rabbit anti-SUN1 (1:1000, Sigma-Aldrich), rabbit anti-SUN2 (1:1000, Sigma-Aldrich) mouse anti-TRF1 antibody (1:500, Abcam) and rabbit anti-SMC2 antibody (1:500; Bethyl Laboratories). Alexa Fluor 488, 568 and 647 (1:2000, Invitrogen) were used as secondary antibodies. Images were acquired using an AxioImager Z1 (63x, plan oil differential interference contract objective lens, 1.4 NA; all from Carl Zeiss) which is coupled with a CCD camera (ORCA-R2; Hamamatsu Photonics). Image acquisition was controlled by Zen software (Carl Zeiss).

5.8. Quantification of DHC-GFP fluorescence intensity

To quantify DHC-GFP fluorescence intensity in immunofluorescence samples, for each individual cell the 3-middle z-stacks containing the NE were collected and sum-projected using ImageJ. To identify the NE, either DHC-GFP signal or Lamin B1, Lamin A or SUN1/2 immunostaining, were used as a guide. Subsequently, four lines were drawn on the NE regions corresponding to each side of the long and of the short nuclear axes. For each line measured, the maximum gray value, which correspond to the NE region, was collected. The four maximum gray values were then averaged for each individual cell. Lastly, the individual mean gray values were average across cells of each experimental group.

5.9. Western Blotting

HeLa cell extracts were collected, washed, and resuspended in 30-50 µL of Lysis Buffer (NP-40, 20 nM HEPES/KOH 775 pH 7.9; 1 mM EDTA pH 8; 1 mM EGTA; 150 mM NaCl; 0.5% NP40; 10% glycerol, 1:50 protease inhibitor; 1:100 Phenylmethylsulfonyl fluoride). The samples were then flash frozen in liquid nitrogen and kept on ice for 30 min. After centrifugation at 14000 rpm for min at 4ºC, the supernatant was collected, and protein concentration was determined by the Bradford protein assay (Bio-Rad). 50 µg of each protein were loaded and ran on 15% SDS-PAGE gels. Next, the loaded proteins were transferred to a nitrocellulose Hybond-C membrane using the iBlot Gel Transfer Device

(Thermo Scientific). Afterwards the membranes were blocked with 5% Milk in triphosphate buffered saline (TBS) with 0.1% Tween-20 (TBS-T) for 1h at RT and subsequently incubated with the primary antibodies overnight at 4ºC with shaking. After three washes in TBS-T, the membranes were incubated with the secondary antibody for 1h at RT. After several washes with TBS-T, the detection was performed with Clarity Western ECL Substrate (Bio-Rad).

The following primary antibodies were used: mouse anti-Lamin A/C (1:500, Abcam), mouse anti-Nde1 (1:500, Abnova), rabbit anti-BicD2 (1:250, Atlas Antibodies) and rat anti-alpha tubulin (1:1000, Bio-Rad). The secondary antibodies used were anti-mouse-HRP, anti-rabbit-HRP and anti-rat-HRP at 1:5000.

5.10. Quantitative analysis of centrosomes, cell membrane and nucleus membrane

Detailed quantitative analysis of centrosomes location and membranes topology (cell and nucleus) was performed using custom made MATLAB scripts (The MathWorks Inc., USA; R2018a). The image analysis took advantage of the different labeling for centrosomes, cell membrane and nuclear membrane. The scripts were separated into three modules with specific workflows: i) centrosomes tracking, ii) nuclear and cellular membrane reconstruction, and iii) nuclear membrane surface dynamics. Tracking of centrosomes position/trajectories was performed in 3D space using image stacks with a pixel size of 0.190μm and z-step of 0.7μm. Images were pre-processed using a Laplacian of Gaussian filter with a user-defined kernel size, associated with the centrosome radius in pixels. Image segmentation was performed using Otsu's method, and morphological operators were used to improve the mask and obtain the centrosomes 3D coordinates. Error correction methods, such as automatic thresholding adjustment or in the limit frame elimination, were implemented to take care of frames where the standard method was unable to uniquely identify 2 centrosomes. For the visualization of the centrosomes trajectories (space and time), the centrosomes coordinates were interpolated using cubic splines. Different metrics, such as the distance between centrosomes (pole-to-pole), were calculated to analyze and characterize the trajectories. Cellular and nuclear membranes were reconstructed in 3D space taking advantage of specific labeling. For each membrane, a mask was produced using Otsu's method and improved with a sequence of morphological operators (namely image close, dilation and erosion, small objects removal). The orientation axis for the membranes were calculated using principal components analysis (PCA) of a large sample of membrane surface points. This method using PCA was found to be more robust than ellipsoid fitting to the membrane surface (followed by extraction of the axis vectors). From the centrosomes locations and nuclear membrane reconstruction, it was possible to

calculate the angle between the centrosomes axis and the nucleus major axis. Quantification of nuclear membrane surface fluctuation was performed in 2D using a single slice with a pixel size of 0.102μm. The coordinates of the pixels in the membrane contour were extracted for each frame by first reducing noise with a median filter (neighborhood of 3×3 pixels) followed by object segmentation. The segmentation used a statistical threshold (median + standard deviation), and was improved with small objects removal and closure morphological operations. A reference membrane contour for the nucleus, obtained from the median intensity projection of all frames, was used as “baseline” for the fluctuation analysis. The (Euclidean) coordinates of the nuclear membrane pixels for each frame were converted to polar coordinates, and fluctuations were calculated as the difference in the radial component to the reference contour. The center of the polar coordinates was defined as the centroid of the reference membrane contour. The polar coordinates allowed the decomposition of the fluctuations normal to the nuclear contour (captured in the radial coordinate). The analysis was limited to 60° angular apertures centered on the membranes main axis, as to minimize the error in the radial component. Different methods were designed to explore, analyze, and visualize the radial components of the membrane contour. In these methods, the membrane radial fluctuations were characterized using statistics such as maximal amplitudes or standard deviation of the radial component. Radial displacement maps were produced as the radial shift of each point in the membrane with respect to the reference (median) membrane contour. Nuclear irregularity index was calculated as described previously [132].

5.11. Statistical analysis and data presentation

Each experiment was repeated independently at least three times and sample sizes are defined in each figure legend. We used three to six independent experiments or biologically independent samples for statistical analysis. When data are represented as box-whisker plots, the box size represents 75% of the population and the line inside the box represents the median of the sample. The size of the bars (whiskers) represents the maximum (in the upper quartile) and the minimum (in the lower quartile) values. Distribution normalities were assessed using the Kolmogorov– Smirnov test. Statistical analysis for multiple group comparison was performed using a parametric one-way analysis of variance (ANOVA) when the samples had a normal distribution. When the sample did not have a normal distribution, multiple group comparison was done using a nonparametric ANOVA (Kruskal-Wallis). When comparing only two experimental groups, a parametric t test was used when the sample had a normal distribution, or a nonparametric Mann-Whitney test was used for samples without normal distribution. No power calculations were used. All statistical analyses were performed using SigmaStat 3.5 (Systat Software, Inc.).

6. References

[1] L. Champion, M.I. Linder, U. Kutay, Cellular Reorganization during Mitotic Entry, Trends Cell Biol. 27 (2017) 26–41. https://doi.org/10.1016/j.tcb.2016.07.004.

[2] N. Mchedlishvili, H.K. Matthews, A. Corrigan, B. Baum, Two-step interphase microtubule disassembly aids spindle morphogenesis, BMC Biol. 16 (2018) 14. https://doi.org/10.1186/s12915-017-0478-z.

[3] P. Meraldi, E.A. Nigg, The centrosome cycle, FEBS Lett. 521 (2002) 9–13. https://doi.org/10.1016/s0014-5793(02)02865-x.

[4] D.A. Compton, Spindle Assembly in Animal Cells, Annu. Rev. Biochem. 69 (2000) 95–114. https://doi.org/10.1146/annurev.biochem.69.1.95.

[5] C. Cadart, E. Zlotek-Zlotkiewicz, M. Le Berre, M. Piel, H.K. Matthews, Exploring the function of cell shape and size during mitosis, Dev. Cell. 29 (2014) 159–169. https://doi.org/10.1016/j.devcel.2014.04.009.

[6] V.T. Dao, A.G. Dupuy, O. Gavet, E. Caron, J. de Gunzburg, Dynamic changes in Rap1 activity are required for cell retraction and spreading during mitosis, J. Cell Sci. 122 (2009) 2996–3004. https://doi.org/10.1242/jcs.041301.

[7] C.L. Dix, H.K. Matthews, M. Uroz, S. McLaren, L. Wolf, N. Heatley, Z. Win, P. Almada, R. Henriques, M. Boutros, X. Trepat, B. Baum, The Role of Mitotic Cell-Substrate Adhesion Re-modeling in Animal Cell Division, Dev. Cell. 45 (2018) 132-145.e3. https://doi.org/10.1016/j.devcel.2018.03.009.

[8] L.P. Cramer, T.J. Mitchison, Investigation of the mechanism of retraction of the cell margin and rearward flow of nodules during mitotic cell rounding, Mol. Biol. Cell. 8 (1997) 109–119. https://doi.org/10.1091/mbc.8.1.109.

[9] A.S. Maddox, K. Burridge, RhoA is required for cortical retraction and rigidity during mitotic cell rounding, J. Cell Biol. 160 (2003) 255–265. https://doi.org/10.1083/jcb.200207130.

[10] P. Chugh, E.K. Paluch, The actin cortex at a glance, J. Cell Sci. 131 (2018). https://doi.org/10.1242/jcs.186254.

[11] P. Kunda, A.E. Pelling, T. Liu, B. Baum, Moesin Controls Cortical Rigidity, Cell Rounding, and Spindle Morphogenesis during Mitosis, Curr. Biol. 18 (2008) 91–101. https://doi.org/10.1016/j.cub.2007.12.051.

[12] P. Kunda, B. Baum, The actin cytoskeleton in spindle assembly and positioning, Trends Cell Biol. 19 (2009) 174–179. https://doi.org/10.1016/j.tcb.2009.01.006.

[13] H.K. Matthews, U. Delabre, J.L. Rohn, J. Guck, P. Kunda, B. Baum, Changes in Ect2 Localization Couple Actomyosin-Dependent Cell Shape Changes to Mitotic Progression, Dev. Cell. 23 (2012) 371–383. https://doi.org/10.1016/j.devcel.2012.06.003.

[14] A. Rosa, E. Vlassaks, F. Pichaud, B. Baum, Ect2/Pbl Acts via Rho and Polarity Proteins to Direct the Assembly of an Isotropic Actomyosin Cortex upon Mitotic Entry, Dev. Cell. 32 (2015) 604–616. https://doi.org/10.1016/j.devcel.2015.01.012.

[15] M.P. Stewart, J. Helenius, Y. Toyoda, S.P. Ramanathan, D.J. Muller, A.A. Hyman, Hydrostatic pressure and the actomyosin cortex drive mitotic cell rounding, Nature. 469 (2011) 226–230. https://doi.org/10.1038/nature09642.

[16] E. Zlotek-Zlotkiewicz, S. Monnier, G. Cappello, M. Le Berre, M. Piel, Optical volume and mass measurements show that mammalian cells swell during mitosis, J. Cell Biol. 211 (2015) 765–774. https://doi.org/10.1083/jcb.201505056.

[17] W. Antonin, H. Neumann, Chromosome condensation and decondensation during mitosis, Curr. Opin. Cell Biol. 40 (2016) 15–22. https://doi.org/10.1016/j.ceb.2016.01.013.

[18] K. Kinoshita, T. Hirano, Dynamic organization of mitotic chromosomes, Curr. Opin. Cell Biol. 46 (2017) 46–53. https://doi.org/10.1016/j.ceb.2017.01.006.

[19] C.L. Rieder, Mitosis in vertebrates: the G2/M and M/A transitions and their associated checkpoints, Chromosome Res. Int. J. Mol. Supramol. Evol. Asp. Chromosome Biol. 19 (2011) 291–306. https://doi.org/10.1007/s10577-010-9178-z.

[20] S. Güttinger, E. Laurell, U. Kutay, Orchestrating nuclear envelope disassembly and reassembly during mitosis, Nat. Rev. Mol. Cell Biol. 10 (2009) 178–191. https://doi.org/10.1038/nrm2641.

[21] R. Ungricht, U. Kutay, Mechanisms and functions of nuclear envelope remodelling, Nat. Rev. Mol. Cell Biol. 18 (2017) 229–245. https://doi.org/10.1038/nrm.2016.153.

[22] S.D. Georgatos, A. Pyrpasopoulou, P.A. Theodoropoulos, Nuclear envelope breakdown in mammalian cells involves stepwise lamina disassembly and microtubule-drive deformation of the nuclear membrane, J. Cell Sci. 110 (Pt 17) (1997) 2129–2140.

[23] J. Beaudouin, D. Gerlich, N. Daigle, R. Eils, J. Ellenberg, Nuclear Envelope Breakdown Proceeds by Microtubule-Induced Tearing of the Lamina, Cell. 108 (2002) 83–96. https://doi.org/10.1016/S0092-8674(01)00627-4.

[24] D. Salina, K. Bodoor, D.M. Eckley, T.A. Schroer, J.B. Rattner, B. Burke, Cytoplasmic Dynein as a Facilitator of Nuclear Envelope Breakdown, Cell. 108 (2002) 97–107. https://doi.org/10.1016/S0092-8674(01)00628-6.

[25] O. Gavet, J. Pines, Progressive activation of CyclinB1-Cdk1 coordinates entry to mitosis, Dev. Cell. 18 (2010) 533–543. https://doi.org/10.1016/j.devcel.2010.02.013.

[26] O. Gavet, J. Pines, Activation of cyclin B1-Cdk1 synchronizes events in the nucleus and the cytoplasm at mitosis, J. Cell Biol. 189 (2010) 247–259. https://doi.org/10.1083/jcb.200909144.

[27] O.M. Lancaster, M. Le Berre, A. Dimitracopoulos, D. Bonazzi, E. Zlotek-Zlotkiewicz, R. Picone, T. Duke, M. Piel, B. Baum, Mitotic rounding alters cell geometry to ensure efficient bipolar spindle formation, Dev. Cell. 25 (2013) 270–283. https://doi.org/10.1016/j.devcel.2013.03.014.

[28] V. Nunes, M. Dantas, D. Castro, E. Vitiello, I. Wang, N. Carpi, M. Balland, M. Piel, P. Aguiar, H. Maiato, J.G. Ferreira, Centrosome-nuclear axis repositioning drives the assembly of a bipolar spindle scaffold to ensure mitotic fidelity, Mol. Biol. Cell. (2020) mbc.E20-01-0047. https://doi.org/10.1091/mbc.E20-01-0047.

[29] J. Cao, J. Crest, B. Fasulo, W. Sullivan, Cortical Actin Dynamics Facilitate Early-Stage Centrosome Separation, Curr. Biol. 20 (2010) 770–776. https://doi.org/10.1016/j.cub.2010.02.060.

[30] R. Uzbekov, I. Kireyev, C. Prigent, Centrosome separation: respective role of microtubules and actin filaments, Biol. Cell. 94 (2002) 275–288. https://doi.org/10.1016/S0248-4900(02)01202-9.

[31] A. De Simone, F. Nédélec, P. Gönczy, Dynein Transmits Polarized Actomyosin Cortical Flows to Promote Centrosome Separation, Cell Rep. 14 (2016) 2250–2262. https://doi.org/10.1016/j.celrep.2016.01.077.

[32] J.A. Raaijmakers, R.G.H.P. van Heesbeen, J.L. Meaders, E.F. Geers, B. Fernandez-Garcia, R.H. Medema, M.E. Tanenbaum, Nuclear envelope-associated dynein drives prophase centrosome separation and enables Eg5-independent bipolar spindle formation, EMBO J. 31 (2012) 4179–4190. https://doi.org/10.1038/emboj.2012.272.

[33] C.M. Whitehead, R.J. Winkfein, J.B. Rattner, The relationship of HsEg5 and the actin cytoskeleton to centrosome separation, Cell Motil. Cytoskeleton. 35 (1996) 298–308. https://doi.org/10.1002/(SICI)1097-0169(1996)35:4<298::AID-CM3>3.0.CO;2-3.

[34] E.N. Cytrynbaum, J.M. Scholey, A. Mogilner, A Force Balance Model of Early Spindle Pole Separation in Drosophila Embryos, Biophys. J. 84 (2003) 757–769. https://doi.org/10.1016/S0006-3495(03)74895-4.

[35] M.E. Tanenbaum, R.H. Medema, Mechanisms of centrosome separation and bipolar spindle assembly, Dev. Cell. 19 (2010) 797–806. https://doi.org/10.1016/j.devcel.2010.11.011.

[36] J. Fink, N. Carpi, T. Betz, A. Bétard, M. Chebah, A. Azioune, M. Bornens, C. Sykes, L. Fetler, D. Cuvelier, M. Piel, External forces control mitotic spindle positioning, Nat. Cell Biol. 13 (2011) 771–778. https://doi.org/10.1038/ncb2269.

[37] S.W. Grill, J. Howard, E. Schäffer, E.H.K. Stelzer, A.A. Hyman, The Distribution of Active Force Generators Controls Mitotic Spindle Position, Science. 301 (2003) 518–521. https://doi.org/10.1126/science.1086560.

[38] O. Hertwig, Das Problem der Befruchtung und der Isotropie des Eies: eine Theorie der Vererbung, Fischer, 1884.

[39] M. Théry, V. Racine, A. Pépin, M. Piel, Y. Chen, J.-B. Sibarita, M. Bornens, The extracellular matrix guides the orientation of the cell division axis, Nat. Cell Biol. 7 (2005) 947–953. https://doi.org/10.1038/ncb1307.

[40] T. Kuga, H. Nie, T. Kazami, M. Satoh, K. Matsushita, F. Nomura, K. Maeshima, Y. Nakayama, T. Tomonaga, Lamin B2 prevents chromosome instability by ensuring proper mitotic chromosome segregation, Oncogenesis. 3 (2014) e94. https://doi.org/10.1038/oncsis.2014.6.

[41] R. Qi, N. Xu, G. Wang, H. Ren, S. Li, J. Lei, Q. Lin, L. Wang, X. Gu, H. Zhang, Q. Jiang, C. Zhang, The lamin-A/C-LAP2α-BAF1 protein complex regulates mitotic spindle assembly and positioning, J. Cell Sci. 128 (2015) 2830–2841. https://doi.org/10.1242/jcs.164566.

[42] M.-Y. Tsai, S. Wang, J.M. Heidinger, D.K. Shumaker, S.A. Adam, R.D. Goldman, Y. Zheng, A Mitotic Lamin B Matrix Induced by RanGTP Required for Spindle Assembly, Science. 311 (2006) 1887–1893. https://doi.org/10.1126/science.1122771.

[43] T. Stiff, F.R. Echegaray-Iturra, H.J. Pink, A. Herbert, C.C. Reyes-Aldasoro, H. Hochegger, Prophase-Specific Perinuclear Actin Coordinates Centrosome Separation and Positioning to Ensure Accurate Chromosome Segregation, Cell Rep. 31 (2020) 107681. https://doi.org/10.1016/j.celrep.2020.107681.

[44] Y. Turgay, L. Champion, C. Balazs, M. Held, A. Toso, D.W. Gerlich, P. Meraldi, U. Kutay, SUN proteins facilitate the removal of membranes from chromatin during nuclear envelope breakdown, J. Cell Biol. 204 (2014) 1099–1109. https://doi.org/10.1083/jcb.201310116.

[45] J. Aureille, V. Buffière-Ribot, B.E. Harvey, C. Boyault, L. Pernet, T. Andersen, G. Bacola, M. Balland, S. Fraboulet, L. Van Landeghem, C. Guilluy, Nuclear envelope deformation controls cell cycle progression in response to mechanical force, EMBO Rep. 20 (2019) e48084. https://doi.org/10.15252/embr.201948084.

[46] S. Huang, C.S. Chen, D.E. Ingber, Control of cyclin D1, p27(Kip1), and cell cycle progression in human capillary endothelial cells by cell shape and cytoskeletal tension, Mol. Biol. Cell. 9 (1998) 3179–3193. https://doi.org/10.1091/mbc.9.11.3179.

[47] M. Uroz, S. Wistorf, X. Serra-Picamal, V. Conte, M. Sales-Pardo, P. Roca-Cusachs, R. Guimerà, X. Trepat, Regulation of cell cycle progression by cell-cell and cell-matrix forces, Nat. Cell Biol. 20 (2018) 646–654. https://doi.org/10.1038/s41556-018-0107-2.

[48] B. Vianay, F. Senger, S. Alamos, M. Anjur-Dietrich, E. Bearce, B. Cheeseman, L. Lee, M. Théry, Variation in traction forces during cell cycle progression, Biol. Cell. 110 (2018) 91–96. https://doi.org/10.1111/boc.201800006.

[49] M. Dantas, A. Oliveira, P. Aguiar, H. Maiato, J.G. Ferreira, Mechanosensitive control of mitotic entry, (2021) 2021.09.23.461473. https://doi.org/10.1101/2021.09.23.461473.

[50] A.D. Stephens, E.J. Banigan, S.A. Adam, R.D. Goldman, J.F. Marko, Chromatin and lamin A determine two different mechanical response regimes of the cell nucleus, Mol. Biol. Cell. 28 (2017) 1984–1996. https://doi.org/10.1091/mbc.e16-09-0653.

[51] A.D. Stephens, E.J. Banigan, J.F. Marko, Chromatin's physical properties shape the nucleus and its functions, Curr. Opin. Cell Biol. 58 (2019) 76–84. https://doi.org/10.1016/j.ceb.2019.02.006.

[52] J. Lammerding, L.G. Fong, J.Y. Ji, K. Reue, C.L. Stewart, S.G. Young, R.T. Lee, Lamins A and C but not lamin B1 regulate nuclear mechanics, J. Biol. Chem. 281 (2006) 25768–25780. https://doi.org/10.1074/jbc.M513511200.

[53] K.N. Dahl, A.J. Engler, J.D. Pajerowski, D.E. Discher, Power-law rheology of isolated nuclei with deformation mapping of nuclear substructures, Biophys. J. 89 (2005) 2855–2864. https://doi.org/10.1529/biophysj.105.062554.

[54] T. Furusawa, M. Rochman, L. Taher, E.K. Dimitriadis, K. Nagashima, S. Anderson, M. Bustin, Chromatin decompaction by the nucleosomal binding protein HMGN5 impairs nuclear sturdiness, Nat. Commun. 6 (2015) 6138. https://doi.org/10.1038/ncomms7138.

[55] R. Biggs, P.Z. Liu, A.D. Stephens, J.F. Marko, Effects of altering histone posttranslational modifications on mitotic chromosome structure and mechanics, Mol. Biol. Cell. 30 (2019) 820–827. https://doi.org/10.1091/mbc.E18-09-0592.

[56] Y. Gruenbaum, A. Margalit, R.D. Goldman, D.K. Shumaker, K.L. Wilson, The nuclear lamina comes of age, Nat. Rev. Mol. Cell Biol. 6 (2005) 21–31. https://doi.org/10.1038/nrm1550.

[57] J. Lammerding, P.C. Schulze, T. Takahashi, S. Kozlov, T. Sullivan, R.D. Kamm, C.L. Stewart, R.T. Lee, Lamin A/C deficiency causes defective nuclear mechanics and mechanotransduction, J. Clin. Invest. 113 (2004) 370–378. https://doi.org/10.1172/JCI19670.

[58] K. Maeshima, T. Matsuda, Y. Shindo, H. Imamura, S. Tamura, R. Imai, S. Kawakami, R. Nagashima, T. Soga, H. Noji, K. Oka, T. Nagai, A Transient Rise in Free Mg2+ Ions Released from ATP-Mg Hydrolysis Contributes to Mitotic Chromosome Condensation, Curr. Biol. CB. 28 (2018) 444-451.e6. https://doi.org/10.1016/j.cub.2017.12.035.

[59] J.D. Pajerowski, K.N. Dahl, F.L. Zhong, P.J. Sammak, D.E. Discher, Physical plasticity of the nucleus in stem cell differentiation, Proc. Natl. Acad. Sci. U. S. A. 104 (2007) 15619–15624. https://doi.org/10.1073/pnas.0702576104.

[60] T. Shimi, K. Pfleghaar, S. Kojima, C.-G. Pack, I. Solovei, A.E. Goldman, S.A. Adam, D.K. Shumaker, M. Kinjo, T. Cremer, R.D. Goldman, The A- and B-type nuclear lamin networks: microdomains involved in chromatin organization and transcription, Genes Dev. 22 (2008) 3409–3421. https://doi.org/10.1101/gad.1735208.

[61] I. Solovei, A.S. Wang, K. Thanisch, C.S. Schmidt, S. Krebs, M. Zwerger, T.V. Cohen, D. Devys, R. Foisner, L. Peichl, H. Herrmann, H. Blum, D. Engelkamp, C.L. Stewart, H. Leonhardt, B. Joffe, LBR and lamin A/C sequentially tether peripheral heterochromatin and inversely regulate differentiation, Cell. 152 (2013) 584–598. https://doi.org/10.1016/j.cell.2013.01.009.

[62] X. Zheng, J. Hu, S. Yue, L. Kristiani, M. Kim, M. Sauria, J. Taylor, Y. Kim, Y. Zheng, Lamins Organize the Global Three-Dimensional Genome from the Nuclear Periphery, Mol. Cell. 71 (2018) 802-815.e7. https://doi.org/10.1016/j.molcel.2018.05.017.

[63] X. Zheng, Y. Kim, Y. Zheng, Identification of lamin B–regulated chromatin regions based on chromatin landscapes, Mol. Biol. Cell. 26 (2015) 2685–2697. https://doi.org/10.1091/mbc.E15-04-0210.

[64] S. Melcer, H. Hezroni, E. Rand, M. Nissim-Rafinia, A. Skoultchi, C.L. Stewart, M. Bustin, E. Meshorer, Histone modifications and lamin A regulate chromatin protein dynamics in early embryonic stem cell differentiation, Nat. Commun. 3 (2012) 910. https://doi.org/10.1038/ncomms1915.

[65] L. Harper, I. Golubovskaya, W.Z. Cande, A bouquet of chromosomes, J. Cell Sci. 117 (2004) 4025–4032. https://doi.org/10.1242/jcs.01363.

[66] L. Crabbe, A.J. Cesare, J.M. Kasuboski, J.A.J. Fitzpatrick, J. Karlseder, Human telomeres are tethered to the nuclear envelope during post-mitotic nuclear assembly, Cell Rep. 2 (2012) 1521–1529. https://doi.org/10.1016/j.celrep.2012.11.019.

[67] D. Castro, V. Nunes, J.T. Lima, J.G. Ferreira, P. Aguiar, Trackosome: a computational toolbox to study the spatiotemporal dynamics of centrosomes, nucleus and cellular membrane, J. Cell Sci. (2020). https://doi.org/10.1242/jcs.252254.

[68] V. Introini, G.R. Kidiyoor, G. Porcella, M. Foiani, P. Cicuta, M.C. Lagomarsino, Centripetal nuclear shape fluctuations associate with chromatin condensation towards mitosis, (2021) 2021.11.25.469847. https://doi.org/10.1101/2021.11.25.469847.

[69] F.-Y. Chu, S.C. Haley, A. Zidovska, On the origin of shape fluctuations of the cell nucleus, Proc. Natl. Acad. Sci. 114 (2017) 10338–10343. https://doi.org/10.1073/pnas.1702226114.

[70] M. Crisp, Q. Liu, K. Roux, J.B. Rattner, C. Shanahan, B. Burke, P.D. Stahl, D. Hodzic, Coupling of the nucleus and cytoplasm: role of the LINC complex, J. Cell Biol. 172 (2006) 41–53. https://doi.org/10.1083/jcb.200509124.

[71] M.L. Lombardi, J. Lammerding, Keeping the LINC: the importance of nucleocytoskeletal coupling in intracellular force transmission and cellular function, Biochem. Soc. Trans. 39 (2011) 1729–1734. https://doi.org/10.1042/BST20110686.

[72] M.L. Lombardi, D.E. Jaalouk, C.M. Shanahan, B. Burke, K.J. Roux, J. Lammerding, The interaction between nesprins and sun proteins at the nuclear envelope is critical for force transmission between the nucleus and cytoskeleton, J. Biol. Chem. 286 (2011) 26743–26753. https://doi.org/10.1074/jbc.M111.233700.

[73] P.J. Stewart-Hutchinson, C.M. Hale, D. Wirtz, D. Hodzic, Structural requirements for the assembly of LINC complexes and their function in cellular mechanical stiffness, Exp. Cell Res. 314 (2008) 1892–1905. https://doi.org/10.1016/j.yexcr.2008.02.022.

[74] M. Versaevel, T. Grevesse, S. Gabriele, Spatial coordination between cell and nuclear shape within micropatterned endothelial cells, Nat. Commun. 3 (2012) 671. https://doi.org/10.1038/ncomms1668.

[75] E. Piskadlo, R.A. Oliveira, A Topology-Centric View on Mitotic Chromosome Architecture, Int. J. Mol. Sci. 18 (2017) E2751. https://doi.org/10.3390/ijms18122751.

[76] S. Bolhy, I. Bouhlel, E. Dultz, T. Nayak, M. Zuccolo, X. Gatti, R. Vallee, J. Ellenberg, V. Doye, A Nup133-dependent NPC-anchored network tethers centrosomes to the nuclear envelope in prophase, J. Cell Biol. 192 (2011) 855–871. https://doi.org/10.1083/jcb.201007118.

[77] T. Hirano, Condensins: organizing and segregating the genome, Curr. Biol. CB. 15 (2005) R265-275. https://doi.org/10.1016/j.cub.2005.03.037.

[78] D.J.-K. Hu, A.D. Baffet, T. Nayak, A. Akhmanova, V. Doye, R.B. Vallee, Dynein Recruitment to Nuclear Pores Activates Apical Nuclear Migration and Mitotic Entry in Brain Progenitor Cells, Cell. 154 (2013) 1300–1313. https://doi.org/10.1016/j.cell.2013.08.024.

[79] D. Splinter, M.E. Tanenbaum, A. Lindqvist, D. Jaarsma, A. Flotho, K.L. Yu, I. Grigoriev, D. Engelsma, E.D. Haasdijk, N. Keijzer, J. Demmers, M. Fornerod, F. Melchior, C.C. Hoogenraad, R.H. Medema, A. Akhmanova, Bicaudal D2, dynein, and kinesin-1 associate with nuclear pore complexes and regulate centrosome and nuclear positioning during mitotic entry, PLoS Biol. 8 (2010) e1000350. https://doi.org/10.1371/journal.pbio.1000350.

[80] A.D. Baffet, D.J. Hu, R.B. Vallee, Cdk1 Activates Pre-mitotic Nuclear Envelope Dynein Recruitment and Apical Nuclear Migration in Neural Stem Cells, Dev. Cell. 33 (2015) 703–716. https://doi.org/10.1016/j.devcel.2015.04.022.

[81] B. van Steensel, T. de Lange, Control of telomere length by the human telomeric protein TRF1, Nature. 385 (1997) 740–743. https://doi.org/10.1038/385740a0.

[82] C.Y. Ho, J. Lammerding, Lamins at a glance, J. Cell Sci. 125 (2012) 2087–2093. https://doi.org/10.1242/jcs.087288.

[83] B. van Steensel, A.S. Belmont, Lamina-Associated Domains: Links with Chromosome Architecture, Heterochromatin, and Gene Repression, Cell. 169 (2017) 780–791. https://doi.org/10.1016/j.cell.2017.04.022.

[84] K. Damodaran, S. Venkatachalapathy, F. Alisafaei, A.V. Radhakrishnan, D. Sharma Jokhun, V.B. Shenoy, G.V. Shivashankar, Compressive force induces reversible chromatin condensation and cell geometry–dependent transcriptional response, Mol. Biol. Cell. 29 (2018) 3039–3051. https://doi.org/10.1091/mbc.E18-04-0256.

[85] V. Boudreau, R. Chen, A. Edwards, M. Sulaimain, P.S. Maddox, PP2A-B55/SUR-6 collaborates with the nuclear lamina for centrosome separation during mitotic entry, Mol. Biol. Cell. 30 (2019) 876–886. https://doi.org/10.1091/mbc.E18-10-0631.

[86] J.C. Gonçalves, S. Quintremil, J. Yi, R.B. Vallee, Nesprin-2 Recruitment of BicD2 to the Nuclear Envelope Controls Dynein/Kinesin-Mediated Neuronal Migration In Vivo, Curr. Biol. CB. 30 (2020) 3116-3129.e4. https://doi.org/10.1016/j.cub.2020.05.091.

[87] T. Kamasaki, E. O'Toole, S. Kita, M. Osumi, J. Usukura, J.R. McIntosh, G. Goshima, Augmin-dependent microtubule nucleation at microtubule walls in the spindle, J. Cell Biol. 202 (2013) 25–33. https://doi.org/10.1083/jcb.201304031.

[88] A. Khodjakov, L. Copenagle, M.B. Gordon, D.A. Compton, T.M. Kapoor, Minus-end capture of preformed kinetochore fibers contributes to spindle morphogenesis, J. Cell Biol. 160 (2003) 671–683. https://doi.org/10.1083/jcb.200208143.

[89] T.J. Maresca, A.C. Groen, J.C. Gatlin, R. Ohi, T.J. Mitchison, E.D. Salmon, Spindle assembly in the absence of a RanGTP gradient requires localized CPC activity, Curr. Biol. CB. 19 (2009) 1210–1215. https://doi.org/10.1016/j.cub.2009.05.061.

[90] S. Petry, R.D. Vale, Microtubule nucleation at the centrosome and beyond, Nat. Cell Biol. 17 (2015) 1089–1093. https://doi.org/10.1038/ncb3220.

[91] S.C. Sampath, R. Ohi, O. Leismann, A. Salic, A. Pozniakovski, H. Funabiki, The chromosomal passenger complex is required for chromatin-induced microtubule stabilization and spindle assembly, Cell. 118 (2004) 187–202. https://doi.org/10.1016/j.cell.2004.06.026.

[92] J. Scrofani, T. Sardon, S. Meunier, I. Vernos, Microtubule nucleation in mitosis by a RanGTP-dependent protein complex, Curr. Biol. CB. 25 (2015) 131–140. https://doi.org/10.1016/j.cub.2014.11.025.

[93] V. Sikirzhytski, F. Renda, I. Tikhonenko, V. Magidson, B.F. McEwen, A. Khodjakov, Microtubules assemble near most kinetochores during early prometaphase in human cells, J. Cell Biol. 217 (2018) 2647–2659. https://doi.org/10.1083/jcb.201710094.

[94] I. Minn, M.M. Rolls, W. Hanna-Rose, C.J. Malone, SUN-1 and ZYG-12, Mediators of Centrosome–Nucleus Attachment, Are a Functional SUN/KASH Pair in Caenorhabditis elegans, Mol. Biol. Cell. 20 (2009) 4586–4595. https://doi.org/10.1091/mbc.e08-10-1034.

[95] X. Zhang, K. Lei, X. Yuan, X. Wu, Y. Zhuang, T. Xu, R. Xu, M. Han, SUN1/2 and Syne/Nesprin-1/2 complexes connect centrosome to the nucleus during neurogenesis and neuronal migration in mice, Neuron. 64 (2009) 173–187. https://doi.org/10.1016/j.neuron.2009.08.018.

[96] N. Wang, Review of cellular mechanotransduction, J. Phys. Appl. Phys. 50 (2017) 233002. https://doi.org/10.1088/1361-6463/aa6e18.

[97] P.A. Janmey, D.A. Weitz, Dealing with mechanics: mechanisms of force transduction in cells, Trends Biochem. Sci. 29 (2004) 364–370. https://doi.org/10.1016/j.tibs.2004.05.003.

[98] D. Ingber, Mechanobiology and diseases of mechanotransduction, Ann. Med. 35 (2003) 564–577. https://doi.org/10.1080/07853890310016333.

[99] I.P. Uray, K. Uray, Mechanotransduction at the Plasma Membrane-Cytoskeleton Interface, Int. J. Mol. Sci. 22 (2021) 11566. https://doi.org/10.3390/ijms222111566.

[100] T.P. Driscoll, B.D. Cosgrove, S.-J. Heo, Z.E. Shurden, R.L. Mauck, Cytoskeletal to Nuclear Strain Transfer Regulates YAP Signaling in Mesenchymal Stem Cells, Biophys. J. 108 (2015) 2783–2793. https://doi.org/10.1016/j.bpj.2015.05.010.

[101] A. Elosegui-Artola, I. Andreu, A.E.M. Beedle, A. Lezamiz, M. Uroz, A.J. Kosmalska, R. Oria, J.Z. Kechagia, P. Rico-Lastres, A.-L.L. Roux, C.M. Shanahan, X. Trepat, D. Navajas, S. Garcia-Manyes, P. Roca-Cusachs, Force Triggers YAP Nuclear Entry by Regulating Transport across Nuclear Pores, Cell. 171 (2017) 1397-1410.e14. https://doi.org/10.1016/j.cell.2017.10.008.

[102] C.T. McKee, V.K. Raghunathan, P.F. Nealey, P. Russell, C.J. Murphy, Topographic modulation of the orientation and shape of cell nuclei and their influence on the measured elastic modulus of epithelial cells, Biophys. J. 101 (2011) 2139–2146. https://doi.org/10.1016/j.bpj.2011.09.042.

[103] O. Afanzar, G.K. Buss, T. Stearns, J.E. Ferrell Jr, The nucleus serves as the pacemaker for the cell cycle, ELife. 9 (2020) e59989. https://doi.org/10.7554/eLife.59989.

[104] F.E. Nolet, A. Vandervelde, A. Vanderbeke, L. Piñeros, J.B. Chang, L. Gelens, Nuclei determine the spatial origin of mitotic waves, ELife. 9 (2020) e52868. https://doi.org/10.7554/eLife.52868.

[105] C.S. Janota, F.J. Calero-Cuenca, E.R. Gomes, The role of the cell nucleus in mechanotransduction, Curr. Opin. Cell Biol. 63 (2020) 204–211. https://doi.org/10.1016/j.ceb.2020.03.001.

[106] M. Maurer, J. Lammerding, The Driving Force: Nuclear Mechanotransduction in Cellular Function, Fate, and Disease, Annu. Rev. Biomed. Eng. 21 (2019) 443–468. https://doi.org/10.1146/annurev-bioeng-060418-052139.

[107] M. Hieda, Signal Transduction across the Nuclear Envelope: Role of the LINC Complex in Bidirectional Signaling, Cells. 8 (2019). https://doi.org/10.3390/cells8020124.

[108] J. Schmitt, R. Benavente, D. Hodzic, C. Höög, C.L. Stewart, M. Alsheimer, Transmembrane protein Sun2 is involved in tethering mammalian meiotic telomeres to the nuclear envelope, Proc. Natl. Acad. Sci. U. S. A. 104 (2007) 7426–7431. https://doi.org/10.1073/pnas.0609198104.

[109] X. Ding, R. Xu, J. Yu, T. Xu, Y. Zhuang, M. Han, SUN1 is required for telomere attachment to nuclear envelope and gametogenesis in mice, Dev. Cell. 12 (2007) 863–872. https://doi.org/10.1016/j.devcel.2007.03.018.

[110] J. Amrichová, E. Lukásová, S. Kozubek, M. Kozubek, Nuclear and territorial topography of chromosome telomeres in human lymphocytes, Exp. Cell Res. 289 (2003) 11–26. https://doi.org/10.1016/s0014-4827(03)00208-8.

[111] T. Jegou, I. Chung, G. Heuvelman, M. Wachsmuth, S.M. Görisch, K.M. Greulich-Bode, P. Boukamp, P. Lichter, K. Rippe, Dynamics of telomeres and promyelocytic leukemia nuclear bodies in a telomerase-negative human cell line, Mol. Biol. Cell. 20 (2009) 2070–2082. https://doi.org/10.1091/mbc.e08-02-0108.

[112] B.J. Vermolen, Y. Garini, S. Mai, V. Mougey, T. Fest, T.C.-Y. Chuang, A.Y.-C. Chuang, L. Wark, I.T. Young, Characterizing the three-dimensional organization of telomeres, Cytom. Part J. Int. Soc. Anal. Cytol. 67 (2005) 144–150. https://doi.org/10.1002/cyto.a.20159.

[113] M.N. Conrad, C.-Y. Lee, G. Chao, M. Shinohara, H. Kosaka, A. Shinohara, J.-A. Conchello, M.E. Dresser, Rapid telomere movement in meiotic prophase is promoted by NDJ1, MPS3, and CSM4 and is modulated by recombination, Cell. 133 (2008) 1175–1187. https://doi.org/10.1016/j.cell.2008.04.047.

[114] H.F. Horn, D.I. Kim, G.D. Wright, E.S.M. Wong, C.L. Stewart, B. Burke, K.J. Roux, A mammalian KASH domain protein coupling meiotic chromosomes to the cytoskeleton, J. Cell Biol. 202 (2013) 1023–1039. https://doi.org/10.1083/jcb.201304004.

[115] J.M. Bupp, A.E. Martin, E.S. Stensrud, S.L. Jaspersen, Telomere anchoring at the nuclear periphery requires the budding yeast Sad1-UNC-84 domain protein Mps3, J. Cell Biol. 179 (2007) 845–854. https://doi.org/10.1083/jcb.200706040.

[116] A. Penkner, L. Tang, M. Novatchkova, M. Ladurner, A. Fridkin, Y. Gruenbaum, D. Schweizer, J. Loidl, V. Jantsch, The nuclear envelope protein Matefin/SUN-1 is required for homologous pairing in C. elegans meiosis, Dev. Cell. 12 (2007) 873–885. https://doi.org/10.1016/j.devcel.2007.05.004.

[117] Y. Hiraoka, A.F. Dernburg, The SUN rises on meiotic chromosome dynamics, Dev. Cell. 17 (2009) 598–605. https://doi.org/10.1016/j.devcel.2009.10.014.

[118] D. Zickler, N. Kleckner, Recombination, Pairing, and Synapsis of Homologs during Meiosis, Cold Spring Harb. Perspect. Biol. 7 (2015) a016626. https://doi.org/10.1101/cshperspect.a016626.

[119] A. Sato, B. Isaac, C.M. Phillips, R. Rillo, P.M. Carlton, D.J. Wynne, R.A. Kasad, A.F. Dernburg, Cytoskeletal forces span the nuclear envelope to coordinate meiotic chromosome pairing and synapsis, Cell. 139 (2009) 907–919. https://doi.org/10.1016/j.cell.2009.10.039.

[120] V. Magidson, C.B. O'Connell, J. Lončarek, R. Paul, A. Mogilner, A. Khodjakov, The Spatial Arrangement of Chromosomes during Prometaphase Facilitates Spindle Assembly, Cell. 146 (2011) 555–567. https://doi.org/10.1016/j.cell.2011.07.012.

[121] D. Splinter, D.S. Razafsky, M.A. Schlager, A. Serra-Marques, I. Grigoriev, J. Demmers, N. Keijzer, K. Jiang, I. Poser, A.A. Hyman, C.C. Hoogenraad, S.J. King, A. Akhmanova, BICD2, dynactin, and LIS1 cooperate in regulating dynein recruitment to cellular structures, Mol. Biol. Cell. 23 (2012) 4226–4241. https://doi.org/10.1091/mbc.e12-03-0210.

[122] Q. Liu, N. Pante, T. Misteli, M. Elsagga, M. Crisp, D. Hodzic, B. Burke, K.J. Roux, Functional association of Sun1 with nuclear pore complexes, J. Cell Biol. 178 (2007) 785–798. https://doi.org/10.1083/jcb.200704108.

[123] B. Enyedi, P. Niethammer, Nuclear membrane stretch and its role in mechanotransduction, Nucleus. 8 (2017) 156–161. https://doi.org/10.1080/19491034.2016.1263411.

[124] I. Liashkovich, A. Meyring, A. Kramer, V. Shahin, Exceptional structural and mechanical flexibility of the nuclear pore complex, J. Cell. Physiol. 226 (2011) 675–682. https://doi.org/10.1002/jcp.22382.

[125] C.E. Zimmerli, M. Allegretti, V. Rantos, S.K. Goetz, A. Obarska-Kosinska, I. Zagoriy, A. Halavatyi, G. Hummer, J. Mahamid, J. Kosinski, M. Beck, Nuclear pores dilate and constrict in cellulo, Science. 374 (2021) eabd9776. https://doi.org/10.1126/science.abd9776.

[126] I. Samejima, C. Spanos, K. Samejima, J. Rappsilber, G. Kustatscher, W.C. Earnshaw, Mapping the invisible chromatin transactions of prophase chromosome remodeling, Mol. Cell. 82 (2022) 696-708.e4. https://doi.org/10.1016/j.molcel.2021.12.039.

[127] A.J. Lomakin, C.J. Cattin, D. Cuvelier, Z. Alraies, M. Molina, G.P.F. Nader, N. Srivastava, P.J. Sáez, J.M. Garcia-Arcos, I.Y. Zhitnyak, A. Bhargava, M.K. Driscoll, E.S. Welf, R. Fiolka, R.J. Petrie, N.S.D. Silva, J.M. González-Granado, N. Manel, A.M. Lennon-Duménil, D.J. Müller, M. Piel, The nucleus acts as a ruler tailoring cell responses to spatial constraints, Science. 370 (2020). https://doi.org/10.1126/science.aba2894.

[128] T. Hirota, D. Gerlich, B. Koch, J. Ellenberg, J.-M. Peters, Distinct functions of condensin I and II in mitotic chromosome assembly, J. Cell Sci. 117 (2004) 6435–6445. https://doi.org/10.1242/jcs.01604.

[129] A. Azioune, N. Carpi, Q. Tseng, M. Théry, M. Piel, Protein micropatterns: A direct printing protocol using deep UVs, Methods Cell Biol. 97 (2010) 133–146. https://doi.org/10.1016/S0091-679X(10)97008-8.

[130] V. Nunes, M. Dantas, J.T. Lima, J.G. Ferreira, High-Resolution Analysis of CentrosomeCentrosomesBehavior DuringMitosisMitosis, in: A.S. Coutts, L. Weston (Eds.), Cell Cycle Oscil. Methods Protoc., Springer US, New York, NY, 2021: pp. 179–194. https://doi.org/10.1007/978-1-0716-1538-6_13.

[131] M. Le Berre, E. Zlotek-Zlotkiewicz, D. Bonazzi, F. Lautenschlaeger, M. Piel, Methods for two-dimensional cell confinement, Methods Cell Biol. 121 (2014) 213–229. https://doi.org/10.1016/B978-0-12-800281-0.00014-2.

[132] A.D. Stephens, P.Z. Liu, E.J. Banigan, L.M. Almassalha, V. Backman, S.A. Adam, R.D. Goldman, J.F. Marko, Chromatin histone modifications and rigidity affect nuclear morphology independent of lamins, Mol. Biol. Cell. 29 (2018) 220–233. https://doi.org/10.1091/mbc.E17-06-0410.

7. Supplementary Figures

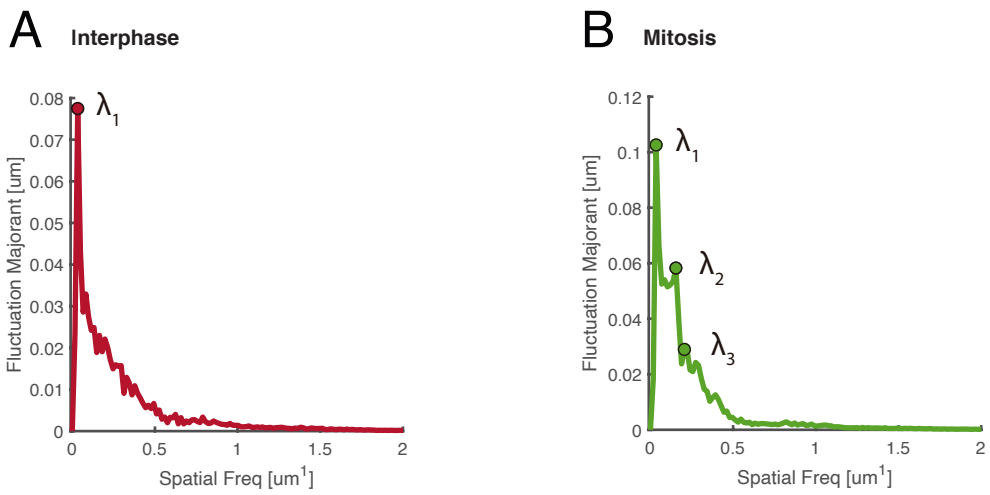


Figure S1: Majorant of frequency-dependent fluctuations, uf, related to Figure 1. **(A)** Majorant of frequency-dependent fluctuations, uf, related to D-D'. Highest FT peak with a wavelength of 0,0775 µm (λ_1)**. (B)** Majorant of frequency-dependent fluctuations, uf, related to E-E'. Highest FT peaks with wavelengths of 0,1026 µm (λ_1), 0,0583 µm (λ_2), and 0,0289 µm (λ_3).

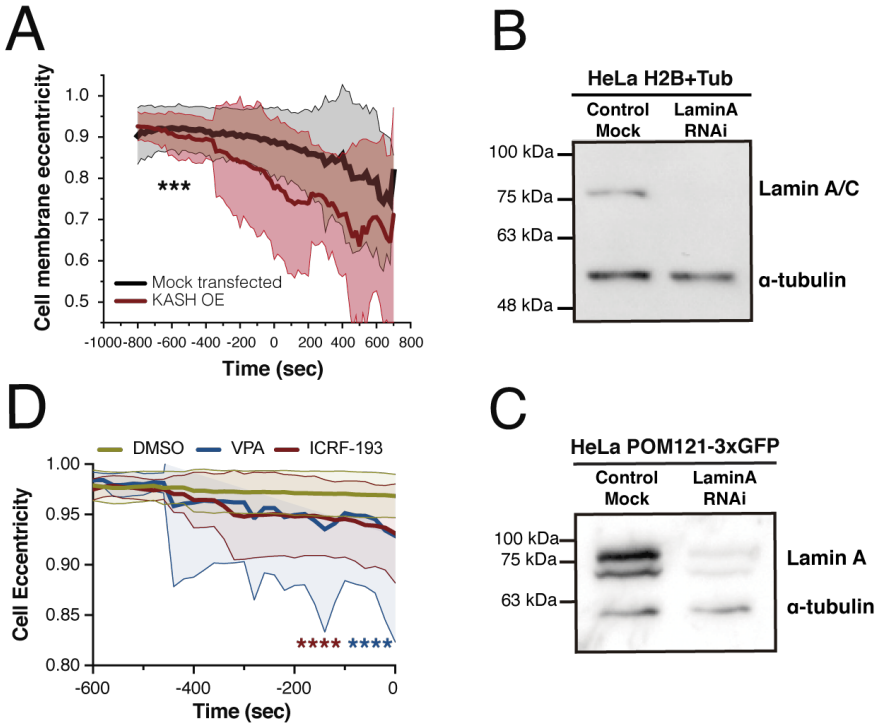


Figure S2: Cell membrane eccentricity and immunoblots related to Figures 2 and 3. **(A)** Cell membrane eccentricity for control cells and pEGFP-KASH transfected cells (KASH OE; n=30; ***p<0.001). Lines correspond to average values and shaded areas correspond to SD. Time zero corresponds to NEP. Representative immunoblots to confirm depletion efficiency by RNAi of LaminA for HeLa H2B-GFP/Tubulin-RFP **(B)** and HeLa POM121-3xGFP **(C)** cell lines. **(D)** Cell membrane eccentricity (dashed lines; ****p<0.000) and

nuclear membrane eccentricity (straight lines; n.s. - not significant) over time for control cells (green; n=28) and LaminA depleted cells (red; n=33). Lines correspond to average values and shaded areas correspond to SD. Time zero corresponds to NEP. **(D)** Cell membrane eccentricity over time for control cells (green; n=50) and cells treated with ICRF-193 (red; n=42; ****p<0.0001) and VPA (blue; n=34; ****p<0.0001). Lines correspond to average values and shaded areas correspond to SD. Time zero corresponds to NEP.

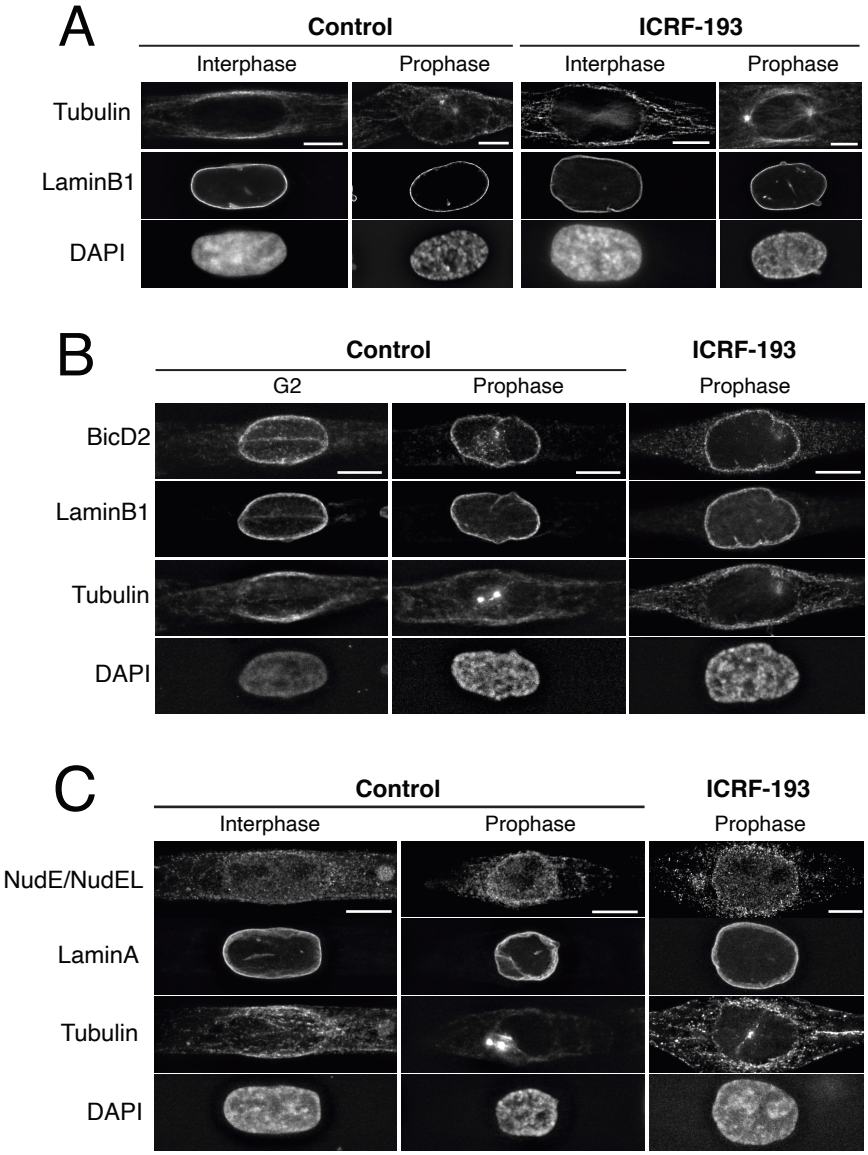


Figure S3: Immunofluorescence analysis of Lamin A and B1 for control and ICRF-193-treated cells, related to Figure 4.**(A)** Representative images of immunofluorescence analysis of Lamin B1, alpha-tubulin and DAPI for controls (n=32) and ICRF-193 (n=30). All images correspond to deconvolved maximal intensity projections. For quantification purposes, sum-projected images were used. Scale bar, 10 µm. **(B)** Representative images of immunofluorescence analysis of BicD2, Lamin B1, alpha-tubulin and DAPI for controls (n=31) and ICRF-193 (n=30). **(C)** Representative images of immunofluorescence analysis of NudE, LaminA, alpha-tubulin and DAPI for controls (n=31) and ICRF-193 (n=30). All images correspond to deconvolved maximal intensity projections. For quantification purposes, sum-projected images were used. Scale bar, 10 µm.

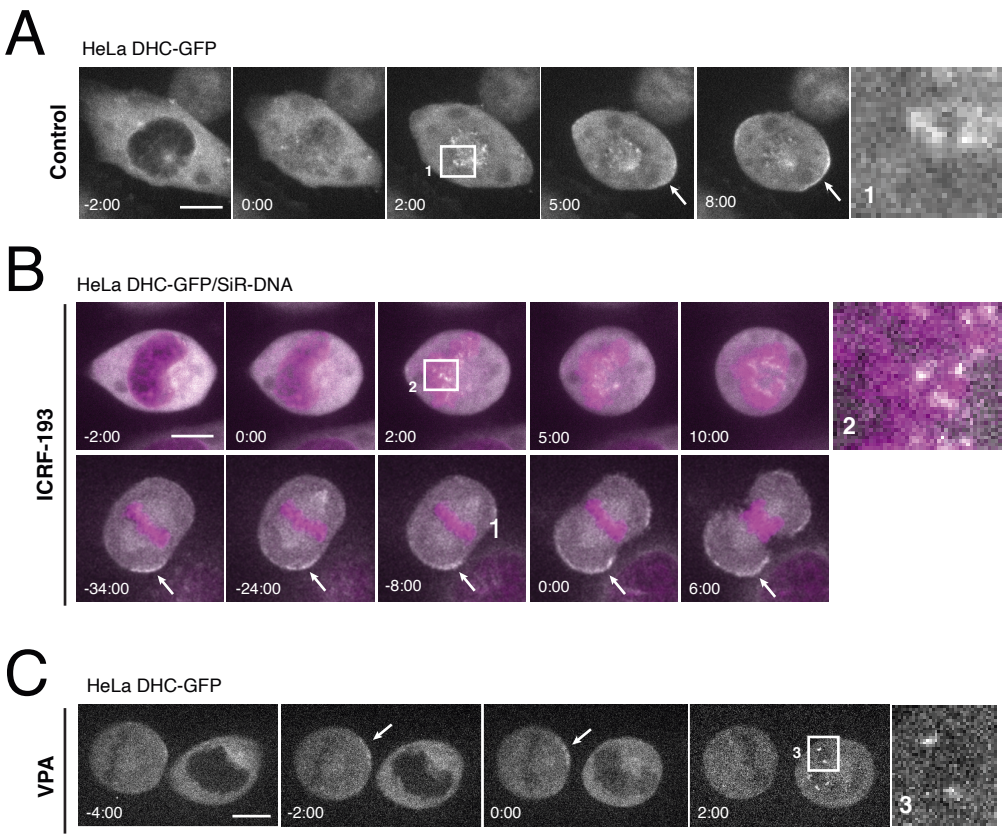


Figure S4: Dynein localizes to kinetochores and cell cortex following treatment with ICRF-193 and VPA, related to Figure 4. **(A)** Representative movie of control HeLa cell expressing DHC-GFP during mitotic entry, highlighting kinetochore (top panel, white box; 1) and cortical (white arrow) Dynein localization. Time is in min:sec. Time zero corresponds to NEP. Scale bar, 10 µm. **(B)** Representative movies of HeLa cells labelled with DHC-GFP and SiR-DNA, treated with ICRF-193, highlighting kinetochore (top panel, white box; 2) and cortical (bottom panel) Dynein localization. Time in in min:sec. Time zero corresponds to NEP (top panel) and anaphase onset (bottom panel). Scale bar, 10 µm. **(C)** Representative movie of HeLa cells labelled with DHC-GFP, treated with VPA, highlighting kinetochore (top panel, white box; 3) and cortical (white arrow) Dynein localization. Time in in min:sec. Time zero corresponds to NEP. Scale bar, 10 µm.

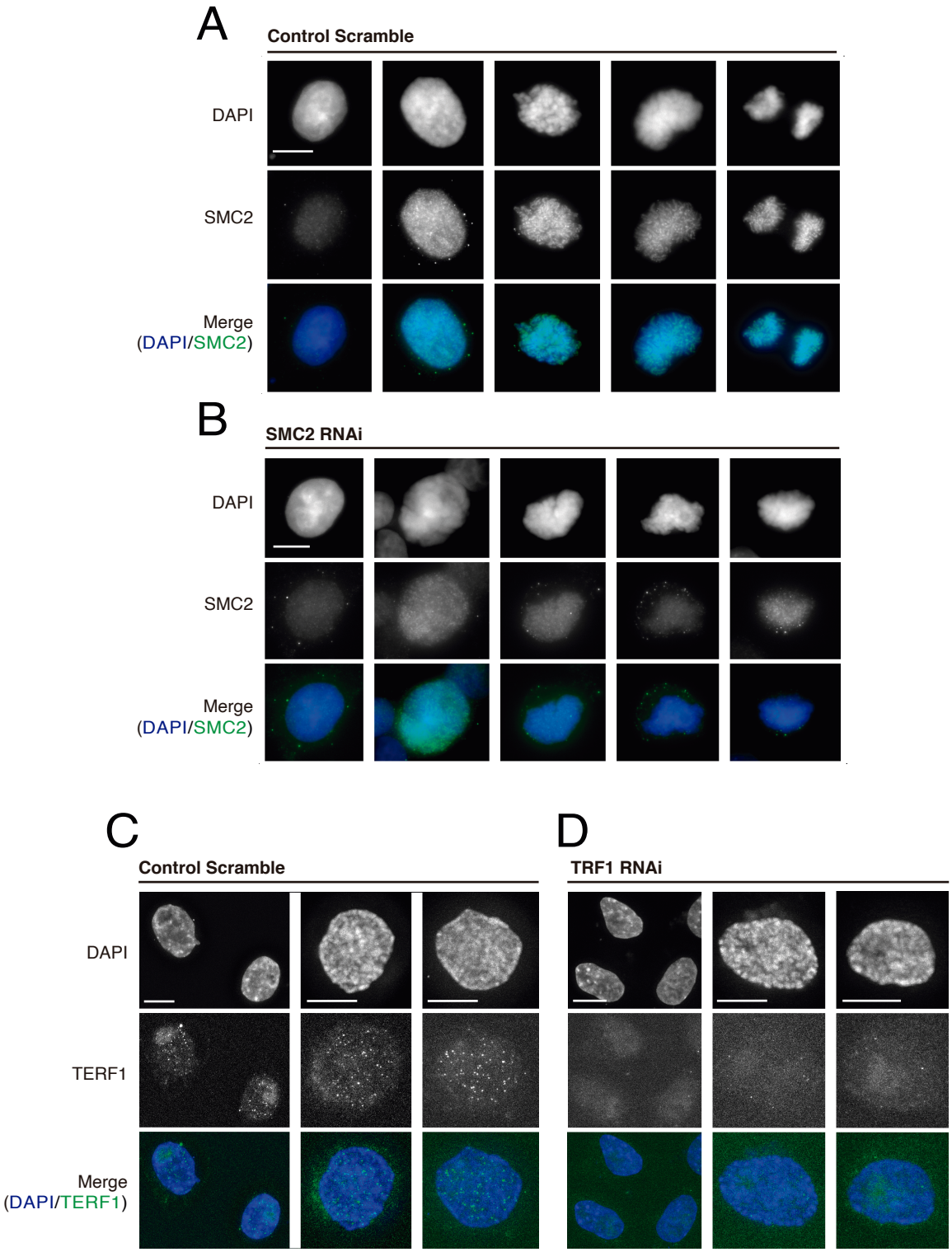


Figure S5: Immunofluorescence analysis to confirm depletion efficiency by RNAi of TRF1 and SMC2, related to Figures 4 and 5. **(A-B)** Representative images of immunofluorescence analysis of DAPI and SMC2 for controls **(A)** and SMC2 depleted cells **(B)**. SMC2 and DAPI correspond to maximal intensity projections. SMC2 and DAPI correspond to maximal intensity projections. Scale bar, 10 μm. **(C-D)** Representative images of immunofluorescence analysis of DAPI and TRF1 for controls **(C)** and TRF1 depleted cells **(D)** expressing DHC-GFP, seeded on 10 μm line micropatterns**.** TRF1 images correspond to deconvolved maximal intensity projections. DAPI correspond to maximal intensity projections. Scale bar, 10 μm.

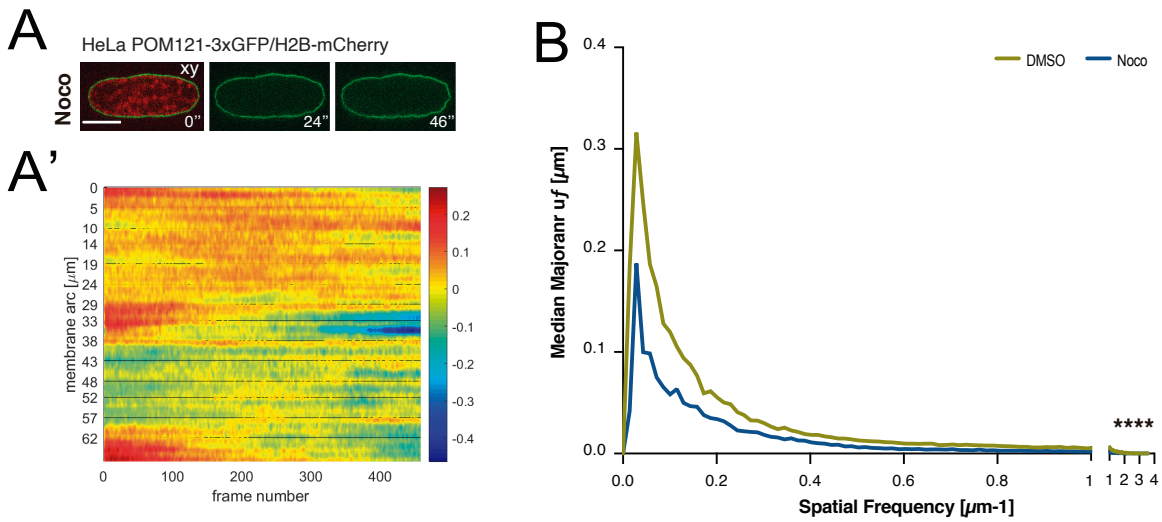


Figure S6: Nuclear envelope fluctuation analysis for cells treated with Nocodozole, related to Figure 4. **(A)** Representative time-frames from movie of a Nocodozole-treated cell expressing POM121-3xGFP/H2B-mCherry, seeded on a 10 µm line micropattern. The NE labeled with POM121-3xGFP (green) is shown at two different time points to illustrate the degree of membrane undulation for the experimental group. Time is in sec. Time zero corresponds to the first recorded frame. Scale bar, 10 µm. **(A')** Corresponding map of the fluctuations amplitude, u_f, obtained for all the frames from the video in A. The *y*-axis corresponds to the arc around the median membrane. **(B)** Medians of the majorant frequency-dependent fluctuations, u_f, for controls (green; n=30) and Nocodozole-treated (red; n=27; ****p<0.0001) cells. Nocodozole treatment caused a significant decrease in the membrane fluctuations in mitosis.

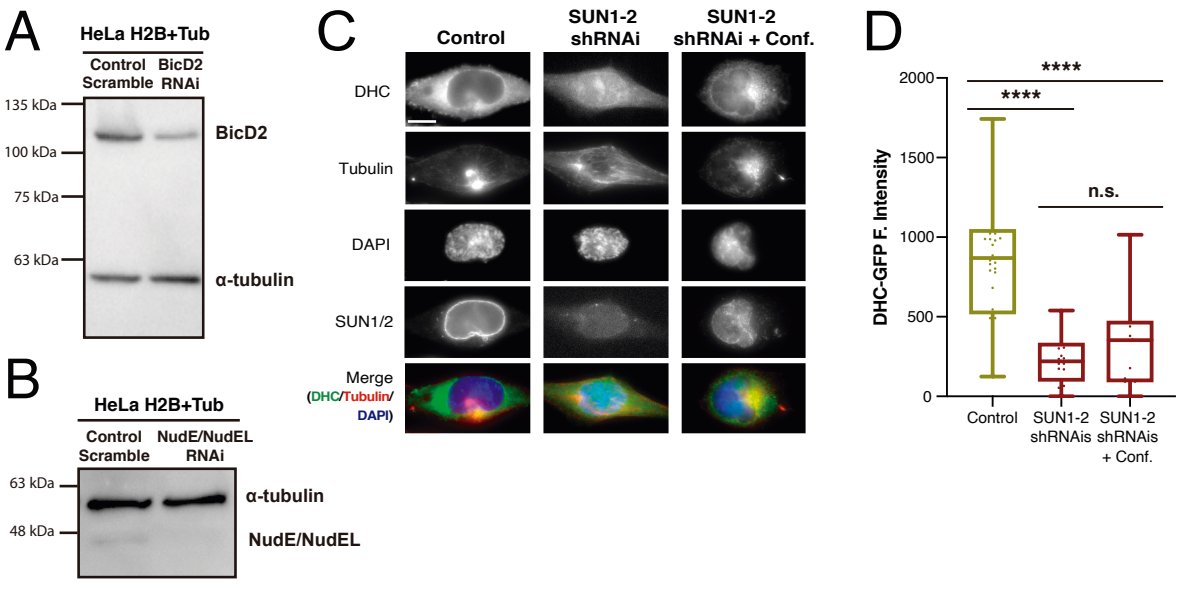


Figure S7: Immunofluorescence analysis of cells treated with ICRF-193 and SUN1/2 shRNA related to Figure 6. **(A)** Representative immunoblot to confirm depletion efficiency by RNAi of BicD2 for HeLa H2B-GFP/Tubulin-RFP. **(B)** Representative immunoblot to confirm depletion efficiency by RNAi of NudE/NudEL for HeLa H2B-GFP/Tubulin-RFP. **(C)** Immunofluorescence images of DHC-GFP, alpha-tubulin, DAPI and SUN1/2 for control cells (n=17) and cells treated with SUN1/2 shRNA before and after confinement and release. Cells

are expressing DHC-GFP and are seeded on 10 μm line micropatterns. DHC-GFP images correspond to sum projections. DAPI, alpha-tubulin and SUN1/2 correspond to maximal intensity projections. Scale bar, 10 μm. **(F)** Quantification of DHC-GFP intensity for prophase of control cells (green; n=30) and cells treated with SUN1/2 shRNA before (red; n=16; ****p<0.0001) and after confinement and release (red; n=13; ****p<0.0001). For quantification purposes, sum-projected images covering the middle nucleus region were used.

CHAPTER VI

General Discussion

1. **Accurate mitotic spindle assembly: A place for everything, everything in its place**

2. **The nucleus as an active regulator of mitotic entry**

Abbreviations

BicD2	Bicaudal D2
CPC	Chromosome Passenger Complex
ECM	Extracellular Matrix
HDACi	Histone Deacetylase Inhibitor
INM	Inner Nuclear Membrane
KT(s)	Kinetochore(s)
LBR	Lamin B Receptor
LINC	Linker of Nucleoskeleton and Cytoskeleton
MT(s)	Microtubule(s)
MTOCs	Microtubule Organizing Centers
NE	Nuclear Envelope
NEB	Nuclear Envelope Breakdown
NPCs	Nuclear Pore Complexes
ONM	Outer Nuclear Membrane
PCM	Pericentriolar Material
PLK1	Polo-like Kinase 1
SAFs	Spindle Assembly Factors
TCJs	Tricellular Junctions
VPA	Valproic Acid
γ − TuRC	Gamma Tubulin Ring Complex

General Discussion

1. Accurate mitotic spindle assembly: A place for everything, everything in its place

In animal somatic cells, centrosome-dependent and -independent pathways cooperate to promote robust spindle assembly [1,2]. In the context of centrosome-independent pathways, chromosomes generate a gradient of RanGTP that greatly enhances microtubule (MT) nucleation in the vicinity of chromatin by promoting the release of spindle assembly factors (SAFs), such as TPX2, from α/β importins [3–7]. In the absence of a RanGTP gradient, MTs are nucleated from centromeric chromatin by another chromatin-mediated pathway involving the chromosome passenger complex (CPC; [8,9]). In fact, chromatin-mediated MT nucleation has been reported in the vicinity of chromosomes [5–9], at kinetochores (KTs; [10,11]), or adjacent to existing MTs due to the activity of the Augmin complex [12,13]. These pathways cooperate to accelerate spindle assembly and facilitate KT-MT capture. Still, in the absence of chromosomes or in presence of substitutes (e.g. viral DNA or plasmid DNA-coated beads), the spindle is still able to form [14–16].

In prophase, when spindle bipolarity is first established, chromatin is not yet exposed to cytoplasmic tubulin dimers [17] and Augmin has not yet been recruited to existing MTs by Aurora A [18] and Polo-like kinase 1 (PLK1; [19]). On the other hand, around this stage, centrosomes are primed to rapidly nucleate MTs due to the recruitment of gamma tubulin ring complex (γ − TuRC) and pericentriolar material (PCM) components by Aurora A and PLK1 [1,20–22] Consequently, in prophase, MT nucleation is largely dominated by the centrosomes, the main MT organizing centers (MTOCs; [1,2]). Through most of interphase, centrosomes usually lie in the cell center [23], close to the outer nuclear envelope (NE; [24]). Around the onset of S-phase centrosomes duplicate [24–26]. In prophase, the duplicated centrosomes separate along the NE to form the mitotic spindle. Centrosome dynamics, which primes centrosome separation and spindle pole formation, is a complex process that is still incompletely understood [1,27]. Nevertheless, it is well established that centrosome loss and incomplete or delayed centrosome separation, despite not being detrimental for the assembly of a functional bipolar spindle [28–30], can cause spindle morphology defects, mitotic delay, chromosome segregation errors and aneuploidy [31–34]. Thus, the centrosome-mediated MT nucleation pathway potentiates the timely and efficient assembly of the mitotic spindle and, consequently, of chromosome segregation fidelity [1,20,27].

Previous reports proposed that cells randomly enter mitosis using one of two pathways: the Prophase pathway, in which centrosomes separate before Nuclear Envelope Breakdown (NEB); and the Prometaphase pathway, in which centrosomes separate after

NEB [34–36]. Contrarily to these reports, our study showed that when cells are seeded under physiological conditions, namely suitable adhesion areas and substrates (e.g., integrin-activating substrates such as fibronectin), centrosome separation occurs in prophase, while the NE is still intact (Chapter II; Supplemental Figure S1), similarly to what was shown in RPE1 cells [37]. This suggests that the dual pathway spindle assembly might be a consequence from cell culture conditions. In prophase, both the nucleus and the cytoplasm are promptly and drastically reorganized to facilitate spindle assembly and prepare cells for chromosome segregation [38,39]. This dynamic remodeling challenges our understanding on the relative contribution of each cellular event for centrosome separation and positioning. Additionally, mitotic spindle assembly is a challenging mechanism to grasp because the spindle is built very fast by multiple players and different pathways [1,27]. Indeed, to date, how centrosomes separate in an accurate and robust manner during prophase is not yet completely understood

Centrosome separation towards opposite sides of the nucleus requires the generation of force. Previous works have identified some of the molecular motors that play a role in this process, such as kinesin-5 (Eg5 in humans; [36,40,41]), Dynein [42,43] and Myosin II [44], in addition to actin and MTs [45–48]. The MT molecular motors Eg5 and NE-associated-Dynein (called “NE-Dynein” hereafter for simplicity) are thought to play a role in initial centrosome separation, the earliest step in establishing spindle bipolarity [27]. The MT plus-end-directed Eg5, which exhibits centrosomal localization in early prophase, drives centrosomes separation by crosslinking and sliding apart antiparallel MTs [40,49,50]. Thus, Eg5 inhibition commonly gives rise to monopolar spindles [40,41]. Interestingly, and in agreement with our observations (Chapter II; Supplemental Figure S5), in many mammalian cells, but not all (e.g., RPE1; [51]), Eg5 is required to establish spindle bipolarity but not for its maintenance [52]. In fact, without a fully functional Eg5, spindle bipolarity is kept by the activity of the plus-end-directed kinesin-12 Kif15 [53,54] and by KT-MT attachment increased stability [51]. On the other hand, in human cells, initial centrosome separation is supported by NE-Dynein, when Eg5 is partially impaired [43]. NE-Dynein was reported to contribute for both initial centrosome separation [43,55,56] and nucleus–centrosome coupling [55,57,58]. NE-Dynein assists initial centrosome separation by generating pulling forces on MTs and, consequently, on their associated centrosomes, along the NE [27]. Interestingly, we found that until NEB, NE-Dynein favors nuclear reorientation instead of centrosome motion (Chapter II; Figure 5 and Supplemental Figure S6). Supporting our results, previous studies have reported NE-Dynein-mediated nuclear rotation [59,60]. For example, wounding assays were shown to trigger nuclear translocation and rotation in a NE-Dynein-dependent manner in migrating fibroblasts [59]. Similarly, in vimentin-null fibroblasts, nuclear rotation was reported to rely on MTs and the associated Dynein [60].

Still, there is no consensus on how centrosome positioning impacts the rate of nuclear rotation. Some authors report that this process is independent of centrosome positioning [59]; whereas others show that centrosome position determines the rate of nuclear rotation by generating asymmetry in the spatial organization of MTs [61]. Interestingly, depletions of vimentin or Lamin B1 were shown to induce nuclear rotation [62]. This suggest that, contrarily to nuclear anchoring, in which the nuclei must be bound to cytoskeleton structures, nuclear rotation is favored by the release of nucleus-cytoskeleton coupling. In line with this idea, our results show that, in prophase, the nucleus needs to be released from its spatial and physical constrains to reorient. This process relies on mitotic cell rounding, when cells lose their adhesion and, consequently, lower the forces exerted by the cell on the substrate (Chapter II; Supplemental Figure S3). In fact, NE-Dynein mediated pulling forces are not enough to drive nuclear reorientation when cellular deadhesion is blocked and, therefore, spatial constrains are kept in place. On the other hand, cellular deadhesion alone seems sufficient to induce nuclear rotation (Chapter II; Figure 4).

In addition to the NE, Dynein is also enriched at the cell cortex, below the plasma membrane. The cortical pool of Dynein was shown to exert pulling forces on astral MTs to position the mitotic spindle in metaphase, in several systems [63–66]. Contrarily to NE-Dynein, that is initially recruited to the NE in late G2 through the RanBP2/Bicaudal D2 (BicD2) pathway [67], cortical Dynein is recruited to the cell cortex only at prometaphase by the LGN complex, which is composed of heterotrimeric Gα protein Gαi, LGN, and NuMA. LGN localization correlates with mitotic spindle positioning [65,66]. While in prometaphase, LGN complex is uniformly distributed along the cell cortex, in metaphase, its localization is limited by polarity cues to two cortical crescents facing the spindle [65,68,69]. The Ran-GTP chromosomal gradient is responsible for the exclusion of the cortical force generators from the vicinity of chromosomes [65]. Therefore, while in prophase, NE-Dynein seems to be a major contributor to position both the nucleus and the centrosomes [43,55,56,70], in metaphase, cortical Dynein determines the orientation of the mitotic spindle [63–66]. Hence, Dynein activity needs to be regulated in a spatiotemporal manner in mitosis [71].

Dynein-mediated pulling forces will only drive centrosome or nuclear motion when asymmetric interactions between centrosomes and the cell cortex and/or NE are established [27]. How this degree of anisotropy in the organization of Dynein-mediated forces is produced, is still not fully comprehended. In *C. elegans* embryos, the displacement of cortically bound Dynein driven by directional actomyosin flows, appears act as the symmetry breaking event [42]. On the other hand, in other systems such as in *Drosophila*, *C. elegans*, frog, and fish embryos, centrosome separation is achieved by an asymmetry in the MT configuration [72–74] driven by depolymerizing motor proteins positioned at the centrosome [75]. In our study, we propose that the MT asymmetry required to induce a

rotational torque on the prophase nucleus mediated by NE-Dynein, arises from centrosome and nucleus positioning during prophase (Chapter II; Figure 1). As previously proposed [74], this configuration is expected to drive centrosome motion, firstly, when centrosomes are still close to each other, by inducing steric interactions between MTs and centrosomes and, later, when centrosomes are positioned at opposite sides of the nucleus, by biasing MT nucleation along the surface of the NE. In addition, we found that NE-Dynein is not homogenously distributed along the NE. Indeed, by analyzing DHC-GFP distribution on the NE of cells seeded on line micropatterns during prophase we found that Dynein was distributed in an asymmetric manner on the NE, concentrating on curved areas of the envelope [76]. We anticipate that NE-Dynein accumulation is sensitive to cell and nuclear shape changes, and that these NE-Dynein spatial asymmetries might also contribute to generate anisotropy and robust centrosome separation and positioning.

Regarding the contribution of the cytoskeleton, the actomyosin cortex has been involved in centrosome separation trough different mechanisms acting at different stages [44,45]. Prior to NEB, in *Drosophila* embryos, Arp2/3- and Formin-mediated actin turnover was suggested to control both cortical actin cap expansion and centrosome separation, independently of myosin II [45]. In this case, centrosome motion was proposed to be powered by cortical Dynein-mediated pulling at the actin cap. Additionally, the Apc2-Armadillo complex, by directly linking the expanding actin cap and astral MTs, could be involved in this process [45]. Still, the mechanism is unclear. After NEB, actin and myosin II based cortical flows were shown to drive late centrosome separation in vertebrate cells (PtK2 cells; [44]). How these actomyosin flows could direct centrosome motion and how the forces produced by the actomyosin network could be transmitted to MTs and centrosomes remains uncertain. A more recent study in *C. elegans* proposed that these cortical flows are initiated by the centrosomes and drive the displacement of cortically anchored motors, which in turn would pull the centrosomes apart [42]. Lastly, in prometaphase, cortical actin was proposed to regulate centrosome separation and spindle positioning by either directly mediating the connection between astral MTs and the cell cortex or by recruiting cortical Dynein [45,69,77,78]. Our results show that in HeLa cells, interfering with the main actin nucleators did not affect cell rounding or nuclear orientation (Chapter II; Figure 5). However, Arp2/3 mediated-actin nucleation, which was previously considered unnecessary for mitotic progression [79] or actomyosin cell cortex assembly [80] at later stages of mitosis, was necessary for centrosome movement in prophase (Chapter II; Figure 6). We proposed that, in prophase, Arp2/3 activity promote centrosome motion by assisting in MT remodeling observed during the G2/M transition [81,82]. In fact, centrosomal Arp2/3 was reported to act as a regulator of MT dynamics, by acting as a “physical barrier” that blocks MT growth and triggers their disassembly [83–85]. Additionally, centrosomes were shown to directly

support Arp2/3-mediated actin nucleation [86,87], under the regulation PCM1 and cell adhesion [86]. Therefore, as we observed (Chapter II; Figure 6) and was previously described [85], in the beginning of mitosis, cellular de-adhesion, coupled to PLK1-mediated recruitment of PCM1 to the centrosomes, favors centrosomal actin nucleation to occur alongside with microtubule nucleation. Arp2/3-mediated MT reorganization also likely aids in generating the anisotropy needed to drive Dynein-mediated nuclear motion. Interestingly, in addition to its centrosomal localization, Arp2/3-mediated F-actin networks were previously described during mitosis, surrounding the nucleus [48,88] or revolving around the cell cortex [89]. The transient accumulation of F-actin overlying the nucleus ("actin cap") was shown to interact with MTs emanating from the centrosome [48] and has been involved in centrosome [70] and chromosome positioning [48,88]. Still, HeLa cells, contrarily to U2OS and RPE-1 cell lines, do not present this specific perinuclear actin structure [48]. The Arp2/3-mediated actin clusters ("actin clouds") circling the subcortex have been described in prometaphase [89]. These actin clouds, together with myosin 10, were reported to contribute to orient the metaphase mitotic spindle in an astral MT-dependent manner [90]. Interestingly, similar revolving Arp2/3-mediated subcortical clouds can be observed during early prophase (our unpublished results). It remains to be determined what is their function at this stage. Therefore, additional work is required to fully understand the role of actin-based structures in early spindle assembly. Nevertheless, all mechanisms described so far highlight the intricate crosstalk between actin and MTs structures and dynamics during both prophase and metaphase.

Metaphase spindle orientation has been extensively studied, given that accurate orientation of the mitotic spindle, and therefore of the cell division axis, is critical for cell size and fate, development and tissue organization [65,90–92]. In this context, the so-called "long axis or Hertwig Rule" is still used as a paradigm, in both single cells and tissues to predict spindle orientation during mitosis [93]. In fact, numerous works have determined that metaphase spindle orientation relies on the distribution of retraction fibres that replicate the interphase adhesion geometry [90,91,94]. However, this is not an universal rule, since it is now well known that certain cell shapes and cell types override this rule (e.g. rectangle or square shapes and sea urchin cells [95]). In these cases, cortical force generators associated with cell polarity [90,91] or with tricellular junctions (TCJs) [96], transmit pulling forces to astral MTs to guide spindle positioning [66,97,98]. In prophase, we observed that centrosomes deviate from the external cues and follow internal cues provided by the cytoskeleton and nucleus to position the centrosomes at the shortest nuclear axis at NEB (Chapter II; Figures 1 and 2). Additionally, we have demonstrated that this particular centrosome-nucleus configuration in prophase depends on cell adhesion area but not on cell shape (Chapter II; Figures 1 and 3). Currently, it is still unclear how centrosome motion

is directed towards this particular configuration. However, our work suggests that additional cues are required to position the centrosome in prophase, which likely come from the nucleus. Nevertheless, centrosome positioning in prophase directly impacts mitotic fidelity (Chapter II; Figure 7).

The timing of mitotic spindle assembly is also under tight control. It was first proposed that, after NEB, centrosome-nucleated MTs search for the chromosomes through a process named “search-and-capture” [99]. It is now well established that timely spindle assembly cannot rely exclusively on MT dynamic instability [100]. Accordingly, both KT-driven MT nucleation [101] and KT expansion [102] facilitate chromosome bi-orientation and, generate less erroneous KT-MTs attachments, thus contributing to mitotic spindle assembly efficiency. Importantly, both chromosome movement [103] and distribution [37] were also implicated in this process, by accelerating MT capture. In fact, while chromosome movements and rotations, described during prometaphase [104], were found to significantly accelerate microtubule capture [103]; chromosome distribution in an equatorial ring during prometaphase was found to favor the exposure of KTs to MTs and, consequently, the formation of amphitelic attachments (attachments where the sister KTs are connected to MTs from opposite poles, resulting in a bioriented chromosome) [37]. This early chromosome positioning fits nicely with our observations of centrosome positioning during prophase. In fact, our data show that, at NEB, centrosomes are well positioned relative to the chromosomal mass, favoring the establishment of appropriate KT-MT attachments, and therefore, also supporting accurate spindle assembly (Chapter II; Figure 7).

In conclusion, we propose that during prophase, centrosomes, nucleus, and chromosomes are actively positioned to facilitate mitotic spindle assembly efficiency.

2. The nucleus as an active regulator of mitotic entry

Chromosomes arms, which cover the bulk of the genome, were once described as “the corpse at a funeral” during mitosis, by Daniel Mazia [105]. Indeed, while chromosome segregation was thought to be the aim of cell division, chromosomes were considered as mere passengers of the mitotic spindle during the process. Obviously, this view has changed considerably in recent years and chromosomes are now acknowledged as active participants in mitosis. As previously described, some of the cellular processes affected by chromosomes are intimately linked to early mitotic spindle assembly. These include chromatin-mediated MT nucleation [5–9] and prometaphase chromosome movement and distribution [37,103]. In addition to chromosomes, other nuclear-associated components directly contribute to assemble the spindle, these include the NL [106–108] and the Linker of Nucleoskeleton and Cytoskeleton (LINC) complex [48,109,110]. Nuclear lamins were

reported to facilitate spindle assembly either by organizing a spindle-associated matrix [107,108] or by modulating mitotic spindle positioning [106]. The LINC complex, on the other hand, was implicated in centrosome separation [48], centrosome–nucleus connection [48,109,110] and NEB [111]. Interestingly, the LINC complex has also been involved in nuclear morphology and positioning [110,112,113], chromatin organization [114,115] and meiotic chromosome movement [116,117] trough NE-Dynein- and MT-dependent mechanisms in other systems.

During prophase, Lamin A is solubilized into the nucleoplasm [118,119] and chromosomes become highly condensed, presumably to assist in the alignment and movement of chromosomes driven by the mitotic spindle [120–122]. These changes in nuclear architecture are expected to elicit changes in the mechanical properties of the nucleus. In fact, it is widely held that both the chromatin compaction status and the amount and distribution of nuclear lamins, determine the mechanical properties of the nuclei [123,124]. Namely, while both chromatin condensation or Lamin A/C overexpression increase nuclear stiffness [124–127], chromatin decompaction, histone hypermethylation, or Lamin A/C depletion, decrease nuclear rigidity and often lead to the formation of nuclear blebs [127–131]. Still, to date, the knowledge on nuclear mechanics impact in early spindle assembly is surprisingly limited.

In our second study we addressed how nuclear mechanics could impact early spindle assembly. We have shown that, indeed, the mechanical properties of the nucleus during prophase are relevant and that chromosome condensation, but not nuclear lamina, determine Dynein recruitment to the NE (Chapter III; Figure 4). We proposed that chromatin condensation generates intranuclear mechanical forces that propagate by the telomeric regions of chromosomes to the SUN proteins at the NE (Chapter III; Figures 4-6). The mechanical strain applied on the SUN protein triggers NE-Dynein recruitment via BicD2 and NudE/NudEL pathways, through mechanisms not yet understood (Chapter III; Figure 6). We speculate that, alongside with chromatin condensation, tension at the NE during prophase changes either globally or locally and this could induce structural modifications on the Nuclear Pore Complexes (NPCs). The resulting changes in the NPCs, could trigger Dynein to the NE. Thus, we propose that nuclear mechanics play an important role in regulating mitotic entry (Chapter III; Figure 7).

The mechanical properties of the nucleus can be estimated using NE fluctuation measurements. NE fluctuations were shown to be actively driven by a balance between forces derived from chromatin and forces generated by the cytoskeleton. Interestingly, it was shown that the fluctuation pattern changes at various cell cycle stages, suggesting an association between cell cycle and nuclear mechanics [132,133]. Even if their purpose is not yet clear, it has been suggested that the NE fluctuations might tune the nucleo-

cytoplasmic shuttling of key molecules across the NPCs [132,134]. NE fluctuations measurements show that, from G2 phase to the onset of mitosis, the transient NE undulations gradually increase their amplitude, which correlates with chromatin condensation (Chapter III; Figure 1; [132,133,135]). This process then culminates in the permeabilization of the NE. By contrast, a recent study reported that a thorough decrease in the amplitude of NE fluctuations upon confinement was consistent with an increase in the NE tension [136]. Thus, an increase in the amplitude of the NE fluctuations during G2-M, given that it is well established that chromatin condensation increases nuclear stiffness [124,126,127], is a puzzling observation. Nevertheless, it should be noticed that cell confinement applies stretching forces at the NE [136], which are expected to be considerably different from the ones applied by chromatin condensation. Additionally, NE dynamics during prophase is significantly richer than in interphase [38,119]. Thus, further comparative studies on how nuclear stiffness and NE fluctuation patterns correlate are needed. Still, overall our fluctuation measurements are in good agreement with previous studies [132,133,135]. Namely, we have shown that affecting either chromatin condensation, nuclear lamina or the nucleo-cytoskeletal coupling increased NE undulations (Chapter III; Figures 2-3), but centrosome positioning and NE-Dynein levels were only affected when chromosome condensation was impaired (Chapter III; Figures 3-4). Interestingly, treatment with Valproic Acid (VPA), a histone deacetylase inhibitor (HDACi), did not significantly alter the NE fluctuations pattern nor centrosome positioning at NEB (Chapter III; Figure 3). Supporting these results, it has been shown that, contrarily to what was initially thought, histone hyperacetylation does not increase mitotic chromosome stiffness, unlike histone hypermethylation [131]. Lamin A depletion and nucleocytoskeleton coupling disruption increased the amplitude of NE fluctuations but did not impact centrosome positioning or NE-Dynein recruitment (Chapter III; Figures 2 and 4). Nevertheless, both treatments were previously shown to affect mitotic progression and fidelity [48,106–108,111]. Based on our results we hypothesized that, under such conditions, the separating centrosomes are able to easily compress and deform the nucleus and, consequently, generate an abnormal local short nuclear axis. This erroneous centrosome-nucleus configuration could potentially contribute to the mitotic problems previously reported. Taken together, these observations show that NE-Dynein recruitment relies specifically on chromosome condensation-mediated tension imposed on the NE.

Mechanotransduction defines the process that enable cells to sense mechanical cues and adjust their organization and function accordingly [137–140]. Research has often focused on mechanotransduction at the focal adhesions, adherens junctions, or at the cell nucleus. Initially, the cell membrane has been considered the only mechanoreceptor given that the forces providing the mechanically stimuli are considered to be generated from

cytoskeletal processes or from the cellular environment (e.g., neighboring cells or the extracellular matrix [138–141]). However, different studies suggested that cells utilize a variety of mechanosensitive elements [142–144]. Regarding the nucleus, several studies have shown that both chromatin and the nuclear lamina can act as mechanosensors that sense the mechanical stimuli and, subsequently, act as mechanotransducers by translating the information into diverse cellular responses (e.g., chromatin-driven change in the global patterns of gene expression [145], nuclear tension-mediated activation of YAP/TAZ pathway [146]; Lamin A-mediated regulation of extracellular matrix (ECM) composition [147–149] or delocalization of heterochromatin in response to Lamin A or Lamin B receptor (LBR) depletion [150]). In fact, most studied cases of nuclear mechanotransduction involve organizational and functional changes of NE proteins or chromatin [137,151,152]. Thus, it is highly likely that additional unanticipated functions of chromatin or nuclear membranes will be discovered, namely regarding when and how these components are involved in mechanotransduction, which is still little studied and understood. In line with this idea, in our latest study we proposed that the forces originated from the nuclear interior, through chromatin condensation, constitute by itself a source of mechanical stimuli for the cell. We then proposed that these forces are transduced to the NE, the mechanosensitive element, resulting in the recruitment of Dynein to this location (Chapter III; Figures 4-5). Supporting our claim, our previous results show that mitotic cell rounding reduces the force exerted by the cells on the ECM (Chapter II; Supplemental Figure S3, A–C). This suggests a significant decrease in cytoskeletal-induced or cytoskeletal-mediated forces at this stage. On the other hand, chromatin condensation was shown to increase nuclear stiffness [124,126,127] and, since the nucleus is the stiffest organelle in the cell, this can severely affect the mechanics of the entire cell [153]. Moreover, many studies support the capacity of the nucleus in modulating cytoskeleton or nuclear elements in response to strain. Namely, cytoskeletal strain transfer to the nucleus was shown to be indispensable for the activation of some mechanoactive signalling pathways (e.g., YAP/TAZ pathway; [146,154]). Also, while in somatic cells mitosis seems be initiated in all parts of the cell simultaneously [155], in larger cells, such as eggs, mitotic events are spatiotemporally regulated [156,157]. Previous findings show that the nucleus, by concentrating Cdc25C and Cyclin B-CDK1, accelerates mitotic entry, thereby acting as the pacemaker for the Xenopus cell cycle [158,159]. These studies suggest that initiating mitosis from a nuclear-based pacemaker, as opposed to a putative location on the cell periphery, should ensure that nuclear events such as chromatin condensation, occur prior to cytoplasmic events such as cell rounding. Therefore, it might be advantageous for the cell to have an internal nuclear signal that cooperates with CDK1 to ensure the proper timing for both nuclear and cytoplasmic events. Lastly, increasing evidence support a link between nuclear mechanics and G1-S [160–163] S-G2 [164], and

G2-M transitions [165]. These observations reinforce the interplay between physical forces and cell cycle progression and withstand with some level of mechanical regulation mediating the events occurring during the G2-M transition.

To convey the mechanical stimuli throughout the cell and enable it to function as a unique mechanically connected system, the nucleus is physically linked to the cytoplasm through the LINC protein complex at the NE [137,166–168]. The LINC complex is constituted by SUN domain-containing proteins (SUN1-5), which interact with lamins and chromatin at the inner nuclear membrane (INM), and KASH domain-containing proteins (nesprins-1–4, KASH5), which are positioned at the outer nuclear membrane (ONM) and interact with different elements of the cytoskeleton [168–171]. As previously mentioned, the LINC complex has been implicated in an increasing plethora of cellular processes in both mitosis and meiosis [48,109–111,114–117]. Importantly, additional protein interactions link chromatin to the nuclear lamina, such as, LAP2ß, MAN1, and emerin bridge via BAF [150,172,173], and LBR via HP1 [150,174,175]. In fact, lamins themselves, by anchoring chromatin to the NE, actively participate in the organization of chromatin [150,176–178]. Also, most nuclear–cytoplasmic communication occurs via NPCs [179]. In our study we proposed that chromosome condensation-mediated forces are transmitted to the SUN protein at the NE by the telomeric regions of chromosomes (Chapter III; Figures 4-6). In agreement with our results, it is not the first time that SUN proteins have been described to interact directly with chromosomes. In fact, recent studies demonstrated that in somatic cells both SUN1 and SUN2 contribute to chromatin anchorage to the NE [180,181]. However, in mitotic cells, SUN1 appears to interacts only with nuclear lamina and KASH domain proteins and does not colocalize with telomeres [181]. Telomere positioning in human cells is also still controversial. In lymphocytes, some authors have reported that telomeres were on average closer to the center of the cell [182]; while others have shown that, in G2 phase, telomeres organize into a disk [183]. Importantly, in human cells, telomeres were described to be anchored to the NE and interact with SUN1 during the process of nuclear reassembly, suggesting a role in chromatin organization during the postmitotic phase [184]. In U2OS osteosarcoma cells, telomeres were observed to display diffusive movements and assemble into transient clusters [185]. Taken together these studies suggest that telomere distribution in human cells is dynamic. Thus, it is crucial to continue dissecting the elements contributing for chromatin-NE interaction.

The LINC complex regulates Dynein loading onto the NE in different cellular processes [110,111,186,187]. Based on our results, KASH proteins are not driving Dynein recruitment to the NE during prophase (Chapter III; Figure 4). Therefore, alternative players should mediate this process. Besides SUN-KASH mediated recruitment, Dynein is recruited to the NE by the consecutive RanBP2-BicD2 [55,67] and Nup133-CENP-F-NudE/NudEL

pathways [58]. Both pathways rely on the association of the Dynein adaptors, BicD2 and NudE/NudEL, with the nucleoporins, RanBP2/Nup358 (RanBP2-BicD2 pathway; [55,67]) and Nup133 (Nup133-CENP-F-NudE/NudEL pathway; [58]) at the NPCs, respectively. Interestingly, our results show that both BicD2 and NudE/NudEL are still present on the NE even after interfering with chromatin condensation (Chapter III; Figure S3). This suggests that NE-Dynein recruitment problems are due to lack of activity of the adaptors and not driven by their absence or loss. Given the direct interaction between the telomeres and SUN proteins, we speculate that chromatin condensation could generate pulling forces at the NE, changing NE tension either globally or locally and inducing conformational changes on the NPCs. These could activate the Dynein adaptors to promote Dynein association. Accordingly, a recent study demonstrated that chromatin remodeling is initiated at nuclear pores [188]. Also, it was shown that SUN1, contrarily to SUN2, can directly interact with the NPCs [189]. Moreover, NE membrane tension was shown to be functionally linked with NPC conformation and nucleocytoplasmic transport activity [154,190–192]. This model could also justify how confinement, either by inducing transient chromatin condensation [193], or imposing mechanical strain on SUN proteins [136], is able to restore NE Dynein localization. NE-Dynein recruitment might, therefore, be a simple physical process regulated by chromatin-mediated tension in the NE. Still, we cannot exclude potential modulatory contributions of other accessory proteins and mechanisms.

Interestingly, in diverse eukaryotic species, it has been extensively reported that SUN1-telomeres interaction is required to drive meiotic chromosome dynamics [181,194–200]. In this context, is has been proposed that cytoplasmic forces generated by Dynein on MTs are transduced to chromosome telomeres trough SUN1/KASH5 bridges. These forces mediate clustering of telomeres at the NE to form the so-called meiotic “chromosome bouquet”, which is considered to aid in homolog chromosome pairing [198,201]. Whether SUN-KASH bridges and telomeres also cooperate to drive Dynein-mediated chromosome motion in mitosis, remains an interesting open question. Thus, it will be important to further characterize chromosomes organization and distribution during mitotic entry and determine its putative roles and/or implications for spindle assembly and mitotic fidelity.

Remarkably, both prophase centrosome separation [70] and NEB [202] and early spindle assembly [58] rely on NE-Dynein-mediated forces and are under the regulation of CDK1 [203]. Thus, the molecular players driving all these processes — MTs, Dynein, LINC complex, NPCs, and centrosomes — are intriguingly similar. Consequently, chromosome condensation-mediated mechanical forces likely regulate and coordinate NEB and centrosome separation, by determining timely Dynein loading. If that is the case, one could imagine that acutely impairing chromosome condensation might directly impact CyclinB1 nuclear translocation. Indeed, it was recently reported that mechanical stimulation triggered

a fast nuclear accumulation of Cyclin B1 [165]. Nevertheless, opposing this hypothesis, abolishing cellular contractility, which was found to be necessary to facilitate Cyclin B1 nuclear translocation [165], did not affect NE-Dynein recruitment (Chapter III; Figure 4).

In conclusion, we propose a new mechanical signaling pathway that relies on the regulation of NE-Dynein recruitment mediated by chromosome condensation. Thus, mechanical signaling pathways appear to cooperate with biochemical signaling pathways (Cyclin B1-CDK1 regulation; [155]), to set the time for mitotic entry and synchronize cytoplasmic and nuclear events. Overall, understanding how the mechanical properties of the nucleus affect cellular processes, such as mitotic entry, will be of special interest to the aging and cancer fields, where lamina mutations and heterochromatin loss are often found [204–209].

3. References

[1] S.L. Prosser, L. Pelletier, Mitotic spindle assembly in animal cells: a fine balancing act, Nat Rev Mol Cell Biol. 18 (2017) 187–201. https://doi.org/10.1038/nrm.2016.162.

[2] C.E. Walczak, R. Heald, Chapter Three - Mechanisms of Mitotic Spindle Assembly and Function, in: K.W. Jeon (Ed.), International Review of Cytology, Academic Press, 2008: pp. 111–158. https://doi.org/10.1016/S0074-7696(07)65003-7.

[3] D.J. Forbes, A. Travesa, M.S. Nord, C. Bernis, Reprint of "Nuclear transport factors: global regulation of mitosis," Curr Opin Cell Biol. 34 (2015) 122–134. https://doi.org/10.1016/j.ceb.2015.07.005.

[4] C.L. Rieder, Kinetochore fiber formation in animal somatic cells: dueling mechanisms come to a draw, Chromosoma. 114 (2005) 310–318. https://doi.org/10.1007/s00412-005-0028-2.

[5] S. Meunier, I. Vernos, Acentrosomal Microtubule Assembly in Mitosis: The Where, When, and How, Trends Cell Biol. 26 (2016) 80–87. https://doi.org/10.1016/j.tcb.2015.09.001.

[6] J. Scrofani, T. Sardon, S. Meunier, I. Vernos, Microtubule nucleation in mitosis by a RanGTP-dependent protein complex, Curr Biol. 25 (2015) 131–140. https://doi.org/10.1016/j.cub.2014.11.025.

[7] S. Petry, R.D. Vale, Microtubule nucleation at the centrosome and beyond, Nat Cell Biol. 17 (2015) 1089–1093. https://doi.org/10.1038/ncb3220.

[8] T.J. Maresca, A.C. Groen, J.C. Gatlin, R. Ohi, T.J. Mitchison, E.D. Salmon, Spindle assembly in the absence of a RanGTP gradient requires localized CPC activity, Curr Biol. 19 (2009) 1210–1215. https://doi.org/10.1016/j.cub.2009.05.061.

[9] S.C. Sampath, R. Ohi, O. Leismann, A. Salic, A. Pozniakovski, H. Funabiki, The chromosomal passenger complex is required for chromatin-induced microtubule stabilization and spindle assembly, Cell. 118 (2004) 187–202. https://doi.org/10.1016/j.cell.2004.06.026.

[10] A. Khodjakov, L. Copenagle, M.B. Gordon, D.A. Compton, T.M. Kapoor, Minus-end capture of preformed kinetochore fibers contributes to spindle morphogenesis, J Cell Biol. 160 (2003) 671–683. https://doi.org/10.1083/jcb.200208143.

[11] V. Sikirzhytski, F. Renda, I. Tikhonenko, V. Magidson, B.F. McEwen, A. Khodjakov, Microtubules assemble near most kinetochores during early prometaphase in human cells, Journal of Cell Biology. 217 (2018) 2647–2659. https://doi.org/10.1083/jcb.201710094.

[12] T. Kamasaki, E. O'Toole, S. Kita, M. Osumi, J. Usukura, J.R. McIntosh, G. Goshima, Augmin-dependent microtubule nucleation at microtubule walls in the spindle, J Cell Biol. 202 (2013) 25–33. https://doi.org/10.1083/jcb.201304031.

[13] S. Lawo, M. Bashkurov, M. Mullin, M.G. Ferreria, R. Kittler, B. Habermann, A. Tagliaferro, I. Poser, J.R.A. Hutchins, B. Hegemann, D. Pinchev, F. Buchholz, J.-M. Peters, A.A. Hyman, A.-C. Gingras, L. Pelletier, HAUS, the 8-subunit human Augmin complex, regulates centrosome and spindle integrity, Curr Biol. 19 (2009) 816–826. https://doi.org/10.1016/j.cub.2009.04.033.

[14] E. Bucciarelli, M.G. Giansanti, S. Bonaccorsi, M. Gatti, Spindle assembly and cytokinesis in the absence of chromosomes during Drosophila male meiosis, J Cell Biol. 160 (2003) 993–999. https://doi.org/10.1083/jcb.200211029.

[15] E. Karsenti, J. Newport, M. Kirschner, Respective roles of centrosomes and chromatin in the conversion of microtubule arrays from interphase to metaphase, J Cell Biol. 99 (1984) 47s–54s. https://doi.org/10.1083/jcb.99.1.47s.

[16] R. Heald, R. Tournebize, T. Blank, R. Sandaltzopoulos, P. Becker, A. Hyman, E. Karsenti, Self-organization of microtubules into bipolar spindles around artificial chromosomes in Xenopus egg extracts, Nature. 382 (1996) 420–425. https://doi.org/10.1038/382420a0.

[17] D. Hayward, J. Metz, C. Pellacani, J.G. Wakefield, Synergy between multiple microtubule-generating pathways confers robustness to centrosome-driven mitotic spindle formation, Dev Cell. 28 (2014) 81–93. https://doi.org/10.1016/j.devcel.2013.12.001.

[18] C.Y. Tsai, B. Ngo, A. Tapadia, P.-H. Hsu, G. Wu, W.-H. Lee, Aurora-A phosphorylates Augmin complex component Hice1 protein at an N-terminal serine/threonine cluster to modulate its microtubule binding activity during spindle assembly, J Biol Chem. 286 (2011) 30097–30106. https://doi.org/10.1074/jbc.M111.266767.

[19] Y. Johmura, N.-K. Soung, J.-E. Park, L.-R. Yu, M. Zhou, J.K. Bang, B.-Y. Kim, T.D. Veenstra, R.L. Erikson, K.S. Lee, Regulation of microtubule-based microtubule nucleation by mammalian polo-like kinase 1, Proc Natl Acad Sci U S A. 108 (2011) 11446–11451. https://doi.org/10.1073/pnas.1106223108.

[20] P.T. Conduit, A. Wainman, J.W. Raff, Centrosome function and assembly in animal cells, Nature Reviews Molecular Cell Biology. 16 (2015) 611–624. https://doi.org/10.1038/nrm4062.

[21] A. Khodjakov, C.L. Rieder, The sudden recruitment of gamma-tubulin to the centrosome at the onset of mitosis and its dynamic exchange throughout the cell cycle, do not require microtubules, J Cell Biol. 146 (1999) 585–596. https://doi.org/10.1083/jcb.146.3.585.

[22] M. Piehl, U.S. Tulu, P. Wadsworth, L. Cassimeris, Centrosome maturation: measurement of microtubule nucleation throughout the cell cycle by using GFP-

tagged EB1, Proc Natl Acad Sci U S A. 101 (2004) 1584–1588. https://doi.org/10.1073/pnas.0308205100.

[23] A. Burakov, E. Nadezhdina, B. Slepchenko, V. Rodionov, Centrosome positioning in interphase cells, J Cell Biol. 162 (2003) 963–969. https://doi.org/10.1083/jcb.200305082.

[24] E.A. Nigg, T. Stearns, The centrosome cycle: Centriole biogenesis, duplication and inherent asymmetries, Nat Cell Biol. 13 (2011) 1154–1160. https://doi.org/10.1038/ncb2345.

[25] T. Stearns, Centrosome Duplication: A Centriolar Pas de Deux, Cell. 105 (2001) 417–420. https://doi.org/10.1016/S0092-8674(01)00366-X.

[26] J. Fu, I.M. Hagan, D.M. Glover, The Centrosome and Its Duplication Cycle, Cold Spring Harb Perspect Biol. 7 (2015) a015800. https://doi.org/10.1101/cshperspect.a015800.

[27] M.E. Tanenbaum, R.H. Medema, Mechanisms of centrosome separation and bipolar spindle assembly, Dev Cell. 19 (2010) 797–806. https://doi.org/10.1016/j.devcel.2010.11.011.

[28] A. Khodjakov, R.W. Cole, B.R. Oakley, C.L. Rieder, Centrosome-independent mitotic spindle formation in vertebrates, Curr Biol. 10 (2000) 59–67. https://doi.org/10.1016/s0960-9822(99)00276-6.

[29] N.M. Mahoney, G. Goshima, A.D. Douglass, R.D. Vale, Making microtubules and mitotic spindles in cells without functional centrosomes, Curr Biol. 16 (2006) 564–569. https://doi.org/10.1016/j.cub.2006.01.053.

[30] R. Basto, J. Lau, T. Vinogradova, A. Gardiol, C.G. Woods, A. Khodjakov, J.W. Raff, Flies without centrioles, Cell. 125 (2006) 1375–1386. https://doi.org/10.1016/j.cell.2006.05.025.

[31] H.-J. Nam, R. Naylor, J.M. van Deursen, Centrosome dynamics as a source of chromosomal instability, Trends Cell Biol. 25 (2015) 65–73. https://doi.org/10.1016/j.tcb.2014.10.002.

[32] W.T. Silkworth, I.K. Nardi, R. Paul, A. Mogilner, D. Cimini, Timing of centrosome separation is important for accurate chromosome segregation, MBoC. 23 (2011) 401–411. https://doi.org/10.1091/mbc.e11-02-0095.

[33] J.-H. Sir, M. Pütz, O. Daly, C.G. Morrison, M. Dunning, J.V. Kilmartin, F. Gergely, Loss of centrioles causes chromosomal instability in vertebrate somatic cells, J Cell Biol. 203 (2013) 747–756. https://doi.org/10.1083/jcb.201309038.

[34] K. Kaseda, A.D. McAinsh, R.A. Cross, Dual pathway spindle assembly increases both the speed and the fidelity of mitosis, Biology Open. 1 (2012) 12–18. https://doi.org/10.1242/bio.2011012.

[35] A. Toso, J.R. Winter, A.J. Garrod, A.C. Amaro, P. Meraldi, A.D. McAinsh, Kinetochore-generated pushing forces separate centrosomes during bipolar spindle assembly, J Cell Biol. 184 (2009) 365–372. https://doi.org/10.1083/jcb.200809055.

[36] C.M. Whitehead, R.J. Winkfein, J.B. Rattner, The relationship of HsEg5 and the actin cytoskeleton to centrosome separation, Cell Motil. Cytoskeleton. 35 (1996) 298–308. https://doi.org/10.1002/(SICI)1097-0169(1996)35:4<298::AID-CM3>3.0.CO;2-3.

[37] V. Magidson, C.B. O'Connell, J. Lončarek, R. Paul, A. Mogilner, A. Khodjakov, The Spatial Arrangement of Chromosomes during Prometaphase Facilitates Spindle Assembly, Cell. 146 (2011) 555–567. https://doi.org/10.1016/j.cell.2011.07.012.

[38] L. Champion, M.I. Linder, U. Kutay, Cellular Reorganization during Mitotic Entry, Trends Cell Biol. 27 (2017) 26–41. https://doi.org/10.1016/j.tcb.2016.07.004.

[39] V. Nunes, J.G. Ferreira, From the cytoskeleton to the nucleus: An integrated view on early spindle assembly, Seminars in Cell & Developmental Biology. 117 (2021) 42–51. https://doi.org/10.1016/j.semcdb.2021.03.006.

[40] N.P. Ferenz, A. Gable, P. Wadsworth, Mitotic functions of kinesin-5, Seminars in Cell & Developmental Biology. 21 (2010) 255–259. https://doi.org/10.1016/j.semcdb.2010.01.019.

[41] T.M. Kapoor, T.U. Mayer, M.L. Coughlin, T.J. Mitchison, Probing Spindle Assembly Mechanisms with Monastrol, a Small Molecule Inhibitor of the Mitotic Kinesin, Eg5, J Cell Biol. 150 (2000) 975–988.

[42] A. De Simone, F. Nédélec, P. Gönczy, Dynein Transmits Polarized Actomyosin Cortical Flows to Promote Centrosome Separation, Cell Rep. 14 (2016) 2250–2262. https://doi.org/10.1016/j.celrep.2016.01.077.

[43] J.A. Raaijmakers, R.G.H.P. van Heesbeen, J.L. Meaders, E.F. Geers, B. Fernandez-Garcia, R.H. Medema, M.E. Tanenbaum, Nuclear envelope-associated dynein drives prophase centrosome separation and enables Eg5-independent bipolar spindle formation, The EMBO Journal. 31 (2012) 4179–4190. https://doi.org/10.1038/emboj.2012.272.

[44] J. Rosenblatt, L.P. Cramer, B. Baum, K.M. McGee, Myosin II-dependent cortical movement is required for centrosome separation and positioning during mitotic spindle assembly, Cell. 117 (2004) 361–372. https://doi.org/10.1016/s0092-8674(04)00341-1.

[45] J. Cao, J. Crest, B. Fasulo, W. Sullivan, Cortical Actin Dynamics Facilitate Early-Stage Centrosome Separation, Current Biology. 20 (2010) 770–776. https://doi.org/10.1016/j.cub.2010.02.060.

[46] M. Plessner, J. Knerr, R. Grosse, Centrosomal Actin Assembly Is Required for Proper Mitotic Spindle Formation and Chromosome Congression, IScience. 15 (2019) 274–281. https://doi.org/10.1016/j.isci.2019.04.022.

[47] W. Wang, L. Chen, Y. Ding, J. Jin, K. Liao, Centrosome separation driven by actin-microfilaments during mitosis is mediated by centrosome-associated tyrosine-phosphorylated cortactin, J Cell Sci. 121 (2008) 1334–1343. https://doi.org/10.1242/jcs.018176.

[48] T. Stiff, F.R. Echegaray-Iturra, H.J. Pink, A. Herbert, C.C. Reyes-Aldasoro, H. Hochegger, Prophase-Specific Perinuclear Actin Coordinates Centrosome Separation and Positioning to Ensure Accurate Chromosome Segregation, Cell Reports. 31 (2020) 107681. https://doi.org/10.1016/j.celrep.2020.107681.

[49] L.C. Kapitein, E.J.G. Peterman, B.H. Kwok, J.H. Kim, T.M. Kapoor, C.F. Schmidt, The bipolar mitotic kinesin Eg5 moves on both microtubules that it crosslinks, Nature. 435 (2005) 114–118. https://doi.org/10.1038/nature03503.

[50] D.J. Sharp, K.L. McDonald, H.M. Brown, H.J. Matthies, C. Walczak, R.D. Vale, T.J. Mitchison, J.M. Scholey, The Bipolar Kinesin, KLP61F, Cross-links Microtubules within Interpolar Microtubule Bundles of Drosophila Embryonic Mitotic Spindles, Journal of Cell Biology. 144 (1999) 125–138. https://doi.org/10.1083/jcb.144.1.125.

[51] A.S. Gayek, R. Ohi, Kinetochore-microtubule stability governs the metaphase requirement for Eg5, Mol Biol Cell. 25 (2014) 2051–2060. https://doi.org/10.1091/mbc.E14-03-0785.

[52] M.W. Elting, P. Suresh, S. Dumont, The spindle: Integrating architecture and mechanics across scales, Trends Cell Biol. 28 (2018) 896–910. https://doi.org/10.1016/j.tcb.2018.07.003.

[53] D. Vanneste, M. Takagi, N. Imamoto, I. Vernos, The Role of Hklp2 in the Stabilization and Maintenance of Spindle Bipolarity, Current Biology. 19 (2009) 1712–1717. https://doi.org/10.1016/j.cub.2009.09.019.

[54] M.E. Tanenbaum, L. Macůrek, A. Janssen, E.F. Geers, M. Alvarez-Fernández, R.H. Medema, Kif15 Cooperates with Eg5 to Promote Bipolar Spindle Assembly, Current Biology. 19 (2009) 1703–1711. https://doi.org/10.1016/j.cub.2009.08.027.

[55] D. Splinter, M.E. Tanenbaum, A. Lindqvist, D. Jaarsma, A. Flotho, K.L. Yu, I. Grigoriev, D. Engelsma, E.D. Haasdijk, N. Keijzer, J. Demmers, M. Fornerod, F. Melchior, C.C. Hoogenraad, R.H. Medema, A. Akhmanova, Bicaudal D2, dynein, and kinesin-1 associate with nuclear pore complexes and regulate centrosome and nuclear positioning during mitotic entry, PLoS Biol. 8 (2010) e1000350. https://doi.org/10.1371/journal.pbio.1000350.

[56] P. Gönczy, S. Pichler, M. Kirkham, A.A. Hyman, Cytoplasmic Dynein Is Required for Distinct Aspects of Mtoc Positioning, Including Centrosome Separation, in the One Cell Stage Caenorhabditis elegans Embryo, Journal of Cell Biology. 147 (1999) 135–150. https://doi.org/10.1083/jcb.147.1.135.

[57] C.J. Malone, L. Misner, N. Le Bot, M.-C. Tsai, J.M. Campbell, J. Ahringer, J.G. White, The C. elegans Hook Protein, ZYG-12, Mediates the Essential Attachment between the Centrosome and Nucleus, Cell. 115 (2003) 825–836. https://doi.org/10.1016/S0092-8674(03)00985-1.

[58] S. Bolhy, I. Bouhlel, E. Dultz, T. Nayak, M. Zuccolo, X. Gatti, R. Vallee, J. Ellenberg, V. Doye, A Nup133-dependent NPC-anchored network tethers centrosomes to the nuclear envelope in prophase, J Cell Biol. 192 (2011) 855–871. https://doi.org/10.1083/jcb.201007118.

[59] J.R. Levy, E.L.F. Holzbaur, Dynein drives nuclear rotation during forward progression of motile fibroblasts, Journal of Cell Science. 121 (2008) 3187–3195. https://doi.org/10.1242/jcs.033878.

[60] M.V. Gerashchenko, I.S. Chernoivanenko, M.V. Moldaver, A.A. Minin, Dynein is a motor for nuclear rotation while vimentin IFs is a “brake,” Cell Biol Int. 33 (2009) 1057–1064. https://doi.org/10.1016/j.cellbi.2009.06.020.

[61] J. Wu, K.C. Lee, R.B. Dickinson, T.P. Lele, How dynein and microtubules rotate the nucleus, Journal of Cellular Physiology. 226 (2011) 2666–2674. https://doi.org/10.1002/jcp.22616.

[62] J.Y. Ji, R.T. Lee, L. Vergnes, L.G. Fong, C.L. Stewart, K. Reue, S.G. Young, Q. Zhang, C.M. Shanahan, J. Lammerding, Cell nuclei spin in the absence of lamin b1, J Biol Chem. 282 (2007) 20015–20026. https://doi.org/10.1074/jbc.M611094200.

[63] T. Nguyen-Ngoc, K. Afshar, P. Gönczy, Coupling of cortical dynein and G alpha proteins mediates spindle positioning in Caenorhabditis elegans, Nat Cell Biol. 9 (2007) 1294–1302. https://doi.org/10.1038/ncb1649.

[64] G.E. Woodard, N.-N. Huang, H. Cho, T. Miki, G.G. Tall, J.H. Kehrl, Ric-8A and Gi alpha recruit LGN, NuMA, and dynein to the cell cortex to help orient the mitotic spindle, Mol Cell Biol. 30 (2010) 3519–3530. https://doi.org/10.1128/MCB.00394-10.

[65] T. Kiyomitsu, I.M. Cheeseman, Chromosome- and spindle-pole-derived signals generate an intrinsic code for spindle position and orientation, Nat. Cell Biol. 14 (2012) 311–317. https://doi.org/10.1038/ncb2440.

[66] S. Kotak, C. Busso, P. Gönczy, Cortical dynein is critical for proper spindle positioning in human cells, J Cell Biol. 199 (2012) 97–110. https://doi.org/10.1083/jcb.201203166.

[67] D. Splinter, D.S. Razafsky, M.A. Schlager, A. Serra-Marques, I. Grigoriev, J. Demmers, N. Keijzer, K. Jiang, I. Poser, A.A. Hyman, C.C. Hoogenraad, S.J. King, A. Akhmanova, BICD2, dynactin, and LIS1 cooperate in regulating dynein recruitment to cellular structures, MBoC. 23 (2012) 4226–4241. https://doi.org/10.1091/mbc.e12-03-0210.

[68] F. di Pietro, A. Echard, X. Morin, Regulation of mitotic spindle orientation: an integrated view, EMBO Rep. 17 (2016) 1106–1130. https://doi.org/10.15252/embr.201642292.

[69] Z. Zheng, Q. Wan, J. Liu, H. Zhu, X. Chu, Q. Du, Evidence for dynein and astral microtubule–mediated cortical release and transport of Gαi/LGN/NuMA complex in mitotic cells, MBoC. 24 (2013) 901–913. https://doi.org/10.1091/mbc.e12-06-0458.

[70] V. Nunes, M. Dantas, D. Castro, E. Vitiello, I. Wang, N. Carpi, M. Balland, M. Piel, P. Aguiar, H. Maiato, J.G. Ferreira, Centrosome-nuclear axis repositioning drives the assembly of a bipolar spindle scaffold to ensure mitotic fidelity, MBoC. (2020) mbc.E20-01-0047. https://doi.org/10.1091/mbc.E20-01-0047.

[71] J.A. Raaijmakers, R.H. Medema, Function and regulation of dynein in mitotic chromosome segregation, Chromosoma. 123 (2014) 407–422. https://doi.org/10.1007/s00412-014-0468-7.

[72] E.N. Cytrynbaum, J.M. Scholey, A. Mogilner, A Force Balance Model of Early Spindle Pole Separation in Drosophila Embryos, Biophysical Journal. 84 (2003) 757–769. https://doi.org/10.1016/S0006-3495(03)74895-4.

[73] M. Wühr, E.S. Tan, S.K. Parker, H.W. Detrich, T.J. Mitchison, A Model for Cleavage Plane Determination in Early Amphibian and Fish Embryos, Current Biology. 20 (2010) 2040–2045. https://doi.org/10.1016/j.cub.2010.10.024.

[74] A. De Simone, P. Gönczy, Computer simulations reveal mechanisms that organize nuclear dynein forces to separate centrosomes, MBoC. 28 (2017) 3165–3170. https://doi.org/10.1091/mbc.e16-12-0823.

[75] S.C. Ems-McClung, C.E. Walczak, Kinesin-13s in mitosis: Key players in the spatial and temporal organization of spindle microtubules, Semin Cell Dev Biol. 21 (2010) 276–282. https://doi.org/10.1016/j.semcdb.2010.01.016.

[76] V. Nunes, M. Dantas, E. Vitiello, I. Wang, N. Carpi, M. Balland, M. Piel, P. Aguiar, H. Maiato, J.G. Ferreira, Spatial Asymmetries of the Prophase Nucleus Regulate Dynein Recruitment to Ensure Mitotic Fidelity, BioRxiv. (2019) 526939. https://doi.org/10.1101/526939.

[77] P. Kunda, B. Baum, The actin cytoskeleton in spindle assembly and positioning, Trends in Cell Biology. 19 (2009) 174–179. https://doi.org/10.1016/j.tcb.2009.01.006.

[78] H. Tuncay, B.F. Brinkmann, T. Steinbacher, A. Schürmann, V. Gerke, S. Iden, K. Ebnet, JAM-A regulates cortical dynein localization through Cdc42 to control planar spindle orientation during mitosis, Nature Communications. 6 (2015) 8128. https://doi.org/10.1038/ncomms9128.

[79] O.M. Lancaster, M. Le Berre, A. Dimitracopoulos, D. Bonazzi, E. Zlotek-Zlotkiewicz, R. Picone, T. Duke, M. Piel, B. Baum, Mitotic rounding alters cell geometry to ensure efficient bipolar spindle formation, Dev Cell. 25 (2013) 270–283. https://doi.org/10.1016/j.devcel.2013.03.014.

[80] P. Chugh, A.G. Clark, M.B. Smith, D.A.D. Cassani, K. Dierkes, A. Ragab, P.P. Roux, G. Charras, G. Salbreux, E.K. Paluch, Actin cortex architecture regulates cell surface tension, Nat Cell Biol. 19 (2017) 689–697. https://doi.org/10.1038/ncb3525.

[81] Y. Zhai, P.J. Kronebusch, P.M. Simon, G.G. Borisy, Microtubule dynamics at the G2/M transition: abrupt breakdown of cytoplasmic microtubules at nuclear envelope breakdown and implications for spindle morphogenesis., J Cell Biol. 135 (1996) 201–214. https://doi.org/10.1083/jcb.135.1.201.

[82] N. Mchedlishvili, H.K. Matthews, A. Corrigan, B. Baum, Two-step interphase microtubule disassembly aids spindle morphogenesis, BMC Biology. 16 (2018) 14. https://doi.org/10.1186/s12915-017-0478-z.

[83] A. Colin, P. Singaravelu, M. Théry, L. Blanchoin, Z. Gueroui, Actin-Network Architecture Regulates Microtubule Dynamics, Current Biology. 28 (2018) 2647-2656.e4. https://doi.org/10.1016/j.cub.2018.06.028.

[84] D. Inoue, D. Obino, J. Pineau, F. Farina, J. Gaillard, C. Guerin, L. Blanchoin, A.-M. Lennon-Duménil, M. Théry, Actin filaments regulate microtubule growth at the centrosome, The EMBO Journal. 38 (2019) e99630. https://doi.org/10.15252/embj.201899630.

[85] F. Farina, N. Ramkumar, L. Brown, D. Samandar Eweis, J. Anstatt, T. Waring, J. Bithell, G. Scita, M. Thery, L. Blanchoin, T. Zech, B. Baum, Local actin nucleation tunes centrosomal microtubule nucleation during passage through mitosis, EMBO J. 38 (2019) e99843. https://doi.org/10.15252/embj.201899843.

[86] F. Farina, J. Gaillard, C. Guérin, Y. Couté, J. Sillibourne, L. Blanchoin, M. Théry, The centrosome is an actin-organizing centre, Nature Cell Biology. 18 (2016) 65–75. https://doi.org/10.1038/ncb3285.

[87] D. Obino, F. Farina, O. Malbec, P.J. Sáez, M. Maurin, J. Gaillard, F. Dingli, D. Loew, A. Gautreau, M.-I. Yuseff, L. Blanchoin, M. Théry, A.-M. Lennon-Duménil, Actin nucleation at the centrosome controls lymphocyte polarity, Nature Communications. 7 (2016) 10969. https://doi.org/10.1038/ncomms10969.

[88] A.J. Booth, Z. Yue, J.K. Eykelenboom, T. Stiff, G.G. Luxton, H. Hochegger, T.U. Tanaka, Contractile acto-myosin network on nuclear envelope remnants positions human chromosomes for mitosis, ELife. 8 (2019) e46902. https://doi.org/10.7554/eLife.46902.

[89] M. Mitsushima, K. Aoki, M. Ebisuya, S. Matsumura, T. Yamamoto, M. Matsuda, F. Toyoshima, E. Nishida, Revolving movement of a dynamic cluster of actin filaments during mitosis, Journal of Cell Biology. 191 (2010) 453–462. https://doi.org/10.1083/jcb.201007136.

[90] J. Fink, N. Carpi, T. Betz, A. Bétard, M. Chebah, A. Azioune, M. Bornens, C. Sykes, L. Fetler, D. Cuvelier, M. Piel, External forces control mitotic spindle positioning, Nature Cell Biology. 13 (2011) 771–778. https://doi.org/10.1038/ncb2269.

[91] M. Théry, V. Racine, A. Pépin, M. Piel, Y. Chen, J.-B. Sibarita, M. Bornens, The extracellular matrix guides the orientation of the cell division axis, Nature Cell Biology. 7 (2005) 947–953. https://doi.org/10.1038/ncb1307.

[92] C.B. O'Connell, Y.L. Wang, Mammalian spindle orientation and position respond to changes in cell shape in a dynein-dependent fashion, Mol. Biol. Cell. 11 (2000) 1765–1774. https://doi.org/10.1091/mbc.11.5.1765.

[93] O. Hertwig, Das Problem der Befruchtung und der Isotropie des Eies: eine Theorie der Vererbung, Fischer, 1884.

[94] M. Théry, M. Bornens, Cell shape and cell division, Current Opinion in Cell Biology. 18 (2006) 648–657. https://doi.org/10.1016/j.ceb.2006.10.001.

[95] N. Minc, D. Burgess, F. Chang, Influence of Cell Geometry on Division-Plane Positioning, Cell. 144 (2011) 414–426. https://doi.org/10.1016/j.cell.2011.01.016.

[96] F. Bosveld, O. Markova, B. Guirao, C. Martin, Z. Wang, A. Pierre, M. Balakireva, I. Gaugue, A. Ainslie, N. Christophorou, D.K. Lubensky, N. Minc, Y. Bellaïche, Epithelial tricellular junctions act as interphase cell shape sensors to orient mitosis, Nature. 530 (2016) 495–498. https://doi.org/10.1038/nature16970.

[97] S.W. Grill, J. Howard, E. Schäffer, E.H.K. Stelzer, A.A. Hyman, The Distribution of Active Force Generators Controls Mitotic Spindle Position, Science. 301 (2003) 518–521. https://doi.org/10.1126/science.1086560.

[98] S.W. Grill, A.A. Hyman, Spindle Positioning by Cortical Pulling Forces, Developmental Cell. 8 (2005) 461–465. https://doi.org/10.1016/j.devcel.2005.03.014.

[99] M.W. Kirschner, T. Mitchison, Microtubule dynamics, Nature. 324 (1986) 621–621. https://doi.org/10.1038/324621a0.

[100] R. Wollman, E.N. Cytrynbaum, J.T. Jones, T. Meyer, J.M. Scholey, A. Mogilner, Efficient chromosome capture requires a bias in the "search-and-capture" process

during mitotic-spindle assembly, Curr Biol. 15 (2005) 828–832. https://doi.org/10.1016/j.cub.2005.03.019.

[101] H. Maiato, C.L. Rieder, A. Khodjakov, Kinetochore-driven formation of kinetochore fibers contributes to spindle assembly during animal mitosis, Journal of Cell Biology. 167 (2004) 831–840. https://doi.org/10.1083/jcb.200407090.

[102] V. Magidson, R. Paul, N. Yang, J.G. Ault, C.B. O'Connell, I. Tikhonenko, B.F. McEwen, A. Mogilner, A. Khodjakov, Adaptive changes in the kinetochore architecture facilitate proper spindle assembly, Nat Cell Biol. 17 (2015) 1134–1144. https://doi.org/10.1038/ncb3223.

[103] R. Paul, R. Wollman, W.T. Silkworth, I.K. Nardi, D. Cimini, A. Mogilner, Computer simulations predict that chromosome movements and rotations accelerate mitotic spindle assembly without compromising accuracy, PNAS. 106 (2009) 15708–15713. https://doi.org/10.1073/pnas.0908261106.

[104] G. Ostergren, J. Mole-Bajer, A. Bajer, An interpretation of transport phenomena at mitosis, Ann N Y Acad Sci. 90 (1960) 381–408. https://doi.org/10.1111/j.1749-6632.1960.tb23258.x.

[105] D. Mazia, CHAPTER 2 - Mitosis and the Physiology of Cell Division, in: J. Brachet, A.E. Mirsky (Eds.), The Cell, Academic Press, 1961: pp. 77–412. https://doi.org/10.1016/B978-0-12-123303-7.50008-9.

[106] R. Qi, N. Xu, G. Wang, H. Ren, S. Li, J. Lei, Q. Lin, L. Wang, X. Gu, H. Zhang, Q. Jiang, C. Zhang, The lamin-A/C-LAP2α-BAF1 protein complex regulates mitotic spindle assembly and positioning, J Cell Sci. 128 (2015) 2830–2841. https://doi.org/10.1242/jcs.164566.

[107] M.-Y. Tsai, S. Wang, J.M. Heidinger, D.K. Shumaker, S.A. Adam, R.D. Goldman, Y. Zheng, A Mitotic Lamin B Matrix Induced by RanGTP Required for Spindle Assembly, Science. 311 (2006) 1887–1893. https://doi.org/10.1126/science.1122771.

[108] T. Kuga, H. Nie, T. Kazami, M. Satoh, K. Matsushita, F. Nomura, K. Maeshima, Y. Nakayama, T. Tomonaga, Lamin B2 prevents chromosome instability by ensuring proper mitotic chromosome segregation, Oncogenesis. 3 (2014) e94. https://doi.org/10.1038/oncsis.2014.6.

[109] I. Minn, M.M. Rolls, W. Hanna-Rose, C.J. Malone, SUN-1 and ZYG-12, Mediators of Centrosome–Nucleus Attachment, Are a Functional SUN/KASH Pair in Caenorhabditis elegans, MBoC. 20 (2009) 4586–4595. https://doi.org/10.1091/mbc.e08-10-1034.

[110] X. Zhang, K. Lei, X. Yuan, X. Wu, Y. Zhuang, T. Xu, R. Xu, M. Han, SUN1/2 and Syne/Nesprin-1/2 complexes connect centrosome to the nucleus during

neurogenesis and neuronal migration in mice, Neuron. 64 (2009) 173–187. https://doi.org/10.1016/j.neuron.2009.08.018.

[111] Y. Turgay, L. Champion, C. Balazs, M. Held, A. Toso, D.W. Gerlich, P. Meraldi, U. Kutay, SUN proteins facilitate the removal of membranes from chromatin during nuclear envelope breakdown, Journal of Cell Biology. 204 (2014) 1099–1109. https://doi.org/10.1083/jcb.201310116.

[112] J.C. Gonçalves, S. Quintremil, J. Yi, R.B. Vallee, Nesprin-2 Recruitment of BicD2 to the Nuclear Envelope Controls Dynein/Kinesin-Mediated Neuronal Migration In Vivo, Curr Biol. 30 (2020) 3116-3129.e4. https://doi.org/10.1016/j.cub.2020.05.091.

[113] K. Wilhelmsen, M. Ketema, H. Truong, A. Sonnenberg, KASH-domain proteins in nuclear migration, anchorage and other processes, J Cell Sci. 119 (2006) 5021–5029. https://doi.org/10.1242/jcs.03295.

[114] J. Aureille, N. Belaadi, C. Guilluy, Mechanotransduction via the nuclear envelope: a distant reflection of the cell surface, Current Opinion in Cell Biology. 44 (2017) 59–67. https://doi.org/10.1016/j.ceb.2016.10.003.

[115] D.-H. Kim, D. Wirtz, Cytoskeletal tension induces the polarized architecture of the nucleus, Biomaterials. 48 (2015) 161–172. https://doi.org/10.1016/j.biomaterials.2015.01.023.

[116] Y. Chikashige, M. Yamane, K. Okamasa, C. Tsutsumi, T. Kojidani, M. Sato, T. Haraguchi, Y. Hiraoka, Membrane proteins Bqt3 and -4 anchor telomeres to the nuclear envelope to ensure chromosomal bouquet formation, Journal of Cell Biology. 187 (2009) 413–427. https://doi.org/10.1083/jcb.200902122.

[117] Y. Chikashige, T. Haraguchi, Y. Hiraoka, Another way to move chromosomes, Chromosoma. 116 (2007) 497–505. https://doi.org/10.1007/s00412-007-0114-8.

[118] S.D. Georgatos, A. Pyrpasopoulou, P.A. Theodoropoulos, Nuclear envelope breakdown in mammalian cells involves stepwise lamina disassembly and microtubule-drive deformation of the nuclear membrane, J Cell Sci. 110 (Pt 17) (1997) 2129–2140.

[119] P. De Magistris, W. Antonin, The Dynamic Nature of the Nuclear Envelope, Curr Biol. 28 (2018) R487–R497. https://doi.org/10.1016/j.cub.2018.01.073.

[120] N. Naumova, M. Imakaev, G. Fudenberg, Y. Zhan, B.R. Lajoie, L.A. Mirny, J. Dekker, Organization of the mitotic chromosome, Science. 342 (2013) 948–953. https://doi.org/10.1126/science.1236083.

[121] W. Antonin, H. Neumann, Chromosome condensation and decondensation during mitosis, Current Opinion in Cell Biology. 40 (2016) 15–22. https://doi.org/10.1016/j.ceb.2016.01.013.

[122] A.S. Belmont, Mitotic chromosome structure and condensation, Current Opinion in Cell Biology. 18 (2006) 632–638. https://doi.org/10.1016/j.ceb.2006.09.007.

[123] A.D. Stephens, E.J. Banigan, S.A. Adam, R.D. Goldman, J.F. Marko, Chromatin and lamin A determine two different mechanical response regimes of the cell nucleus, MBoC. 28 (2017) 1984–1996. https://doi.org/10.1091/mbc.e16-09-0653.

[124] A.D. Stephens, E.J. Banigan, J.F. Marko, Chromatin's physical properties shape the nucleus and its functions, Current Opinion in Cell Biology. 58 (2019) 76–84. https://doi.org/10.1016/j.ceb.2019.02.006.

[125] J. Lammerding, L.G. Fong, J.Y. Ji, K. Reue, C.L. Stewart, S.G. Young, R.T. Lee, Lamins A and C but not lamin B1 regulate nuclear mechanics, J Biol Chem. 281 (2006) 25768–25780. https://doi.org/10.1074/jbc.M513511200.

[126] K.N. Dahl, A.J. Engler, J.D. Pajerowski, D.E. Discher, Power-law rheology of isolated nuclei with deformation mapping of nuclear substructures, Biophys J. 89 (2005) 2855–2864. https://doi.org/10.1529/biophysj.105.062554.

[127] T. Furusawa, M. Rochman, L. Taher, E.K. Dimitriadis, K. Nagashima, S. Anderson, M. Bustin, Chromatin decompaction by the nucleosomal binding protein HMGN5 impairs nuclear sturdiness, Nat Commun. 6 (2015) 6138. https://doi.org/10.1038/ncomms7138.

[128] J.D. Pajerowski, K.N. Dahl, F.L. Zhong, P.J. Sammak, D.E. Discher, Physical plasticity of the nucleus in stem cell differentiation, Proc Natl Acad Sci U S A. 104 (2007) 15619–15624. https://doi.org/10.1073/pnas.0702576104.

[129] J. Lammerding, P.C. Schulze, T. Takahashi, S. Kozlov, T. Sullivan, R.D. Kamm, C.L. Stewart, R.T. Lee, Lamin A/C deficiency causes defective nuclear mechanics and mechanotransduction, J Clin Invest. 113 (2004) 370–378. https://doi.org/10.1172/JCI19670.

[130] Y. Gruenbaum, A. Margalit, R.D. Goldman, D.K. Shumaker, K.L. Wilson, The nuclear lamina comes of age, Nat Rev Mol Cell Biol. 6 (2005) 21–31. https://doi.org/10.1038/nrm1550.

[131] R. Biggs, P.Z. Liu, A.D. Stephens, J.F. Marko, Effects of altering histone posttranslational modifications on mitotic chromosome structure and mechanics, MBoC. 30 (2019) 820–827. https://doi.org/10.1091/mbc.E18-09-0592.

[132] F.-Y. Chu, S.C. Haley, A. Zidovska, On the origin of shape fluctuations of the cell nucleus, PNAS. 114 (2017) 10338–10343. https://doi.org/10.1073/pnas.1702226114.

[133] D. Castro, V. Nunes, J.T. Lima, J.G. Ferreira, P. Aguiar, Trackosome: a computational toolbox to study the spatiotemporal dynamics of centrosomes, nucleus and cellular membrane, J Cell Sci. (2020). https://doi.org/10.1242/jcs.252254.

[134] T. Menais, S. Mossa, A. Buhot, Polymer translocation through nano-pores in vibrating thin membranes, Scientific Reports. 6 (2016) 38558. https://doi.org/10.1038/srep38558.

[135] V. Introini, G.R. Kidiyoor, G. Porcella, M. Foiani, P. Cicuta, M.C. Lagomarsino, Centripetal nuclear shape fluctuations associate with chromatin condensation towards mitosis, (2021) 2021.11.25.469847. https://doi.org/10.1101/2021.11.25.469847.

[136] A.J. Lomakin, C.J. Cattin, D. Cuvelier, Z. Alraies, M. Molina, G.P.F. Nader, N. Srivastava, P.J. Sáez, J.M. Garcia-Arcos, I.Y. Zhitnyak, A. Bhargava, M.K. Driscoll, E.S. Welf, R. Fiolka, R.J. Petrie, N.S.D. Silva, J.M. González-Granado, N. Manel, A.M. Lennon-Duménil, D.J. Müller, M. Piel, The nucleus acts as a ruler tailoring cell responses to spatial constraints, Science. 370 (2020). https://doi.org/10.1126/science.aba2894.

[137] C.S. Janota, F.J. Calero-Cuenca, E.R. Gomes, The role of the cell nucleus in mechanotransduction, Curr Opin Cell Biol. 63 (2020) 204–211. https://doi.org/10.1016/j.ceb.2020.03.001.

[138] N. Wang, Review of cellular mechanotransduction, J. Phys. D: Appl. Phys. 50 (2017) 233002. https://doi.org/10.1088/1361-6463/aa6e18.

[139] P.A. Janmey, D.A. Weitz, Dealing with mechanics: mechanisms of force transduction in cells, Trends in Biochemical Sciences. 29 (2004) 364–370. https://doi.org/10.1016/j.tibs.2004.05.003.

[140] D. Ingber, Mechanobiology and diseases of mechanotransduction, Annals of Medicine. 35 (2003) 564–577. https://doi.org/10.1080/07853890310016333.

[141] I.P. Uray, K. Uray, Mechanotransduction at the Plasma Membrane-Cytoskeleton Interface, Int J Mol Sci. 22 (2021) 11566. https://doi.org/10.3390/ijms222111566.

[142] F. Martino, A.R. Perestrelo, V. Vinarský, S. Pagliari, G. Forte, Cellular Mechanotransduction: From Tension to Function, Frontiers in Physiology. 9 (2018). https://www.frontiersin.org/article/10.3389/fphys.2018.00824 (accessed March 8, 2022).

[143] V. Swaminathan, M. Gloerich, Decoding mechanical cues by molecular mechanotransduction, Current Opinion in Cell Biology. 72 (2021) 72–80. https://doi.org/10.1016/j.ceb.2021.05.006.

[144] V. Kanoldt, L. Fischer, C. Grashoff, Unforgettable force - crosstalk and memory of mechanosensitive structures, Biol Chem. 400 (2019) 687–698. https://doi.org/10.1515/hsz-2018-0328.

[145] Y.A. Miroshnikova, M.M. Nava, S.A. Wickström, Emerging roles of mechanical forces in chromatin regulation, Journal of Cell Science. 130 (2017) 2243–2250. https://doi.org/10.1242/jcs.202192.

[146] T.P. Driscoll, B.D. Cosgrove, S.-J. Heo, Z.E. Shurden, R.L. Mauck, Cytoskeletal to Nuclear Strain Transfer Regulates YAP Signaling in Mesenchymal Stem Cells, Biophys J. 108 (2015) 2783–2793. https://doi.org/10.1016/j.bpj.2015.05.010.

[147] J.H. Van Berlo, J.W. Voncken, N. Kubben, J.L.V. Broers, R. Duisters, R.E.W. van Leeuwen, H.J.G.M. Crijns, F.C.S. Ramaekers, C.J. Hutchison, Y.M. Pinto, A-type lamins are essential for TGF-beta1 induced PP2A to dephosphorylate transcription factors, Hum Mol Genet. 14 (2005) 2839–2849. https://doi.org/10.1093/hmg/ddi316.

[148] L. Hernandez, K.J. Roux, E.S.M. Wong, L.C. Mounkes, R. Mutalif, R. Navasankari, B. Rai, S. Cool, J.-W. Jeong, H. Wang, H.-S. Lee, S. Kozlov, M. Grunert, T. Keeble, C.M. Jones, M.D. Meta, S.G. Young, I.O. Daar, B. Burke, A.O. Perantoni, C.L. Stewart, Functional coupling between the extracellular matrix and nuclear lamina by Wnt signaling in progeria, Dev Cell. 19 (2010) 413–425. https://doi.org/10.1016/j.devcel.2010.08.013.

[149] J. de la Rosa, J.M.P. Freije, R. Cabanillas, F.G. Osorio, M.F. Fraga, M.S. Fernández-García, R. Rad, V. Fanjul, A.P. Ugalde, Q. Liang, H.M. Prosser, A. Bradley, J. Cadiñanos, C. López-Otín, Prelamin A causes progeria through cell-extrinsic mechanisms and prevents cancer invasion, Nat Commun. 4 (2013) 2268. https://doi.org/10.1038/ncomms3268.

[150] I. Solovei, A.S. Wang, K. Thanisch, C.S. Schmidt, S. Krebs, M. Zwerger, T.V. Cohen, D. Devys, R. Foisner, L. Peichl, H. Herrmann, H. Blum, D. Engelkamp, C.L. Stewart, H. Leonhardt, B. Joffe, LBR and lamin A/C sequentially tether peripheral heterochromatin and inversely regulate differentiation, Cell. 152 (2013) 584–598. https://doi.org/10.1016/j.cell.2013.01.009.

[151] G.R. Fedorchak, A. Kaminski, J. Lammerding, Cellular mechanosensing: getting to the nucleus of it all, Prog Biophys Mol Biol. 115 (2014) 76–92. https://doi.org/10.1016/j.pbiomolbio.2014.06.009.

[152] T.J. Kirby, J. Lammerding, Emerging views of the nucleus as a cellular mechanosensor, Nat Cell Biol. 20 (2018) 373–381. https://doi.org/10.1038/s41556-018-0038-y.

[153] C.T. McKee, V.K. Raghunathan, P.F. Nealey, P. Russell, C.J. Murphy, Topographic modulation of the orientation and shape of cell nuclei and their influence on the measured elastic modulus of epithelial cells, Biophys J. 101 (2011) 2139–2146. https://doi.org/10.1016/j.bpj.2011.09.042.

[154] A. Elosegui-Artola, I. Andreu, A.E.M. Beedle, A. Lezamiz, M. Uroz, A.J. Kosmalska, R. Oria, J.Z. Kechagia, P. Rico-Lastres, A.-L.L. Roux, C.M. Shanahan, X. Trepat, D. Navajas, S. Garcia-Manyes, P. Roca-Cusachs, Force Triggers YAP Nuclear Entry by Regulating Transport across Nuclear Pores, Cell. 171 (2017) 1397-1410.e14. https://doi.org/10.1016/j.cell.2017.10.008.

[155] O. Gavet, J. Pines, Activation of cyclin B1-Cdk1 synchronizes events in the nucleus and the cytoplasm at mitosis, J Cell Biol. 189 (2010) 247–259. https://doi.org/10.1083/jcb.200909144.

[156] K. Hara, P. Tydeman, M. Kirschner, A cytoplasmic clock with the same period as the division cycle in Xenopus eggs, Proc Natl Acad Sci U S A. 77 (1980) 462–466. https://doi.org/10.1073/pnas.77.1.462.

[157] J.B. Chang, J.E. Ferrell, Mitotic trigger waves and the spatial coordination of the Xenopus cell cycle, Nature. 500 (2013) 603–607. https://doi.org/10.1038/nature12321.

[158] O. Afanzar, G.K. Buss, T. Stearns, J.E. Ferrell Jr, The nucleus serves as the pacemaker for the cell cycle, ELife. 9 (2020) e59989. https://doi.org/10.7554/eLife.59989.

[159] F.E. Nolet, A. Vandervelde, A. Vanderbeke, L. Piñeros, J.B. Chang, L. Gelens, Nuclei determine the spatial origin of mitotic waves, ELife. 9 (n.d.) e52868. https://doi.org/10.7554/eLife.52868.

[160] J. Aureille, V. Buffière-Ribot, B.E. Harvey, C. Boyault, L. Pernet, T. Andersen, G. Bacola, M. Balland, S. Fraboulet, L. Van Landeghem, C. Guilluy, Nuclear envelope deformation controls cell cycle progression in response to mechanical force, EMBO Rep. 20 (2019) e48084. https://doi.org/10.15252/embr.201948084.

[161] S. Huang, C.S. Chen, D.E. Ingber, Control of cyclin D1, p27(Kip1), and cell cycle progression in human capillary endothelial cells by cell shape and cytoskeletal tension, Mol Biol Cell. 9 (1998) 3179–3193. https://doi.org/10.1091/mbc.9.11.3179.

[162] M. Uroz, S. Wistorf, X. Serra-Picamal, V. Conte, M. Sales-Pardo, P. Roca-Cusachs, R. Guimerà, X. Trepat, Regulation of cell cycle progression by cell-cell and cell-matrix forces, Nat Cell Biol. 20 (2018) 646–654. https://doi.org/10.1038/s41556-018-0107-2.

[163] B. Vianay, F. Senger, S. Alamos, M. Anjur-Dietrich, E. Bearce, B. Cheeseman, L. Lee, M. Théry, Variation in traction forces during cell cycle progression, Biol Cell. 110 (2018) 91–96. https://doi.org/10.1111/boc.201800006.

[164] E. Vitiello, P. Moreau, V. Nunes, A. Mettouchi, H. Maiato, J.G. Ferreira, I. Wang, M. Balland, Acto-myosin force organization modulates centriole separation and PLK4

recruitment to ensure centriole fidelity, Nature Communications. 10 (2019) 52. https://doi.org/10.1038/s41467-018-07965-6.

[165] M. Dantas, A. Oliveira, P. Aguiar, H. Maiato, J.G. Ferreira, Mechanosensitive control of mitotic entry, (2021) 2021.09.23.461473. https://doi.org/10.1101/2021.09.23.461473.

[166] M. Maurer, J. Lammerding, The Driving Force: Nuclear Mechanotransduction in Cellular Function, Fate, and Disease, Annu Rev Biomed Eng. 21 (2019) 443–468. https://doi.org/10.1146/annurev-bioeng-060418-052139.

[167] M. Hieda, Signal Transduction across the Nuclear Envelope: Role of the LINC Complex in Bidirectional Signaling, Cells. 8 (2019). https://doi.org/10.3390/cells8020124.

[168] M.L. Lombardi, J. Lammerding, Keeping the LINC: the importance of nucleocytoskeletal coupling in intracellular force transmission and cellular function, Biochem Soc Trans. 39 (2011) 1729–1734. https://doi.org/10.1042/BST20110686.

[169] D.N. Simon, K.L. Wilson, The nucleoskeleton as a genome-associated dynamic "network of networks," Nature Reviews Molecular Cell Biology. 12 (2011) 695–708. https://doi.org/10.1038/nrm3207.

[170] P. Meinke, E.C. Schirmer, LINC'ing form and function at the nuclear envelope, FEBS Letters. 589 (2015) 2514–2521. https://doi.org/10.1016/j.febslet.2015.06.011.

[171] D.A. Starr, H.N. Fridolfsson, Interactions Between Nuclei and the Cytoskeleton Are Mediated by SUN-KASH Nuclear-Envelope Bridges, Annu Rev Cell Dev Biol. 26 (2010) 421–444. https://doi.org/10.1146/annurev-cellbio-100109-104037.

[172] M. Cai, Y. Huang, R. Ghirlando, K.L. Wilson, R. Craigie, G.M. Clore, Solution structure of the constant region of nuclear envelope protein LAP2 reveals two LEM-domain structures: one binds BAF and the other binds DNA, EMBO J. 20 (2001) 4399–4407. https://doi.org/10.1093/emboj/20.16.4399.

[173] S.M. Schreiner, P.K. Koo, Y. Zhao, S.G.J. Mochrie, M.C. King, The tethering of chromatin to the nuclear envelope supports nuclear mechanics, Nature Communications. 6 (2015) 7159. https://doi.org/10.1038/ncomms8159.

[174] R. Burla, M. La Torre, K. Maccaroni, F. Verni, S. Giunta, I. Saggio, Interplay of the nuclear envelope with chromatin in physiology and pathology, Nucleus. 11 (n.d.) 205–218. https://doi.org/10.1080/19491034.2020.1806661.

[175] R. Czapiewski, M.I. Robson, E.C. Schirmer, Anchoring a Leviathan: How the Nuclear Membrane Tethers the Genome, Front Genet. 7 (2016) 82. https://doi.org/10.3389/fgene.2016.00082.

[176] T. Shimi, K. Pfleghaar, S. Kojima, C.-G. Pack, I. Solovei, A.E. Goldman, S.A. Adam, D.K. Shumaker, M. Kinjo, T. Cremer, R.D. Goldman, The A- and B-type nuclear lamin

networks: microdomains involved in chromatin organization and transcription, Genes Dev. 22 (2008) 3409–3421. https://doi.org/10.1101/gad.1735208.

[177] X. Zheng, J. Hu, S. Yue, L. Kristiani, M. Kim, M. Sauria, J. Taylor, Y. Kim, Y. Zheng, Lamins Organize the Global Three-Dimensional Genome from the Nuclear Periphery, Mol Cell. 71 (2018) 802-815.e7. https://doi.org/10.1016/j.molcel.2018.05.017.

[178] X. Zheng, Y. Kim, Y. Zheng, Identification of lamin B–regulated chromatin regions based on chromatin landscapes, MBoC. 26 (2015) 2685–2697. https://doi.org/10.1091/mbc.E15-04-0210.

[179] K.E. Knockenhauer, T.U. Schwartz, The Nuclear Pore Complex as a Flexible and Dynamic Gate, Cell. 164 (2016) 1162–1171. https://doi.org/10.1016/j.cell.2016.01.034.

[180] J. Schmitt, R. Benavente, D. Hodzic, C. Höög, C.L. Stewart, M. Alsheimer, Transmembrane protein Sun2 is involved in tethering mammalian meiotic telomeres to the nuclear envelope, Proc Natl Acad Sci U S A. 104 (2007) 7426–7431. https://doi.org/10.1073/pnas.0609198104.

[181] X. Ding, R. Xu, J. Yu, T. Xu, Y. Zhuang, M. Han, SUN1 is required for telomere attachment to nuclear envelope and gametogenesis in mice, Dev Cell. 12 (2007) 863–872. https://doi.org/10.1016/j.devcel.2007.03.018.

[182] J. Amrichová, E. Lukásová, S. Kozubek, M. Kozubek, Nuclear and territorial topography of chromosome telomeres in human lymphocytes, Exp Cell Res. 289 (2003) 11–26. https://doi.org/10.1016/s0014-4827(03)00208-8.

[183] B.J. Vermolen, Y. Garini, S. Mai, V. Mougey, T. Fest, T.C.-Y. Chuang, A.Y.-C. Chuang, L. Wark, I.T. Young, Characterizing the three-dimensional organization of telomeres, Cytometry A. 67 (2005) 144–150. https://doi.org/10.1002/cyto.a.20159.

[184] L. Crabbe, A.J. Cesare, J.M. Kasuboski, J.A.J. Fitzpatrick, J. Karlseder, Human telomeres are tethered to the nuclear envelope during post-mitotic nuclear assembly, Cell Rep. 2 (2012) 1521–1529. https://doi.org/10.1016/j.celrep.2012.11.019.

[185] T. Jegou, I. Chung, G. Heuvelman, M. Wachsmuth, S.M. Görisch, K.M. Greulich-Bode, P. Boukamp, P. Lichter, K. Rippe, Dynamics of telomeres and promyelocytic leukemia nuclear bodies in a telomerase-negative human cell line, Mol Biol Cell. 20 (2009) 2070–2082. https://doi.org/10.1091/mbc.e08-02-0108.

[186] H.N. Fridolfsson, N. Ly, M. Meyerzon, D.A. Starr, UNC-83 coordinates kinesin-1 and dynein activities at the nuclear envelope during nuclear migration, Dev Biol. 338 (2010) 237–250. https://doi.org/10.1016/j.ydbio.2009.12.004.

[187] J. Yu, K. Lei, M. Zhou, C.M. Craft, G. Xu, T. Xu, Y. Zhuang, R. Xu, M. Han, KASH protein Syne-2/Nesprin-2 and SUN proteins SUN1/2 mediate nuclear migration

during mammalian retinal development, Hum Mol Genet. 20 (2011) 1061–1073. https://doi.org/10.1093/hmg/ddq549.

[188] I. Samejima, C. Spanos, K. Samejima, J. Rappsilber, G. Kustatscher, W.C. Earnshaw, Mapping the invisible chromatin transactions of prophase chromosome remodeling, Molecular Cell. 82 (2022) 696-708.e4. https://doi.org/10.1016/j.molcel.2021.12.039.

[189] Q. Liu, N. Pante, T. Misteli, M. Elsagga, M. Crisp, D. Hodzic, B. Burke, K.J. Roux, Functional association of Sun1 with nuclear pore complexes, J Cell Biol. 178 (2007) 785–798. https://doi.org/10.1083/jcb.200704108.

[190] C.E. Zimmerli, M. Allegretti, V. Rantos, S.K. Goetz, A. Obarska-Kosinska, I. Zagoriy, A. Halavatyi, G. Hummer, J. Mahamid, J. Kosinski, M. Beck, Nuclear pores dilate and constrict in cellulo, Science. 374 (n.d.) eabd9776. https://doi.org/10.1126/science.abd9776.

[191] B. Enyedi, P. Niethammer, Nuclear membrane stretch and its role in mechanotransduction, Nucleus. 8 (2017) 156–161. https://doi.org/10.1080/19491034.2016.1263411.

[192] I. Liashkovich, A. Meyring, A. Kramer, V. Shahin, Exceptional structural and mechanical flexibility of the nuclear pore complex, J Cell Physiol. 226 (2011) 675–682. https://doi.org/10.1002/jcp.22382.

[193] K. Damodaran, S. Venkatachalapathy, F. Alisafaei, A.V. Radhakrishnan, D. Sharma Jokhun, V.B. Shenoy, G.V. Shivashankar, Compressive force induces reversible chromatin condensation and cell geometry–dependent transcriptional response, MBoC. 29 (2018) 3039–3051. https://doi.org/10.1091/mbc.E18-04-0256.

[194] M.N. Conrad, C.-Y. Lee, G. Chao, M. Shinohara, H. Kosaka, A. Shinohara, J.-A. Conchello, M.E. Dresser, Rapid telomere movement in meiotic prophase is promoted by NDJ1, MPS3, and CSM4 and is modulated by recombination, Cell. 133 (2008) 1175–1187. https://doi.org/10.1016/j.cell.2008.04.047.

[195] H.F. Horn, D.I. Kim, G.D. Wright, E.S.M. Wong, C.L. Stewart, B. Burke, K.J. Roux, A mammalian KASH domain protein coupling meiotic chromosomes to the cytoskeleton, J Cell Biol. 202 (2013) 1023–1039. https://doi.org/10.1083/jcb.201304004.

[196] J.M. Bupp, A.E. Martin, E.S. Stensrud, S.L. Jaspersen, Telomere anchoring at the nuclear periphery requires the budding yeast Sad1-UNC-84 domain protein Mps3, J Cell Biol. 179 (2007) 845–854. https://doi.org/10.1083/jcb.200706040.

[197] A. Penkner, L. Tang, M. Novatchkova, M. Ladurner, A. Fridkin, Y. Gruenbaum, D. Schweizer, J. Loidl, V. Jantsch, The nuclear envelope protein Matefin/SUN-1 is

required for homologous pairing in C. elegans meiosis, Dev Cell. 12 (2007) 873–885. https://doi.org/10.1016/j.devcel.2007.05.004.

[198] Y. Hiraoka, A.F. Dernburg, The SUN rises on meiotic chromosome dynamics, Dev Cell. 17 (2009) 598–605. https://doi.org/10.1016/j.devcel.2009.10.014.

[199] D. Zickler, N. Kleckner, Recombination, Pairing, and Synapsis of Homologs during Meiosis, Cold Spring Harb Perspect Biol. 7 (2015) a016626. https://doi.org/10.1101/cshperspect.a016626.

[200] A. Sato, B. Isaac, C.M. Phillips, R. Rillo, P.M. Carlton, D.J. Wynne, R.A. Kasad, A.F. Dernburg, Cytoskeletal forces span the nuclear envelope to coordinate meiotic chromosome pairing and synapsis, Cell. 139 (2009) 907–919. https://doi.org/10.1016/j.cell.2009.10.039.

[201] L. Harper, I. Golubovskaya, W.Z. Cande, A bouquet of chromosomes, J Cell Sci. 117 (2004) 4025–4032. https://doi.org/10.1242/jcs.01363.

[202] D. Salina, K. Bodoor, D.M. Eckley, T.A. Schroer, J.B. Rattner, B. Burke, Cytoplasmic Dynein as a Facilitator of Nuclear Envelope Breakdown, Cell. 108 (2002) 97–107. https://doi.org/10.1016/S0092-8674(01)00628-6.

[203] A.D. Baffet, D.J. Hu, R.B. Vallee, Cdk1 Activates Pre-mitotic Nuclear Envelope Dynein Recruitment and Apical Nuclear Migration in Neural Stem Cells, Dev Cell. 33 (2015) 703–716. https://doi.org/10.1016/j.devcel.2015.04.022.

[204] E.A. Booth, S.T. Spagnol, T.A. Alcoser, K.N. Dahl, Nuclear stiffening and chromatin softening with progerin expression leads to an attenuated nuclear response to force, Soft Matter. 11 (2015) 6412–6418. https://doi.org/10.1039/c5sm00521c.

[205] K.L. Reddy, A.P. Feinberg, Higher order chromatin organization in cancer, Semin Cancer Biol. 23 (2013) 109–115. https://doi.org/10.1016/j.semcancer.2012.12.001.

[206] V. Butin-Israeli, S.A. Adam, A.E. Goldman, R.D. Goldman, Nuclear lamin functions and disease, Trends Genet. 28 (2012) 464–471. https://doi.org/10.1016/j.tig.2012.06.001.

[207] M. Zwerger, C.Y. Ho, J. Lammerding, Nuclear mechanics in disease, Annu Rev Biomed Eng. 13 (2011) 397–428. https://doi.org/10.1146/annurev-bioeng-071910-124736.

[208] K.-H. Chow, R.E. Factor, K.S. Ullman, The nuclear envelope environment and its cancer connections, Nat Rev Cancer. 12 (2012) 196–209. https://doi.org/10.1038/nrc3219.

[209] J.I. de Las Heras, D.G. Batrakou, E.C. Schirmer, Cancer biology and the nuclear envelope: a convoluted relationship, Semin Cancer Biol. 23 (2013) 125–137. https://doi.org/10.1016/j.semcancer.2012.01.008.

ANNEX A

High-Resolution Analysis of Centrosome Behavior During Mitosis

The content of this chapter is published in the following original research paper:

V. Nunes, M. Dantas, J.T. Lima, J.G. Ferreira, High-Resolution Analysis of Centrosomes Behavior During Mitosis, in: A.S. Coutts, L. Weston (Eds.), Cell Cycle Oscil. Methods Protoc., Springer US, New York, NY, 2021: pp. 179–194. https://doi.org/10.1007/978-1-0716-1538-6_13.

This is an original research paper and it is presented for the first time in a thesis.



Chapter 13

High-Resolution Analysis of Centrosome Behavior During Mitosis

Vanessa Nunes, Margarida Dantas, Joana T. Lima, and Jorge G. Ferreira

Abstract

Cell division requires a dynamic reorganization of cytoskeletal and nuclear components. One essential step is the separation of centrosomes, which allows the assembly of a microtubule-based mitotic spindle. This has to be spatially and temporally coordinated with other events such as adhesion complex disengagement, assembly of an actin-rich cell cortex and nuclear envelope breakdown (NEB), to ensure chromosome segregation fidelity. Previous methodologies often focused on a single event and failed to provide an integrated view of the process. In this chapter, we describe a method to study mitosis with high resolution, by analyzing the dynamic interplay between centrosomes, nucleus, and cell membrane, using a combination of live-cell imaging and micromanipulation with custom-designed computational tools.

Key words Centrosome, Mitosis, Automated tracking, Nucleus, Cell membrane

1 Introduction

Mitosis is the process by which cells segregate duplicated chromosomes between two daughter cells. Chromosome segregation is accomplished through a chain of highly regulated events, which include extensive reorganization of the cytoskeleton and cell nucleus [1, 2]. Many of these changes take place during the first stage of mitosis, termed "prophase." During this stage, cells lose adhesion [3–5], and their volume changes [6–8] to allow the assembly of a microtubule-based mitotic spindle [9–12]. At the same time, within the nucleus chromosomes condense [13, 14] and the nuclear lamina disassembles [15, 16]. How these events are coordinated to ensure efficient chromosome segregation remains unclear.

In animal cells, the duplicated centrosomes migrate in opposite directions along the nuclear envelope (NE), to originate the two spindle poles [17]. The molecular players involved in centrosome separation and positioning have been previously identified and include microtubules and microtubule-associated motors, such as

Amanda S. Coutts and Louise Weston (eds.), *Cell Cycle Oscillators: Methods and Protocols*, Methods in Molecular Biology, vol. 2329, https://doi.org/10.1007/978-1-0716-1538-6_13, © Springer Science+Business Media, LLC, part of Springer Nature 2021

Eg5 and dynein [12, 18–20], but also myosin II [21], actin [22] and Arp2/3 [12]. However, a comprehensive understanding of how these molecular factors cross talk in space and time to regulate centrosome behavior during prophase is absent.

The study of highly dynamic events such as cell division has greatly benefited from live-cell imaging techniques, because they allow us to probe the spatiotemporal characteristics of the process [23]. This has been facilitated by the development of new microscopy techniques [24] and improved fluorescent probes [25], which are less phototoxic to cells [26, 27]. Importantly, live-cell imaging can be used in combination with microfabrication techniques that aim to recapitulate or mimic the complexity of the cellular microenvironment [28–30], or with cell confinement systems, that allow us to physically constrain the height and the stiffness applied onto cells [31, 32]. Used separately or in combination, these methods have provided a more realistic picture of the process of mitosis [12, 29, 33].

The ability to extract quantitative data from live-cell imaging datasets using image analysis software, has allowed the detailed characterization of key events that take place during mitosis [12, 34, 35]. In particular, analysis of centrosome motion has been extensively studied using both commercial and custom-designed tools [36–38]. However, current approaches fail to analyze the changes that occur at the cell membrane, nucleus and cytoskeleton in an integrated manner.

In this chapter, we describe a methodology established in our laboratory to study centrosome, nucleus and cell membrane behavior during mitosis in human cells, using state-of-the-art, live-cell microscopy in combination with cell micropatterning and/or cell confinement techniques and posterior bio-image reconstruction and analysis. Using a custom-designed computation tool [39], we are able to precisely measure and correlate the dynamic changes that occur during mitosis.

2 Materials

Prepare, use, store, and dispose all the reagents according to the Material Safety Data Sheet (MSDS) guidelines. All the mediums and buffers used in the cell culture procedures should be pre-warmed, unless otherwise stated.

2.1 Cell Lines and Culture Conditions

Unless otherwise noted, all human cell lines are cultured in complete medium and grown in a 37 °C humidified incubator with 5% CO_2 (*see* **Notes 1–3**).

1. Human cell lines of interest.
2. Disposable 25 and 75 cm^2 tissue culture flasks and 6-well plates.
3. Complete medium: Dulbecco's Modified Eagle Medium supplemented with 10% heat-inactivated fetal bovine serum (FBS).
4. Trypsin: Trypsin-EDTA solution 0.25%. Can be prepared by adding 2.5 g porcine trypsin and 0.2 g EDTA.4Na to 1 L of Hanks' Balanced Salt Solution.
5. Sterile phosphate-buffered solution (PBS), pH 7.4.
6. Disposable sterile pipettes (1, 5, and 10 mL).
7. Disposable conical tubes (15 and 50 mL).

2.2 Transient Plasmid DNA and Small Interfering RNAs (siRNAs) Transfections

1. Complete medium.
2. Reduced serum medium: DMEM supplemented with 5% FBS.
3. Opti-MEM.
4. Lipofectamine 2000.
5. Lipofectamine RNAiMAX.
6. Plasmid DNA of interest or siRNA oligos.
7. Solution A:
   (a) For DNA: Dilute 5 µL of Lipofectamine 2000 in 250 µL of Opti-MEM.
   (b) For siRNAs: Dilute 5 µL of Lipofectamine RNAiMAX in 250 µL of Opti-MEM.
8. Solution B:
   (a) For DNA: Dilute 1 ng/mL of the plasmid DNA of interest in 250 µL of Opti-MEM.
   (b) For siRNAs: Dilute 2 µL of the siRNA of interest (Stock Concentration = 20 mM; Final Concentration = 20 nM) in 250 µL of Opti-MEM.
9. Selection antibiotics, depending on the plasmid to be used (e.g., for HeLa cells, G418 at 200–400 µg/mL, puromycin at 1–2 µg/mL).

2.3 Micropatterning on Glass Coverslip with Deep UV Light

1. Deep UV lamp (185 nm wavelength; Novascan).
2. Synthetic quartz mask (Delta Mask B.V.).
3. Plasma cleaner (Zepto Plasma System, Diener Electronic).
4. Glass coverslips: 22 × 22 mm No. 1.5.
5. Milli-Q water.
6. 10 mM Hepes, pH 7.4: Dilute 238.30 g of Hepes (MW = 238.30) in 1 L of ddH_2O to make a 1 M stock. To adjust the pH, use HCl 37% or 0.1 M NaOH inside a flow hood. Filter-sterilize or autoclave the buffer. Dilute 5 mL of stock solution in 500 mL of dH_2O for 10 mM solution.

7. PLL-g-PEG: 0.1 mg/mL PLL(20)-g[3.5]-PEG(2) (SuSoS) in 10 mM Hepes pH 7.4. Dissolve PLL-g-PEG powder in 10 mM Hepes pH 7.4 to obtain a stock solution of 1 mg/mL. Before usage, dilute the stock solution in 10 mM Hepes pH 7.4 to obtain the working concentration of 0.1 mg/mL.
8. 100 mM $NaHCO_3$, pH 8.6: Dilute 84 mg of $NaHCO_3$ in 10 mL ddH_2O. To adjust the pH, use HCl 37% or 0.1 M NaOH, inside a flow hood.
9. Fibronectin (FBN) solution: 25 μg/mL, diluted in 100 mM NaHCO3 (pH 8.6).
10. Alexa546 or 647-conjugated fibrinogen: 5 μg/mL, diluted in 100 mM NaHCO3 (pH 8.6).
11. Air gun.
12. Isopropanol.
13. Stainless steel forceps, 0.4 mm with angled tip.
14. PTFE forceps, 145 mm with pointed ends.

2.4 Cell Confinement

1. Microfluidic pressure pump and generator (AF1 Dual, ElveFlow).
2. PDMS cell confiner [custom-designed as described in [32] or obtained from 4Dcell]. The size of the PDMS confiner device will depend on the size of the imaging chamber.
3. Cell confinement slides (custom-designed or obtained from 4Dcell). To prepare custom-designed confinement slides, use round cover glass, 10 mm, 0.17 mm thickness, coated with PDMS micropillars according to [32].
4. FluoroDishes 35 mm well, glass-bottom 0.17 mm thickness (World Precision Instruments).
5. Plasma cleaner (Zepto, Diener Electronics).
6. FBN solution.
7. Stainless steel forceps, 0.4 mm with angled tip.

2.5 Live-Cell Imaging

1. Spinning disk microscope.
2. Magnetic imaging chamber (Live Cell Instrument).
3. 6-well plates.
4. FluoroDishes 35 mm well, glass-bottom 0.17 mm thickness (World Precision Instruments).
5. Glass coverslips: 22 × 22 mm No. 1.5.
6. Complete medium.
7. Imaging medium: Leibovitz's L-15 medium supplemented with 10% FBS.
8. Antibiotics (e.g., penicillin–streptomycin solution, antibiotic–antimycotic solution).

2.6 Analysis and Data Extraction from Live-Cell Imaging Datasets

1. Live-Cell Imaging datasets.
2. Bio-image analysis software.
   (a) ImageJ/Fiji.
   (b) MATLAB 2018 or newer version.
   (c) Tracking and reconstruction tools (e.g., Trackosome: available at https://github.com/Trackosome).

3 Methods

3.1 Transient Plasmid DNA and Small Interfering RNAs (siRNAs) Transfections

Day 0

1. Seed the human cell line of interest in a 6-well plate well with 2 mL of complete medium (*see* **Note 4**).
2. Grow cells in a 37 °C humidified incubator with 5% CO_2, until they are 50–75% confluent.

Day 1

3. Rinse the cells with sterile phosphate-buffered solution (PBS) and replace the cell culture medium with 1.5 mL of reduced serum medium.
4. Incubate cells in a 37 °C humidified incubator with 5% CO_2.
5. For cell transfection, prepare solutions A and B (*see* **Notes 5** and **6**).
6. Incubate solutions A and B separately for 5 min at room temperature (RT).
7. Mix solutions A and B and incubate for 30 min at RT.
8. Add the oligo-lipid complexes to the cells, dropwise.
9. Incubate the cells for 5–6 h in a 37 °C humidified incubator with 5% CO_2.
10. Replace the culture medium with 2 mL of complete medium.
11. Grow cells in a 37 °C humidified incubator with 5% CO_2 for 24, 48, or 72 h (*see* **Note 7**).
12. Analyse cells (*see* **Note 8**).

3.2 Micropatterning on Glass Coverslip with Deep UV Light

3.2.1 Coating of Glass Coverslips with PLL-g-PEG

1. Activate glass coverslips with air plasma for 2 min (Fig. 1a1).
2. Incubate the activated side of the coverslip in 50–200 µL of PLL-g-PEG for 30 min-1 h at RT (*see* **Note 9**) (Fig. 1a2).
3. Rinse the coverslips with dH_2O, dry and store them at RT (*see* **Note 10**).

3.2.2 UV Illumination of PLL-g-PEG-coated Glass Coverslips Using a Quartz Photomask

1. Wash the quartz mask with isopropanol and air-dry it if necessary (*see* **Notes 11** and **12**).
2. Illuminate the brown side of the quartz mask with the UV lamp for 5 min (*see* **Note 13**) (Fig. 1a3).

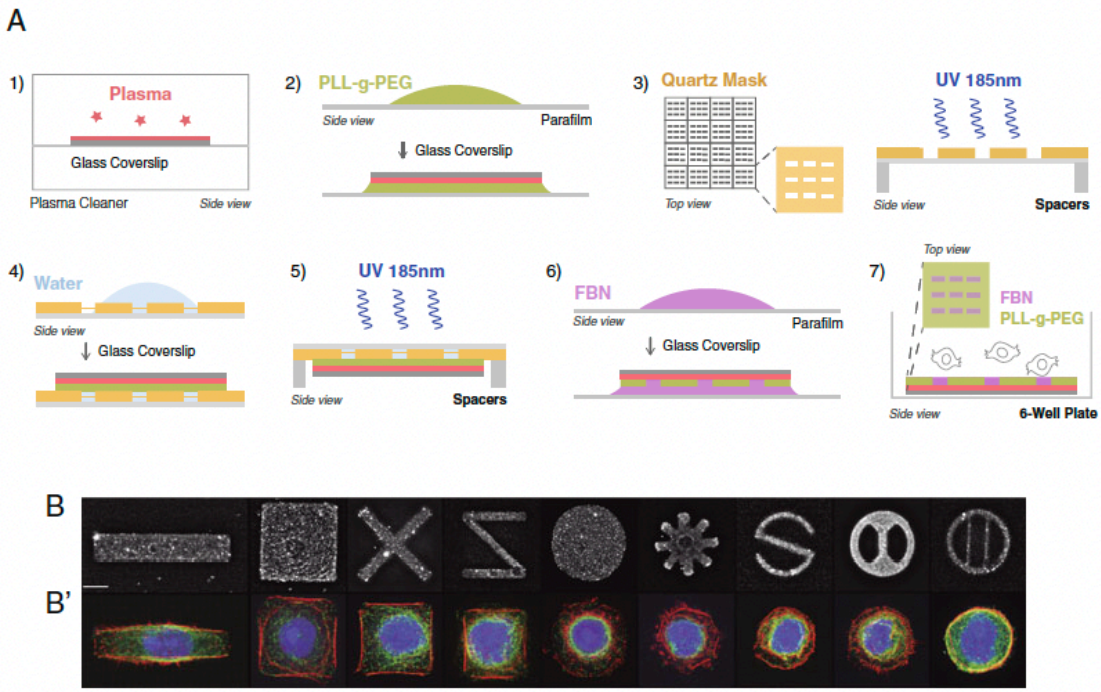


Fig. 1 (**a**) Diagram depicting the deep-UV based method for micropattern generation on glass coverslips [28]. Glass coverslip is activated with plasma (1) and incubated with PLL-g-PEG (2). The pegylated side of the coverslip is sealed onto the previously activated (3) brown side of the quartz mask using Milli-Q water (4). To degrade the PLL-g-PEG coating with the desired micropatterns, the silver side of the quartz mask with the coverslip attached is irradiated with deep UV at a wavelength of 185 nm (5). Finally, the coverslip is incubated with an extracellular matrix component such as fibronectin (FBN; 6) and cells can be seeded (7). (**b**) Representative immunofluorescence images of FBN micropatterns of different geometries labeled with fibrinogen-Alexa 594. (**b′**) Representative immunofluorescence images of HeLa cells labeled with DAPI, SiR Actin, and alpha-tubulin seeded on the micropatterns. Scale bar is 10 m

3. Seal the pegylated side of the coverslip onto the brown side of the quartz mask using 2–3 µL of Milli-Q water (*see* **Notes 9** and **14**) (Fig. 1a4).
4. Illuminate the silver side of the quartz mask with the UV lamp for 5 min (*see* **Notes 13** and **15**) (Fig. 1a5).
5. To detach the coverslips from the quartz mask, pour 2 to 5 mL of dH_2O onto the coverslips and incubate for 2–3 min.
6. Collect the coverslips and stored them at RT after drying (*see* **Note 16**).

3.2.3 Seeding Cells on FBN-Patterned Glass Coverslips

1. Incubate the patterned face of the coverslip with 50–200 µL of FBN solution and Alexa-conjugated fibrinogen for 1 h, at RT (*see* **Notes 9**, **17**, and **18**) (Fig. 1a6).
2. Rinse the coverslips with PBS (*see* **Notes 19** and **20**).
3. Harvest human cell line of interest by washing with PBS and incubating with the Trypsin solution for 2 min. Trypsin volume

will vary according to the surface area (e.g., for a 25mm^2 flask, use 2 mL of Trypsin and for a 6-well plate well, use 1 mL of Trypsin).

4. Seed 50,000–200,000 cells in the FBN-patterned coverslips with 2 mL of complete medium supplemented with antibiotics (*see* **Note 21** and **22**) (Fig. 1a7).
5. Incubate the cells in a 37 °C humidified incubator with 5% CO_2 for 1–2 h (*see* **Note 22**).
6. Gently wash the unattached cells with complete medium.
7. Grow cells in a 37 °C humidified incubator with 5% CO_2 for 12–24 h.
8. Image cells on the microscope (*see* Subheading 3.4).

3.3 Cell Confinement

3.3.1 Cell Seeding for Confinement

1. Activate the FluoroDishes with air plasma for 2 min.
2. Coat the activated FluoroDishes with FBN solution for 30 min to 1 h, at RT.
3. Rinse FluoroDishes three times with dH_2O.
4. Seed cells in the coated FluoroDishes with 2 mL complete medium supplemented with antibiotics. Number of cells to be seeded will depend on the cell type used (*see* **Note 21**).
5. Incubate the cells overnight at 37 °C in a 5% CO_2 humidified incubator.

3.3.2 Using the Dynamic Cell Confiner

1. Replace the cell culture medium with 500 μL of imaging medium supplemented with antibiotics (*see* **Note 23**).
2. Add the confinement slide to the PDMS piston in the confiner cell (Fig. 2a). Assemble the dynamic confiner setup by connecting the PDMS pillar to the pressure/vacuum generator (*see* **Note 24**).
3. Gently place the PDMS pillar on top of the FluoroDishes with the cells. Gently press it down to ensure that the PDMS confiner is attached to the bottom and turn on the vacuum generator.
4. Lower the confinement slide onto the cells by generating a vacuum (Fig. 2b).
5. Proceed with live-cell image acquisition. Confinement can be modulated by increasing or decreasing the pressure on the vacuum line.

3.4 Live-Cell Imaging

Day 0

1. 12–24 h prior to each experiment, seed 50,000–200,000 cells (depending on cell type; *see* **Note 21**) in FBN-patterned coverslips with 2 mL of complete medium supplemented with antibiotics (*see* **Note 1**).

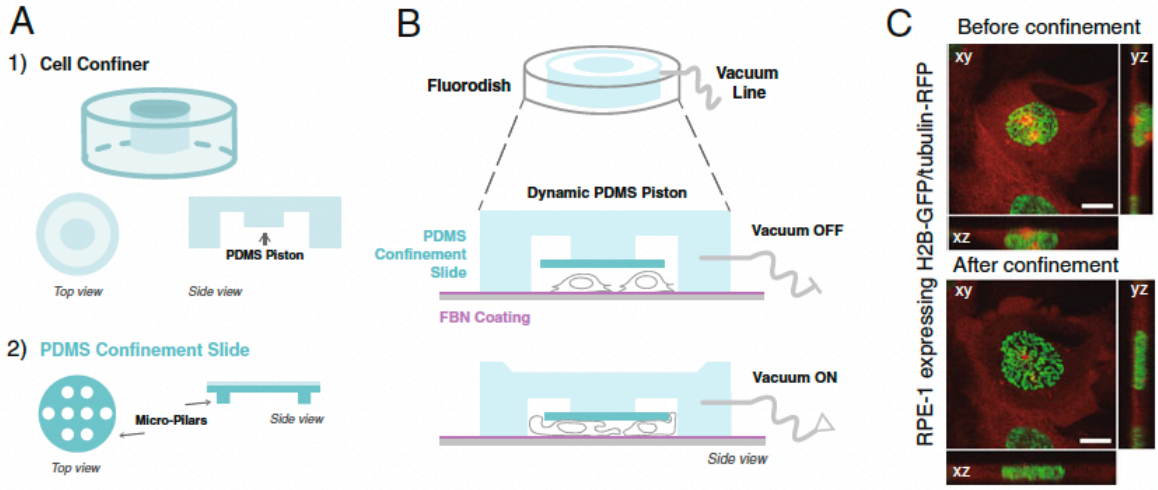


Fig. 2 (**a**) Graphic representation of cell confiner (1) and PDMS confinement slides (2). (**b**) Diagram of the experimental setup used to dynamically confine the cells during time-lapse acquisition. A vacuum line is attached to the PDMS confiner, allowing temporal control of pressure. (**c**) Representative images of an RPE-1 cell expressing H2B-GFP/tubulin-RFP before (top panel) and after (bottom panel) confinement. Scale bar, 10 m

Day 1

2. Approximately 30 min to 2 h prior to each experiment, assemble the magnetic imaging chamber and replace the cell culture medium with 1–2 mL of imaging medium supplemented with antibiotics. Add SiR-dyes or drugs of interest (acute pharmacological inhibition) to the cell culture medium at this time point (*see* **Notes 1** and **25**).
3. Turn ON all the imaging equipment and set the appropriate temperature and CO_2 levels (37 °C and 5% CO_2) for the microscope chamber (*see* **Note 26**).
4. Set up your experimental conditions, namely the appropriate illumination wavelengths, laser power intensities, exposure times, and time-lapse conditions (*see* **Notes 27** and **28**).
5. If using a confinement setup, additional adjustments to your imaging setup are required at this stage. Refer to **step 2**.
6. Start imaging. Representative frames from a movie of a human U2-OS cell expressing H2B-GFP/tubulin-RFP, seeded on a line micropattern can be seen in Fig. 3a, b.

3.5 Analysis and Data Extraction from Live-Cell Imaging Datasets

Bio-image analysis and data extraction can be performed with our custom-designed tool [39]. For the purpose of this chapter, we will focus on the use of the Centrosome Dynamics and Compile Data modules.

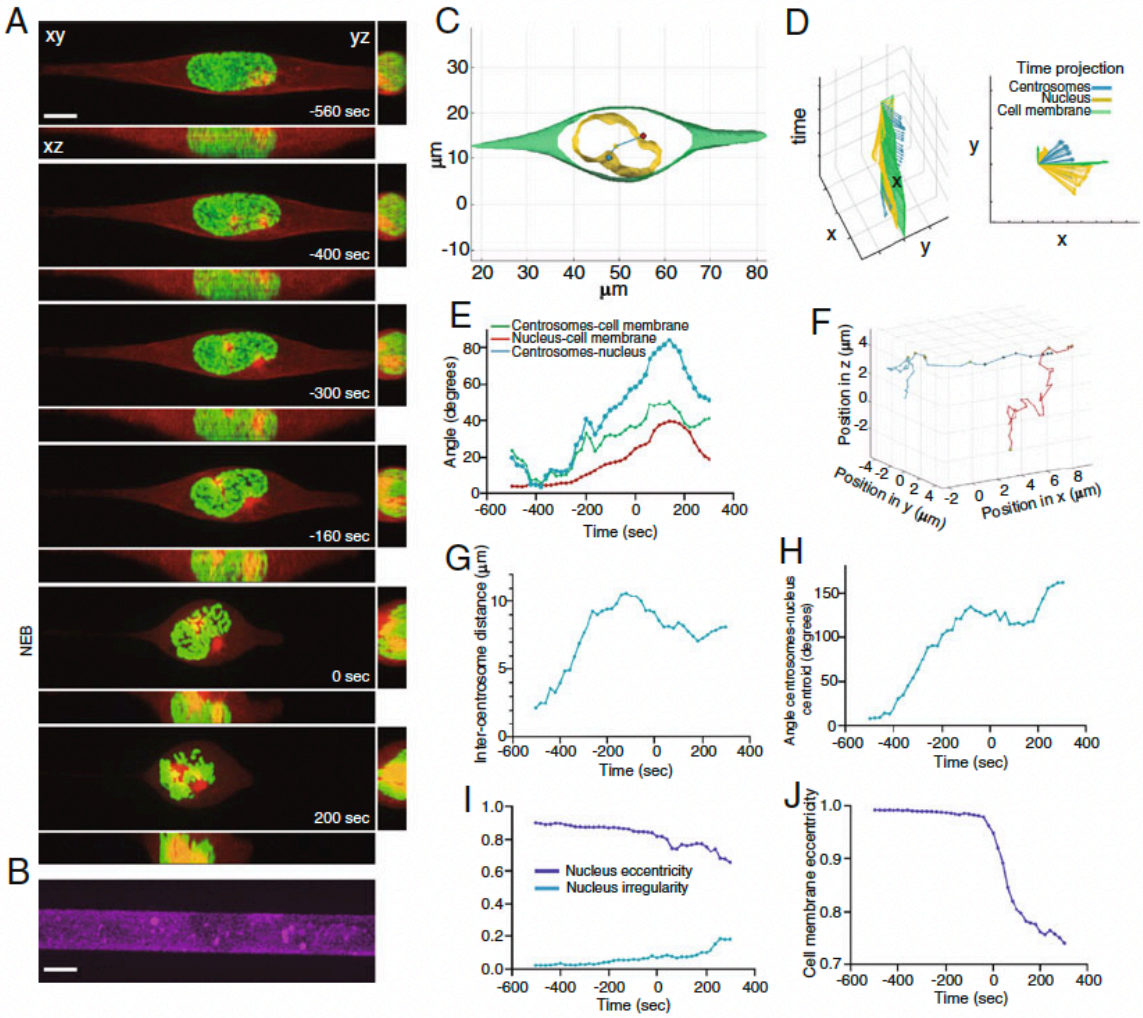


Fig. 3 Detailed spatiotemporal analysis of spindle assembly. (**a**) Human U2-OS cell expressing H2B-GFP and tubulin-RFP seeded on a line micropattern during mitotic entry. Time-lapse is 20 s. Time is in seconds. Time zero corresponds to NEB. Scale bar, 10 m. (**b**) Micropatterned surface (10 m line) coated with fibronectin and fluorescently labeled fibrinogen (647 nm) corresponding to the cell represented in (**a**). (**c**) 3D reconstruction of the U2-OS cell in (**a**), showing cell membrane (green), nucleus (yellow), and the two centrosomes (blue and red dots). The vector connecting both centrosomes is shown as a blue line. (**d**) Reconstruction and correlation between centrosomes vector (blue arrows), long cellular axis (large green arrows), and long nuclear axis (large yellow arrows). Each set of arrows corresponds to a time-point extracted from a live-cell imaging movie, using our software. Right panel shows a temporal projection of left panel. (**e**) Correlation of the angles between nucleus and cell membrane (red), centrosomes and cell membrane (green), and centrosomes and nucleus (blue) over time. (**f**) Reconstruction of centrosomes trajectories in 4D. Each point corresponds to a time-point extracted from a live-cell imaging movie. (**g**) Intercentrosome distances over time. (**h**) Angle between the two centrosome and the nucleus centroid over time. (**i**) Nuclear eccentricity and irregularity over time. (**j**) Cell membrane eccentricity over time

3.5.1 Single-Cell Analysis

1. Open 4D dataset files (e.g., *.nd2, *.tiff) using ImageJ/Fiji software.
2. Split channels (Image→Color→Split Channels) (*see* **Note 29**).
3. Adjust image brightness and contrast (Image→Adjust→Brightness/Contrast→Reset).
4. Convert image to 8-bit (Image - > Type - > 8-bit).
5. Save each channel as a *.tiff file (e.g., Centrosomes.tiff, Nucleus.tiff, and Membrane.tiff).
6. Install the analysis tool in the MATLAB working directory.
7. Open MATLAB and run the command "GUI_Main_Menu".
8. Select "Load Data."
9. Load "Centrosomes Projection" (e.g., Centrosomes.tiff).
10. Set parameters (e.g., define the pixel and z-step sizes) (*see* **Note 30**).
11. Repeat procedure to load additional files containing the nucleus labeling and cell membrane labeling using "Nuclear Membrane Projection" and "Cell Membrane Projection," respectively.
12. Select "Crop," adjust window size on the "Centrosome Projection" image and click "Save."
13. Select "Next."
14. Select the frames of interest and click "Ok."
15. Manually locate both centrosomes in the projection and click "Confirm."
16. Select Filter and then "Next."
17. Select "Run" (*see* **Note 31**).
18. Click "Results" (Fig. 3c–j).
19. Save results and figures (*see* **Note 32**).
20. The same procedure can be applied to cells seeded on regular dishes (i.e., without any surface modification) or subjected to micromanipulation or confinement (Fig. 4).

3.5.2 Compile Results

1. Open MATLAB and run the command "GUI_Compile_Data".
2. Select "Import Files."
3. Define saving settings at "Save as."
4. Select "Compile & Export" (*see* **Note 33**).
5. Results are exported in *.xls and *.csv format.

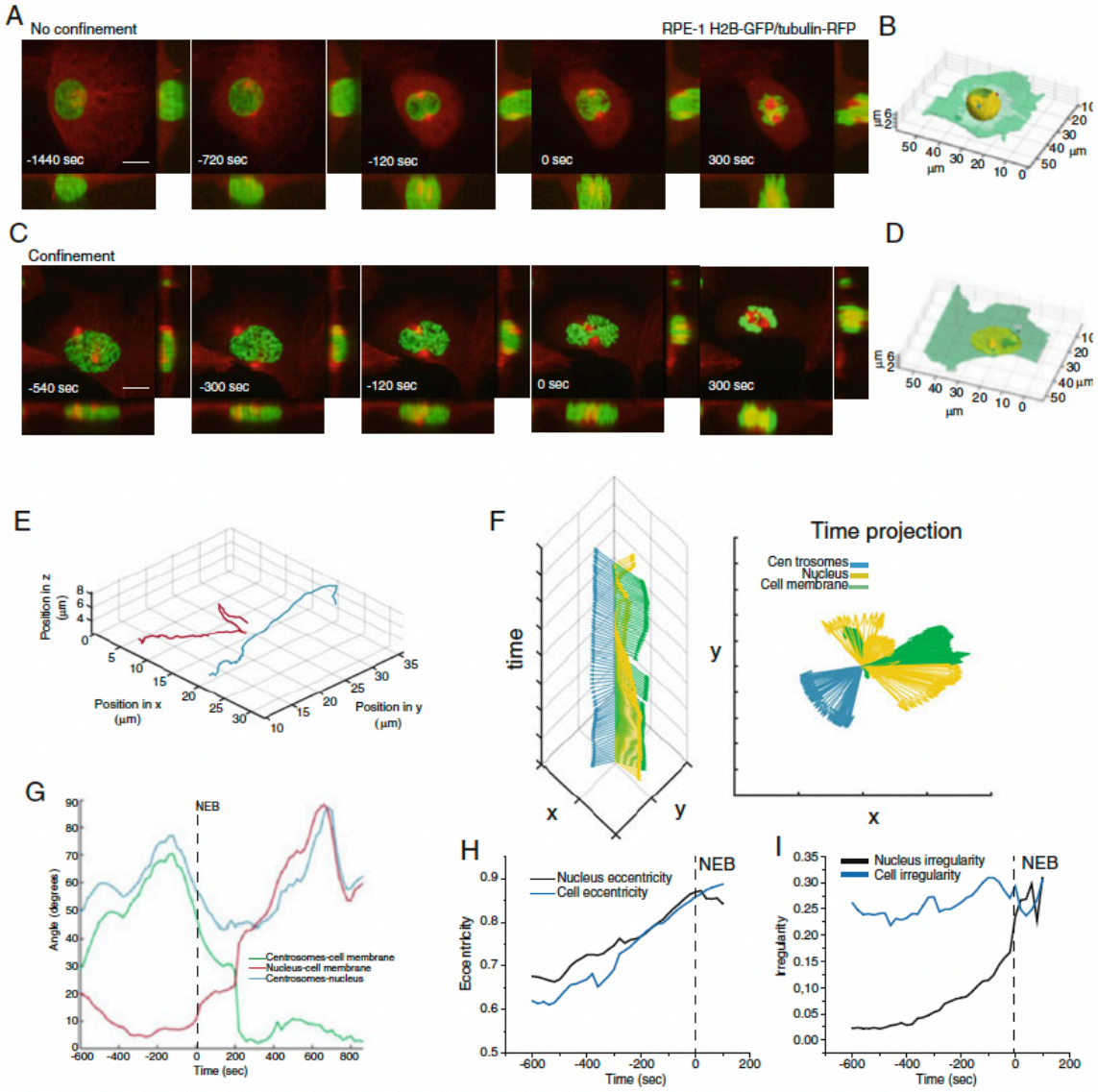


Fig. 4 (**a**) Time-lapse images of an RPE-1 cell expressing H2B-GFP/tubulin-RFP, dividing without confinement. (**b**) 3D reconstruction of the RPE-1 cell in (**a**), showing cell membrane (green), nucleus (yellow), and the two centrosomes (blue and red dots). The vector connecting both centrosomes is shown as a blue line. (**c**) Time-lapse images of an RPE-1 cell expressing H2B-GFP/tubulin-RFP, dividing under confinement. (**d**) 3D reconstruction of the RPE-1 cell in (**c**). Time zero corresponds to NEB (nuclear envelope breakdown). Time is in seconds and time-lapse is 20 s. Scale bar corresponds to 10 m. (**e**) Reconstruction of centrosomes trajectories in 4D. Each point corresponds to a time-point extracted from a live-cell imaging movie. (**f**) Reconstruction and correlation between centrosomes vector (blue arrows), long cellular axis (large green arrows), and long nuclear axis (large yellow arrows). Each set of arrows corresponds to a time-point extracted from a live-cell imaging movie. Right panel shows a temporal projection of left panel. (**g**) Correlation of the angles between nucleus and cell membrane (red), centrosomes and cell membrane (green) and centrosomes and nucleus (blue) over time for the cell shown in (**c**). (**h**) Cell membrane (blue) and nucleus (black) eccentricity over time for the cell shown in (**c**). (**i**) Cell (blue) and nuclear (black) irregularity over time for cell shown in (**c**). Dashed lines correspond the NEB

4 Notes

1. The continuous use of antibiotics in the cell culture medium should be avoided as it may select resistant subclones. When necessary (e.g., imaging the cells), the use of antibiotic–antimycotic solutions (e.g., penicillin–streptomycin) is recommended.
2. A sterile laminar flow hood should be used to perform all cell manipulation procedures.
3. Cells should be used at a low-passage number.
4. It is advised to grow cells for experimental and control conditions in parallel.
5. Prepare solutions A and B for the control condition in parallel. For controls, add 2 μL of Scrambled RNAi or perform a mock transfection.
6. Adjust the concentration according to the oligo and the type of cells used.
7. When the transiently transfected plasmid contains a selection marker, positive cells can be selected by adding the appropriate selection drug to the cell culture medium for 1–2 weeks.
8. When siRNAs are transiently transfected, monitor protein depletion efficiency by collecting cell extracts for Western blot analysis and by fixing cells for phenotypic analysis.
9. For 22 × 22 mm^2 coverslips, use 100 μL of PLL-g-PEG or FBN. For other coverslip sizes, adjust the volume accordingly.
10. PLL-g-PEG-coated glass coverslips can be store dried, at RT, for 3–5 weeks.
11. The micropattern designs on the quartz mask should be customized according to requirements (e.g., size and shape of the micropatterns) (Fig. 1b–b′).
12. Use soft tissues (e.g., Kimwipes) to avoid scratching the mask during the cleaning process. Repeat washing steps if necessary. Occasionally, wash the mask with soap and tap water to remove greasy debris.
13. Use plastic or glass spacers to avoid contact of the mask with the bottom of the lamp box.
14. Try to remove all the air bubbles using a plastic tip to press the coverslip against the mask. The presence of air bubbles will enlarge and distort the underlying pattern.
15. Illumination time might need to be adjusted for different cell types.
16. Patterned glass coverslips can be store dried, at RT, for 2–3 weeks.

17. Never allow the coverslips to dry after FBN incubation.
18. The use of fibrinogen is not mandatory but advised to evaluate micropatterning efficiency and quality.
19. To store the coverslips after FBN incubation (no longer then 1–2 days), incubate the coverslips with PBS at 4 °C. The best results are obtained when the FBN incubation step is performed immediately before seeding the cells.
20. It is possible to UV-sterilize the coverslips in the Laminar Flow Hood, at this point. Keep the coverslips in PBS during UV exposure.
21. Optimal seeding density will vary depending on cell size. Typical number of cells per 22 × 22 mm^2 coverslip or 6-well plate well are: U2-OS, approximately 50,000 cells; HeLa and RPE-1, approximately 75,000 cells; HCT116, approximately 150,000 cells; MDA-MB-468, approximately 200,000 cells.
22. Optimal seeding time should be predetermined for each cell line, taking into account its properties. For more adherent cells such as RPE-1 or U2-OS, a 15–20 min incubation is sufficient, whereas HCT116 and MDA-MB-468 require 20–30 min and HeLa cells typically require 30–40 min.
23. Using a small volume of cell culture medium avoids suction of the culture medium into the vacuum line attached to the pressure/vacuum generator.
24. The cell confiner and the cell confinement slides can be bought or microfabricated in the lab, as previously described [31, 32]. There are different devices (e.g., static vs dynamic cell confiner) and types of confinement coverslips (e.g., slides with PDMS pillars or with hydrogels with tunable stiffness) commercially available (e.g., 4DCell, France). Adjust the equipment according to the requirements of your experiment.
25. Leibovitz's L-15 is a phenol red-free and a CO_2-independent medium. The phenol red dye usually used as a pH indicator in the cell culture medium should be avoided. CO_2-independent medium should be used when pH cannot be controlled by the standard $NaHCO_2/CO_2$-buffering system.
26. Mitosis is tremendously sensitive to temperature; minor temperature changes might induce mitotic delay [40]. It is crucial that the appropriate temperature is set prior to mounting the imaging chamber on the microscope stage. The temperature should be kept stable during the acquisition time.
27. To precisely track centrosome, nucleus, and cell membrane behavior during mitosis, cells should be expressing suitable fluorescent tags (e.g., tubulin, actin, and H2B). Acquisition time will vary according to the temporal resolution required. For high spatiotemporal resolution such as centrosome

tracking during mitotic entry, cells can be filmed every 20 s, capturing 17–21 z-stacks with a 0.5–0.7 μm step. For lower temporal resolution (e.g., follow a complete mitosis), cells can be filmed every 2–5 min, capturing 10–15 z-stacks with a 0.7–1 μm step.

28. To keep the cells healthy during the acquisition process, cells must be protected from light-induced damage. Excessive illumination often leads to cell cycle arrest at G2, or delayed G2–M transition. Reduce light exposure time and laser intensity to a minimum, just enough to guarantee the appropriate temporal and spatial resolutions required for the study.
29. The Centrosome Dynamics module of Trackosome was designed to track centrosomes in 4D and to correlate their trajectories with cell and nuclear membrane metrics. Therefore, live-cell imaging datasets where the three cellular components of interest are independently labeled are required.
30. When metadata information is available on the 4D dataset, the image parameters (e.g., pixel size, time step, and z step) are automatically loaded.
31. Using the option "Correct Centrosomes Coordinates" in Trackosome, allows the manual editing of the centrosomes coordinates in specific time frames.
32. It is recommended to save both the excel and MATLAB files. MATLAB files can be used to edit or reanalyze the data at later time points.
33. Results include key metrics for centrosome, nucleus, and cell membrane such as intercentrosome distances; angles between long nuclear axis/long cell axis, angles between centrosomes/long cell axis and centrosomes/long nuclear axis; and nucleus and cell membrane eccentricity and irregularity.

References

1. Champion L, Linder MI, Kutay U (2017) Cellular reorganization during mitotic entry. Trends Cell Biol 27:26–41. https://doi.org/10.1016/j.tcb.2016.07.004
2. McIntosh JR (2016) Mitosis. Cold Spring Harb Perspect Biol 8. https://doi.org/10.1101/cshperspect.a023218
3. Cramer LP, Mitchison TJ (1997) Investigation of the mechanism of retraction of the cell margin and rearward flow of nodules during mitotic cell rounding. Mol Biol Cell 8:109–119. https://doi.org/10.1091/mbc.8.1.109
4. Dao VT, Dupuy AG, Gavet O, Caron E, de Gunzburg J (2009) Dynamic changes in Rap1 activity are required for cell retraction and spreading during mitosis. J Cell Sci 122:2996–3004. https://doi.org/10.1242/jcs.041301
5. Marchesi S, Montani F, Deflorian G, D'Antuono R, Cuomo A, Bologna S, Mazzoccoli C, Bonaldi T, Di Fiore PP, Nicassio F (2014) DEPDC1B coordinates de-adhesion events and cell-cycle progression at mitosis. Dev Cell 31:420–433. https://doi.org/10.1016/j.devcel.2014.09.009
6. Matthews HK, Delabre U, Rohn JL, Guck J, Kunda P, Baum B (2012) Changes in Ect2 localization couple actomyosin-dependent cell shape changes to mitotic progression. Dev Cell 23:371–383. https://doi.org/10.1016/j.devcel.2012.06.003

7. Stewart MP, Helenius J, Toyoda Y, Ramanathan SP, Muller DJ, Hyman AA (2011) Hydrostatic pressure and the actomyosin cortex drive mitotic cell rounding. Nature 469:226–230. https://doi.org/10.1038/nature09642
8. Zlotek-Zlotkiewicz E, Monnier S, Cappello G, Le Berre M, Piel M (2015) Optical volume and mass measurements show that mammalian cells swell during mitosis. J Cell Biol 211:765–774. https://doi.org/10.1083/jcb.201505056
9. Kunda P, Pelling AE, Liu T, Baum B (2008) Moesin controls cortical rigidity, cell rounding, and spindle morphogenesis during mitosis. Curr Biol 18:91–101. https://doi.org/10.1016/j.cub.2007.12.051
10. Lancaster OM, Le Berre M, Dimitracopoulos A, Bonazzi D, Zlotek-Zlotkiewicz E, Picone R, Duke T, Piel M, Baum B (2013) Mitotic rounding alters cell geometry to ensure efficient bipolar spindle formation. Dev Cell 25:270–283. https://doi.org/10.1016/j.devcel.2013.03.014
11. Mchedlishvili N, Matthews HK, Corrigan A, Baum B (2018) Two-step interphase microtubule disassembly aids spindle morphogenesis. BMC Biol 16(14). https://doi.org/10.1186/s12915-017-0478-z
12. Nunes V, Dantas M, Castro D, Vitiello E, Wang I, Carpi N, Balland M, Piel M, Aguiar P, Maiato H, Ferreira JG (2020) Centrosome-nuclear axis repositioning drives the assembly of a bipolar spindle scaffold to ensure mitotic fidelity. Mol Biol Cell 2020:mbc.E20-01-0047. https://doi.org/10.1091/mbc.E20-01-0047
13. Antonin W, Neumann H (2016) Chromosome condensation and decondensation during mitosis. Curr Opin Cell Biol 40:15–22. https://doi.org/10.1016/j.ceb.2016.01.013
14. Belmont AS (2006) Mitotic chromosome structure and condensation. Curr Opin Cell Biol 18:632–638. https://doi.org/10.1016/j.ceb.2006.09.007
15. Güttinger S, Laurell E, Kutay U (2009) Orchestrating nuclear envelope disassembly and reassembly during mitosis. Nat Rev Mol Cell Biol 10:178–191. https://doi.org/10.1038/nrm2641
16. Kutay U, Hetzer MW (2008) Reorganization of the nuclear envelope during open mitosis. Curr Opin Cell Biol 20:669–677. https://doi.org/10.1016/j.ceb.2008.09.010
17. Khodjakov A, Rieder CL (2001) Centrosomes enhance the fidelity of cytokinesis in vertebrates and are required for cell cycle progression. J Cell Biol 153:237–242. https://doi.org/10.1083/jcb.153.1.237
18. Whitehead CM, Winkfein RJ, Rattner JB (1996) The relationship of HsEg5 and the actin cytoskeleton to centrosome separation. Cell Motil Cytoskeleton 35:298–308. https://doi.org/10.1002/(SICI)1097-0169(1996)35:4<298::AID-CM3>3.0.CO;2-3
19. Bolhy S, Bouhlel I, Dultz E, Nayak T, Zuccolo M, Gatti X, Vallee R, Ellenberg J, Doye V (2011) A Nup133-dependent NPC-anchored network tethers centrosomes to the nuclear envelope in prophase. J Cell Biol 192:855–871. https://doi.org/10.1083/jcb.201007118
20. Kotak S, Busso C, Gönczy P (2013) NuMA phosphorylation by CDK1 couples mitotic progression with cortical dynein function. EMBO J 32:2517–2529. https://doi.org/10.1038/emboj.2013.172
21. Rosenblatt J, Cramer LP, Baum B, McGee KM (2004) Myosin II-dependent cortical movement is required for centrosome separation and positioning during mitotic spindle assembly. Cell 117:361–372. https://doi.org/10.1016/s0092-8674(04)00341-1
22. Cao J, Crest J, Fasulo B, Sullivan W (2010) Cortical actin dynamics facilitate early-stage centrosome separation. Curr Biol 20:770–776. https://doi.org/10.1016/j.cub.2010.02.060
23. Khodjakov A, Rieder CL (2006) Imaging the division process in living tissue culture cells. Methods San Diego Calif 38:2–16. https://doi.org/10.1016/j.ymeth.2005.07.007
24. Walther N, Ellenberg J (2018) Quantitative live and super-resolution microscopy of mitotic chromosomes. Methods Cell Biol 145:65–90. https://doi.org/10.1016/bs.mcb.2018.03.014
25. Shcherbo D, Murphy CS, Ermakova GV, Solovieva EA, Chepurnykh TV, Shcheglov AS, Verkhusha VV, Pletnev VZ, Hazelwood KL, Roche PM, Lukyanov S, Zaraisky AG, Davidson MW, Chudakov DM (2009) Far-red fluorescent tags for protein imaging in living tissues. Biochem J 418:567–574. https://doi.org/10.1042/BJ20081949
26. Douthwright S, Sluder G (2017) Live cell imaging: assessing the phototoxicity of 488 and 546 nm light and methods to alleviate it. J Cell Physiol 232:2461–2468. https://doi.org/10.1002/jcp.25588
27. Magidson V, Khodjakov A (2013) Circumventing photodamage in live-cell microscopy. Methods Cell Biol 114:545–560. https://doi.org/10.1016/B978-0-12-407761-4.00023-3

28. Azioune A, Storch M, Bornens M, Théry M, Piel M (2009) Simple and rapid process for single cell micro-patterning. Lab Chip 9:1640–1642. https://doi.org/10.1039/b821581m
29. Théry M, Jiménez-Dalmaroni A, Racine V, Bornens M, Jülicher F (2007) Experimental and theoretical study of mitotic spindle orientation. Nature 447:493–496. https://doi.org/10.1038/nature05786
30. Velve-Casquillas G, Le Berre M, Piel M, Tran PT (2010) Microfluidic tools for cell biological research. Nano Today 5:28–47. https://doi.org/10.1016/j.nantod.2009.12.001
31. Le Berre M, Zlotek-Zlotkiewicz E, Bonazzi D, Lautenschlaeger F, Piel M (2014) Methods for two-dimensional cell confinement. Methods Cell Biol 121:213–229. https://doi.org/10.1016/B978-0-12-800281-0.00014-2
32. Le Berre M, Aubertin J, Piel M (2012) Fine control of nuclear confinement identifies a threshold deformation leading to lamina rupture and induction of specific genes. Integr Biol Quant Biosci Nano Macro 4:1406–1414. https://doi.org/10.1039/c2ib20056b
33. Fink J, Carpi N, Betz T, Bétard A, Chebah M, Azioune A, Bornens M, Sykes C, Fetler L, Cuvelier D, Piel M (2011) External forces control mitotic spindle positioning. Nat Cell Biol 13:771–778. https://doi.org/10.1038/ncb2269
34. Harder N, Mora-Bermúdez F, Godinez WJ, Wünsche A, Eils R, Ellenberg J, Rohr K (2009) Automatic analysis of dividing cells in live cell movies to detect mitotic delays and correlate phenotypes in time. Genome Res 19:2113–2124. https://doi.org/10.1101/gr.092494.109
35. Neumann B, Walter T, Hériché J-K, Bulkescher J, Erfle H, Conrad C, Rogers P, Poser I, Held M, Liebel U, Cetin C, Sieckmann F, Pau G, Kabbe R, Wünsche A, Satagopam V, Schmitz MHA, Chapuis C, Gerlich DW, Schneider R, Eils R, Huber W, Peters J-M, Hyman AA, Durbin R, Pepperkok R, Ellenberg J (2010) Phenotypic profiling of the human genome by time-lapse microscopy reveals cell division genes. Nature 464:721–727. https://doi.org/10.1038/nature08869
36. Collins E, Mann BJ, Wadsworth P (2014) Eg5 restricts anaphase B spindle elongation in mammalian cells. Cytoskeleton (Hoboken NJ) 71:136–144. https://doi.org/10.1002/cm.21158
37. De Simone A, Nédélec F, Gönczy P (2016) Dynein transmits polarized actomyosin cortical flows to promote centrosome separation. Cell Rep 14:2250–2262. https://doi.org/10.1016/j.celrep.2016.01.077
38. Boudreau V, Chen R, Edwards A, Sulaimain M, Maddox PS (2019) PP2A-B55/SUR-6 collaborates with the nuclear lamina for centrosome separation during mitotic entry. Mol Biol Cell 30:876–886. https://doi.org/10.1091/mbc.E18-10-0631
39. Castro D, Nunes V, Lima JT, Ferreira JG, Aguiar P (2020) Trackosome: a computational toolbox to study the spatiotemporal dynamics of centrosomes, nuclear envelope and cellular membrane. J Cell Sci 133: jcs252254. https://doi.org/10.1242/jcs.252254
40. Rieder CL, Maiato H (2004) Stuck in division or passing through: what happens when cells cannot satisfy the spindle assembly checkpoint. Dev Cell 7:637–651. https://doi.org/10.1016/j.devcel.2004.09.002

ANNEX B

Trackosome: a computational toolbox to study the spatiotemporal dynamics of centrosomes, the nucleus and cellular membrane

The content of this chapter is published in the following original research paper:

D. Castro, V. Nunes, J.T. Lima, J.G. Ferreira, P. Aguiar, Trackosome: a computational toolbox to study the spatiotemporal dynamics of centrosomes, nucleus and cellular membrane, J. Cell Sci. (2020). https://doi.org/10.1242/jcs.252254

This is an original research paper and it is presented for the first time in a thesis.

© 2020. Published by The Company of Biologists Ltd | Journal of Cell Science (2020) 133, jcs252254. doi:10.1242/jcs.252254

TOOLS AND RESOURCES

Trackosome: a computational toolbox to study the spatiotemporal dynamics of centrosomes, nuclear envelope and cellular membrane

Domingos Castro[1], Vanessa Nunes[1], Joana T. Lima[1], Jorge G. Ferreira[1,2,*,‡] and Paulo Aguiar[1,*,‡]

ABSTRACT

During the initial stages of mitosis, multiple mechanisms drive centrosome separation and positioning. How they are coordinated to promote centrosome migration to opposite sides of the nucleus remains unclear. Here, we present Trackosome, an open-source image analysis software for tracking centrosomes and reconstructing nuclear and cellular membranes, based on volumetric live-imaging data. The toolbox runs in MATLAB and provides a graphical user interface for easy access to the tracking and analysis algorithms. It provides detailed quantification of the spatiotemporal relationships between centrosomes, nuclear envelope and cellular membrane, and can also be used to measure the dynamic fluctuations of the nuclear envelope. These fluctuations are important because they are related to the mechanical forces exerted on the nucleus by its adjacent cytoskeletal structures. Unlike previous algorithms based on circular or elliptical approximations, Trackosome measures membrane movement in a model-free condition, making it viable for irregularly shaped nuclei. Using Trackosome, we demonstrate significant correlations between the movements of the centrosomes, and identify specific oscillation modes of the nuclear envelope. Overall, Trackosome is a powerful tool that can be used to help unravel new elements in the spatiotemporal dynamics of subcellular structures.

KEY WORDS: Tracking subcellular structures, Centrosome movement correlations, Membrane reconstruction, Nuclear envelope fluctuations, Mitosis, Free and open-source software

INTRODUCTION

Mitosis is a highly regulated stage of the cell cycle in which multiple subcellular structures take part in a complex chain of events that culminate in chromosome segregation. As cells prepare to enter mitosis, adhesion complexes disassemble (Dao et al., 2009) and the cytoskeleton reorganizes (Matthews et al., 2012; Mchedlishvili et al., 2018). At the same time, duplicated centrosomes need to migrate along the nuclear envelope (NE) so that a bipolar spindle can form (Tanenbaum and Medema, 2010). This process requires the activity of multiple players, such as microtubule-associated motors kinesin-5 (Whitehead et al., 1996) and dynein (Raaijmakers et al., 2012), but also actin (Cao et al., 2010) and myosin II (Rosenblatt et al., 2004). How the dynamic changes in all these events are coordinated in space and time to ensure efficient centrosome separation and spindle assembly remains unknown.

Recent advances in live-cell imaging and image analysis techniques have made it possible to access the subcellular environment and quantitatively examine its underlying mechanisms (Gerlich et al., 2001; Otsuka et al., 2018). Commercial imaging software such as Imaris and Metamorph are equipped with automatic particle tracking functions, which have been used to track centrosome pairs in three dimensions (Collins et al., 2014; De Simone et al., 2016; Yamashita et al., 2015). The open-source freeware ImageJ (Eliceiri et al., 2012) with its particle-tracking plugin Trackmate (Tinevez et al., 2017) has also been used for centrosome tracking in several studies (Boudreau et al., 2019; Mahen, 2018; Stiff et al., 2020). However, these generic tracking tools are not fine-tuned for the appearance and motion dynamics of centrosome pairs, which limits their tracking performance and often requires exhaustive parameter optimization, particularly when high-quality videos are not available. Moreover, when studying the dynamics of spindle formation, it is often necessary to analyze centrosome movement in reference to the cellular and nuclear membrane (and, therefore, in a non-canonical coordinate system). To the best of our knowledge, the available computational tools do not directly allow analysis of the coordinated changes between different structures in specific subcellular frames of reference (such as the nuclear membrane).

The NE also exhibits rich spatiotemporal dynamics, displaying measurable oscillations that correlate with the forces exerted by chromatin, nuclear lamina and the cytoskeleton (Chu et al., 2017; Schreiner et al., 2015; Stephens et al., 2017) and strongly influence nuclear functions (Jahed and Mofrad, 2019; Stephens et al., 2019). One way to study this complex interplay between cytoskeletal forces imposed on the nucleus and the resistive forces triggered by chromatin and nuclear lamina is by measuring the dynamics of NE membrane fluctuations (Chu et al., 2017; Hampoelz et al., 2011; Schreiner et al., 2015), which allow the distinction between thermally driven and active fluctuations (Chu et al., 2017). Importantly, during mitotic entry, chromosomes condense (Antonin and Neumann, 2016) and the nuclear lamina disassembles (Georgatos et al., 1997). How these events affect the pattern of NE oscillations and impact other aspects of early spindle assembly remains to be determined. Current methods used to calculate NE fluctuations were developed under the assumption that each point of the membrane oscillates radially around its time-averaged position (Almonacid et al., 2019; Blanchoud et al., 2010; Caragine et al., 2018; Chu et al., 2017; Schreiner et al., 2015). However, describing the membrane deformations as a radial displacement is a coarse approximation that can lead to erroneous results. Also, to the best of our knowledge, there are no available toolboxes for calculating these membrane fluctuations.

Driven by these computational limitations and the need to better characterize the crosstalk between subcellular structures during mitotic entry, we developed the open-source software Trackosome. This novel computational tool enables a quantitative analysis of the

[1]i3S - Instituto de Investigação e Inovação em Saúde, Universidade do Porto, 4200-135 Porto, Portugal. [2]Departamento de Biomedicina, Faculdade de Medicina, Universidade do Porto, 4200-450 Porto, Portugal.
*These authors contributed equally to this work

‡Authors for correspondence (jferreir@ibmc.up.pt; pauloaguiar@ineb.up.pt)

V.N., 0000-0001-8568-4269; J.T.L., 0000-0002-2327-8852; J.G.F., 0000-0001-6802-3696; P.A., 0000-0003-4164-5713

Handling Editor: David Stephens
Received 26 July 2020; Accepted 2 November 2020

spatiotemporal dynamics of three cellular components: centrosomes, NE and cellular membrane. Trackosome relies on live-cell imaging datasets, where the structures of interest are independently tagged. The tool has two modules: (1) the Centrosome Dynamics module, used for tracking the centrosomes (or other subcellular organelles) in 3D and study their spatiotemporal relations with the nucleus and cell membrane; (2) the Nuclear Envelope Fluctuations module, used to reconstruct, measure and analyze the dynamic fluctuations of the nuclear membrane (or other membranes) in 2D. The accurate 3D reconstruction of the centrosome trajectories relative to the nucleus and cell membranes (in ellipsoidal coordinates) allowed us to unravel and quantify a significant correlation between centrosome trajectories that has not previously been characterized. In addition, the Nuclear Envelope Fluctuations module allowed us to observe and quantify distinct patterns of membrane oscillations in 2D in different stages of the cell cycle.

Trackosome is made publically available (open-source) as a platform-independent MATLAB toolbox and can be downloaded from https://github.com/Trackosome.

RESULTS

Dynamics of cellular reorganization during early spindle assembly

Tracking and trajectory analysis of centrosomes is performed in the Trackosome toolbox through the Centrosome Dynamics module. This module has a graphical user interface (Fig. 1A; Fig. S1, Movies 1-3) that provides useful feedback about the automatic tracking status, and allows manual or semi-automatic corrections whenever needed. The accuracy of the tracking algorithm was tested and validated in synthetic data, created with imposed controlled conditions. The videos generated had two centrosome-like objects moving in 3D with biologically realistic dynamics (coordinates taken from real centrosome trajectories), in a noisy environment. We set three levels of tracking difficulty by varying the signal-to-noise ratio (Fig. 1B). The coordinates obtained by the Trackosome algorithm were then compared with the original coordinates used to create the videos (Fig. 1C). Our tool was able to track the centrosomes with high fidelity even in highly noisy environments (signal-to-noise ratio of 0.7) where the particles were almost indistinguishable from the background. For all videos analyzed, the root mean squared error associated with the tracking (Fig. 1C) was at the subpixel level (1 pixel=0.189 µm).

We then recorded cells seeded on line micropatterns to normalize cell and nuclear shape (Versaevel et al., 2012). Note, however, that Trackosome does not require cells to be seeded in such micropatterns and can be used in unconstrained conditions (Fig. S3A-D). Taking advantage of the precision provided by Trackosome, we quantified specific spatiotemporal relations between three cellular structures during mitotic entry, namely centrosome pair, nuclear membrane and cell membrane. We chose this stage of the cell cycle as it involves extensive dynamic reorganization of the entire cell (Champion et al., 2017), providing a good benchmark to test the ability of Trackosome to detect these dynamic changes. Here, Trackosome was able to reconstruct in 3D the surfaces of the membranes, together with the trajectories of centrosomes (Fig. 2A,B). Based on their relative positions, the software was able to output different quantitative metrics, such as the distance and angles between centrosomes (Fig. 2C,D), the eccentricity of the nuclear and cellular membranes (Fig. 2E) and the angles between the major axes of the nucleus, cell and centrosomes (Fig. 2F). These metrics describe the intracellular reorganization that occurs as cells enter mitosis, such as movement of the centrosomes to opposite sides of the nucleus (Fig. 2B-D) and nucleus-centrosome axis reorientation (Fig. 2B,F), which we previously described (Nunes et al., 2020).

Centrosome trajectories are not independent

HeLa or U2OS cells labeled with histone H2B-GFP/α-tubulin-RFP/SiR-actin or EB3-GFP/Lifeact-mCherry/SiR-DNA, respectively, were tracked until nuclear envelope breakdown (NEB). During this stage, nuclear shape remained approximately constant and correlated with the labeled chromatin, allowing us to define the median nucleus membrane (Fig. 2G, grey mask) based on the 3D reconstructions of the NE. The centrosomes, on the other hand, exhibited complex trajectories that resembled a search or adaptive path around the nucleus (Fig. 2G). For this reason, to infer the coordination of movement between centrosomes, their trajectories were analyzed using the nucleus as a reference. An ellipsoid was fitted to the median nuclear membrane, setting the frame of reference for the new coordinate system (Fig. S3F-H). Each point of the centrosome trajectory was defined by a latitude ϕ, longitude λ

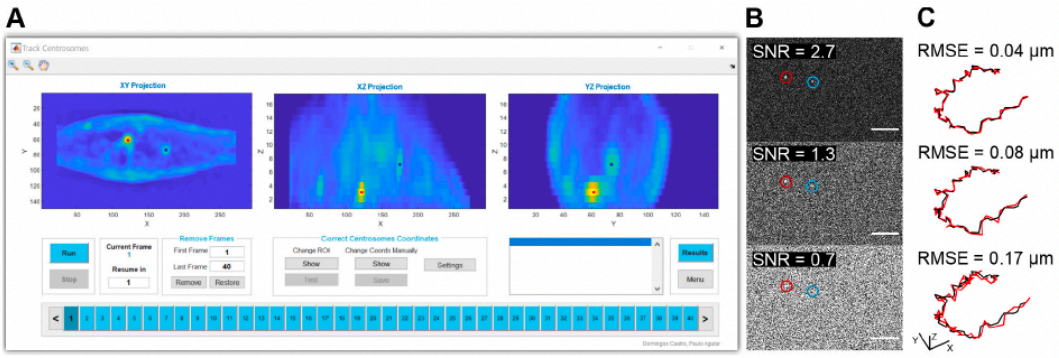


Fig. 1. Evaluation of centrosome tracking. (A) User interface for centrosome tracking showing the XY, XZ and YZ maximum projections for a video of a mitotic cell with the corresponding automatically identified centrosome positions (red and blue dots). (B) Frame extracted from the three synthetic videos with varying levels of signal-to-noise ratio (SNR). Centrosomes are inside the red and blue circles. (C) Ground-truth trajectory (black) and trajectory obtained by Trackosome (red) for the centrosome on the left in B (red circle), and associated root mean square of the error (RMSE) obtained for both centrosomes. Scale bars: 10 µm (B), 1 µm (C).

Journal of Cell Science (2020) 133, jcs252254. doi:10.1242/jcs.252254

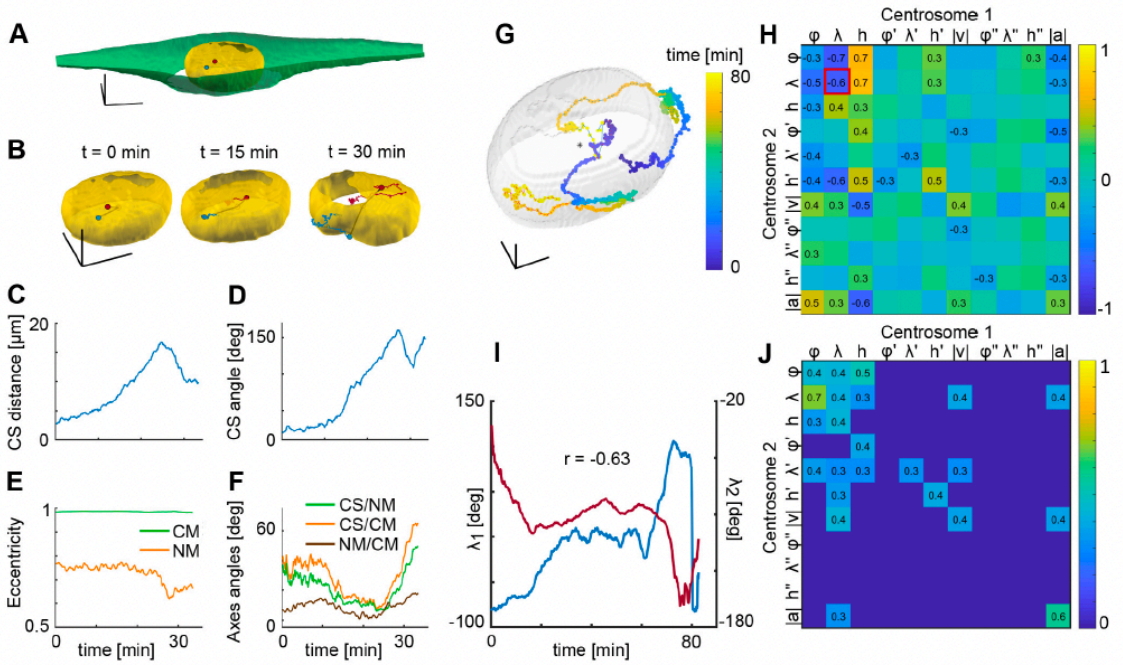


Fig. 2. Spatiotemporal relations between cellular structures during early mitosis. (A-F) Example of Trackosome outputs for a representative cell in mitosis. (A) 3D reconstruction of the cellular membrane (green), nuclear envelope (yellow) and centrosomes (red and blue dots). (B) Nuclear membrane and centrosomes at three distinct time stamps. The centrosome trajectories (red and blue lines) highlight their migration to opposite poles of the nucleus, followed by progressive nuclear deformation. (C) Distance between centrosomes (CS) over time. The distance increases gradually during centrosome migration and decreases once the centrosomes start compressing the nucleus. (D) Angles formed between the centrosomes and the nucleus centroid over time. Note how the decrease in distance between the centrosomes (C) occurs after centrosomes are on opposite sides of the nucleus, corresponding to the highest value for the centrosome-nucleus angle. (E) Eccentricity of the cellular (CM, green) and nuclear (NM, orange) membranes evidencing that, although the cellular membrane remains morphologically stable, the nuclear membrane undergoes conformational changes after the centrosomes start deforming the nucleus. (F) Angles formed between the centrosome axis and the nucleus major axis (orange), centrosome axis and the cell major axis (green), and the nucleus major axis and the cell major axis (brown). The centrosome pair progressively moves towards a disposition perpendicular to the major axis of the nucleus and cell. (G-J) Trajectories of centrosome pairs are spatiotemporally correlated. (G) Centrosome positions across time (color-coded for elapsed time) surrounding the nucleus (gray). (H) Correlation matrix of the movement components (in ellipsoidal coordinates) for the trajectories shown in G. (I) Example of the correlated features highlighted in H (red square), corresponding to the longitude components of both centrosomes, which suggests a potential mechanical coupling between both structures. (J) Median of the absolute correlation matrices obtained from videos of different cells (n=5), thresholded at 0.3 for visualization purposes, showing consistent correlations between centrosome trajectories across different cells. Scale bars: 10 μm (A,B), 5 μm (G).

and height h; the respective ellipsoidal velocities ϕ', λ', h' and velocity norm $|v|$; and the ellipsoidal accelerations ϕ'', λ'', h'' and acceleration norm $|a|$. We calculated the correlation matrix of these features for each centrosome pair (Fig. 2H), revealing which components were temporally correlated between the two trajectories. Our results indicate a considerable degree of similarity and synchrony among trajectory pairs (Fig. 2I), with correlation values as high as 0.7, in contrast to a previous report (Waters et al., 1993). By calculating the median of the absolute correlation matrices obtained, we produced a map of the most consistent correlations (Fig. 2J). Interestingly, the positions of the centrosomes, ϕ, λ, h, and the acceleration norm $|a|$, showed significant correlations. The latter is particularly relevant because the acceleration of a particle reflects the force applied to it, suggesting a synchronous variation of the forces applied to both centrosomes, probably driven by kinesin-5 (Whitehead et al., 1996) or dynein (Raaijmakers et al., 2012). It is worth emphasizing that if the movement of centrosomes had been described in Cartesian coordinates (i.e. ignoring the nuclear surface constraint), the observed correlations would not be evident.

Dynamics of nuclear envelope fluctuations driving mitotic entry

The dynamic morphology of the NE was analyzed using the Membrane Fluctuations module of Trackosome (Fig. S2; Movies 4 and 5). The membrane oscillations were determined by calculating the orthogonal displacement of each point of the membrane with respect to its medial position (Fig. S3I,J). Our new method does not rely on prior assumptions regarding the nucleus shape. We believe that this approach leads to a more realistic description of the membrane displacements than the radial displacement approximations (with respect to the centroid of the membrane) usually described in the literature (Almonacid et al., 2019; Blanchoud et al., 2010; Caragine et al., 2018; Chu et al., 2017; Schreiner et al., 2015). The radial displacements are particularly flawed for an irregularly shaped nucleus with wide fluctuations (Fig. 3A), which generally limits its use to cells in interphase. Here, we were able to quantify and compare the nuclear deformations for cells in interphase and early mitosis.

As before, we recorded cells seeded on line micropatterns. From our analysis, it is possible to confirm that cells in interphase present subtle but measurable nuclear membrane movements. As a negative

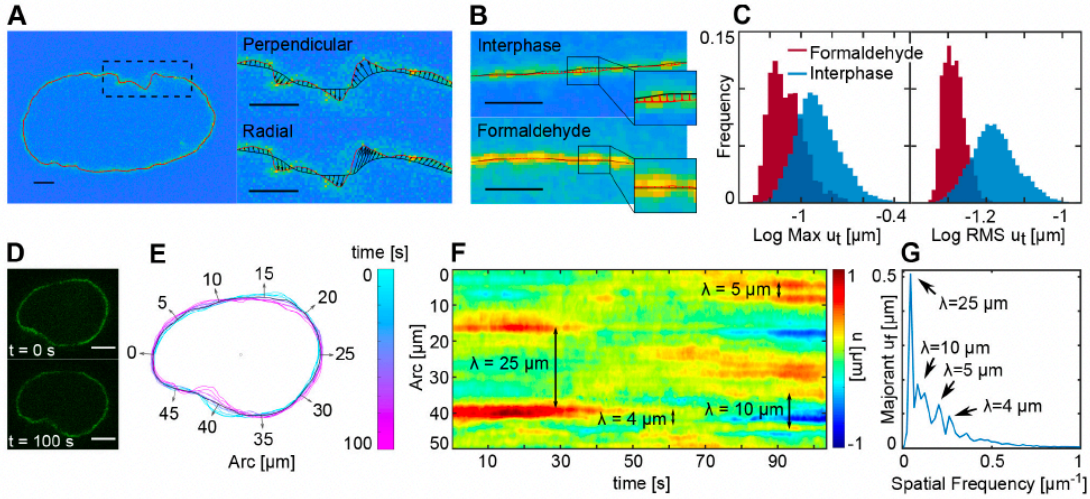


Fig. 3. Nuclear membrane fluctuations captured with Trackosome. (A-C) The perpendicular membrane displacements measured with Trackosome are sensitive to subtle membrane movements. (A) Membrane segmentation (red) of a representative nucleus in prophase (left) and a detailed view of the upper region of the membrane (right) illustrating the difference between defining the fluctuations (black vectors) as perpendicular (top right) or radial (bottom right) movements of the current membrane (red) around the median membrane (black). For the radial displacements, the centroid of the median membrane is used as origin. Perpendicular displacements offer a more realistic description of the membrane movement around its basal position. (B) Representative examples of the nuclear membrane fluctuations (red vectors) of a cell in interphase (top) and a cell fixed in formaldehyde (bottom). The small fluctuations measured for the cell in interphase are clearly larger than those obtained for the fixed cell, suggesting that they are the result of subtle membrane movements. (C) Distributions of the maximum fluctuation per frame, Max u_t (left), and the root mean square (RMS) of the fluctuation per frame, RMS u_t (right), for cells in interphase (44 cells with approximately 600 frames each) and in formaldehyde (4 cells with approximately 500 frames each). With logarithmic scales, the distributions are approximately Gaussian and easily distinguishable. (D-G) Typical nuclear fluctuations results obtained with Trackosome for a cell in prophase. (D) Two frames of the original video. (E) Centered nucleus membrane extracted from the video in D at different time stamps (colored scale), with vectors (gray) indicating the arc in micrometers around the median membrane (black), pointing in the direction along which the fluctuations are calculated. (F) Map of the fluctuations amplitude, u, obtained for all the frames. The y-axis corresponds to the arc around the median membrane, marked by the vectors in E. (G) Majorant of frequency-dependent fluctuations, u_f, obtained by finding the maximum amplitude of the spatial Fourier transform (FT) for each frequency across frames. This FT curve shows the maximum fluctuation amplitude of each wavelength; thus, its peaks reveal the amplitude and wavelength of the most significant curvatures of the nuclear envelope, evidenced both in E and F. Scale bars: 2 μm (A), 2 μm (B), 5 μm (D).

control, fluctuation measurements were made for interphase cells fixed with formaldehyde, which showed a significant decrease in undulations upon fixation (Fig. 3B,C).

During mitotic entry, chromosomes condense (Antonin and Neumann, 2016) and the nuclear lamina disassembles (Georgatos et al., 1997). Whether these events change nuclear behavior remains to be determined. We analyzed the nuclear membrane fluctuations of cells using Trackosome (Fig. 3D-G). After segmenting and registering (centering on centroid) the NE (Fig. 3E), the fluctuations (u) of each frame were calculated assuming normal displacements (Fig. 3A, top). The values obtained were concatenated frame-by-frame and filtered in time and space with a 2D Gaussian kernel. The resulting fluctuations map reveals how the envelope curvatures are dominated by specific wavelengths (Fig. 3F). These wavelengths are determined by calculating the spatial Fourier transform (FT) of the fluctuations, u_f, for each frame and then obtaining the maximum magnitude of each wavelength across frames (Fig. 3G). Calculating the majorant for each frequency component u_f has the advantage of highlighting the most well-defined spatial frequencies, even if they occur for a limited number of frames. On the other hand, averaging the FT curves of all frames would attenuate these components, and the magnitude of the final FT peaks would not correspond to the magnitude of the actual membrane waves that originated them, thus providing a less intuitive readout.

The FT curve allowed us to identify and quantify the most prominent spatial frequencies and obtain relevant information about the dynamics of NE fluctuation. For the cell in prophase exemplified in Fig. 3D-G, the highest FT peak, with a wavelength of 25 μm (half of the nucleus perimeter), was the result of the large membrane displacement seen around the 15 and 40 μm arc landmarks in Fig. 3E,F. As prophase progressed, exertion of compression forces in these two separate points made the nuclear membrane wobble, with a wavelength that was half of the membrane perimeter (Fig. S4A). In addition, the FT analysis allowed the identification of membrane 'wrinkles' with spatial signatures defined by wavelengths of approximately 10, 5 and 4 μm (Fig. 3F,G). Trackosome captures these spatial signatures with high accuracy, even for curvatures with amplitudes at the subpixel level under noisy backgrounds (Fig. S4B-I).

To help uncover the processes behind these observed spatial frequencies, membrane fluctuations were calculated for cells in early mitosis and interphase (Fig. 4A,B). We calculated the majorant u_f for all cells (as in Fig. 3G) and then the median curve across trials for each group. Our results showed a significant difference in the FT curves of the two groups (Fig. 4B). In interphase, the magnitude of the fluctuations was very low through the entire spectrum of wavelengths, indicating that the membrane barely deviated from its basal position. Still, the u_f magnitude was above the noise floor established by the formaldehyde curve. This behavior changed in prophase, as there was an increase in the fluctuation amplitude for the entire range of wavelengths. This increase was particularly significant for the low frequency components, reflecting the occurrence of nucleus-wide deformations as described above.

Journal of Cell Science (2020) 133, jcs252254. doi:10.1242/jcs.252254

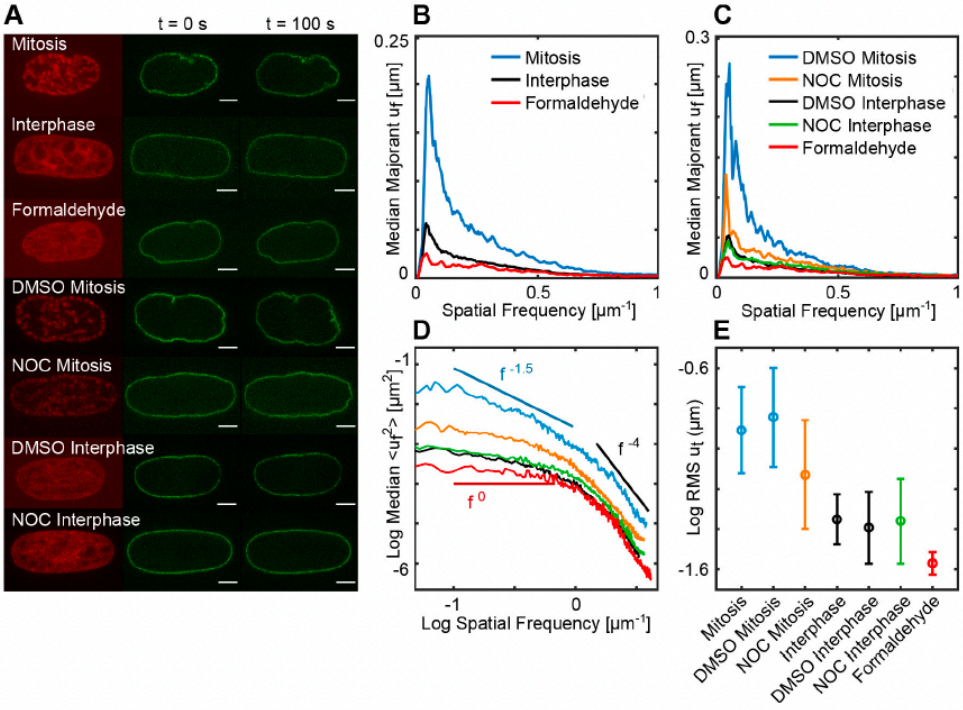


Fig. 4. Nuclear membrane fluctuations vary with the stage of the cell cycle and the physiological treatment. (A) Representative images of H2B-mCherry for each experimental group. The phase of the cell cycle is evidenced by the marked histone (red), taken from the first frame of each video. The nuclear envelope (green) is shown at two different time stamps to illustrate the degree of membrane undulation in each group. (B) Median of the majorant frequency-dependent fluctuations, u_f, obtained for groups of cells in interphase (n=44) and early mitosis (n=26). The curve for cells fixed with formaldehyde (n=4) was also included to set the noise limit. (C) Median of the majorant u_f obtained for groups of cells in interphase and mitosis, treated with DMSO (n=25 and n=15, respectively), nocodazole (NOC) (n=17 and n=16, respectively) and fixed with formaldehyde (n=4). NOC caused a significant decrease in the membrane fluctuations in mitosis. (D) Median across cells of the average FT of the squared fluctuations of each cell, $\langle u_f^2 \rangle$, for the groups represented in C. In logarithmic scales, the $\langle u_f^2 \rangle$ curves show regions dominated by different frequency dependencies, limited by the solid lines with slopes f^0, $f^{-1.5}$ and f^{-4}. (E) Mean and standard deviation of the log root mean square (RMS) of the fluctuations for all the tested groups. Using a logarithmic scale, the RMS fluctuations distributions are approximately normal and can thus be described by their mean value and standard deviation. Scale bars: 5 µm.

Fluctuations of the NE are known to depend on the cytoskeleton and, in particular, on the microtubule (MT) network (Chu et al., 2017; Hampoelz et al., 2011). To assess whether Trackosome was sensitive enough to detect these changes, we treated cells with low doses of nocodazole (NOC) to suppress the polymerization of MTs without affecting overall cell structure. Interphase cells treated with NOC had an FT curve similar to the control curve obtained for interphase cells treated with DMSO only (Fig. 4A,C). On the other hand, nuclear fluctuations of mitotic cells were significantly altered with the addition of NOC. The FT obtained for this experimental condition showed a decrease in the low-frequency peak compared with the control group. This suggests that disruption of the MT cytoskeleton led to a decreased nuclear compression, which is in agreement with reports that the MTs induce large-scale deformations of the NE (Hampoelz et al., 2011; Schreiner et al., 2015). The frequency components beyond the peak were also severely attenuated, which means that the shorter membrane wrinkles were also mitigated. Most of these effects can be qualitatively evaluated by examining the nuclei images directly (Fig. 4A), but Trackosome provides a precise quantification.

Biological membranes exhibit passive fluctuations, which are thermally excited at physiological temperatures. The equilibrium properties of these undulating systems can be modeled by Helfrich-type models (Helfrich, 1978). To evaluate the spectral dependencies in line with Helfrich theory, we calculated the average FT of the squared fluctuations for each cell, $\langle u_f^2 \rangle$, and then the median curve across cells for each group. The curves of the fluctuations obtained for the NOC and control groups showed regions with distinct spectral dependencies (Fig. 4D). For frequencies above 1.5 µm^{-1} (wavelengths below 0.7 µm), the FT curves followed a f^{-4} power law, consistent with what is expected for thermally driven fluctuations at short wavelengths (Brandt et al., 2011). At lower frequencies, each group followed a different power law, ranging from close to f^0 for formaldehyde, up to $f^{-1.5}$ for the control group in mitosis. These can be attributed to different nonequilibrium active forces governing each system. It is important to note that in Helfrich theory these spectral dependencies are defined in terms of the adimensional wavenumber q, and not spatial frequency. However, for the frequency ranges marked by the solid lines in Fig. 4D, the slopes were equivalent in both scales (Fig. S4J-L).

Finally, we compared the fluctuation amplitude [in terms of log root mean square (RMS) of u_f as in Fig. 3C, right] for all groups (Fig. 4E). NOC led to a significant decrease in the fluctuation amplitude during prophase. Importantly, this decrease was not caused by DMSO, because prophase cells in the presence of DMSO exhibited higher fluctuations than the untreated prophase cells. Also,

the fluctuations obtained for the interphase cells were similar among the different groups and the range of amplitudes was consistent with those already described in the literature (Schreiner et al., 2015).

Overall, our results indicate that nuclear membrane fluctuations increase as cells transition from interphase to mitosis and that interfering with the MT network significantly reduces the large scale deformations of the nucleus during this stage.

DISCUSSION

Recent developments in light microscopy have generated extensive datasets that allow unprecedented access to subcellular events with high spatiotemporal resolution. Here, we report on Trackosome, a new open-source software that enables an automated quantitative analysis of the spatiotemporal dynamics of subcellular structures even in conditions of low signal-to-noise ratio. During the transition from G2 to mitosis, chromosomes condense (Antonin and Neumann, 2016), cells round up (Matthews et al., 2012) and centrosomes separate (Whitehead et al., 1996). In this context, the extent of centrosome separation at the time of NEB remains a matter of debate. Although some reports show that cells can enter mitosis with unseparated centrosomes (Kaseda et al., 2012; Whitehead et al., 1996), others indicate that centrosomes are fully separated at NEB (Magidson et al., 2011; Mardin et al., 2013; Nunes et al., 2020). These discrepancies highlight the need to determine carefully how the events leading up to mitosis are coordinated to ensure efficient spindle assembly. By using the different modules available on Trackosome, we were able to correlate centrosome movement accurately and centrosome-nucleus axis reorientation during mitotic entry. Our results, using cells seeded on fibronectin micropatterns, indicate that centrosomes are fully separated before NEB and that their movement is coordinated to optimize their positioning on opposite sides of the nucleus (Magidson et al., 2011), in contrast to previous observations (Waters et al., 1993). This coordination was evidenced using elliptical coordinates to describe the centrosome trajectories around the nucleus. Interestingly, the high correlation scores between movement components of both centrosomes strongly indicate a mechanical coupling between the two structures. This coupling could be provided by specific pools of dynein on the cell cortex (Kotak et al., 2012; Woodard et al., 2010) or at the NE (Bolhy et al., 2011; Splinter et al., 2012), which are known to generate pulling forces on centrosomal microtubules to position asters (Laan et al., 2012). Determining the exact nature of this mechanical coupling between the centrosomes during mitotic entry will be of interest in the future.

The mechanical properties of the nucleus depend on the chromatin condensation state (Stephens et al., 2017, 2018) and the nuclear lamina (Lammerding et al., 2006). Given that Lamin A levels (Chu et al., 2017; Moir et al., 2000) and chromatin compaction (Hinde et al., 2012) change throughout the cell cycle, it is possible that the mechanical properties of the nucleus change accordingly. In agreement, NE fluctuations, which reflect forces imposed on the nucleus, were shown to vary depending on the cell cycle stage (Chu et al., 2017). However, whether the mechanical properties of the nucleus change during the transition from G2 to mitosis, when mitotic chromosomes condense and the nuclear lamina disassembles, remains unclear. Here, we report on a new tool for analyzing NE fluctuations during mitotic entry that measures orthogonal displacements relative to the medial position of the nuclear membrane. We reveal that chromosome condensation, together with microtubules, triggers significant changes in the spatial pattern of NE fluctuations as cells prepare to enter mitosis. To the best of our knowledge, it is the first time that the transition from G2 to prophase has been characterized in terms of NE fluctuations. In the future, it will be interesting to determine how these fluctuations reflect the mechanical properties of the nucleus.

The novel algorithms compiled in the computational toolbox Trackosome provide a reliable and accurate instrument with subpixel precision to help uncover new elements in the spatiotemporal dynamics of subcellular structures. Importantly, Trackosome is not restricted to centrosomes and the nucleus or cell membrane; its algorithms can be used to track other subcellular structures, providing these structures can be adequately segmented from 3D live imaging data (in its current version, Trackosome can simultaneously track two particles and two membranes sets). Moreover, this toolbox has the potential to be adapted to other experimental conditions such as the study of cell migration and cell polarity, where the capacity to analyze dynamic datasets with high accuracy is highly relevant. Being specifically developed in MATLAB and made publically available as open-source software allows other researchers to easily modify Trackosome and integrate additional functions or metrics to suit their needs.

MATERIALS AND METHODS

Biological methods

Cell culture

Cell lines were cultured in Dulbecco's modified Eagle medium (DMEM; Life Technologies) supplemented with 10% fetal bovine serum (FBS; Life Technologies) and grown in a 37°C humidified incubator with 5% CO_2. The HeLa POM121-3×GFP/H2B-mCherry cell line was a kind gift from the laboratory of Katharine Ullman (University of Utah, Salt Lake City, UT, USA). The HeLa cell line expressing histone H2B-GFP/mRFP-α-tubulin was generated in our laboratory using lentiviral vectors. All cell lines were authenticated in the laboratory of origin. All cell lines used in this study are routinely tested for mycoplasma contamination and always found to be negative.

Micropatterning

Micropatterns to control individual cell shape and adhesion pattern were produced as previously described (Azioune et al., 2009). Briefly, glass coverslips (22×22 mm No. 1.5; VWR) were activated with plasma (Zepto Plasma System, Diener Electronic) for 1 min and incubated with 0.1 mg/ml of PLL(20)-g[3,5]-PEG(2) (SuSoS) in 10 mM HEPES at pH 7.4, for 1 h at room temperature. After rinsing and air-drying, the coverslips were placed on a synthetic quartz photomask (Delta Mask), previously activated with deep-UV light (PSD-UV, Novascan Technologies) for 5 min. MiliQ water (3 µl) was used to seal each coverslip to the mask. The coverslips were then irradiated through the photomask with the UV lamp for 5 min. Afterwards, coverslips were incubated with 25 µg/ml of fibronectin (Sigma-Aldrich) and 5 µg/ml of Alexa Fluor 546 or 647-conjugated fibrinogen (ThermoFisher Scientific) in 100 mM $NaHCO_3$ at pH 8.6, for 1 h at room temperature. Cells were seeded at a density of 50,000 cells/coverslip and allowed to spread for 10-15 h before imaging. Non-attached cells were removed by changing the medium 2-5 h after seeding.

Time-lapse microscopy

For time-lapse microscopy, 12-24 h before the experiments, 5×10^4 cells were seeded on coverslips coated with FBN (25 µg/ml; F1141, Sigma). Prior to each experiment, cell culture medium was changed from DMEM with 10% FBS to Leibovitz-L15 medium (Life Technologies) supplemented with 10% FBS and Antibiotic-Antimycotic 100× (AAS; Life Technologies). When SiR dyes were used, they were added to the culture medium 30-60 min before acquisition (20 nM SiR-tubulin or 10 nM SiR-DNA; Spirochrome). Where stated, nocodazole was added to the cells 30 min before the experiment (20 nM; Sigma-Aldrich). Live-cell imaging was performed using temperature-controlled Nikon TE2000 microscopes equipped with a modified Yokogawa CSU-X1 spinning-disc head (Yokogawa Electric), an electron multiplying iXon+ DU-897 EM-CCD

camera (Andor) and a filter-wheel. Three laser lines were used for excitation at 488, 561 and 647 nm. For nuclear membrane fluctuations, an oil-immersion 100×1.4 NA Plan-Apo DIC (Nikon) was used. All the remaining experiments were done with an oil-immersion 60×1.4 NA Plan-Apo DIC (Nikon). Image acquisition was controlled by NIS Elements AR software. For centrosome tracking, 17-21 z-stacks with a 0.5 µm separation were collected every 20 s or, to analyze centrosome correlations, every 10 s. For NE fluctuation measurements, a single z-stack was collected every 100 ms.

Trackosome toolbox: Centrosome Dynamics

Trackosome is made publically available (open-source) as a platform-independent MATLAB toolbox and can be downloaded from https://github.com/Trackosome.

Tracking algorithm

A 3D Laplacian of Gaussian filter is applied to the video of centrosomes to highlight centrosome-like blobs. The user must then select the approximate position of the two centrosomes in an XY maximum projection of the first frame. These are the seeding points for the tracking loop that follows. For each frame, two 3D regions of interest (ROIs) are centered at the coordinates of the centrosomes obtained for the previous frame (for the first frame, it uses the coordinates selected by the user). The ROIs are large enough to encompass the centrosome displacements between frames. This ensures that the ROIs, centered in the coordinates of the centrosomes at the previous frame, still contain the centrosomes in the current frame. The ROIs are thresholded to isolate regions of high intensity. Then, each ROI is iteratively shortened, one-dimension at a time, until it confines a high-intensity blob with the approximate size of the centrosome. Once each centrosome is enclosed by a 3D mask, the centroids are found by projecting the masked intensities along the three axes and fitting a Gaussian curve to each intensity profile – the coordinates of the centrosome correspond to the peaks of the fitted Gaussian curves (Fig. S3E).

Nuclear and cellular membrane reconstruction

The images from each video (nucleus and cellular membrane) are filtered with a 4D (three spatial dimensions and one temporal dimension) average filter. Then, they are binarized using Otsu's method and submitted to an iterative set of morphological operations intended to create a closed, smooth, binary volume. The membrane of each structure corresponds to the outer pixels of their binary volume. The major axes of the cell and nucleus are obtained by calculating the principal components of the binary volumes for each frame.

Correlation of centrosome trajectories

The correlations among displacements of the centrosomes were evidenced by defining their movements as two ellipsoidal trajectories surrounding the approximately ellipsoidal nucleus (Fig. S3F-H). The nucleus was centered to ensure a common centroid in each frame. The median nucleus was obtained by calculating the median binary volume across time. The videos were analyzed until NE breakdown. An ellipsoid was fitted to the median nucleus, setting the coordinate system used to define the ellipsoidal trajectories. The trajectories of the centrosomes were normalized with regards to the centroid of the nucleus for each frame. The transformed trajectories were converted to ellipsoidal coordinates, using the fitted ellipsoid as a referential of the coordinate system. The trajectories were also characterized by the norm of the ellipsoidal velocity and acceleration, and by their decomposition along the latitude, longitude and altitude directions at each point. Once all the features of both centrosome trajectories were calculated, the correlation matrix was directly obtained. We only included videos with long and changing centrosome trajectories, because short monotonic trajectories would invariantly have high, but misleading, correlation coefficients. We also excluded videos with a nonstationary nucleus because a moving referential would lead to fallacious correlation values.

Trackosome toolbox: Membrane Fluctuations

We consider that the points of the model-free membrane move in a direction perpendicular to its surface. This is an important novelty, compared with the frequently used methodology that relies on the, much easier to calculate, but flawed, radial direction (see Fig. 3A). We define the fluctuations as being the distance from each point of the median membrane to the membrane at a given frame, along a direction normal to the median membrane. The membranes are segmented for all frames and then centered, assuring a common centroid among frames. To calculate the basal position (the reference membrane) of the NE, we calculate the median projection of the centered frames and segment the resulting membrane. Each point of the reference membrane is associated with a normal vector that defines the direction of the membrane displacements. The fluctuations are then measured by calculating the distance from the reference membrane to the membrane of each frame, along the directions defined by the normal vectors (see Fig. S3I,J).

Acknowledgements

The authors would like to thank Margarida Dantas for the critical reading of the manuscript and Helder Maiato for providing access to microscopes and equipment. The authors would like to thank Katharine Ullman for the HeLa POM121-3×GFP/H2B-mCherry.

Competing interests

The authors declare no competing or financial interests.

Author contributions

Conceptualization: D.C., J.G.F., P.A.; Methodology: D.C., J.G.F., P.A.; Software: D.C., P.A.; Formal analysis: D.C., J.G.F., P.A.; Investigation: D.C., V.N., J.T.L., J.G.F., P.A.; Resources: J.G.F., P.A.; Data curation: D.C., V.N., J.T.L., J.G.F., P.A.; Writing - original draft: D.C., J.G.F., P.A.; Writing - review & editing: D.C., J.G.F., P.A.; Supervision: J.G.F., P.A.; Project administration: P.A.; Funding acquisition: J.G.F., P.A.

Funding

This work was funded by grants from Fundo Europeu de Desenvolvimento Regional (FEDER) through the COMPETE 2020 - Operacional Programme for Competitiveness and Internationalization (POCI), Portugal 2020, and by Portuguese funds through Fundação para a Ciência e a Tecnologia/Ministério da Ciência, Tecnologia e Ensino Superior (FCT) in the framework of the project PTDC/BEX-BCM/1758/2014 (POCI-01–0145-FEDER-016589). V.N. is supported by grant PD/BD/135545/2018 from the BiotechHealth Fundação para a Ciência e a Tecnologia/Ministério da Ciência, Tecnologia e Ensino Superior PhD program. J.T.L. is supported by grant SFRH/BD/147169/2019 from Fundação para a Ciência e a Tecnologia/Ministério da Ciência, Tecnologia e Ensino Superior. The laboratory of Helder Maiato has received funding for research and equipment from the European Research Council (ERC) under the European Union's Horizon 2020 research and innovation program (grant agreement No 681443).

Supplementary information

Supplementary information available online at
https://jcs.biologists.org/lookup/doi/10.1242/jcs.252254.supplemental

Peer review history

The peer review history is available online at
https://jcs.biologists.org/lookup/doi/10.1242/jcs.252254.reviewer-comments.pdf

References

Almonacid, M., Al Jord, A., El-Hayek, S., Othmani, A., Coulpier, F., Lemoine, S., Miyamoto, K., Grosse, R., Klein, C., Piolot, T. et al. (2019). Active fluctuations of the nuclear envelope shape the transcriptional dynamics in oocytes. *Dev. Cell* **51**, 145-157.e10. doi:10.1016/j.devcel.2019.09.010

Antonin, W. and Neumann, H. (2016). Chromosome condensation and decondensation during mitosis. *Curr. Opin. Cell Biol.* **40**, 15-22. doi:10.1016/j.ceb.2016.01.013

Azioune, A., Storch, M., Bornens, M., Théry, M. and Piel, M. (2009). Simple and rapid process for single cell micro-patterning. *Lab. Chip* **9**, 1640. doi:10.1039/b821581m

Blanchoud, S., Budirahardja, Y., Naef, F. and Gönczy, P. (2010). ASSET: a robust algorithm for the automated segmentation and standardization of early Caenorhabditis elegans embryos. *Dev. Dyn.* **239**, 3285-3296. doi:10.1002/dvdy.22486

Bolhy, S., Bouhlel, I., Dultz, E., Nayak, T., Zuccolo, M., Gatti, X., Vallee, R., Ellenberg, J. and Doye, V. (2011). A Nup133-dependent NPC-anchored network tethers centrosomes to the nuclear envelope in prophase. *J. Cell Biol.* **192**, 855-871. doi:10.1083/jcb.201007118

Boudreau, V., Chen, R., Edwards, A., Sulaimain, M. and Maddox, P. S. (2019). PP2A-B55/SUR-6 collaborates with the nuclear lamina for centrosome separation during mitotic entry. *Mol. Biol. Cell* **30**, 876-886. doi:10.1091/mbc.E18-10-0631

Brandt, E. G., Braun, A. R., Sachs, J. N., Nagle, J. F. and Edholm, O. (2011). Interpretation of fluctuation spectra in lipid bilayer simulations. *Biophys. J.* **100**, 2104-2111. doi:10.1016/j.bpj.2011.03.010

Cao, J., Crest, J., Fasulo, B. and Sullivan, W. (2010). Cortical actin dynamics facilitate early-stage centrosome separation. *Curr. Biol.* **20**, 770-776. doi:10.1016/j.cub.2010.02.060

Caragine, C. M., Haley, S. C. and Zidovska, A. (2018). Surface fluctuations and coalescence of nucleolar droplets in the human cell nucleus. *Phys. Rev. Lett.* **121**, 148101. doi:10.1103/PhysRevLett.121.148101

Champion, L., Linder, M. I. and Kutay, U. (2017). Cellular reorganization during mitotic entry. *Trends Cell Biol.* **27**, 26-41. doi:10.1016/j.tcb.2016.07.004

Chu, F.-Y., Haley, S. C. and Zidovska, A. (2017). On the origin of shape fluctuations of the cell nucleus. *Proc. Natl. Acad. Sci. USA* **114**, 10338-10343. doi:10.1073/pnas.1702226114

Collins, E., Mann, B. J. and Wadsworth, P. (2014). Eg5 restricts anaphase B spindle elongation in mammalian cells. *Cytoskeleton* **71**, 136-144. doi:10.1002/cm.21158

Dao, V. T., Dupuy, A. G., Gavet, O., Caron, E. and de Gunzburg, J. (2009). Dynamic changes in Rap1 activity are required for cell retraction and spreading during mitosis. *J. Cell Sci.* **122**, 2996-3004. doi:10.1242/jcs.041301

De Simone, A., Nédélec, F. and Gönczy, P. (2016). Dynein transmits polarized actomyosin cortical flows to promote centrosome separation. *Cell Rep.* **14**, 2250-2262. doi:10.1016/j.celrep.2016.01.077

Eliceiri, K. W., Berthold, M. R., Goldberg, I. G., Ibáñez, L., Manjunath, B. S., Martone, M. E., Murphy, R. F., Peng, H., Plant, A. L., Roysam, B. et al. (2012). Biological imaging software tools. *Nat. Methods* **9**, 697-710. doi:10.1038/nmeth.2084

Georgatos, S. D., Pyrpasopoulou, A. and Theodoropoulos, P. A. (1997). Nuclear envelope breakdown in mammalian cells involves stepwise lamina disassembly and microtubule-drive deformation of the nuclear membrane. *J. Cell Sci.* **110**, 2129-2140.

Gerlich, D., Beaudouin, J., Gebhard, M., Ellenberg, J. and Eils, R. (2001). Four-dimensional imaging and quantitative reconstruction to analyse complex spatiotemporal processes in live cells. *Nat. Cell Biol.* **3**, 852-855. doi:10.1038/ncb0901-852

Hampoelz, B., Azou-Gros, Y., Fabre, R., Markova, O., Puech, P.-H. and Lecuit, T. (2011). Microtubule-induced nuclear envelope fluctuations control chromatin dynamics in Drosophila embryos. *Development* **138**, 3377-3386. doi:10.1242/dev.065706

Helfrich, W. (1978). Steric interaction of fluid membranes in multilayer systems. *Zeitschrift für Naturforschung A* **33**, 305-315. doi:10.1515/zna-1978-0308

Hinde, E., Cardarelli, F., Digman, M. A. and Gratton, E. (2012). Changes in chromatin compaction during the cell cycle revealed by micrometer-scale measurement of molecular flow in the nucleus. *Biophys. J.* **102**, 691-697. doi:10.1016/j.bpj.2011.11.4026

Jahed, Z. and Mofrad, M. R. K. (2019). The nucleus feels the force, LINCed in or not!. *Curr. Opin. Cell Biol.* **58**, 114-119. doi:10.1016/j.ceb.2019.02.012

Kaseda, K., McAinsh, A. D. and Cross, R. A. (2012). Dual pathway spindle assembly increases both the speed and the fidelity of mitosis. *Biol. Open* **1**, 12-18. doi:10.1242/bio.2011012

Kotak, S., Busso, C. and Gönczy, P. (2012). Cortical dynein is critical for proper spindle positioning in human cells. *J. Cell Biol.* **199**, 97-110. doi:10.1083/jcb.201203166

Laan, L., Pavin, N., Husson, J., Romet-Lemonne, G., van Duijn, M., López, M. P., Vale, R. D., Jülicher, F., Reck-Peterson, S. L., Dogterom, M. et al. (2012). Cortical dynein controls microtubule dynamics to generate pulling forces that position microtubule asters. *Cell* **148**, 502-514. doi:10.1016/j.cell.2012.01.007

Lammerding, J., Fong, L. G., Ji, J. Y., Reue, K., Stewart, C. L., Young, S. G. and Lee, R. T. (2006). Lamins A and C but not lamin B1 regulate nuclear mechanics. *J. Biol. Chem.* **281**, 25768-25780. doi:10.1074/jbc.M513511200

Magidson, V., O'Connell, C. B., Lončarek, J., Paul, R., Mogilner, A. and Khodjakov, A. (2011). The spatial arrangement of chromosomes during prometaphase facilitates spindle assembly. *Cell* **146**, 555-567. doi:10.1016/j.cell.2011.07.012

Mahen, R. (2018). Stable centrosomal roots disentangle to allow interphase centriole independence. *PLoS Biol.* **16**, e2003998. doi:10.1371/journal.pbio.2003998

Mardin, B. R., Isokane, M., Cosenza, M. R., Krämer, A., Ellenberg, J., Fry, A. M. and Schiebel, E. (2013). EGF-induced centrosome separation promotes mitotic progression and cell survival. *Dev. Cell* **25**, 229-240. doi:10.1016/j.devcel.2013.03.012

Matthews, H. K., Delabre, U., Rohn, J. L., Guck, J., Kunda, P. and Baum, B. (2012). Changes in Ect2 localization couple actomyosin-dependent cell shape changes to mitotic progression. *Dev. Cell* **23**, 371-383. doi:10.1016/j.devcel.2012.06.003

Mchedlishvili, N., Matthews, H. K., Corrigan, A. and Baum, B. (2018). Two-step interphase microtubule disassembly aids spindle morphogenesis. *BMC Biol.* **16**, 14. doi:10.1186/s12915-017-0478-z

Moir, R. D., Yoon, M., Khuon, S. and Goldman, R. D. (2000). Nuclear lamins A and B1: different pathways of assembly during nuclear envelope formation in living cells. *J. Cell Biol.* **151**, 1155-1168. doi:10.1083/jcb.151.6.1155

Nunes, V., Dantas, M., Castro, D., Vitiello, E., Wang, I., Carpi, N., Balland, M., Piel, M., Aguiar, P., Maiato, H. et al. (2020). Centrosome-nuclear axis repositioning drives the assembly of a bipolar spindle scaffold to ensure mitotic fidelity. *Mol. Biol. Cell* **31**, 1675-1690. doi:10.1091/mbc.E20-01-0047

Otsuka, S., Steyer, A. M., Schorb, M., Hériché, J.-K., Hossain, M. J., Sethi, S., Kueblbeck, M., Schwab, Y., Beck, M., Ellenberg, J. et al. (2018). Postmitotic nuclear pore assembly proceeds by radial dilation of small membrane openings. *Nat. Struct. Mol. Biol.* **25**, 21-28. doi:10.1038/s41594-017-0001-9

Raaijmakers, J. A., van Heesbeen, R. G. H. P., Meaders, J. L., Geers, E. F., Fernandez-Garcia, B., Medema, R. H. and Tanenbaum, M. E. (2012). Nuclear envelope-associated dynein drives prophase centrosome separation and enables Eg5-independent bipolar spindle formation. *EMBO J.* **31**, 4179-4190. doi:10.1038/emboj.2012.272

Rosenblatt, J., Cramer, L. P., Baum, B. and McGee, K. M. (2004). Myosin II-dependent cortical movement is required for centrosome separation and positioning during mitotic spindle assembly. *Cell* **117**, 361-372. doi:10.1016/S0092-8674(04)00341-1

Schreiner, S. M., Koo, P. K., Zhao, Y., Mochrie, S. G. J. and King, M. C. (2015). The tethering of chromatin to the nuclear envelope supports nuclear mechanics. *Nat. Commun.* **6**, 7159. doi:10.1038/ncomms8159

Splinter, D., Razafsky, D. S., Schlager, M. A., Serra-Marques, A., Grigoriev, I., Demmers, J., Keijzer, N., Jiang, K., Poser, I., Hyman, A. A. et al. (2012). BICD2, dynactin, and LIS1 cooperate in regulating dynein recruitment to cellular structures. *Mol. Biol. Cell* **23**, 4226-4241. doi:10.1091/mbc.e12-03-0210

Stephens, A. D., Banigan, E. J., Adam, S. A., Goldman, R. D. and Marko, J. F. (2017). Chromatin and lamin A determine two different mechanical response regimes of the cell nucleus. *Mol. Biol. Cell* **28**, 1984-1996. doi:10.1091/mbc.e16-09-0653

Stephens, A. D., Liu, P. Z., Banigan, E. J., Almassalha, L. M., Backman, V., Adam, S. A., Goldman, R. D. and Marko, J. F. (2018). Chromatin histone modifications and rigidity affect nuclear morphology independent of lamins. *Mol. Biol. Cell* **29**, 220-233. doi:10.1091/mbc.E17-06-0410

Stephens, A. D., Banigan, E. J. and Marko, J. F. (2019). Chromatins physical properties shape the nucleus and its functions. *Curr. Opin. Cell Biol.* **58**, 76-84. doi:10.1016/j.ceb.2019.02.006

Stiff, T., Echegaray-Iturra, F. R., Pink, H. J., Herbert, A., Reyes-Aldasoro, C. C. and Hochegger, H. (2020). Prophase-specific perinuclear actin coordinates centrosome separation and positioning to ensure accurate chromosome segregation. *Cell Rep.* **31**, 107681. doi:10.1016/j.celrep.2020.107681

Tanenbaum, M. E. and Medema, R. H. (2010). Mechanisms of centrosome separation and bipolar spindle assembly. *Dev. Cell* **19**, 797-806. doi:10.1016/j.devcel.2010.11.011

Tinevez, J.-Y., Perry, N., Schindelin, J., Hoopes, G. M., Reynolds, G. D., Laplantine, E., Bednarek, S. Y., Shorte, S. L. and Eliceiri, K. W. (2017). TrackMate: an open and extensible platform for single-particle tracking. *Methods* **115**, 80-90. doi:10.1016/j.ymeth.2016.09.016

Versaevel, M., Grevesse, T. and Gabriele, S. (2012). Spatial coordination between cell and nuclear shape within micropatterned endothelial cells. *Nat. Commun.* **3**, 671. doi:10.1038/ncomms1668

Waters, J. C., Cole, R. W. and Rieder, C. L. (1993). The force-producing mechanism for centrosome separation during spindle formation in vertebrates is intrinsic to each aster. *J. Cell Biol.* **122**, 361-372. doi:10.1083/jcb.122.2.361

Whitehead, C. M., Winkfein, R. J. and Rattner, J. B. (1996). The relationship of HsEg5 and the actin cytoskeleton to centrosome separation. *Cell Motil. Cytoskelet.* **35**, 298-308. doi:10.1002/(SICI)1097-0169(1996)35:4<298::AID-CM3>3.0.CO;2-3

Woodard, G. E., Huang, N.-N., Cho, H., Miki, T., Tall, G. G. and Kehrl, J. H. (2010). Ric-8A and Giα recruit LGN, NuMA, and dynein to the cell cortex to help orient the mitotic spindle. *Mol. Cell. Biol.* **30**, 3519-3530. doi:10.1128/MCB.00394-10

Yamashita, N., Morita, M., Legant, W. R., Chen, B.-C., Betzig, E., Yokota, H. and Mimori-Kiyosue, Y. (2015). Three-dimensional tracking of plus-tips by lattice light-sheet microscopy permits the quantification of microtubule growth trajectories within the mitotic apparatus. *J. Biomed. Opt.* **20**, 101206. doi:10.1117/1.JBO.20.10.101206